FETAL DEVELOPMENT AND EVOLUTION OF THE HUMAN CRANIAL BASE

Nathan Jeffery

September 1999

A dissertation submitted to University College London in partial fulfilment of the requirements for the degree of Doctor of Philosophy.

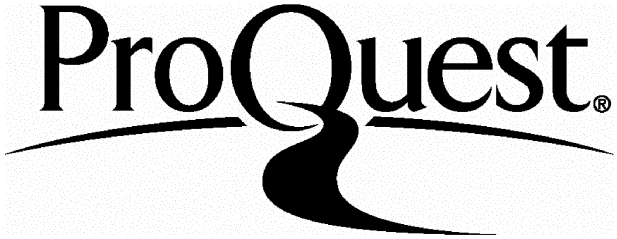

" *A hidden assumption of much writing ... is that the great apes are appropriate surrogates for human ancestors. ... the best prototype among living forms is the human fetus or juvenile.* "

Stephen Jay Gould, from " Of prototypes" in Ontogeny and Phylogeny (1977).

To the memory of my mother

ABSTRACT

One of the principal morphological features that distinguishes *Homo sapiens* from other primates is the major reorganisation of its cranial base. Pivotally positioned as the interface between the neurocranium and the face, the cranial base has long been recognised as a key area to our understanding of the origins of modern human skull form. A number of authors have hypothesised that the unique architectural features of the modern human cranial base result from changes in the size of the brain. However, the ontogenetic mechanisms underlying this relationship have yet to be investigated. This study assesses a number of evolutionary hypotheses regarding the relationship between brain and cranial base morphology in a sample of human fetuses.

Forty-two formalin preserved human fetuses, 53-205mm crown-rump length (11-23 weeks gestation +/- 1 week), were imaged using high resolution magnetic resonance imaging. This approach was used in this study in order to non-invasively image soft-tissues as well as base morphology. Transverse T2 (TE = 40msecs; TR = 9secs) weighted images were acquired contiguously through the head, interpolated and then resampled. Cranial base angle, angle of palate orientation, orientation of the petrous temporal bones, orientation of the orbits, sagittal orientation of the tentorium cerebelli, and infra and supratentorial brain volumes were measured using the images produced.

Bivariate analysis of the data indicates that whilst many parts of the fetal cranial base are indeed interrelated with brain development some are not. In particular the study shows that the substantial 47-fold increase of brain size during the period studied does not correlate with an increase in base flexion. Thus, these results suggest that there are indeed ontogenetic relationships between brain development and cranial base morphology, but rather than being a simple continuous process these interactions likely involve different parts of the cranial base at different times.

CONTENTS

List of Figures

CHAPTER 2.

CHAPTER 3.

CHAPTER 6.

CHAPTER 7.

List of Tables

ACKNOWLEDGEMENTS

I would like to gratefully acknowledge the enthusiastic and patient supervison of Dr. Fred Spoor without whom this thesis would not exist. He gave me the opportunity to enter a field in which I had no prior form and apply novel imaging techniques to the study of human evolution. Not everyone would have taken the time to guide a physicist through the intricacies of the anthropological sciences.

I would also like to thank the following people: Prof. Chris Dean, Dr. Callum Ross (Stonybrook, USA) and Dr. Daniel Lieberman (Washington D.C., USA) for their advice and discussions concerning the cranial base and brain; Dr. Paul Kinchesh (Queen Mary and Westfield College, London) for help with the NMR spectrometer system; University of London Intercollegiate Research Services for providing the NMR service at Queen Mary and Westfield College; Dr. M. Bird for access to the fetal collection at Queen Mary and Westfield College, London; Dr. Paul O'Higgins, Dr Gary Schwartz, Nick Jones, Jane Moore, and Sam Cobb for their general support and opposing viewpoints; Dr. Brad Smith (Duke University, USA) for an insight into the field of MRI microscopy; Wendy Birch and Derek Dudley for the preparation of material and a subtle sense of humour; and finally I thank Samantha Peacock for safeguarding my sanity.

My appreciation goes to the Medical Research Council for the financial support they have given me over the past three years.

CHAPTER 1. INTRODUCTION

One of the principal morphological features that distinguishes *Homo sapiens* from other primates is the major reorganisation of its cranial base. Pivotally positioned as the interface between the neurocranium and the face the cranial base has long been recognised as a key area to our understanding of the origins of modern human skull form. Gaining insight into the biological factors underlying this unique basicranial architecture and its associations with facial morphology and brain enlargement is a prerequisite for interpreting the fossil hominid record and the evolutionary history it represents.

Compared with other primates the human basioccipital has a more inclined orientation relative to the anterior cranial base, shown as a high degree of basicranial flexion, and the foramen magnum faces more inferiorly and has a more anterior position. The petrous pyramids are more coronally oriented and, like the basioccipital, their posterior surface is more inclined relative to the orientation of the anterior cranial base. Consequently, the human posterior cranial fossa is much wider and deeper than in other primates, which primarily seems to reflect the large human brain. Indeed, the major spatial changes in basicranial architecture that must have occurred during human evolutionary history have been linked with the process of encephalization, the major expansion of brain size, although other factors, such as upright posture, have been proposed as well (Moss *et al.*, 1956; Kier, 1976; Dean, 1988; Ross and Ravosa, 1993; Spoor, 1997; Lieberman and McCarthy, 1999). More in particular, the hypotheses have been postulated that human midline basicranial

flexion is the consequence of a combination of a large brain and a short cranial base length (Ross and Ravosa, 1993) and that lateral expansion of the human cerebellum associated with a short posterior base underlies the coronal orientation of the petrous pyramids (Dean, 1988). Evidence from interspecific studies of adult primate species corroborate these hypothetical correlations (Ross and Ravosa, 1993; Spoor, 1997), and seem to support the notion that, as an evolutionary process, brain growth and development forms the predominant influence on endocranial aspects of basicranial morphology.

Early histological development of the basicranium is distinct from that of the face. The cranial base forms by chondrification of mesodermal derived tissues that subsequently ossify endochondrally whereas the neural-crest derived tissues of the face ossify intramembranously. However, the spatial proximity of these structures and the position of the cranial base between the face and endocranial cavity has led some researchers to associate changes of facial morphology with that of the basicranium and also, therefore, the process of encephalization (e.g. Weidenreich, 1941; Scott, 1956, 1958; Biegert, 1964). As such the face and cranial base are structurally and morphologically continuous and effectively integrated within a single complex. Hence, the influence of brain enlargement is transmitted to the face via changes of cranial base architecture. In particular, it has been postulated that the orthognathic position of the maxilla in modern humans compared with other primates is the consequence of increased base flexion (Cameron, 1924; Enlow and Bang, 1965; Enlow, 1975). It has also been proposed that the forward orientation of the orbits in humans results from an increase of brain size within the anterior and middle cranial fossae (Enlow, 1968; Enlow and McNamara, 1973; Sperber, 1981). Indeed, correlations of maxillary prognathism, palate orientation, and orbital

orientation with cranial base angulation and similarities between growth of the anterior cranial base and face appear to support the notion of a unified complex on both an evolutionary and ontogenetic level (e.g. Kvinnland, 1971; Sirianni and Swindler, 1979; Ross and Ravosa, 1993; Ross and Henneberg, 1995). However, the ontogenetic mechanisms underlying the relationship of brain enlargement with basicranial architecture and the effect on facial morphology have yet to be investigated. The question can be asked whether in humans increased fetal brain growth directly and mechanically drives a stronger ontogenetic reorientation of the basioccipital and the petrous pyramids than in other primates and whether this relates to changes of facial morphology. Interestingly, the opposite notion, that the distinctiveness of the human skull is a consequence of humans departing less from their fetal form than other primates has also been proposed (Gould, 1977). The alternative to hypotheses centred on major ontogenetic change in basicranial morphology, dependent or independent of surrounding soft-tissues, is that the morphology characteristic of humans and other primates is largely present at the onset of the fetal period and subsequently shows little change other than scaled growth.

The most direct way of addressing the afore-mentioned issues is by examining fetal growth patterns in human and other primate species. The few studies that have investigated fetal basicranial morphology in humans are largely inconclusive and contradictory because of limited sample sizes and the use of less-suitable radiological techniques (e.g. Levihn, 1967; Dimitriadis *et al.*, 1995). Hence, before the question of possible interactions between the fetal cranial base and brain and influences on facial morphology can be addressed there is a need for even the

most basic quantitative description of morphological change shown by these structures during development.

Magnetic resonance imaging (MRI) studies of human fetuses in *utero* and post-mortem have shown the way forward for non-invasive quantification of prenatal morphologies in conjunction with the soft-tissues of the brain (e.g. Foster *et al.*, 1983; Weinreb *et al.*, 1985; Hata *et al.*, 1990; Adrias-Mendoza *et al.*, 1991; Hansen *et al.*, 1993; Baker *et al.*, 1995; Garden and Roberts, 1996; Gong *et al.*, 1998). MRI has the ability to differentiate many more tissues than either plain radiography or computed tomography (CT) and is therefore ideal for imaging the varied tissue types found in the fetus (e.g. brain, muscle, cartilage, and bone). At present, however, such clinically orientated works as the ones cited above provide insufficient contrast and resolution to accurately define the homologous landmarks that are essentially for quantifying cranial base architecture. Nonetheless, more sensitive equipment can be used to obtain higher resolutions and better image contrast, and these allow for a comprehensive study of human fetal development. This study aims to use the new technique of high-resolution magnetic resonance imaging (hrMRI) to visualise and quantify for the first time the afore-mentioned features of the cranial base as well as the face in relation to the brain. On this basis evolutionary hypotheses are investigated in an ontogenetic context, thereby yielding information as to the mechanisms underlying some of the uniquely modern human features of the cranial base.

This thesis explores a wide range of topics from evolution to the quantum mechanics of hydrogen spins. Nonetheless, the biological aspects are interrelated and are well placed with MRI under the aims of the present study. Hence, to maintain an overall perspective chapters have been organised to follow on from one another

rather than as separate units. In Chapter 2 a review of the literature on prenatal development of the brain, cranial base, face, and other associated structures is given. This review, unlike most others, follows human development according to specific age groups as opposed to individual structures and covers both embryonic and fetal periods. Chapter 3 begins with a brief overview of genetic and epigenetic factors in skull formation and provides the general framework in which more specific biomechanical hypotheses are considered. Following this, more in depth assessments of a few evolutionary hypotheses covering the biomechanical relationships amongst basicranial morphology, facial morphology, and brain enlargement are given using evidence from the existing literature. This together with the information covered in Chapter 2 was used to interpret selected hypotheses in terms of prenatal development. These are summarised in the form of testable predictions at the end of Chapter 3. In Chapter 4 an introduction to MRI is provided that includes subsections on all the basic principles required to understand the practical aspects of high-resolution MRI, its advantages, and its disadvantages. Subsequently, Chapter 5 describes the hrMRI technique, fetal sample, landmarks and measures, and statistical analyses used in the present study. Chapters 6 and 7 contain the results and discussion, respectively.

CHAPTER 2. A REVIEW OF PRENATAL DEVELOPMENT OF THE HUMAN CRANIAL BASE WITH REFERENCE TO THE BRAIN AND OTHER ASSOCIATED STRUCTURES

Development of the brain, the surrounding cranial base, and the face has been the focus of numerous studies and reviews in the past (e.g. De Beer, 1937; Bartelmez and Blount, 1954; Burdi, 1976; Gasser, 1976; Müller and O'Rahilly, 1980; Diewert, 1985). However, only a few of these have documented their development in relation to each other. Indeed, those authors that have described cranial base and facial development in conjunction with that of the brain typically confined their observations to the embryonic stages (e.g. Gasser, 1976; Müller and O'Rahilly, 1980).

In order to provide a descriptive framework for the quantitative analysis, which is at the heart of this thesis, the following section reviews development of the brain, basicranium, face, and some associated structures from one to forty weeks (term) gestation as compiled from a wide range of studies (e.g. Streeter, 1918; De Beer, 1937; Noback and Robertson, 1951; Burdi, 1976; Gasser, 1976; Kodama, 1976a-c; Shapiro and Robinson, 1980; Sperber, 1981; Moore, 1982; Kjaer, 1990a-c; O'Rahilly and Müller, 1994; Kjaer and Fischer-Hansen, 1995). Because the appearance and development of most, if not all, of these structures are subject to some degree of normal biological variation, the timing of certain observations reported in the literature is inconsistent. This is complicated by further inconsistencies in the terminology and definitions used to denote 'age' (e.g. crown rump length, CR or CRL; greatest Length, GL; stage; horizon; number of somites;

post-ovulatory days; post-conception days). Hence, it is not always possible to accurately order observations chronologically from different investigations. Thus, many aspects of this review are likely to be equivocal and deficient in both content and the sequence of events reported. It should not, therefore, be considered irrefutable, but more a consensus of the literature. A table for converting some of the measures used to denote age into weeks is given in Appendix 1a.

The review is divided into different age (weeks) groupings and then subdivided according to anatomical structure (brain, basicranium, face, and other). The method of description preferred here is mostly in the past and occasionally the future tense since this more openly reflects the cross-sectional nature of the stages studied in the works reviewed. More eloquent descriptions, which lack a rolling temporal order, are given by Keith (1948), Sperber (1981), Moore (1982), and Moore and Persaud (1998). A summary of the major events occurring during prenatal development and the differences in the reported timing of these events are shown at the end of this section in Table 2.1. Some of the synonyms encountered are listed in Appendix 1b.

2.1 Week 1-5

2.1.1 *Brain*

The neural groove is discerned along the midline of the primitive head as an invagination of the neural plate (a thickened layer of ectoderm superior to the notochord) and is bound on either side by neural folds. These structures represent the first indication of a primitive brain.

Formation of the neural tube by fusion of the neural folds above the neural groove (referred to as neuralation) is first seen in the primitive head region some six days after the groove is visible. Openings at either end of the tube, the caudal and rostral neuropores, ensure that lumen of the tube communicates with the amniotic cavity. This lumen is the precursor to the ventricular system of the brain.

Neural crest cells, derived from the neural folds, are observed in the mesoblast between the neural tube and surface ectoderm. Amongst other things these eventually contribute to the formation of the pia mater and arachnoid coverings of the brain and the pharyngeal arches that give rise to the face. Migration of neuroblastic cells has also formed a medial and lateral pair of lamina along the floor of the neural tube. Medial and lateral pairs of lamina are known as basal and alar plates, respectively. Later in prenatal life the alar plates are involved in the formation of the cerebellum.

A ventral bend in the neural tube, the cephalic flexure, marks off the rostral margin of the mesencephalon or midbrain (Figure 2.1). Also visible are the other two main divisions of the embryonic brain, namely the rhombencephalon or hindbrain and the prosencephalon or forebrain. Occasionally, diencephalic (consisting of thalamic and optic portions) and telencephalic parts of the prosencephalon are also distinguished.

2.1.2 *Basicranium*

The first indications of the cranial base are visible between the developing hindbrain and foregut as parachordal condensations of mesenchyme derived from the neural crests and primitive streak (Figure 2.1). Otic placodes are visible as regions of thickened ectoderm on either side of the primitive hindbrain. The surface of each placode invaginates to form an otic pit that subsequently develops into an otocyst or otic vesicle (Bartelmez and Blount, 1954; Bartelmez and Dekaban, 1962).

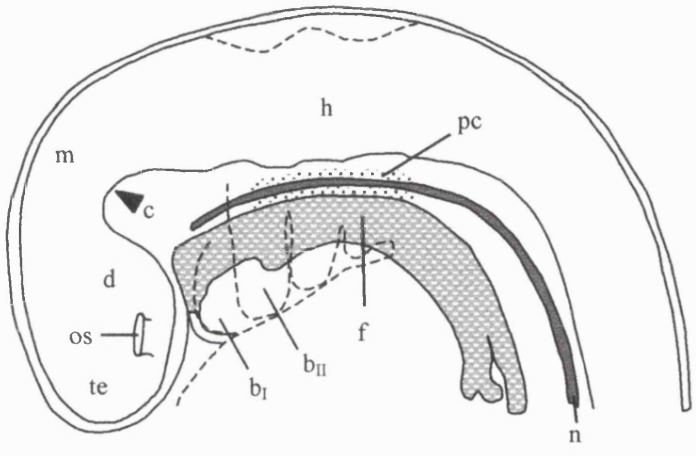

Figure 2.1. Lateral view of a human embryo (5mm crown-rump length): telencephalon (te); optic stalk (os); cephalic flexure (c); diencephalon (d); mesencephalon (m); foregut (f); hindbrain (h); notochord (n); first or mandibular branchial arch (b_I); second or hyoid branchial arch (b_{II}); and parachordal condensations of mesenchyme (pc). The latter eventually fuse and give rise to the basal plate of the cranial base (from Gasser, 1976).

2.1.3 *Face*

Optic sulci are visible at the end of each neural fold and subsequently develop into optic vesicles by about the fifth week. These are the precursors to the eyes and their development influences the orbital morphology of the face. Bilateral swellings of surface ectoderm on each side of the frontonasal region mark the positions of the nasal placodes. Within a week, mesenchyme has collected on the margins of each placode to form nasal pits.

The anterior of six pairs of processes or pharyngeal arches projecting from the base of the cerebral capsule represents the first signs of the face. Two processes on the first or mandibular arch are the precursors to the maxilla and Meckel's cartilage, respectively (Figure 2.2). Meckel's cartilage is the forerunner to the mandible. The second or hyoid arch eventually contributes to the formation of hard tissue structures such as the middle ear ossicles, and the styloid and hyoid structures of the neck region.

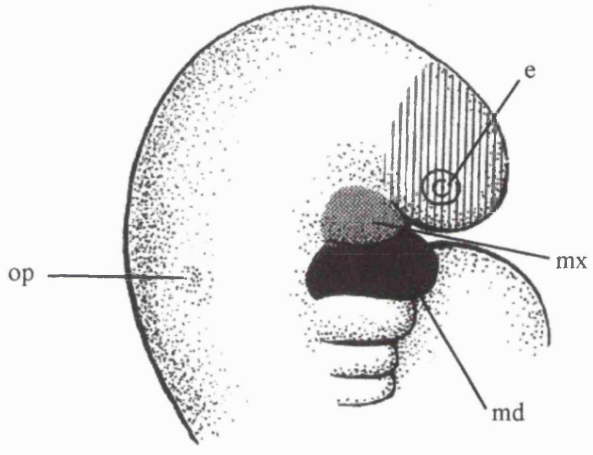

Figure 2.2. Lateral view of the embryo at 4 weeks showing: an early stage of eye development (e); otic placode (op); frontonasal area (vertical stripes); and the maxillary (mx) and mandibular processes (md) of the first pharyngeal arch.

2.1.4 *Other*

Differentiation of paraxial mesoderm (derived from the intra-embryonic mesoderm) into occipital somites along the rostral end of the neural tube is detectable at around the same time as the parachordal condensations are seen. Within the cephalic flexure, the precursor of the medial part of the tentorium cerebelli (Figure 2.3), which is partially derived from and connected to the notochord, is discernible (O'Rahilly and Müller, 1986).

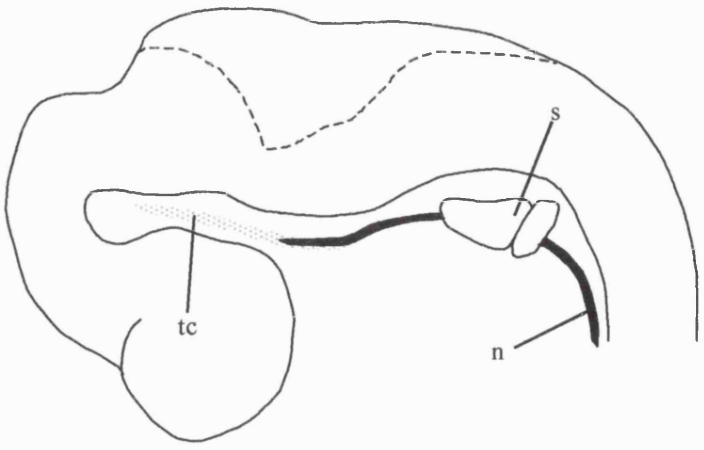

Figure 2.3. Lateral view of the embryonic head (stage 15) showing the medial part of the early tentorium cerebelli (tc) within the cephalic flexure and its relationship to the notochord (n). Also shown are the occipital somites (s) (from O'Rahilly and Müller, 1986).

Primitive blood capillary channels in the mesenchymal tissue around the ventral part of the neural tube and lateral surface of the brain, mark the position of the internal carotid artery and primary head vein respectively. The primary head vein is established not long after and drains a meshwork of capillaries over the brain analogon. These are arranged into three plexuses: (1) the anterior plexus, containing anterior cerebral veins that drain the forebrain, midbrain and otic region into the pre-trigeminal portion of the primary head vein; (2) the middle plexus, containing middle cerebral veins that drain the cerebellar region; and (3) the posterior plexus, containing posterior cerebral veins. The primary head vein also receives tributaries from the optic region, nerve-ganglia, and the first two pharyngeal arches (see Streeter, 1918 for further details).

2.2 Week 5-6

2.2.1 *Brain*

The cephalic flexure has pushed the prosencephalon into an almost perpendicular position relative to the mesencephalon and an additional flexure, the cervical flexure, separates the rhombencephalon from the spinal cord. The caudal and lateral parts of the rhombencephalon are marked by hypoglossal nuclei and the fourth and fifth hypoglossal roots. Differential growth in the rhombencephalon has given rise to the pontine flexure by the end of this period. This divides the hindbrain into the myelencephalon (future medulla oblongata) caudually and the metencephalon (future pons) rostrally. All five secondary brain vesicles are discernible at six weeks (Figure 2.4).

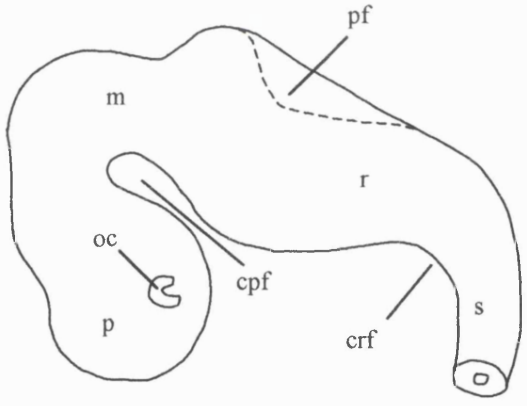

Figure 2.4. Lateral view of the three brain flexures at the end of the 6th week: the pontine flexure (pf), cervical flexure (crf), cephalic flexure (cpf). Also shown are the spinal cord (s), rhombencephalon (r), mesencephalon (m), prosencephalon (p), and an optic cup (oc).

A recess in the base of the brain, caudal to the developing infundibular region (neurohypophysis), identifies the position of the mammillary body. The precursor to the hypophyseal or Rathke's pouch is seen as a small diverticulum rostral to the tip of the notochord and is traversed on either side by the internal carotid arteries. Both parts of the future hypophysis (*hypophysis cerebri*), the

adenohypophyseal part (a small invagination of oral ectoderm occupying Rathke's pouch) and the neurohypophyseal part (derived from neuroectoderm in the diencephalon), have differentiated. The *sulcus hypothalamicus* marks the dorsal boundary of the hypothalamus, which is visible between the infundibular and mammillary regions. Amygdaloid, hippocampal and olfactory regions of the prosencephalon are visible as well.

Cerebral vesicles are visible as dorso-lateral outpouchings of the forebrain and are distinguished from the rest of the telencephalon by the *torus hemisphericus* internally and the ditelencephalic sulcus externally (O'Rahilly and Muller, 1994). Thickening in the ventro-lateral wall of the cerebral hemispheres (vesicles) marks the position of the corpus striatum.

Within the fourth ventricle, bilateral swellings (enlarged alar plates) derived from the rhombencephalon and isthmus areas mark the future position of cerebellum. These swellings, after growing dorso-medially over the ventricle and fusing, are visible some time later as the cerebellar segments (Larsell and Jansen, 1972; O'Rahilly and Müller, 1994).

2.2.2 *Basicranium*

The parachordal condensations have extended bilaterally, superior to the pharynx, towards the hypophyseal region of the brain (Figure 2.5). The sclerotomes, which are derived from the medial and ventral walls of the occipital somites, are visible in the occipital region. At the end of this period, the sclerotic tissue is seen bilaterally around part of the hypoglossal (XII) nerves in the form of the hypoglossal incisures and occipital arches. The first signs of chondrification are visible in this region by the sixth week as discrete chondrogenic cells which are thought to arise in

relation to development of the notochord and brain stem (Kingsbury, 1924; Holtzer, 1964).

Lateral extensions of mesenchyme from the midline basal region represent the otic capsule posteriorly and the *ala temporalis* (alisphenoid; greater wing of sphenoid) anteriorly. The *ala orbitalis* (orbitosphenoid; lesser wing of sphenoid) consists of a smaller extension of mesenchyme ventral to the *ala temporalis*. Mesenchyme collected around the otic vesicles has formed the otic capsules.

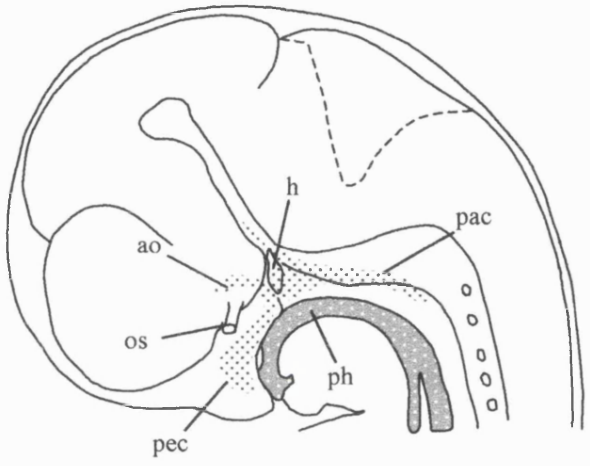

Figure 2.5. Lateral view of an embryo (stage 19) showing mesenchymal condensations (black and white stippled areas). These include the prechordal condensation (pec), parachordal condensation (pac), and *ala orbitalis* (ao). Also shown are the hypophysis (h), primitive pharynx (ph), and optic stalk (os)(from Gasser, 1976).

2.2.3 *Face*

Prechordal mesenchyme has given rise to the prechordal condensations which extend into the olfactory region as the basis for the ethmoid structures, and the nasal capsules (Figure 2.5). Mesenchyme originating from around the base of the brain, but now covering most of the brain, represents the precursor of the neurocranium (Burdi, 1976). The second or hyoid pharyngeal arch has overgrown the third and fourth arches, giving that region of the neck a smoother appearance. Meckel's cartilage is visible within the first pharyngeal arch and forms the template around which part of the mandible will develop.

2.2.4 *Other*

The pia mater covering of the brain is almost complete (O'Rahilly and Müller, 1986) and the future falx cerebri consists of loose mesenchyme between the cerebral vesicles. Internal carotid arteries supply most of the forebrain via anterior and middle cerebral arteries, and posterior communicating divisions while other blood vessels have penetrated the walls of the brain (Padgett, 1957).

2.3 Week 6-7

2.3.1 *Brain*

Five longitudinal zones in the diencephalon mark the positions of the epithalamus, dorsal thalamus, ventral thalamus, subthalamus and hypothalamus. All twelve cranial nerves are visible. Lateral choroid plexuses are present in the roof of each lateral ventricle, though as yet little cerebrospinal fluid is produced.

Enlargement of the cerebral hemispheres dorsally towards the midline has deepened the longitudinal fissure and posteriorly it covers much of the diencephalon. Within the cerebral cortex of each hemisphere, ventricular, intermediate, and marginal strata are distinguishable and a fourth subventricular layer is visible some time later. Olfactory fibres have entered the wall of the diencephalon at the site of the future olfactory bulb.

2.3.2 *Basicranium*

Parachordal, prechordal, and sections of mesenchymal condensation around the hypophyseal region are now chondrified. Fusion of the parachordal cartilages between the rhombencephalon and primitive pharynx has formed the basal plate (De

Beer, 1937: Figure 2.6). Rostrally, this plate is continuous with the fused hypophyseal or polar cartilages in the future sella turcica area and the trabecula cartilages of the prechordal condensation. Trabecula cartilages are continuous anteriorly with the nasal capsules and parts of the palate. The otic capsules are fused with the lateral aspect of the basal plate and show signs of chondrification. The dorsum sellae is represented as a bar of cartilage connected to the clivus via a fibrous band (Shapiro and Robinson, 1980).

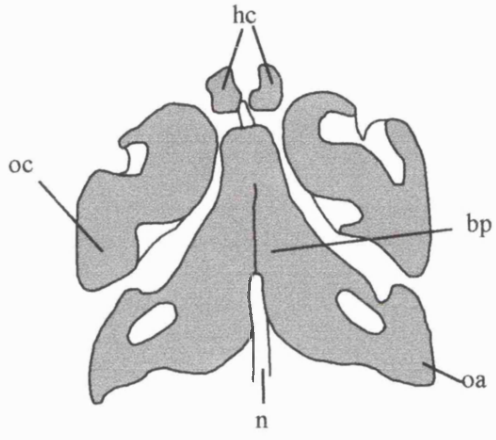

Figure 2.6. Dorsal view of the cartilaginous basicranium in an embryo (14mm crown-rump length) showing the notochord (n), otic capsule (oc), basal plate (bp), occipital arch (oa), and the paired hypophyseal cartilages (from De Beer, 1937).

2.3.3 *Face*

Mesenchymal cells collecting between the nasal pits, formed by invagination of ectoderm below the cerebral vesicles, have contributed to the formation of the frontonasal area. Subsequent condensations of mesenchyme around the nasal pits forms the nasal capsules. By the seventh week the maxillary processes have grown forward and fused with the nasal capsules of the frontonasal region. Ledges projecting vertically from the medial surface of each maxillary process represent the palatine processes of the palate. These are separated by the tongue, which extends from the floor of the primitive pharynx. A mesenchymal condensation representing

the future nasal septum, or mesethmoid, is also discerned at some point during this period. Intramembranous ossification centres for each half of the mandible are visible lateral to Meckel's cartilage. The expanding cerebral hemispheres have forced the optic cups into a more frontal position on the head.

The first signs of tooth development are visible in the anterior mandibular and maxillary regions as localised thickenings of oral epithelium, the dental laminae, protruding into the underlying layer of mesenchyme. The tooth buds or germs for the deciduous dentition are visible some seven days later following proliferation of cells around the dental lamina.

2.3.4 *Other*

Carotid arteries have joined with others in forming the circle of Willis. Brain enlargement has compressed the dura and cut off many of the superficial networks of capillaries covering the brain (vascular cleavage). This leaves the remaining vessels at three anatomical levels: external, dural, and cerebral. The future tentorium cerebelli now extends from within the cephalic flexure to the lateral parts of the diencephalon.

2.4 Week 7-8

2.4.1 *Brain*

Further cerebral expansion has extended the hemispheres beyond the well-developed olfactory bulbs anteriorly and the thalamus posteriorly and the flattened medial surface of each hemisphere is marked by the insular region.

Lateral outpouchings of the midbrain at its posterior end mark the positions of the inferior colliculi. Afferent and efferent cranial nerves have formed from neuroblastic cells derived from the alar and basal plates, respectively. At this stage the adenohypophysis is closely related to the neurohypophysis (infundibulum), forming the anterior and posterior lobes of the pituitary (hypophysis), respectively. Development of these structures together with the hypophyseal condensations define the floor of the future sella turcica.

2.4.2 *Basicranium*

Chondrification of the cranial base is well underway (Figure 2.7). The cartilaginous orbitosphenoid extends antero-laterally from the prehypophyseal segment of the developing sphenoid (presphenoid), but has yet to fuse with it. The greater part of the cartilaginous alisphenoid connects to the central stem by the *alar processus*. The space between the alisphenoid and orbitosphenoid, occupied by the oculomotor (III), trochlear (IV), ophthalmic (V), abducens (VI) nerves and

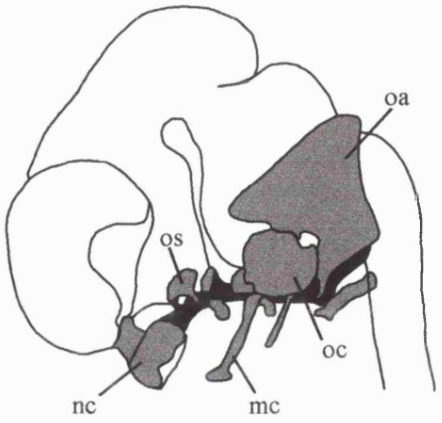

Figure 2.7. Lateral view of the chondrocranium at 8 weeks showing the occipital arches (oa), otic capsule (oc), orbitosphenoid (os), nasal capsule (nc), and Meckel's cartilage (mc) (from Keith, 1948).

ophthalmic veins, defines the superior and inferior limits of the superior orbital fissure. A region of intramembranous ossification is detected in the squamous part of

the future temporal bone, close to the root of the zygomatic process (Viraponges *et al.*, 1985).

2.4.3 *Face*

Continued fusion between the maxillary process and the frontonasal region has established a continuity between the sides of the nasal capsules and the future maxilla. The lateral palatine processes have moved to a more horizontal position superior to the tongue (palatal elevation), fusing together and with the lower edge of the nasal septum to form the palate. Apart from ossification and proportional changes, gross development of the nasomaxillary area is almost complete.

2.4.4 *Other*

The choroid plexus of the fourth ventricle has started to produce cerebrospinal fluid (CSF). Experimental evidence suggests that the production of CSF together with closure of the rostral and caudal neuropores (1-5 weeks), which prevents the ventricular system communicating with the surrounding amniotic fluid, contributes to the rapid expansion of the cerebral vesicles (Desmond and Jacobson, *1977*).

The tentorium cerebelli consists of condensed fibrous tissue extending from within the cephalic flexure over the lateral and posterior parts of the diencephalon (Figure 2.8). Blood from the middle dural plexus, which originally drained into the primary head vein, now drains into the posterior dural plexus (Streeter, 1918). Sigmoid sinuses and a primitive transverse sinus, both derived from the dural plexuses, are visible in the posterior cranial fossa. Caudal remnants of the primary

head vein contribute to the formation of the petrosal and stylomastoid veins (Padgett, 1957).

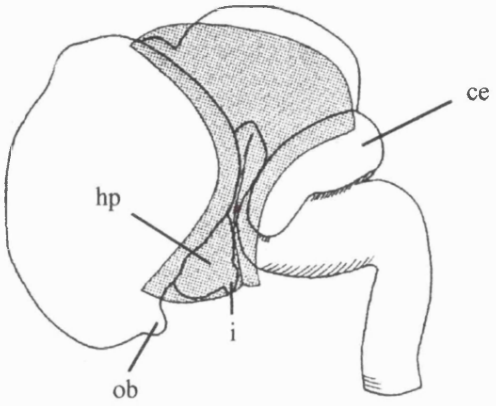

Figure 2.8. Lateral view of the brain showing the tentorium cerebelli (stippled area) at 7 weeks. Also shown are the cerebellum (ce), hypothalamus (hp), infundibulum (i), and olfactory bulb (ob).

2.5 Week 8-9

2.5.1 *Brain*

The cerebelli segments which are differentiated by fissures into several lobules have extended medially, assisted earlier by continued pontine and midbrain flexion, to become the cerebellum. External swellings on each side of the cerebellum mark the future flocculi. The cervical flexure is less prominent than in previous stages and the cerebral hemispheres cover much of the diencephalon. Optic nerve fibres, formed from retinal ganglion cells, connect the optic chiasma of the brain with the retinal nerve layer in each of the primitive eyes (O'Rahilly, 1975).

2.5.2 *Basicranium*

The otic capsules connect posteriorly to the occipital cartilage and medially to the basal plate. The glossopharyngeal (IX), vagus (X), spinal accessory (XI) nerves and the jugular vein exit from the cranium via the jugular foramen which lies between the otic capsule and the basal plate. Mastoid processes are discernible on the lateral wall of the otic capsule and bulges on the inferior surface of the occipital represent the occipital condyles. Fusion between the dorsal edge of the mesethmoid and trabecula cartilages has given rise to the crista galli (Figure 2.9). Cartilage of the dorsum sellae is continuous with that of the basal plate. Superiorly, the orbital cartilages are attached to the roof of the nasal capsules.

An endochondral ossification centre, which is initially visible in the zygomatic portion of the temporal, has spread and is fused with a single intramembranous centre originating from the inferior half of the squamosal part of the temporal. In the otic capsule, the semicircular canals are visible. Of the canals, the anterior canal was first to appear followed by the posterior, and finally the lateral (Nemzek *et al.*, 1996).

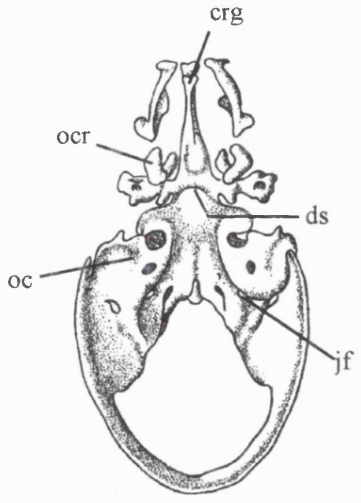

Figure 2.9. Dorsal view of the cranial base at 20mm crown-rump length showing the crista galli (crg), orbital cartilage (ocr), dorsum sellae (ds), otic capsule (oc), and the jugular foramen (jf) (adapted from De Beer, 1937).

According to Sperber (1981), a pair of intramembranous centres are visible in the supranuchal squamous (interparietal) portion of the occipital during this period and two endochondral centres are visible a short time later for the infranuchal squamous portion (supraoccipital). The latter is consistent with De Beer's (1937) observations. However, some reports indicate that supranuchal and infranuchal portions ossify from two and three pairs, respectively (Kodama, 1973; Gopinathan, 1992; Srivastava, 1992). Cartilaginous styloid processes are visible, having formed by fusion of a lateral prong of chondrogenic material derived from Meckel's cartilage in the hyoid region.

2.5.3 *Face*

The cap stage of deciduous tooth development is visible: Dental papilla has pushed the mesenchymal surface of anterior tooth buds towards the oral cavity. Intramembranous ossification is visible at two centres on either side of the midline in the frontal region, superior to the orbital arch. These centres spread over the forehead and into the inner wall of the orbit and ultimately fuse medially to occlude the metopic suture and form the frontal bone. The palatine shows signs of intramembranous ossification from one centre just dorsal to the lateral wall of the nasal capsule and the vomer has two intramembranous centres either side of the midline (De Beer, 1937).

According to De Beer (1937) a separate premaxilla centre of intramembranous ossification is visible at this stage and has started to fuse with a main maxilla centre, ascending laterally to form the sides of the external nostril and medially to form the palatine process (De Beer, 1937). However, evidence that is

more recent indicates that the whole of the maxilla starts to ossify in membrane from a single centre in the body during this period (Berkovitz and Moxham, 1988).

2.5.4 *Other*

The medial part of the tentorium extends from sella turcica to the mammillary body and has shifted backwards with increases in the size of the cerebrum. Changes in the topography of the brain have also forced the anterior and middle plexuses to combine into a tentorial plexus or sinus between the cerebral hemispheres and the anterior margin of the cerebellum. This eventually gives rise to the confluence of sinuses and contributes to the formation of the superior sagittal sinus, but at present it only receives the deep and superficial telencephalic veins, and the ventral diencephalic vein (Padgett, 1957). The head vein has a cavernous portion that receives ophthalmic, maxillary veins and a large cerebral vein. Tissue in the subarachnoid space is clearly visible at this stage and the falx cerebri is discernible in the rostral part of the longitudinal fissure towards the newly formed crista galli (Figure 2.10).

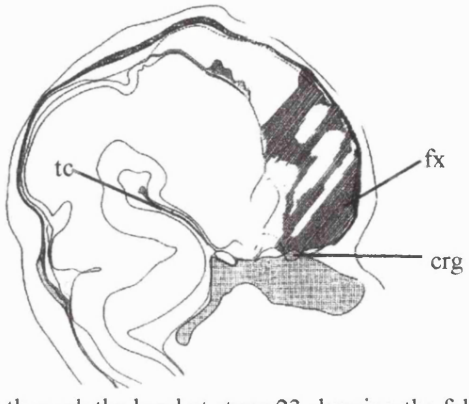

Figure 2.10. Midline section through the head at stage 23 showing the falx cerebri (fx) and its attachment to the crista galli (crg) and the tentorium cerebelli (tc) (adapted from O'Rahilly and Müller, 1986).

2.6 Week 9-10

2.6.1 *Brain*

The insula is visible as an indented region on the surface of each cerebral hemisphere which are still smooth in appearance (Figure 2.11). In contrast, the cerebellum is marked by a number of fissures. The commissural plate is distinguishable as a thickening of the anterior commissure. The brain at this stage, with the exception of gyri and sulci and proportional changes, has much the same basic structure as that of a new born.

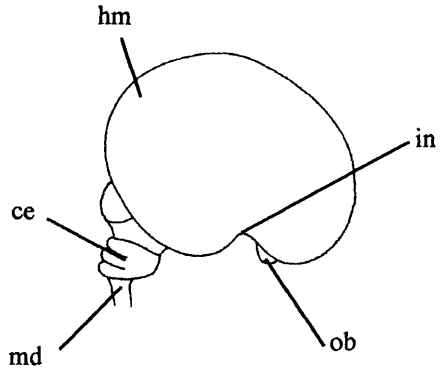

Figure 2.11. Lateral view of the brain at 9 weeks: smooth cerebral hemisphere (hm); insula region (in); olfactory bulb (ob); medulla (md); and cerebellum (ce).

2.6.2 *Basicranium*

Orbitosphenoids extend to the mesethmoid, but are separated from it by the spheno-ethmoidal suture. Medially, the orbitosphenoids have encircled the optic nerves to form the optic foramina (Figure 2.12). Ossification of the alisphenoids has commenced from endochondral centres surrounding each foramen rotundum which transmit the maxillary division of the trigeminal nerve (V^{II}). Within a short time, a closely associated intramembranous centre is also visible for the alisphenoid in close contact with the endochondral centre. These centres eventually spread into the

orbital part surrounding foramen ovale (De Beer, 1937), which transmits the mandibular division of the trigeminal nerve (V^{III}).

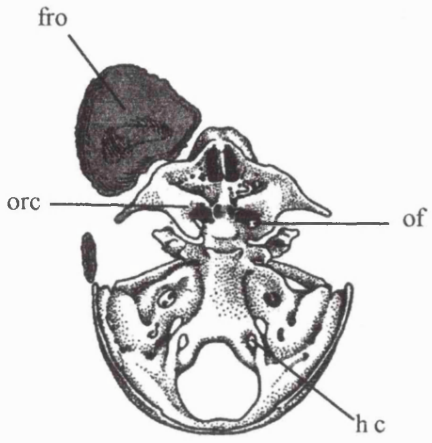

Figure 2.12. Dorsal view of the cranial base of a fetus (40mm crown-rump length) showing the frontal bone (fro), orbital cartilages (orc), optic foramen (of), and hypoglossal foramen (hc).

Ossification is visible in the hamulus of the medial pterygoid plate, the basioccipital (a single median endochondral centre which defines the anterior border of foramen magnum), and in the outer wall of the tympanic segment of the temporal. Ossification in the tympanic ring is said to commence from three (anterior, inferior, and posterior) (De Beer, 1937) or four (Viraponges *et al.*, 1985) intramembranous centres.

The condylar part of the occipital (exoccipital) shows signs of endochondral ossification around the hypoglossal incisure (De Beer, 1937), demarcating the hypoglossal or anterior condylar canal. This transmits the hypoglossal nerve (XII), the meningeal branch of the ascending pharyngeal artery, and an emissary vein.

2.6.3 *Face*

Intramembranous ossification from the maxilla has spread into the wall of the nasal capsule, orbital floor, and palate medially. Ossification is also visible in membrane around the body and ramus of the mandible and the posterior part of the

palatal bone. Centres for lacrimal (or lachrymal: De Beer, 1937) bones have appeared in membrane as a single pair lateral to the posterior part of the nasal capsular walls.

Tooth buds for permanent teeth with deciduous predecessors are visible deep within the dental laminae, lingual to the deciduous teeth and are surrounded by a dental sac consisting of condensed mesenchyme. The ectodermal part of the developing deciduous teeth has differentiated into the enamel organ (early bell stage). Tooth buds for those permanent teeth without deciduous predecessors become visible much later in fetal life and postnatally (i.e. molars).

2.6.4 *Other*

The falx cerebri is attached to the crista galli and cribriform plate anteriorly and the tentorium posteriorly. The tentorium stretches anteriorly from this junction to the dorsum sellae, between the cerebrum to the petrous ridges posterolaterally, and the occipital posteriorly.

Previous median consolidation of plexuses, which formed the primitive midline sagittal plexus, has given rise to primitive versions of the straight sinus, great cerebral vein, and the internal cerebral vein (Padgett, 1957).

2.7 Week 10-11

2.7.1 *Brain*

Except for continued enlargement of the cerebrum, particularly in the region of the temporal and occipital lobes, the brain has changed little from the previous period.

2.7.2 *Basicranium*

Ossification in the squamal part of the occipital, condylar part of the occipital, nasal region, and vomer is visible using plain radiographs (Kjaer, 1990c; Bach-Petersen and Kjaer, 1993). Centres are also present in the medial pterygoid plate (intramembranous) and the anterior part of *ala processus* (endochondral) (Shapiro and Robinson, 1980). The tympanic centres have fused to produce an annulus or ring that is missing the superior part. The zygomatic process of the squamosal temporal bone is almost fully articulate with the zygomatic process of the zygomatic bone (Noback, 1944).

Bone remodelling is evident on the surfaces of the frontal bone and the anterior cranial fossa (see Enlow, 1976 for details: Figure 2.13). The ectocranial and endocranial surfaces of the frontal region are largely depository and resorptive respectively. In contrast to the postnatal pattern, endocranial and ectocranial surfaces of the anterior fossa are depository and resorpitive, respectively. The orbital floor is also resorptive, reflecting growth of the eye.

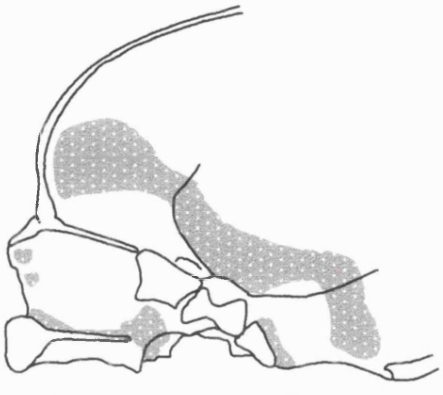

Figure 2.13. Midline lateral view of the fetal skull showing resorptive (stipple) and depository (the remaining area) endocranial surface fields (from Enlow, 1976).

2.7.3 *Face*

Turbinal cushions have fused and the lumens of the ethmoid sinuses are visible. The frontal process of the maxilla extends superiorly along side the developing nasal bones. Secondary cartilages have started to appear in the mandible to form the head of the condyle, part of the coronoid process, and the mental protuberance.

2.7.4 *Other*

Venous drainage and arterial supply of the head undergo positional changes during subsequent weeks, but has the same general structure as in the neonate (Figure 2.14).

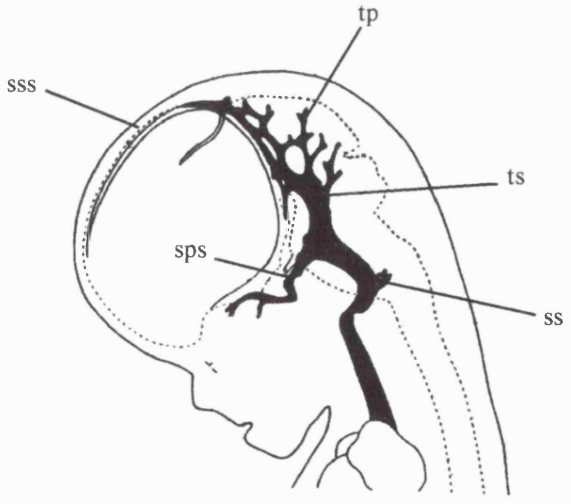

Figure 2.14. Lateral view of the fetal head (35mm crown-rump length) showing the tentorial plexus (tp), transverse sinus (ts), sigmoid sinus (ss), superior petrosal sinus (sps) and the superior sagittal sinus (sss) (adapted from Streeter, 1918).

2.8 Weeks 11-16

2.8.1 *Brain*

The characteristic shape of the cerebellum, formed by the cerebellar hemispheres and vermis, is recognisable and is divided into the neocerebellum (posterior lobe), paleocerebellum (anterior lobe and vermis) and archicerebellum (flocculonodular lobe) (Figure 2.15). Phylogentically these represent the new, the old, and the ancient parts of the cerebellum, respectively. Enlargement of the cerebellar hemispheres has covered the vermis and given rise to the paravermian sulci and many of the horizontal fissures.

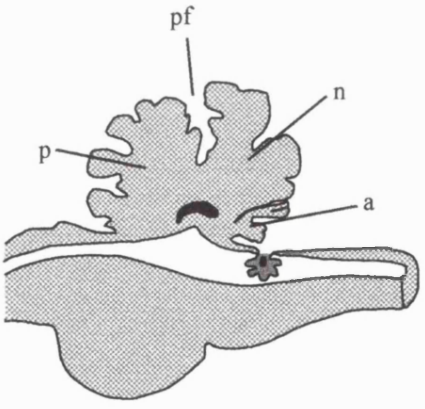

Figure 2.15. Midsagittal lateral view of the cerebellum showing the paleocerebellum (p), primary fissure (pf), neocerebellum (n), and archicerebellum (a) (from Moore, 1982).

2.8.2 *Basicranium*

The endochondral ossification centre originating from the orbitosphenoid has spread posteriorly into the anterior clinoid process and anteriorly around the optic foramen (Noback and Robertson, 1951; Kodama, 1976b). This foramen transmits the ophthalmic artery and optic (II) nerve.

The bony centres of the squamosal part of the occipital are fused and a pair of condylar endochondral centres are visible in the sclerotome cartilage along the lateral boundaries of the foramen magnum (Sperber, 1981). Lateral and medial pairs (four pieces) of endochondral ossification centres are also discernible on either side of the midline in the basisphenoid (De Beer, 1937; Noback, 1944; Noback and Robertson, 1951; Sasaki and Kodama, 1976; Shapiro and Robinson, 1980). The medial pair lie on either side of the midline in the region of the future sella turcica and the lateral pair are visible in the *alar processus* part of the basisphenoid (postsphenoid). The crista galli shows signs of ossification. Middle ear ossicles are adult sized and show signs of progressive ossification, starting with the incus, the malleus (both arising in the posterior region of Meckel's cartilage), and finally the stapes (De Beer, 1937; Noback, 1944; Nemzek *et al.*, 1996).

According to Bast (1930) and De Beer (1937), ossification is visible in the otic capsule by about 16 weeks or 110mm (CRL), after the labyrinth has reached adult size. Bast (1930) suggests the capsule arises from some fourteen separate centres, while De Beer divides the structure into opisthotic, prootic and epiotic parts each containing several centres. In general, these regions correspond to those centres reported by Bast (1930).

2.8.3 *Face*

The ethmoid cavities have enlarged into sinuses containing rings of cartilage (Monteiro and Dias, 1997). The maxilloturbinals have started to ossify endochondrally and the ossification centres of the vomer have fused, forming a groove in which the lower part of the developing nasal septum rests (Shapiro and Robinson, 1980). Secondary cartilages of the mandible have started to ossify starting

in the condyle region. Deciduous tooth development has advanced to the bell stage, characterised by degeneration of the dental lamina between tooth cap and the oral epithelium.

2.8.4 *Other*

With expansion of the cerebral hemispheres the primitive transverse sinus has moved posteriorly to its characteristic position on the endocranial surface of the occipital, superior to the cerebellum (Figure 2.16). A definitive confluence of sinuses is also visible during this period (Padgett, 1957).

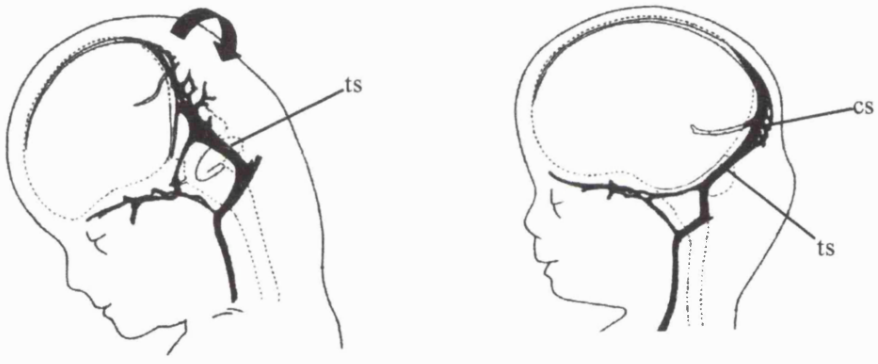

Figure 2.16. Expansion of the occipital lobes of the cerebrum (black arrow) pushes the transverse sinus (ts) and the tentorium cerebelli into a more posterior orientation, thereby forming a confluence of sinuses (cs) (adapted from Streeter, 1918).

2.9 Weeks 16-25

2.9.1 *Brain*

The lateral surfaces of the brain is still comparatively smooth, but marked by the insula, central sulcus, and lateral sulcus. Calcarine and parieto-occipital fissures mark the medial surfaces. An oblique fissure is usually discernible on the lateral surface of the occipital lobe some time later and is associated with the appearance of

a cingulate sulcus on the medial surface of each hemisphere (Dorovini-Zis and Dolman, 1977).

2.9.2 *Basicranium*

Ossification is visible around the apical and basal turns of the cochlea (Nemzek *et al.*, 1996; Sperber, 1981). Vestibulocochlear (VIII) and facial (VII) nerves and labyrinthine vessels traverse the internal acoustic meatus, which remains patent within the otic capsule. Most of the otic capsule shows signs of ossification, except for the subarcuate fossa (Nemzek *et al.*, 1996). A small diverticulum from the tympanic cavity, which is the precursor to the antrum and mastoid air cells, is visible in the epiotic part of the otic capsule.

In general, the presphenoid region contains several ossification centres at this age (nine pieces in total consisting of three pairs and three individuals: see Kodama, 1976a). There is, however, some confusion in the literature as to the terminology and the age at which particular centres become visible (compare for example De Beer, 1937; Noback, 1944; Kodama, 1976a; Sperber, 1981). According to Kodama, the first centres, a pair of main centres, are visible endochondrally in the presphenoid close to the posterior crus of the orbitosphenoid (Figure 2.17). These are followed by the remaining ossification centres of the presphenoid: Anterior and posterior accessory pairs of endochondral centres are seen in their respective positions relative to the main centres and two corporal middle centres are visible along the midline separated by an intermediate centre (middle accessory centre). Fusion between the median unpaired and median paired centres of the presphenoid has commenced (De Beer, 1937).

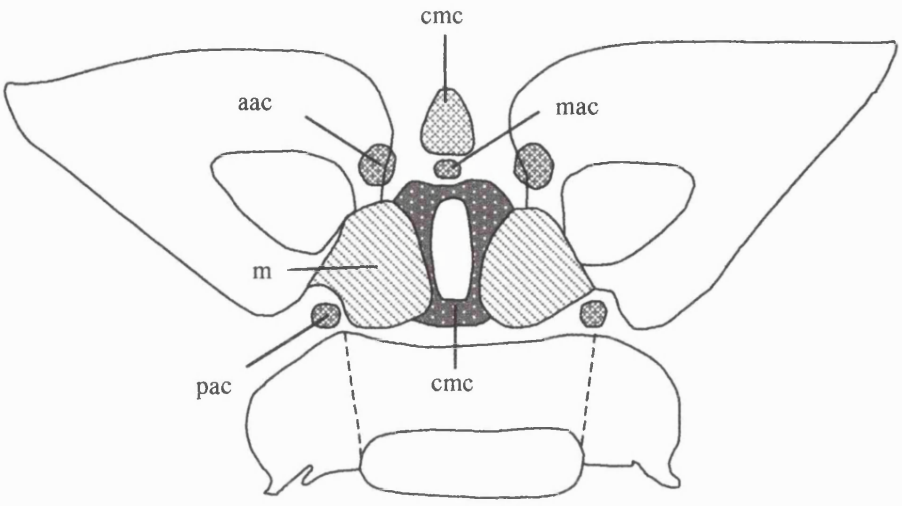

Figure 2.17. Coronal view of the ossification centres of the presphenoid: (m) main centre, (aac) anterior accessory centre, (pac) posterior accessory centre, (mac) middle accessory centre, (cmc) corporeal middle centre (from Kodama, 1976a).

Fusion between the orbitosphenoids and the lateral part of the presphenoid bone (De Beer, 1937; Kodama, 1976b) has formed the floors of the optic canals. Ossification in the basisphenoid has invaded the tuberculum sellae anteriorly and the dorsum sellae posteriorly. Both the pterygoid process and lateral pterygoid plate are fused. In addition, the alisphenoid has started to fuse with the pterygoid plate and basisphenoid. Osseous fusion between the four centres of the basisphenoid is detectable (Shapiro and Robinson, 1980) and occludes the track left by Rathke's pouch (Sperber, 1981). On plain radiographs, bony tissue is seen in the corpus of the sphenoid, petrosal part of the temporal, and around the carotid canal and jugular fossa (Kjaer, 1990a; Kjaer, 1990b; Bach-Petersen and Kjaer, 1993).

2.9.3 *Face*

Endochondral ossification centres are visible in the inferior and superior ethmoturbinals (Noback, 1944). Ossification centres for the inferior nasal conchae are present in the lateral part of the ossifying nasal capsule (Sperber, 1981). Centres

for the lateral parts of the ethmoid, which form the orbital lamina, are also visible. Much of Meckel's cartilage has disappeared through resorption, leaving centres of endocranial ossification in the secondary cartilages of the mandible and intramembranous ossification around the body and ramus.

2.9.4 *Other*

The folds of the tentorium cerebelli are united posteriorly with the falx cerebri and straight sinus, to form a tense, diaphragmatic membrane supporting the occipital lobes of the cerebral hemispheres. This meningeal layer serves to separate the contents of the posterior cranial fossa (infratentorial elements) from the prosencephalic parts of the brain (supratentorial elements), though the two segments remain connected via a hiatus superior to the dorsum sellae (Figure 2.18).

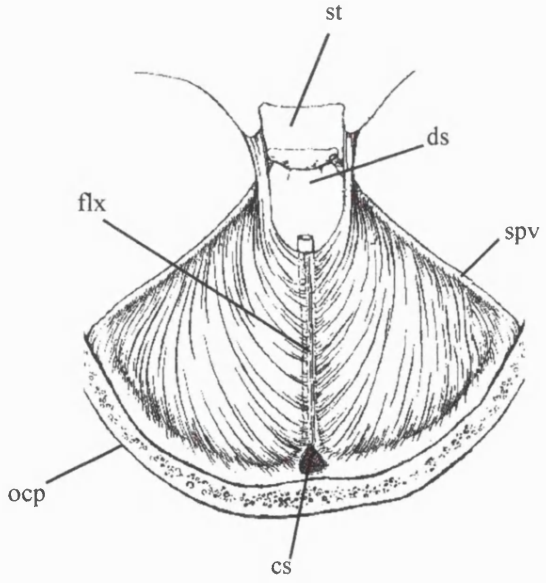

Figure 2.18. Dorsal view of the tentorium cerebelli at term: sella turcica (st); dorsum sellae (ds); superior petrosal vein (spv); confluence of sinuses (cs); occipital bone (ocp); and the junction between the falx cerebri and tentorium (flx).

2.10 Weeks 25-40 (term).

2.10.1 *Brain*

Existing cerebral fissures have deepened and frontal, intraparietal, and superior temporal sucli are evident (Figure 2.19). Many more gyri and sulci appear from 28-30 weeks as the brain undergoes a growth spurt. Barron (1950) suggests that sucli and gyri develop as a result of differential growth between the inner and outer cortical layers of the brain.

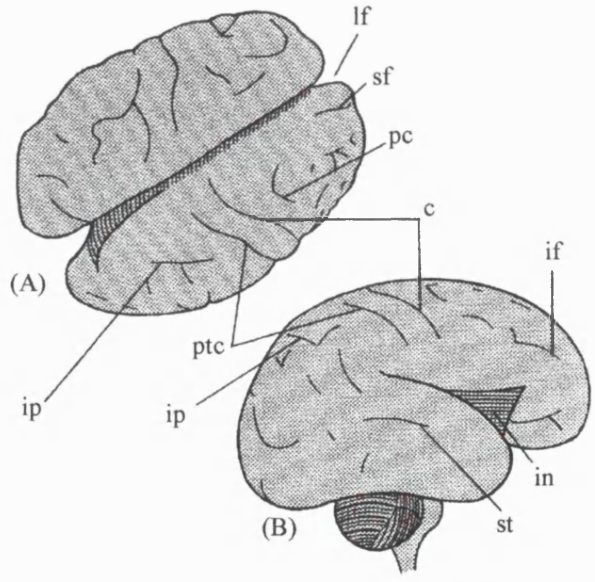

Figure 2.19. Dorsal (A) and lateral (B) views of the brain at 26 weeks. Many grooves are present including: longitudinal fissure (lf); superior frontal fissure (sf); precentral fissure (pc); central fissure (c); inferior frontal fissure (if); insula (in); superior temporal fissure (st); intraparietal fissure (ip); and postcentral fissure (ptc) (adapted from O'Rahilly and Müller, 1994).

2.10.2 *Basicranium*

The subarcuate fossa is less prominent than in previous stages due to progressive ossification of the otic capsule. Ossification centres in the basisphenoid are completely fused and the united bony structure of the basisphenoid, the presphenoid, and the orbitosphenoids show signs of fusion with one another

(Shapiro and Robinson, 1980; Sasaki and Kodama, 1976). Consequently, the mid-sphenoidal synchondrosis is no longer seen separating the presphenoid from the basisphenoid (Ford, 1958). Ossification of the pterygoid canal, through which a nerve and an artery of the same name pass, is almost complete.

The tympanic ring is adult sized and has started to fuse with the squamosal part of the temporal bone. Parts of the hyoid (laterohyal, stylohyal, basihyal, and thyrohyal) show signs of endochondral ossification and the maxillary, ethmoidal, and sphenoidal sinuses are clearly visible.

2.10.3 *Face*

Ossification in the ethmoid extends into the cribriform plate and the ossified ethmoturbinates. Dentin and enamel formations are discernible in the developing deciduous teeth.

2.10.4 *Other*

Little has changed since the last period described.

2.11 Summary

This section has described development of the brain in conjunction with that of the cranial base, face, and other associated structures, such as the vascular system and meninges. Despite inconsistencies in the timing of events (see Table 2.1) the consensus appears to be that many aspects of neural and meningeal development are both spatially and temporally related to changes in the face and cranial base. For example, development of the cerebrum effects venous drainage of the head and the position of the tentorium cerebelli. In addition, development of the

hypophyseal cartilages, which eventually form the floor of sella turcica, is temporally related to the formation of the pituitary gland.

It is interesting to note that discrepancies between the reported timings of certain events appear to increase with age. It seems likely that this is partly due to the stochastic accumulation of individual variation (most studies cited in this review are cross-sectional). However, it is not clear whether or not this variation increases in relative terms from that observed during the early stages of development (e.g. 10% variation at 10 days is 1day whereas at 10 weeks it is 1 week or 7 times the absolute variation observed at 10 days). It seems possible that some of this increased variation is the result of there being fewer studies covering older material, particularly the third trimester. Thus, more first-hand observations, preferably from longitudinal studies, are required to bring our knowledge of fetal development in line with that of the embryonic period. Notwithstanding this limitation, the present review provides a workable framework for assessing evolutionary hypotheses on the basis of prenatal human ontogeny.

Table 2.1. Developmental events and discernible structures during prenatal development.

Discernible structure or event	Size *	Reference	Age	Reference
Neural groove	1-1.5	George, 1942	3 wk	Gasser, 1976
	1-3 smts	O'Rahilly, 1966	18 dy	Moore and Persaud, 1998
	0.4-1.5 GL	O'Rahilly *et al.*, 1984	18 dy PO	O'Rahilly *et al.*, 1984
	0.4 GL	O'Rahilly and Müller, 1986		
	1-1.5	O'Rahilly and Müller, 1994		
	1-1.5	Larsen, 1997		
Neuralation commences	10 smts	O'Rahilly, 1966	4 wk	Gasser, 1976
	2-3.5 GL	O'Rahilly and Gardner, 1971	22-23 dys	Moore, 1982
	2.1 GL	O'Rahilly *et al.*, 1984	18 dy	Johnson, 1988
	2-3.4 GL	O'Rahilly and Müller, 1986	22 dy	Kjaer, 1998
	2-3.5	O'Rahilly and Müller, 1994	end 3 wk	Moore and Persaud, 1998
	2-3.5	Larsen, 1997	22 dy PO	O'Rahilly *et al.*, 1984
Optic sulci	2-3.5 GL	O'Rahilly and Gardner, 1971	22 dy PO	O'Rahilly, 1975
	2.1 GL	O'Rahilly *et al.*, 1984	22 dy	Moore,1982
			22 dy PO	Sadler, 1995
Otic placodes	1.5-2.5 GL	O'Rahilly and Gardner, 1971	21-24 dy	Sperber, 1981
	0.4-1.5 GL	O'Rahilly *et al.*, 1984	early 4 wk	Moore, 1982
			22 dy PO	Sadler,1995
			3 wk GA	Nemzek *et al.*, 1996
Cephalic flexure	1.5-2.5 GL	O'Rahilly and Gardner, 1971	4 wk	Gasser, 1976
			3 wk	Moore, 1982
Blood plexuses	4	Streeter, 1918	4 wk	Gasser,1976
	2.5-4.5 GL	O'Rahilly and Müller, 1986		
Parachordal condensations	11-14 GL	O'Rahilly and Müller, 1986	4 wk	Burdi, 1976
			5 wk	Gasser, 1976
			4 wk	Sperber, 1981
Otic vesicle	3-5 GL	O'Rahilly, 1963	5 wk	Burdi, 1976
	17-19 smts	O'Rahilly, 1966	4 wk GA	Nemzek *et al.*, 1996
	2.5-4.5 GL	O'Rahilly and Gardner, 1971		
	4-6	Larsen, 1997		
Optic vesicle	3-5 GL	Bartelmez and Dekaban, 1962	24 dy PO	O'Rahilly, 1975
	3.4 GL	O'Rahilly *et al.*, 1984	5 wk	Gasser, 1976
	2.5-4.5	Larsen, 1997	28 dy	Moore, 1982
Pharyngeal arches	5-8	Padgett, 1957	4 wk IU	Sperber, 1981
	2-3.5	Larsen, 1997	24 dy	Moore, 1982
			4-5 wk	Sadler, 1995
Somites	-	-	21 dy	Sperber, 1981
			20 dy	Moore, 1982
			end 3 wk	Moore and Persaud, 1998
Cerebral vesicles	5.5-7.3 GL	Bartelmez and Dekaban, 1962	6 wk	Gasser, 1976
	6.6 GL	O'Rahilly *et al.*, 1984	35 dy	Kjaer, 1998
	5-7	Larsen, 1997		
Pontine flexure	6-12	Padgett, 1957	6 wk	Keith, 1948
	5.5-7.3 GL	Bartelmez and Dekaban, 1962	6 wk	Gasser,1976
	5-7 GL	O'Rahilly and Gardner, 1971		
	7	O'Rahilly and Müller, 1994		
Corpus striatum	7-11 GL	Bartelmez and Dekaban, 1962	-	-
	2.5-4.5 GL	O'Rahilly and Gardner, 1971		
Cervical flexure	4-6 GL	O'Rahilly and Gardner, 1971	4 wk	Keith, 1948
			5 wk	Gasser,1976
			6 wk	Moore, 1982

Table 2.1. Developmental events (contd.)

Rathke's pouch present	-	-	5 wk 24 dy	Gasser, 1976 Moore, 1982
Cerebellum	7 11-14	O'Rahilly and Müller, 1994 Larsen, 1997	-	-
Lateral choroid plexus	10.8-14.2 GL 13-17 GL	Bartelmez and Dekaban, 1962 O'Rahilly and Gardner, 1971	-	-
Otic capsule	10-16	Padgett, 1957	6 wk	Gasser, 1976
Nasal capsule	-	-	6 wk	Gasser, 1976
Basal plate	14 CRL	De Beer, 1937	7 wk	Gasser, 1976
Venous sinuses	24	Streeter, 1918	-	-
Ossification of squamous temporal	-	-	8 wk GA 8 wk 7 wk GA	Shapiro and Robinson, 1980 Sperber, 1981 Viraponges *et al.*, 1985
Ossification of maxilla	15 CRL 28 CRL	De Beer, 1937 Noback and Robertson, 1951	early 8 wk	Sperber, 1981
Reorientation of palatal shelves	29 CRL	Diewert, 1985	6 wk 47-54 dy IU	Keith, 1948 Sperber, 1981
Mesethmoid	13-17 GL	O'Rahilly and Müller, 1986	8 wk	Gasser, 1976
Ossification of frontal bone	25 CRL 25 35 CRL	De Beer, 1937 Keith, 1948 Noback and Robertson, 1951	8 wk GA 8 wk 23 H	Shapiro and Robinson, 1980 Sperber, 1981 O'Rahilly, 1966
Ossification of vomer	30 CRL 35 CRL	De Beer, 1937 Noback and Robertson, 1951	8 wk GA 8 wk	Shapiro and Robinson, 1980 Sperber, 1981
Supraoccipital endochondral ossification	-	-	9-10 wk GA 10 wk IU	Shapiro and Robinson, 1980 Sperber, 1981
Semicircular canals	-	-	8 wk GA 6 wk	Nemzek *et al.*, 1996 Sadler, 1995
Supraoccipital membranous ossification	-	-	9-10 wk GA 8 wk IU 9 wk	Shapiro and Robinson, 1980 Sperber, 1981 Srivastava, 1992
Ossification of Mandible	24 CRL	Noback and Robertson, 1951	7 wk	Keith, 1948
Ossification of alisphenoid	37 CRL 52 CRL	De Beer, 1937 Noback and Robertson, 1951	12 wk GA	Shapiro and Robinson, 1980
Ossification of hamulus	30 CRL 35 CRL	De Beer, 1937 Noback and Robertson, 1951	9 wk GA	Shapiro and Robinson, 1980
Ossification of tympanic	32 CRL 40 CRL	De Beer, 1937 Noback and Robertson, 1951	9 wk GA 3 mnth IU 10 wk GA	Shapiro and Robinson, 1980 Sperber, 1981 Viraponges *et al.*, 1985
Ossification of exoccipital	37 CRL 45 CRL	De Beer, 1937 Noback and Robertson, 1951	early 3 mnth	Keith, 1948
Ossification of basiocciput	51 CRL 60 CRL	De Beer, 1937 Noback and Robertson, 1951	early 3 mnth 11 wk IU	Keith, 1948 Sperber, 1981
Ossification of basisphenoid, medial centres	65 CRL 83 CRL 125 BL 120 BL	De Beer, 1937 Noback and Robertson, 1951 Kodama, 1976c Sasaki and Kodama, 1976	4 mnth IU	Sperber, 1981

Table 2.1. Developmental events (contd.)

Ossification of basisphenoid, lateral centres	90 CRL 145 BL 130 BL	De Beer, 1937 Kodama, 1976c Sasaki and Kodama, 1976	-	-
Ossification of Orbitosphenoid	60 CRL 71 CRL 125 BL	De Beer, 1937 Noback and Robertson, 1951 Kodama, 1976b	11 wk GA 13 wk GA	Shapiro and Robinson, 1980 Viraponges *et al.*, 1985
Ossification of otic capsule	110-161 CRL	De Beer, 1937	16-17 wk GA 5 mnth IU 18 wk GA	Shapiro and Robinson, 1980 Sperber, 1981 Nemzek *et al.*, 1996
Membranous and endochondral portions of supraoccipital fuse	-	-	14 wk GA 12 wk IU	Shapiro and Robinson, 1980 Sperber, 1981
Ossification of middle ear ossicles	110-139 CRL	De Beer, 1937	16 wk GA 4 mnth IU 15 wk GA	Viraponges *et al.*, 1985 Sperber, 1981 Nemzek *et al.*, 1996
Ossification of presphenoid, lateral centres	90 CRL 133 CRL	De Beer, 1937 Noback and Robertson, 1951	4 mnth IU	Sperber, 1981
Ossification of presphenoid, medial centres	168 CRL 235 CRL 180 BL	De Beer, 1937 Noback and Robertson, 1951 Kodama, 1976a	12 wk GA	Shapiro and Robinson, 1980
Basisphenoid centres fuse	110 CRL 180 BL 235 BL	De Beer, 1937 Kodama, 1976c Sasaki and Kodama, 1976	20 wk GA end 4 mnth IU	Shapiro and Robinson, 1980 Sperber, 1981
Orbitosphenoid and presphenoid centres fuse.	135 CRL	De Beer, 1937	6 mnth 8 mnth	Kodama, 1976a Kodama, 1976b
Otic centres fuse	200 CRL	De Beer, 1937	6 mnth IU	Sperber, 1981
Basisphenoid and presphenoid centres fuse	165 CRL 315 BL 280 BL	De Beer, 1937 Kodama, 1976c Sasaki and Kodama, 1976	7 mnth 28 wk GA 8 mnth IU	Kodama, 1976a Shapiro and Robinson, 1980 Sperber, 1981

BL, body length ; CRL, crown-rump length; GA, gestational age; GL, greatest length; H-horizon; IU, in utero; PO, postovulatory; wk, week(s); mnth, month(s); dy, day(s); smts, somites; *, size is in mm unless otherwise stated.

CHAPTER 3. GENETIC AND EPIGENETIC REGULATION OF CRANIAL BASE ARCHITECTURE

It has long been suggested, albeit implicitly, that genes and epigenetic factors influence cranial base morphology directly and indirectly during human ontogeny. That is, basicranial architecture is determined not only directly by gene expression within the basicranium, but also by factors such as brain growth and therefore indirectly by genes controlling neurological development. However, the argument as to whether genetics or epigenetics has and has had the greatest direct impact on cranial base morphology during human development and evolution, respectively, remains equivocal (see review in Herring, 1993).

On the one hand, some workers propose that many features of the cranial base are chiefly genetic constructs, being the product of evolutionary gene selection (e.g. Nur and Hasson, 1984; Bailey, 1986; Thomason and Russel, 1986). In contrast, evidence from biomechanical studies suggests that epigenetic factors have a considerable, if not greater influence on cranial base architecture (e.g. Virchow, 1857; Pratt, 1948; Avis 1959; Biegert, 1964; Enlow, 1975; Enlow and McNamara, 1973; Smith, 1981). Developmental studies, on the other hand, indicate that the dominance of either factor is dependent on developmental stage (e.g. Manson, 1968) or the type of tissue present (e.g. Scott, 1954; Dorenbos, 1972).

This chapter covers some earlier and more recently proposed hypotheses encompassing biomechanical epigenetic factors, as defined by Hall (1983, 1984), and genetic factors affecting skull growth. Additional influences included within Hall's definition of epigenetic, i.e. any non-genetic factor affecting skull growth, and other definitions of the term 'epigenetic' are discussed elsewhere (e.g. Watt and

Williams, 1951; Moore, 1965; Steegman and Platner, 1968; Heath, 1984). A number of biomechanical hypotheses presented in this section (highlighted with bold Arabic numerals) are used to the validate the predominantly epigenetic thesis of fetal skull development. Testable predictions from these hypotheses are summarised at the end of the section.

3.1 Inheritance of form

3.1.1 *Preformation, transcendentalism, and heterochrony*

Although the Mendelian theory of inheritance (Mendel, 1866) was not readily accepted until after the eighteen hundreds, a number of ideas were conceived during the preceding centuries that implied, albeit unintentionally, that form is in some way inherited, i.e. determined by genes (see Gould, 1977 for a review).

One group, the Preformationists, believed that ontogeny only involved an increase in size from a miniature human, the homunculus (Figure 3.1), inside the egg or sperm (Bonnet, 1769). Accordingly, they suggested that humans inherited the form of Eve via an infinite number of homunculi. This illustrates that as early as the eighteenth century many biologists believed that morphology was determined by structural 'information' (the homunculi) contained within the gametes and was passed from one generation to the next via this medium.

The theory of transcendentalism also contains an underlying concept of inheritance. Derived from the ideas of Aristotle and qualified by Meckel (1811), transcendentalism suggests that embryological development recapitulates or parallels the adult structures of animals below it on a perceived scale of beings, ranging from the primitive to the advanced (Figure 3.2). While Von Baer (1828) disputed this

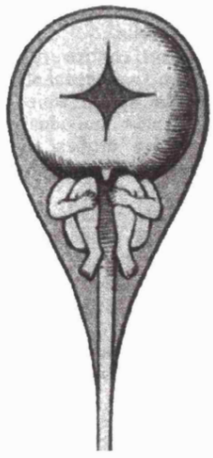

Figure 3.1. Sketch of a Homunculus in the sperm (from Moore, 1982).

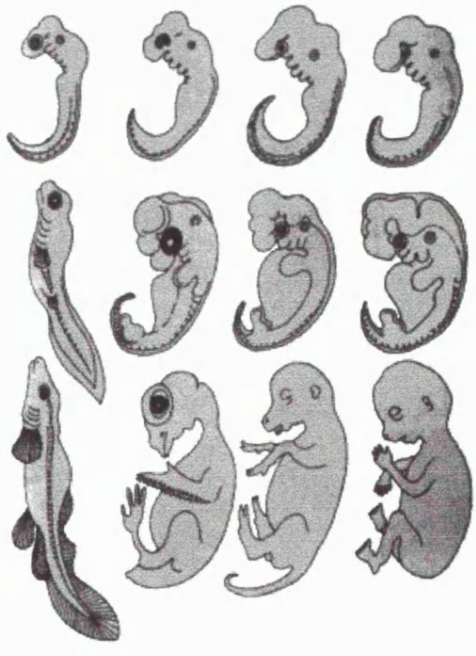

Figure 3.2. Sketches of, from left to right, fish, chick, calf, and human embryos showing the similarity between early and late stages (adapted from Haeckel, 1879)

theory, post-Darwinists such as Haeckel (1879) and De Beer (1940) later used a modified version to explain evolution in terms of changes in the onset of development in descendent ontogeny relative to an ancestor's ontogeny, referred to as heterochrony (see Gould, 1977 for a review of the many facets and consequences of heterochrony)

Recapitulation implies that some sort of shared process or component exists between descendent and ancestral ontogeny. Moreover, since the epigenetic factors involved in, for example, fish development are unlikely to be exactly the same as those for humans, it therefore follows that the element common to both ontogenies and responsible for the perceived similarities is predominantly genetic. As such recapitulation represents the sequential expression of archaic genes now common to a number of species, both extant and extinct. Heterochrony, on the other hand, is the time difference in the expression of such genes during the ontogeny of one species as compared with another on different taxonomic levels. This results in either paedomorphosis (time hypomorphosis, rate hypomorphosis, and neoteny) or peramorphosis (rate hypermorphosis, time hypermorphosis, acceleration). Thus, rate hyper- or hypomorphosis is the heterochronic product of changes in expression time and the extent of gene activity. In other words, recapitulation and heterochrony can be seen as manifestations of genetic regulation on different species-specific time scales.

3.1.2 *Modern genetics*

For the majority of pre-twentieth century theories of inheritance, the mode and means of passing structural information from one generation to the next remained unclear. That is, until the rediscovery of Mendel's ideas in the early 1900's

(Corren, 1900; Vries, 1900; Tschermak, 1900; Bateson, 1909). With this new era of genetics came a greater understanding of the contribution made by genes to the process of skull formation. Indeed, a specific group of genes within the genome, the regulatory genes, were investigated and identified as major determinants of ontogeny and, thus, possibly morphological evolution by heterochrony (King and Wilson, 1975).

Evidence from studies on morphology and dysmorphology of, for example, the mandible (Johnson, 1986; Grüneberg, 1975), cranial vault (Grüneberg, 1963), otic capsule (Green, 1951), and maxilla (Gluecksohn-Waelsh *et al.*, 1956) in gene mutants appears to support the notion of a predominantly genetic view of skull formation. Moreover, disruptions in homeobox (HOX) gene expressions often lead to characteristic abnormalities of the face and hindbrain regions (Hill *et al.*, 1991; Winter, 1996). These genes are regulatory and contain ancient and conserved regions that specify positional information (Figure 3.3) and segment identity along the long axis of the body (Akam, 1989).

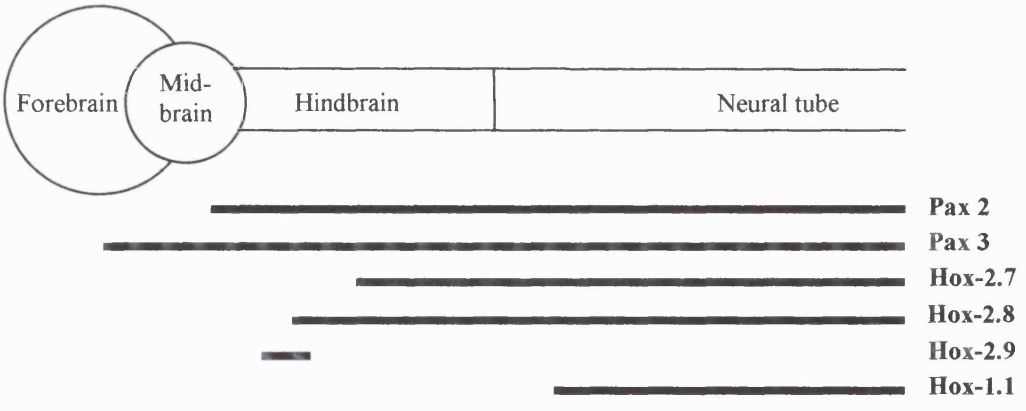

Figure 3.3. Anterior expression of certain homeobox genes (adapted from Kessel and Guss, 1990).

This molecular evidence seems to indicate that most skeletal patterning is 'pre-programmed' in the neural crest cells and their epithelial precursors (Noden, 1986; Robert *et al.*, 1989) as genes like *Hox* 2.9, *Hox* 1.1, or *Xhox* 3 (e.g. Balling *et al.*, 1989; Ruiz i Altaba and Melton, 1989; Hunt *et al.*, 1991; Froham *et al.*, 1990). However, what most geneticists define as a skeletal pattern, i.e. regions of mesenchyme growth, is somewhat different to the subtler and mostly post-embryonic morphological features with some direct significance to human evolutionary studies (e.g. facial orientation relative to the basicranium). Though such features may well be associated with heterochrony (e.g. base flexion: see review in Gould, 1977) as in the activation of archaic genes, the direct role of genes in the formation of such details remains unclear.

3.1.3 *Genetic and epigenetic morphogenesis*

Workers advocating a more unified view of skull formation propose that both genetics and epigenetic factors make similar, if not equal overall contributions to skull formation during ontogeny. In other words, the dominance of one precedes or succeeds the dominance of the other in determining cranial base architecture, but neither governs the whole of ontogeny.

There are two main propositions within this group. The first suggests that genes govern prenatal skull growth whilst epigenetics govern the functioning postnatal skull (Baker, 1941). The second theory, originally proposed by Scott (1954), marks the boundary between genetic and epigenetic control according to tissue type rather than age. This hypothesis predicts that cartilage is subject to genetic regulation while bone is epigenetically determined. In general, both propositions imply a gradual change in the dominant influence on cranial base

morphology from one of genetic to mostly epigenetic.

Scott's (1954) proposition, appears to be supported by experimental evidence showing that certain cartilages develop almost normally in vitro and that mechanical forces (epigenetic) influence bone growth (e.g. Washburn, 1947; Avis, 1959; Hall, 1970; Rönning and Kylämarkula, 1982; Hohl, 1983; Copray, 1986). However, the principal distinction made between cartilage and bone is not corroborated by Ede's (1983) study of development which indicates that mechanical forces also effect primary cartilages. Similarly, the validity of the first proposition, which distinguishes between developmental stages, is also undermined by experimental evidence showing that mechanical forces, e.g. differential tissue growth (Tuckett and Morris-Kay, 1985), influence prenatal as well as postnatal development.

More recently, Thorogood (1987, 1988) has attempted to revive a more holistic view of skull development with his 'fly-paper' model. This model integrates epigenetic and genetic factors, suggesting that genes regulate the direction and substance of cells in cranial morphogenesis whilst biomechanical forces determine their point of aggregation and ultimately therefore form. In other words, the developing brain and face act as a three-dimensional structural template around which the architectural foundations of the skull form.

3.2 Biomechanical epigenetic influences

3.2.1 *Basicranial architecture: 'spatial-packing' hypothesis*

Perhaps the most reported morphometric feature of the basicranium, noted as early as 1867 by Huxley, is the angle between the posterior (basioccipital) and anterior cranial base (midline floor of the anterior cranial fossa) seen in hemisected skulls (Figure 3.4). Many different measures of this angle, known as the cranial base

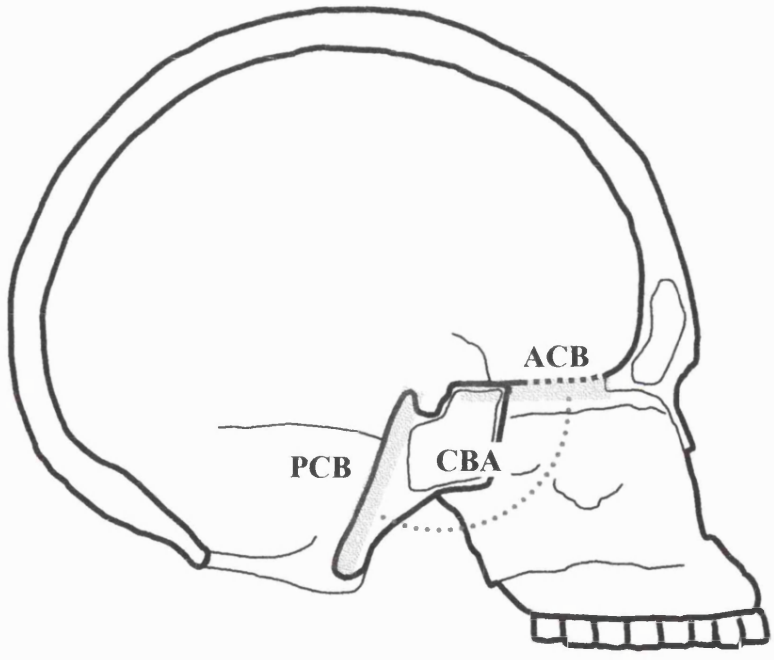

Figure 3.4. Midline lateral sketch of a human skull showing cranial base angle (CBA) between the anterior cranial base (ACB) and posterior cranial base (PCB).

angle (CBA), have been proposed (see review in Lieberman and McCarthy, 1999). Nonetheless, studies consistently show a considerable variation of CBA across anthropoids, ranging by 30 degrees from a relatively flat basicranium in prosimians to a more ventrally flexed posterior cranial base in great apes (e.g. Keith, 1910; Duckworth, 1915; Zuckerman, 1926; Cameron, 1930; Ashton, 1957). More importantly, modern human basicrania appear to exhibit the greatest degree of flexion, and therefore the smallest CBA when compared with extant African apes

and amongst mammals in general (Scott, 1958; Ross and Henneberg, 1995; Spoor, 1997). Phylogenetically, this implies that some evolutionary mechanism has influenced the modern human cranial base, resulting in a decrease in CBA from an ancestral condition similar to that in extant African apes. As ever, the fossil evidence remains equivocal on this point. In general, hominid studies indicate that modern human CBA is reduced in comparison with *Australopithecines* but greater than that of archaic species of *Homo* (Ross and Henneberg, 1993; Spoor, 1997). This suggests that the evolutionary process of base flexion is polyphasic in nature with both periods of flexion and more recently retroflexion, through this is not shown by primate trends.

Two of the hypotheses often used to expound the reduced CBA in modern humans compared with non-human primates are those posited by Biegert (1964) and Gould (1977). Other hypotheses, such those relating to posture and locomotion (see review in Ross and Ravosa, 1993; Strait and Ross, 1999), are difficult to test due to the complex nature in which primates interact with their environment. Biegert's and Gould's hypotheses, on the other hand, are more readily tested since the characteristic human CBA is explained in terms of measurable quantities e.g. endocranial space and brain size.

Biegert's (1964) hypothesis proposes that CBA increases with increasing size of the masticatory apparatus and decreases with enlargement of definitive areas of the brain such as the neopallium (cerebral hemispheres). In contrast, Gould's hypothesis, as interpreted by Ross and Ravosa (1993), indicates that the reduced CBA in moderns humans is a solution to the 'spatial-packing' problem caused by a phylogenetic increase of brain size relative to cranial base length. In order to accommodate a larger brain relative to the midline cranial base length, the anterior

part of the human basicranium has deflected ventrally while the posterior part moved anteriorly (Figure 3.5), displacing the foramen magnum into a more inferior position. This is similar in many respects to Enlow's (1976) early notion that prenatal and postnatal human base flexion is a consequence of brain growth relative to the slower

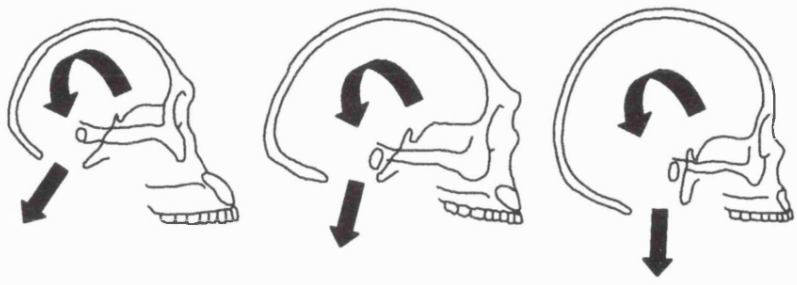

Figure 3.5. Increases in base flexion due to enlargement of the brain relative to base length in *Australopithecus*, *Homo erectus*, and *Homo sapiens* (after Biegert, 1963).

growing midline basicranium. The classic analogy is one of an inflating balloon that is tethered along it's base. As the balloon inflates it curls around the area where expansion is limited, thereby producing a flexure.

Gould's hypothesis is supported by two interspecific studies. Firstly, Ross and Ravosa (1993) investigated correlation between CBA and relative brain size among primates. The authors measured CBA in lateral radiographs between midline planes of the basioccipital, clivus, and sphenoid body (Figure 3.6a) as well as neurocranial volumes from 68 extant primates. Relative brain size (Index of Relative Encephalization #1: IRE1) was defined as the cube root of neurocranial volume over base length.

Ross and Ravosa (1993) thus found significant negative correlations amongst all primates investigated (Pearson's correlation coefficient $r = -0.645$, $P<0.001$) as well as on many subordinal levels. Biegert's (1964) hypothesis, which predicts a correlation between increases of neocortical volume relative to masticatory apparatus (Ross and Ravosa use palate length) and decreases of CBA, was also investigated but

only found a significant correlation amongst platyrrhines ($r = -0.624$, $P<0.05$).

A second study, Spoor's (1997) report on Sts 5 (*Australopithecus africanus*), also includes an interspecific analysis of CBA and relative brain size amongst extant non-human primates. Rather than use the cranial base measurements defined by Ross and Ravosa (1995), which excludes the contribution of the cribriform plate to the length of the anterior cranial base (see section 5.2), Spoor measured CBA on CT scans of 42 extant non-human primates and 48 modern humans as the angle between basion, sella, and foramen caecum (see Figure 3.6b). Furthermore, he uses these same landmarks to measure base length (see Figure 3.6a). Consequently, his calculated values of relative brain size are smaller than those reported by Ross and Ravosa (1993) since the denominator base length includes cribriform plate length. This approach is considered more appropriate than Ross and Ravosa's measure since it takes into account that in anthropoids the frontal lobes of the cerebrum extend beyond the anterior border of planum sphenoideum. Moreover, during human development it has been shown that the planum sphenoideum and ethmoid (including the cribriform plate) contribute almost equally to increases in the length of the anterior cranial base (Kvinnsland, 1971). It has also been shown that a large proportion of forward growth along the anterior cranial base during the second half of prenatal gestation is determined by the distance from the spheno-ethmoidal synchondrosis to nasion (Anagnostopoulou *et al.*, 1988). Nevertheless, Spoor's results are, in general, consistent with those reported by Ross and Ravosa's (1993) in that they show a significant negative correlation ($r = -0.786$, $P<0.001$) between relative brain size and CBA amongst non-human primates.

Thus, results from these studies appear to support the proposition that decreases in cranial base angle are associated with increases of brain size relative to

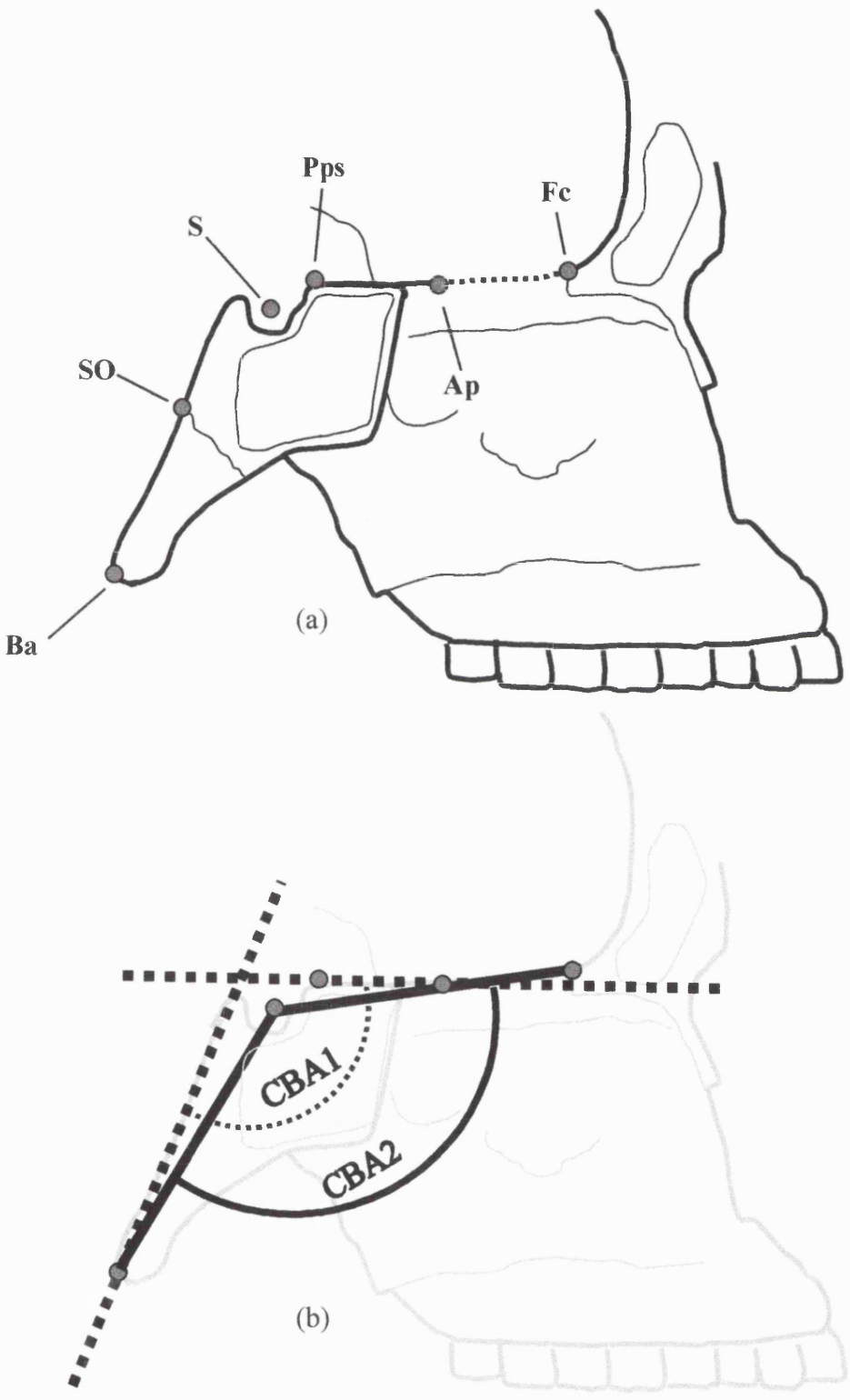

Figure 3.6. Midsagittal view of the skull showing the (a) landmarks used by Ross and Ravosa (1993) [Basion, Ba; SO, posterior edge of spheno-occipital synchondrosis; Pps, posterior edge of planum sphenoideum; Ap, anterior border of planum sphenoideum] and Spoor (1997) [Basion, Ba; Sella, S; Foramen caecum, Fc] and (b) cranial base angle (CBA1) used by Ross and Ravosa (1993) and the cranial base angle (CBA2) used by Spoor (1997).

base length. However, there is insufficient evidence to determine whether this association constitutes a causal relationship and also the analyses fail to take into account the influence of the phylogenetic relationships amongst species within the sample (see Harvey and Pagel, 1991 for details of this effect). Results from within specific primate taxa and amongst modern humans fail to support the Gould hypothesis. In the first instance, Ross and Ravosa (1993) found little evidence to substantiate the hypothesis within the primate order at the subordinal level of Strepsirrhini (-0.360,ns), Cercopithecoidea (r = -0.335,ns), and Cercopithecinae (r = 0.203, ns). The authors also note an insignificant correlation at the level of Hominoidea (r = -0.790, ns), but this is at least in part caused by the small number of species studied (six species studied). Ross and Henneberg (1995) have shown that there is no significant correlation between CBA and relative brain size amongst modern humans.

Employing the same measurements used by Ross and Ravosa (1993), Ross and Henneberg (1995) have shown that while modern human basicrania (mean CBA of 111.8 degs.) are more flexed than in most other primates, CBA remains greater than that predicted from the non-human primate trend. This difference between predicted and measured modern human CBA is consistent with, but considerably greater than that reported by Spoor (1997). Using the RMA equations for CBA vs. IRE1 amongst non-human primates reported by Ross and Henneberg (1995) and Spoor (1997), the expected outcome for modern humans is 59 and 133 degrees, respectively. The mean values for measured human CBA, however, were 112 and 137 degrees, respectively (Figure 3.7). Spoor's (1997) calculated result for modern humans is closer to the measured value for two possible reasons. Firstly, Spoor included two species of prosimian in his primate trend for CBA whereas Ross and

Henneberg only used the anthropoid sample reported by Ross and Ravosa (1993). Secondly, Spoor includes the length of the cribriform plate as part of the base length measurement when calculating relative brain size. This gives an IRE1 value of 1.17 for modern humans as opposed to the 1.65 reported by Ross and Henneberg.

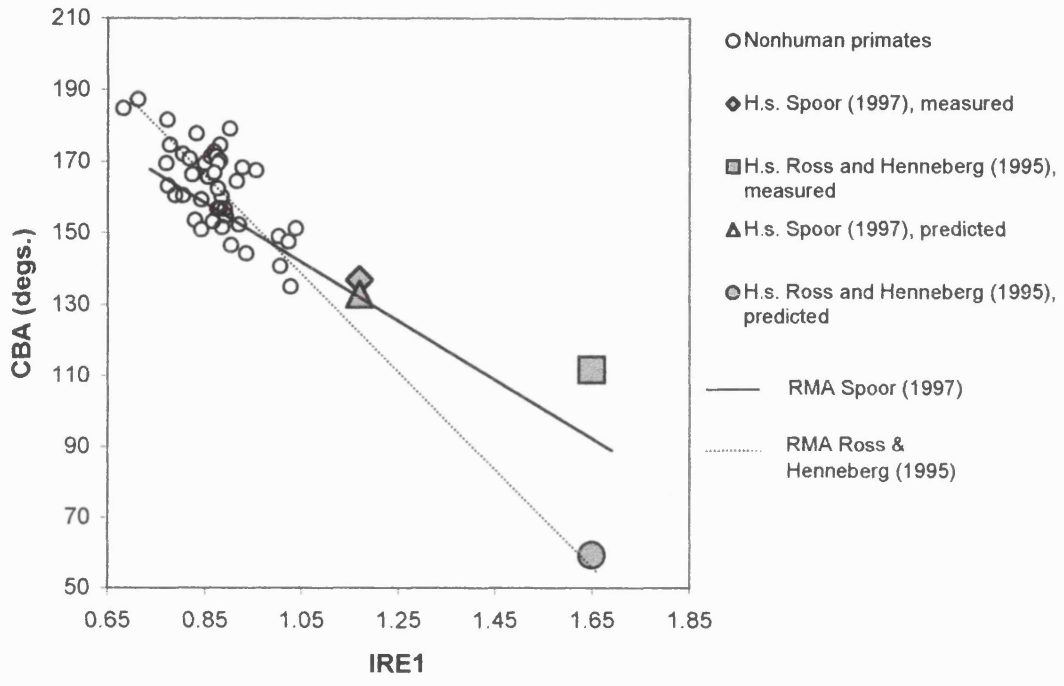

Figure 3.7. Graph of cranial base angle (CBA) vs. relative brain size (IRE1) showing the non-human primate data reported by Ross and Ravosa (1993); the RMAs reported by Ross and Henneberg (1995) and Spoor (1997) for non-hominid and non-human primates, respectively; the predicted modern human (H.s.) values for CBA from the RMA slopes reported by Spoor (1997) and Ross and Henneberg (1995); and the mean measured CBA values reported by Spoor (1997) and Ross and Henneberg (1995) for modern humans.

Thus, evidence from interspecific studies of non-human primates appears to support Gould's hypothesis whereas the intraspecific study of modern humans fails to support the hypothesis. More in particular, it is shown that modern humans do not follow the non-human primate trend for CBA vs. IRE1 reported by Ross and Henneberg (1995).

There are a number of possible explanations for why modern humans do not show a significant correlation between CBA and IRE1 and deviate from the non-human primate trend. The first and most obvious possibility is that the lack of

correlation is due to intraspecific noise, i.e. the variation in individual growth patterns makes it difficult to evaluate the allometric signal in a general population representing the end-product of human ontogeny and evolution. This contention is testable by studying an intraspecific sample in which the signal, if any exists, is likely to be greater than the sample noise generated. Human fetal material, in which the brain undergoes a number of orders magnitude increase in size (see Jeffery and Spoor, 1999), fits the criterion for such a sample. Secondly, it seems feasible that medio-lateral increases of human brain size exceed increases along the cranial base. This realises a major limitation with the model of 'spatial-packing' proposed by Ross and Ravosa (1993) (i.e. IRE = cube root brain volume/ total base length). While cube root volume can increase due to, for example, lateral and longitudinal (antero-posterior) brain enlargement, it is compared with only the longitudinal component of the cranial base, namely total base length. Hence, an alternative human model can be proposed were the brain 'inflates' laterally around the base rather than along it. This would produce an increase of relative brain size that projects only a minor force upon the length of the cranial base. Thus, the absence of any correlated change in CBA may result from isometric scaling between midline endocranial area and base length while relative brain size increases due to lateral expansion of the brain.

A third possible explanation for why modern humans deviate from the nonhuman primate trend by having a larger CBA than predicted by Ross and Henneberg (1995) is that flexion is structurally limited. In other words, the functional space of the pharynx prevents further antero-inferior rotation of the basioccipital in modern humans (Ross and Ravosa, 1993). Although beyond the scope of this thesis, the possible relationship between maximum base flexion and the size of the pharynx has been used to investigate the evolution of speech (e.g.

Laitman and Heimbuch, 1982; Lieberman *et al.*, 1992). Thus, the phylogenetic retroflexion from archaic to modern humans may relate to this evolutionary process.

The final point, which may elucidate the unique modern human condition, is the suggestion that the adult human skull is paedomorphic (neotenic), in that it exhibits juvenile characters of other primates (Bolk, 1926). The higher degree of base flexion observed in juvenile primates compared with adults is therefore retained amongst modern humans by retardation of somatic development (see Gould, 1977, for a review). Further clarification indicates that differences between humans and apes appear during prenatal rather than juvenile development (Dean and Wood, 1984; Dean, 1988). Indeed, Gould himself argues for a human fetal model of human paedomorphosis in preference to comparisons with juvenile chimps or gorillas. Hence, it is expected that because of 'fetalization' adult modern humans have a similar CBA to prenatal humans as is suggested by developmental studies that propose that the adult modern human base flexure is established prenatally and then, with a few minor deviations, maintained throughout life (Scott, 1958; Diewert, 1983).

At present the literature on human fetal cranial base angulation seems to suggest that flexion is not a linear process, but more polyphasic in nature. This reflects in many ways the apparent changes of CBA seen in the fossil hominid record. However, like the fossil record work pertaining to the fetal process of flexion is often confusing and contradictory. Numerous authors report that the basicranium flexes (chordal to prechordal angle) during the early part of the embryonic period from a relatively open position to a more acute angle and retroflexes during the late embryonic period (e.g. Müller and O'Rahilly, 1980; Diewert, 1983; Lemire, 1986). It has also been shown that the basicranium retroflexes during the third trimester and

flexes again postnatally (e.g. Zuckerman, 1955; Ford, 1956; Burdi, 1969; George, 1978; Lang, 1983). The former may relate in some way to a reduced rate of brain growth towards birth (see Guihard-Costa and Larroche, 1992) that possibly evolved to safeguard against difficult births of comparatively large headed infant humans. Moloy (1942) has indicated that base flexion in humans is associated with molding of the head during birth itself, though this remains to be tested.

Burdi (1969) has reported that the cranial base angle remains essentially unchanged during the second trimester with mean values ranging from 126 to 131 degrees. Similarly, though Levihn (1967) maintains that CBA generally increases, there is little evidence to support this conclusion in his results, which show a total increase of 3.5 degrees from 12 to 40 weeks (no sample standard deviations given). His cranial base angles vary from 149.5 degrees at 12-15 weeks to 148 degrees at 25-28 weeks and therefore appear consistent with those of Burdi. In contrast, Kvinnsland (1971) and Dimitriadis *et al* (1995) report increases (retroflexion) of 17 and 27 degrees respectively during the second trimester (Kvinnsland's fetal parameters were converted to ages using the data published by Chitty *et al.*, 1994). Van den Eynde *et al.* (1992) and Erdoglija (1989), on the other hand report decreases (flexion) of 12 and 20 degrees, respectively.

These results lead to contradictory conclusions when applied to Gould's hypothesis: either base length increases in relation to brain size resulting in retro-flexion (e.g. Kvinnsland, 1971; Dimitriadis *et al.*, 1995), brain size increases relative to base length resulting in flexion (e.g. Erdoglija, 1989; van den Eynde *et al*, 1992), or brain size and base length scale isometrically resulting in very little change in CBA (e.g. Levihn, 1967; Burdi, 1969). The apparent differences between measured values of CBA may be attributed to the use of nasion as the anterior-most landmark

and differences in the visualisation techniques used. Nasion has been shown to be variable with age and across species in a way that is independent of cranial base morphology (Scott, 1956; Scott, 1958; Sirianni and Van Ness, 1978). In addition, it is possible that the radiographic images (CT and plain film) used by Dimitriadis *et al.* (1995), van den Eynde *et al.* (1992), and Erdoglija (1989) were insufficiently contrasted, due to the greater radio-translucency of cartilage, to accurately locate landmarks in the younger specimens.

The work cited above can be grouped into two main hypotheses containing a number of supplements. These propose that (**1**) increases of brain volume relative to cranial base length creates a spatial-packing problem that mechanically drives base flexion during human fetal development. This predicts two possible outcomes: Firstly, variations in cranial base angulation significantly correlate with changes of brain volume relative to base length; Second, the cranial base remains essentially unchanged if cranial base length scales isometrically with cube root brain volume (i.e. relative brain size remains unchanged). However, the supplementary proposition suggests that increases of human fetal brain size arise primarily through lateral as opposed to longitudinal expansion, thereby leading to an increase of relative brain size that is not projected along the cranial base. Thus, the suitability of the proposed model of spatial-packing must be tested with the null hypothesis that increases of square root midline area are the same as or greater than increases of cube root brain volume. This predicts that the slope of square root midline area against cube root brain volume is equal to or significantly greater than one. The second hypothesis suggests that (**2**) the high degree of base flexion observed in adult modern humans is a fetal character established during prenatal human ontogeny. This predicts that the

cranial base angle observed in adult modern humans is the same as, or not significantly different from that found in the human fetus.

3.2.2 *Basicranial architecture: posterior cranial fossa*

In addition to the 'spatial-packing' hypotheses discussed earlier, other theories have been proposed in order to explained changes in the cranial base angle in relation to the size and shape of the posterior cranial fossa and its contents. In particular, Moss (1958) and Dean (1988) attribute cranial base flexion, lateral expansion of the posterior cerebral fossa, and inferior displacement of the foramen magnum to enlargement of the infratentorial elements of the brain, namely the cerebellum and brain stem. Moss (1958) compares the 28 degree downward and backward rotation of the foramen magnum relative to the plane of the lateral semicircular canals during life, two thirds of which occurs prenatally (Fenart, 1953; Bergerhoff and Martin, 1954; Bjork, 1955), with vertical deformation of American Indian skulls. In these skulls, both supero-inferior and posterior expansion was restricted by artificial means during growth. According to Moss (1958) this

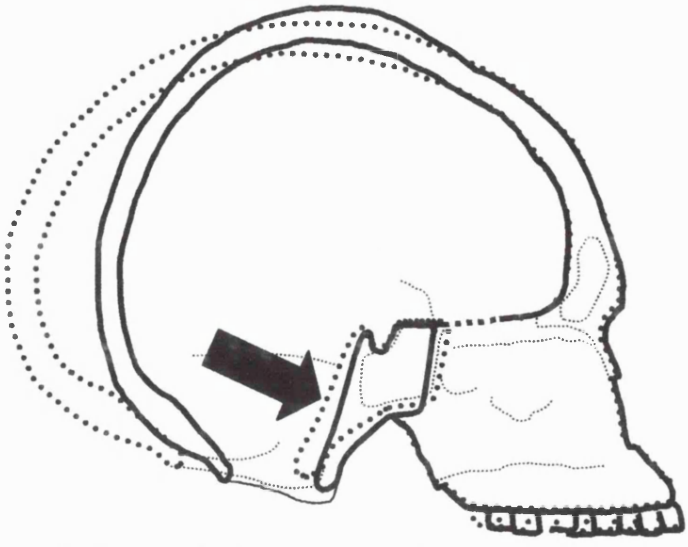

Figure 3.8. Illustration showing the decrease in cranial base angle from a normal skull (interrupted line) to that of a vertically deformed Indian skull (adapted from Moss, 1958).

redirected the force of the expanding cerebellum onto the posterior cranial base, thereby inducing cranial base flexion (Figure 3.8).

Ross and Ravosa (1993) only find limited evidence of a relationship between absolute cerebellum size and CBA across primates ($r = -0.466$, $P<0.01$; raw data). At the subordinal level significant correlations were only found in Haplorhines ($r = 0.464$,$P<0.05$; raw data) and Cercopithecines ($r = -0.968$, $P<0.05$:$\log_e$ data), leading the authors to conclude that there is little evidence to support the contention of Moss (1958) and Dean (1988).

Moss drew further evidence for his hypothesis from changes in the position of the dura, particularly the tentorium, and petrous temporal bones, both of which he considers part of the same functional unit and significant determinants of skull formation (Moss *et al.*, 1956; Moss, 1958). The tentorium has become increasingly important in supporting enlargement of the forebrain, thereby preventing herniation of the cranial contents through the foramen magnum, during hominid evolution (Aiello and Dean, 1990) and human development (Klintworth, 1967). Klintworth (1968) suggests that the tentorium emerged relatively late in evolution, being absent or rudimentary in all but the 'highest' mammals. He also reports that successive evolutionary stages of the tentorium in comparative subjects are recapitulated to a certain extent during human development. Similarly, Bull (1969) indicates that the characteristic incline of the human tentorium evolved in order to efficiently dissipate the phylogenetic increased load of the brain, brought about by the adoption of an upright posture and cerebral enlargement, towards the skull. Thus, it can be proposed that the orientation of the tentorium during development and evolution influences the load of the cerebrum upon the contents of the posterior fossa. In other words, rotation of the tentorium towards the foramen magnum limits the superior expansion

of the cerebellum and is therefore associated with an increase in the force of the developing cerebellum on the walls and floor of the posterior fossa. Indeed, Hochstetter (1939) and Moss *et al.* (1956) report that the human fetal tentorium in *norma lateralis* rotates posteriorly towards the foramen magnum (Figure 3.9) during the first fourteen weeks of gestation (90mm CRL; Streeter, 1920). Furthermore, Moss indicates that this rotation relates to changes in the proportions of the brain, i.e. infra and supratentorial parts. He also suggests that the orientation of the tentorium remains essentially unchanged once the brain has attained its topographical proportions at around fourteen to seventeen weeks. This is almost contemporaneous with a general increase in the rate of growth of the cerebellum (Rakic and Sidman, 1970) and an increase in the width of the cerebellum relative to the length of the cerebrum (Noback and Moss, 1956). Before sixteen weeks the latter relationship is approximated by cerebellum width = (cerebrum length/b)$^{1/2.1}$ while after sixteen

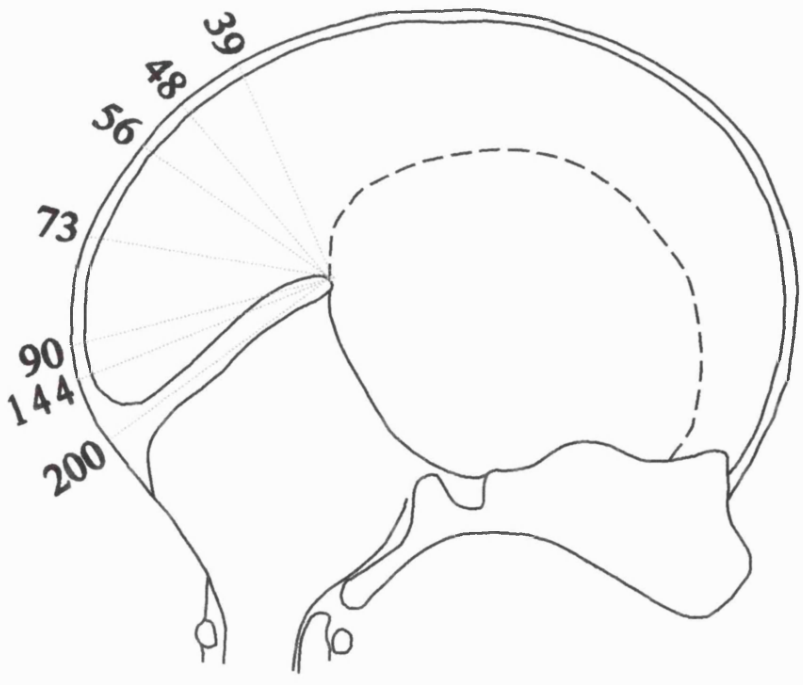

Figure 3.9. Midline sagittal sketch of the skull showing the backward and downward rotation of the tentorium cerebelli from 38.5-200mm CRL (adapted from Hochstetter, 1939).

weeks it is given by cerebellum width = (cerebrum length/b)$^{1/0.9}$, where b is a constant (equations derived from those published by Noback and Moss, 1956). In other words, for every increase in the length of the cerebrum there is a greater increase in the width of the cerebellum after sixteen weeks than before (Figure 3.10).

A number of studies based on exocranial landmarks have shown that the human petrous bones are more coronally orientated than in great apes. The authors propose that such differences are due to increases of human cerebelli size, possibly

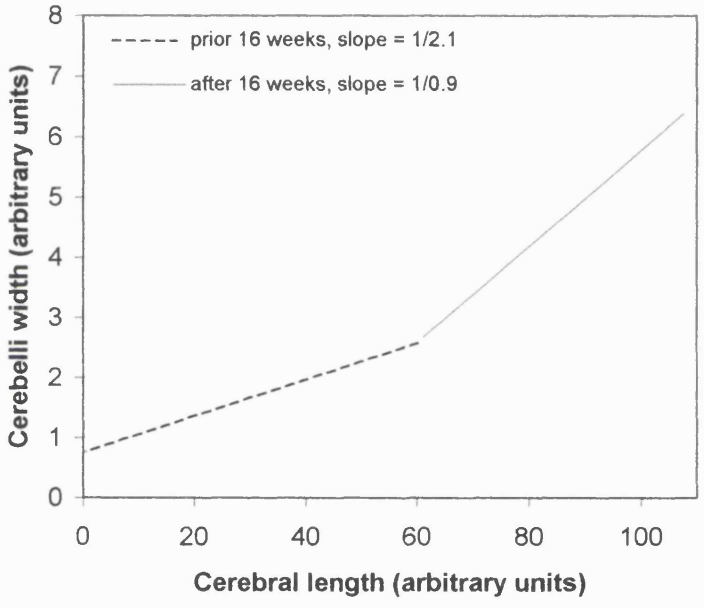

Figure 3.10. Graph showing the different growth rates of the width of the cerebellum relative to the length of the cerebrum before and after 16 weeks gestation (data from Noback and Moss, 1956).

as a consequence of increased manual dexterity, relative to the posterior cranial base (Dean and Wood, 1981; Dean, 1988). Indeed, Spoor (1997) has shown that petrous angle is interspecifically correlated with IRE1 and suggests that more coronally orientated petrous bones are associated with brain enlargement. This is consistent with Moss's (1958) earlier notion that enlargement of the infratentorial parts of the brain increases the width of the posterior fossa. Comparing the size of the cerebellum relative to, for example, the length of the posterior cranial base as opposed to

analyzing absolute volumes may overcome the limitations of Ross and Ravosa's (1993) evaluation of the Moss hypothesis.

Developmentally, Ford (1956) suggests that progressive widening of the posterior fossa during human fetal development is a compensatory mechanism for the slower growth rate of the posterior cranial base compared with the anterior cranial base and brain. This is confirmed by findings that the anterior cranial base grows faster than the posterior cranial base in human (Mestre, 1959; Burdi, 1969; Levihn, 1967; Houpt, 1970; Johnston, 1974; Eriksen *et al.*, 1995) and non-human primate fetuses (Sirianni and Newell-Morris, 1980). Thus, it can be conjectured that the slower rate of posterior cranial base elongation compared to growth of the infratentorial parts of the brain (see Guihard-Costa and Larroche, 1992) leads to an increase of relative infratentorial size during fetal development. This increase, perhaps facilitated by tentorial rotation, may therefore be associated with a relatively wider posterior fossa, cranial base flexion, and more coronally orientated petrous pyramids. This is supported in an evolutionary context by reports that the posterior cranial base is shorter in adult modern humans than in *Gorilla*, *Pan*, and particularly *Pongo* (Dean and Wood, 1981). It is also supported by reports that the cerebellum is larger in modern humans than in non-human primates (Stephan *et al.*, 1981; Rilling and Insel, 1998), probably due to the demands of increased of manual dexterity or other cognitive functions (e.g. Stein *et al.*, 1987; Kim *et al.*, 1994; Thach, 1996; Matano and Hirasaki, 1997).

However, Lee *et al.* (1996) in their study of normal Korean fetuses have shown that the angle between the otic capsules, intersected at the centre of the sphenoid, rapidly decreases during the early part of the third trimester (22-30 weeks) and subsequently plateaus towards the end of the third trimester. Unless base length

rapidly increases in relation to the cerebellum, which is unlikely (see earlier references), this result seems to contradict the proposition made earlier stating that increases in relative infratentorial size results in more coronally orientated petrous pyramids. Nonetheless, is not clear from Lee *et al.*'s (1996) report whether the orientation of the otic capsules is coronal and the angle decreases because the true intersection between the capsules, which in any case is unlikely to lie at the centre of the sphenoid, shifts posteriorly.

Taking into account the evidence presented, the third hypothesis to be tested in this study (**3**) states that differential growth between infra- and supratentorial parts of the brain drives the tentorium cerebelli posteriorly towards foramen magnum and effects a change in the shape, i.e. relative width, of the posterior cranial fossa. Here, the hypothesis predicts that changes in the angle between the tentorium and anterior cranial base correlate with variations in the ratio between the infra- and supratentorial volumes and that once these volumes attain their fetal topographical proportions the tentorium ceases to rotate. The hypothesis also predicts that variations of brain topography are directly correlated with proportional changes of the posterior cranial fossa and the orientation of the petrous pyramids. The corollary hypothesis suggests that variations of cranial base angulation, in particular increases of cranial base angle, complements the influence of changing brain topography by further varying the space available for subtentorial parts of the brain to develop. Both increases of supratentorial relative to infratentorial size and base retroflexion limit supero-inferior development of subtentorial parts of the brain, thereby creating a spatial-packing problem that effects the proportions of the posterior fossa and petrous pyramid orientation. This predicts that variations of brain topography and

cranial base angulation correlate with changes in the proportions of the posterior cranial fossa and the orientation of the petrous pyramids.

It is also hypothesised that (**4**) increases in the size of the cerebellum relative to the length of the posterior cranial base affects the proportions of the posterior cranial fossa, petrous temporal orientation, and in contrast to hypothesis 3 actively drives cranial base flexion. Thus, it is expected that increases in infratentorial volume relative to posterior cranial base length correlate with changes to the proportions of the posterior cranial fossa, the angle between the petrous pyramids and cranial base angulation.

3.2.3 *Basicranial and facial complex: facial kyphosis and maxillary prognathism*

A number of researchers have suggested that the face and basicranium are closely related both spatially and developmentally and have been during much of human evolution (Scott, 1958; Knowles, 1963; Riesenfeld, 1967; Enlow and Hunter, 1968; Sarnat, 1973; Enlow, 1975; Baer and Nanda, 1976; Enlow, 1976; Du Brul, 1977). This relationship, between the face and cranial base, consists of both biomechanical and spatial influences (e.g. respiratory spaces and masticatory apparatus). It is arguably one of the most complex in the skull since many of the contributing factors are both interrelated and mutually interdependent (Figure 3.11) (see Enlow and Hunter, 1968 for further details). One particular aspect of this complex is the downward and forward growth of the mid-face that is only permitted during human and non-human primate development by the presence of sutures and synchondroses between the face and cranial base (Scott, 1956; Scott, 1958; Enlow and Hunter, 1968; Sirianni and Swindler, 1979). Considering the close relationship between the face and cranial base, it seems logical to suppose that changes in facial

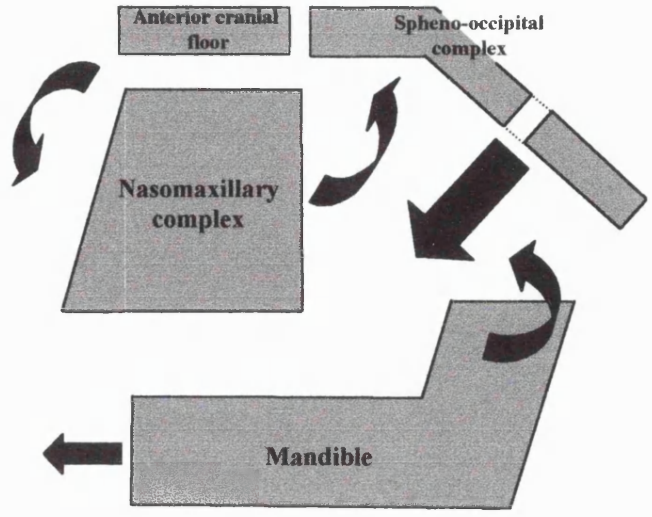

Figure 3.11. Schematic showing the various components of the face and cranial base that are closely related and mutually interdependent as indicated by the arrows (adapted from Enlow and Hunter, 1968).

prognathism and orientation are associated, perhaps via a complex matrix of ontogenetic and phylogenetic mechanisms involving the synchondroses of the cranial base, with cranial base flexure and brain size (Weidenreich, 1941; Scott, 1956; Ashton, 1957; Young, 1959; Biegert, 1964; Riesenfeld, 1967;Enlow and Hunter, 1968; Enlow, 1976; Sirianni and Swindler, 1979; Ross and Ravosa, 1995; Lieberman and McCarthy, 1999). Indeed, specific parts of the brain have been implicated: Enlow (1976) reports that during human growth, the mid-face becomes more vertically orientated in order to remain perpendicular to the olfactory bulbs. These, the author proposes, have rotated forward and downward at some point during human evolution and become reduced in comparison with body size (olfactory regression). This is consistent with earlier notions that facial prognathism in primates is determined by the size of the olfactory organs (Biegert, 1964; Cartmill, 1970) and that the cribriform plate changes orientation in relation to the olfactory bulbs during rodent ontogeny (Hoyte, 1971).

Development of the secondary palate (palatogenesis) in humans, formed by movement of the palatal shelves into a horizontal position above the tongue at the end of the embryonic period (8 weeks: Sperber, 1981), is the key event associated with extensive proportional and spatial changes in the craniofacial complex (Wragg *et al.*, 1970). During this period the nasomaxillary complex (mid-face) tends to lift up and the angle of the maxilla, relative to the anterior cranial base, increases (Diewert, 1983: Figure 3.12). The force regulating the direction of this displacement is said by some workers to be nasal septal cartilage growth, providing both a 'thrust' and 'pull' (septomaxillary ligament) force in the mid-face region (Scott, 1953,1954, 1967; Sperber, 1981). Moss-Salentijn (1969), however, proposes that the septum provides structural support in the region while the orofacial complex provides the directional force. This is consistent with studies showing that there is little disproportionate septal growth relative to the rest of the nasal area during fetal development (Ford, 1956; Burdi, 1969).

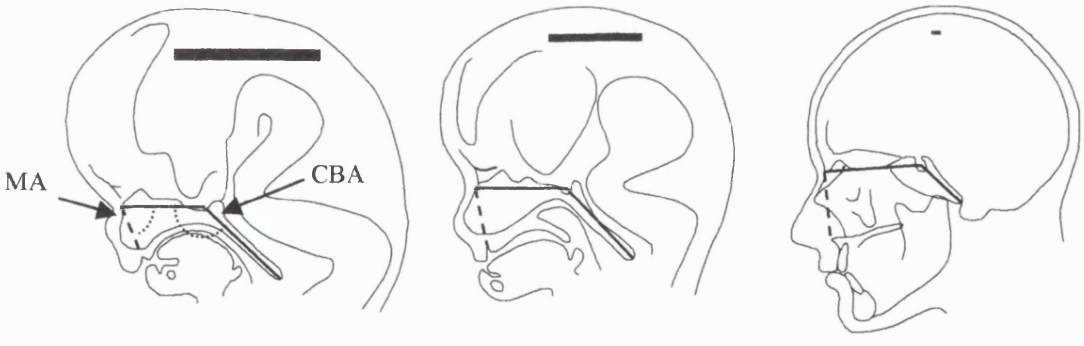

Figure 3.12. Midline lateral illustrations of the face in, from the left, a 7 week embryo, a 9 week fetus, and an adult human showing general changes in the orientation of the nasomaxillary complex (mid-face) and the increase in the angle of the maxilla relative to the anterior cranial base (MA). Bar equals 5mm (adapted from Diewert, 1983).

After development of the secondary palate, the angle of the palate to posterior cranial base and the angle of the maxilla to anterior cranial base are said to remain unchanged as the head extends superiorly and dorsally (Johnston, 1974;

Diewert, 1983). Moreover, the craniofacial pattern formed, according to Diewert (1983), is similar to that found by other workers for later prenatal periods and postnatally (e.g. Burdi, 1969; Levihn, 1967; Johnston, 1974; Reidel, 1952). Hence, Diewert suggests that the pattern of facial form created during the late embryonic-early fetal period is maintained throughout the second and third trimesters and into the postnatal period. This is substantiated by Ford's (1956) results, which indicate that after 10 weeks there is no significant change in the pituitary-nasion-prosthion angle during fetal development.

The results obtained by Burdi (1969) and Levihn (1967), which indicate that CBA also remains essentially unchanged during the second trimester, appear to support the notion that variations of cranial base flexure are contemporaneous with those of facial orientation. This is further supported by Kvinnsland's (1971) results that show a positive correlation ($r = 0.44$-0.48; no significance given) between CBA and the angle between the anterior cranial base and palate from about 10-25 weeks. It is also corroborated by evidence from studies of craniofacial abnormalities (Burston, 1959; Latham, 1976) and Björk's (1955) suggestion that flattening of the cranial base in subadult humans effects a tilting of the face upwards.

Studies of non-human primates have shown that growth of the cranial base, in particular the anterior cranial base, is related to growth and development of the facial complex (Sirianni and Swindler, 1979). Indeed, a similar condition to that described earlier for human fetuses, showing that the facial angle and cranial base angle remain relatively unchanged, is evident during the fetal period of *Macaca nemestrina* (Sirianni and Newell-Morris, 1980).

Ross and Ravosa (1993) have found a significant positive correlation between cranial base angle and orientation of the palate relative to the posterior

cranial base (facial kyphosis) amongst adult nonhuman primates ($r = 0.469$, $P<0.001$). This correlation indicates that increased ventral kyphosis of the face corresponds to increased base flexion amongst nonhuman primates. However, no significant correlations were observed at the level of Strepsirhini ($r = 0.422$, ns), Catarrhini ($r = -0.033$, ns), Cercopithecoidae ($r = 0.232$,ns), Colobinae ($r = 0.360$, ns) or Hominoidea ($r = 0.054$,ns). Hence, the authors reticent suggestion that facial orientation 'may' be affected by basicranial morphology. Nevertheless a similar correlation to that found across non-human primates by Ross and Ravosa (1993) is also found amongst adult modern humans ($r = 0.492$; Ross and Henneberg, 1995), though the significance of this value is not given but presumed to be lower than 0.05. The mean value for palate orientation amongst adult modern humans is some 30 degrees less than that of the African apes suggesting that the palate has become ventrally deflected during human evolution (Ross and Henneberg, 1995).

Thus, it can be hypothesised that (**5**) changes of facial morphology are associated with variations in cranial base architecture, in particular cranial base angulation, and increases of relative brain size. This predicts that variations in palate orientation (angle of facial kyphosis) and maxillary prognathism correlate with variations of cranial base angulation and relative brain size.

3.2.4 *Basicranial and facial complex: orbital convergence and frontation*

Orbital regions of the face are structurally continuous with the basicranium and are therefore an integral part of the basicranial and facial complex. The midline cranial base sits between the supero-medial walls of the orbits and the sphenoid wings and anterior cranial floor separates the orbits from the temporal and frontal lobes of the brain, respectively. Hence, increases of brain size that are said to affect

basicranial architecture have also been linked to changes of orbital morphology (Enlow and McNamara, 1973; Enlow, 1976).

Across mammals, Enlow (1976) intimates that sagittal orbital axis orientation is related to facial prognathism when he describes how the former is, in general, positioned perpendicular to the posterior maxillary plane which is said to represent the interface between the face and neurocranium (Lieberman, 1998; Spoor *et al.*, 1999). It has also been proposed that the orientation of the orbital rims in *norma laterlis* has increased to a more perpendicular position relative to the anterior cranial base (referred to as frontation) during primate evolution as a result of phylogenetic enlargement of the prefrontal and frontal lobes of the brain (Cartmill, 1970; Enlow and McNamara, 1973). Moreover, the characteristic forward facing orbits in humans are said to be a consequence of ventral rotation of the orbital axes and vertical displacement of the orbital rims during primate evolution (Enlow and McNamara, 1973; Enlow, 1976: Figure 3.13).

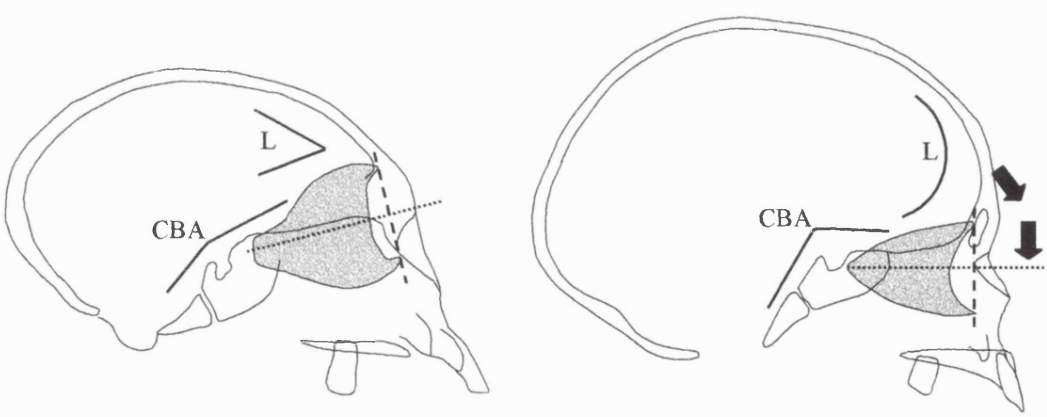

Figure 3.13. Lateral diagrams of a nonhuman primate skull (left) and human skull (right) showing the difference between the sagittal orientation of the orbital axes (dotted lines) and orbital rims (dashed lines; sagittal frontation) in relation to cranial base angle (CBA) and the extent of frontal lobe expansion (L) (adapted from Duterloo and Enlow, 1970).

The posited association between orbital axis orientation, cranial base flexure, and facial prognathism is to a certain degree supported by evidence of significant correlations across primates (Ravosa, 1991; Ross and Ravosa, 1993). In particular, Ross and Ravosa (1993) have found highly significant positive correlations between cranial base angle and orbital axis orientation (measured relative to the posterior cranial base) across non-human primates ($r = 0.608$, $P<0.001$). In addition, adult modern humans appear to have a mean orbital axis orientation (114.6 degs.) relative to cranial base angle that is not significantly different from the predicted value from the non-hominid primate trend (Ross and Henneberg, 1995).

From this evidence it can be hypothesised that (**6**) orbital morphology in the sagittal plane is structurally associated with changes in the cranial base and with variations of brain size relative to base length. This predicts that orbital axis and rim orientations in the sagittal plane correlate with variations of basicranial angulation and relative brain size

During fetal development, the eyes and orbits rotate medially in the transverse plane (Sperber, 1981; Diewert, 1985). Zimmerman *et al.* (1934) have shown that the angle between the optic nerves, measured from the eyeball to the optic chiasma, decreases during human fetal development from 180 degrees in the second lunar month to 71 degrees at birth. The greatest part of this convergence, from 180 to 105 degrees, is said to occur from 8 to 12 weeks during development of the face and cranial base. This suggests that expansion of the telencephalon, especially the frontal and temporal lobes, against the mostly unossified and separate components of the orbit is responsible for the convergence of the eyes, displacing the orbits and therefore the axis of the optic nerves medially.

Orbital convergence towards the midline during primate evolution has been associated with facial recession and olfactory regression, thereby yielding stereoscopic vision (Jones, 1917; Smith, 1924; Napier and Napier, 1967; Cartmill, 1970). In particular, Biegert (1964) and Enlow (1968) suggest that orbital convergence during primate evolution corresponds to increases of the frontal and temporal lobes of the brain (Figure 3.14). As such it represents an alternative solution to the 'spatial-packing' problem arising from increases of relative brain size and leads to a reduction in interorbital breadth. Kurihara *et al.*, (1980) have shown that the interorbital distance continues to shorten during human ontogeny up until the midline sutures have fused at around three years. After this period bone deposition on the orbital lamina leads to an increase of interorbital breadth (Lang, 1983; Hoyte, 1991). The interorbital region forms part of the matrix supporting the face, particularly the snout, and therefore shortening may associate with facial orthognathism (Enlow and McNamara, 1973).

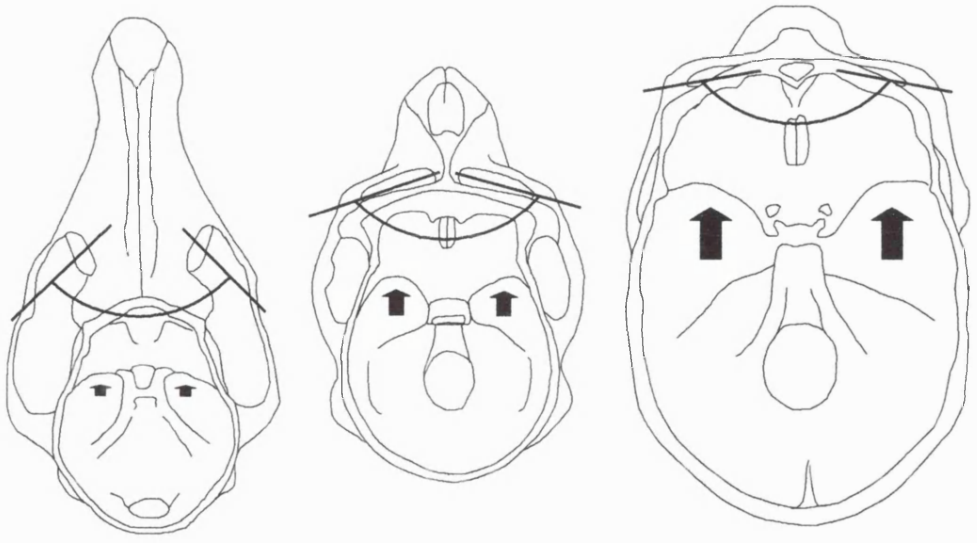

Figure 3.14. Superior view of, from the left, a dog, Rhesus monkey, and human skull showing that in comparative terms temporal lobe expansion (arrows) moves the orbits (thick black lines) into a more frontal position in the face (adapted from Enlow and McNamara, 1973).

Considering the above, it can be hypothesised that (**7**) orbital convergence and frontation in the transverse plane correlate with variations of basicranial angulation and relative brain size. The final synthesised hypothesis, which is summarised together with the other hypotheses in Figure 3.15, therefore states that (**8**) the face and cranial base form a complex in which changes of morphology are interrelated and determined by increases of brain size. This predicts correlations amongst facial kyphosis, maxillary prognathism, orbital convergence, orbital frontation (transverse and sagittal), cranial base flexion and ultimately with increases of relative brain size. It is also predicted that differential growth between the anterior cranial base and palate correlates with maxillary prognathism.

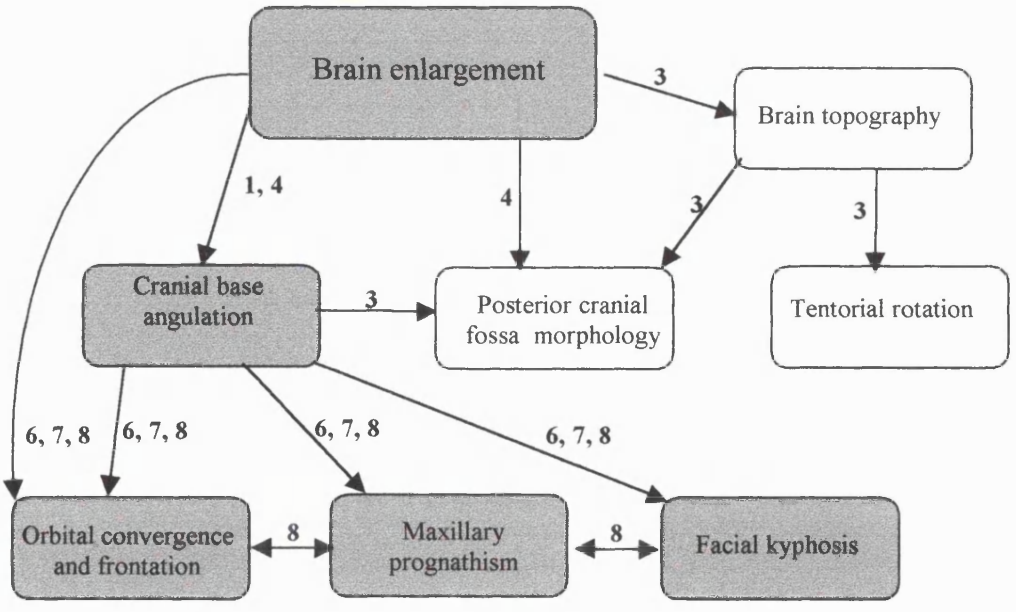

Figure 3.15. Flow chart of the relationships to be investigated in the present study. Numbers indicate the relevant predictions (see body of text) that will be used to test the proposed hypotheses. The synthesis between basicranial and facial morphology and the cascading influence of brain enlargement on this complex is highlighted in grey. Hypotheses 2 is not shown.

3.3 Summary of testable predictions

1) Increases of brain size relative to base length correlate with a decrease of cranial base angle. Thus isometric scaling between base length and brain size will have no effect on cranial base angulation. The corollary hypothesis is that if lateral expansion of the brain is dominant then increases of relative brain size will have little effect on cranial base angle. To evaluate this hypothesis, it is predicted that increases of linearised midline brain area (square root) are equal to or greater than increases of linearised brain volume (cube root).
2) The mean value of human fetal cranial base angulation is not significantly different to that observed amongst adult modern humans.
3) Increases of supratentorial volume in relation to infratentorial volume drives posterior tentorial rotation and correlates with variations in the proportions of the posterior cranial fossa and petrous pyramid orientation. Similarly, it is also predicted that variations in cranial base angulation correlate with changes to the proportions of the posterior fossa and petrous pyramid orientation as well.
4) Increases of infratentorial volume in relation to posterior cranial base length correlate with variations in the proportions of the posterior cranial fossa, and petrous pyramid orientation.
5) Changes to the architecture of the basicranium and increases of relative brain size correlate with variations of palate orientation and maxillary prognathism.
6) Changes to the architecture of the basicranium and increases of relative brain size correlate with variations of orbital axis and rim orientation in the sagittal plane.
7) Changes to the architecture of the basicranium and increases of relative brain size correlate with orbital frontation and convergence in the transverse plane.

8) Palate orientation, maxillary prognathism, orbital frontation and convergence all inter-correlate with each other, cranial base angle, and increases of relative brain size. Maxillary prognathism correlates with increases of palate length in relation to anterior cranial base length.

CHAPTER 4. MAGNETIC RESONANCE IMAGING (MRI)

Magnetic Resonance Imaging (MRI) was developed during the 1970's (Mansfield *et al.*, 1976; Mansfield and Pykett, 1978), on the basis of techniques and principles developed for chemical Nuclear Magnetic Resonance (NMR) spectroscopy (Bloch *et al.*, 1946) and Computed Tomography (Lauterbur, 1973). Later, it was applied in medicine as a non-invasive imaging tool (Edelstein *et al.*, 1980).

MRI has the ability to produce high quality images of internal morphology by applying pulses of radiofrequency electromagnetic radiation and weak magnetic field gradients to map the spatial localisation of ^{1}H protons in the presence of a strong magnetic field. The non-invasive nature of MRI and the high quality of the images formed, in which more soft tissues are more readily differentiated than with CT, make it ideal for visualising and quantifying human fetal morphology. This chapter briefly reviews the general principles and some practical aspects of MRI relevant to the present study. A glossary in Appendix 2 explains some specific terms given in the text in bold.

4.1 Basic principles

4.1.1 *Atomic nuclei and moments*

All particles within an atom, **protons** (p+), **neutrons** and, **electrons** (e-) exhibit **quantum** motion: electrons spin about their axes whilst orbiting around the nucleus, and protons and neutrons spin within the nucleus. Such spins can be described by the spin quantum number I. In, for example, the deuterium atom (^{2}H),

which has one unpaired electron, one proton, and one neutron, the total electron spin = ½ and the total nuclear spin =1. In MR, nuclei with an odd number of protons or neutrons (e.g. one neutron, two protons) are used because the overall nuclear charge generates a magnetic field, known as the magnetic **dipole** moment, normal to the plane of spin rotation. Such nuclei, also referred to as MR active nuclei, include ^{13}C (unpaired protons = 0; unpaired neutrons = 1; total nuclear spin = ½), ^{19}F (0;1;½), ^{31}P (0;1;½), and more importantly ^{1}H (1;0; ½). Of these, hydrogen protons are the most widely studied in MRI because: (a) hydrogen protons are abundant in soft tissues, and (b) the single proton (nuclear I=½) provides a large magnetic **moment**.

Normally, spin ½ moments are distributed randomly such that there is no net or bulk magnetic moment in any particular direction. However, in the presence of a strong magnetic field, with flux density B_0, the moments assume either a parallel or anti-parallel state relative to B_0, also known as spin-up and spin-down respectively. The proportion of moments in either state depends on the **magnetic flux** density of the field and the thermal energy of the system, since the parallel state corresponds to a lower energy level than the antiparallel state. In other words, moments from nuclei with high thermal energy occupy the more energetic antiparallel state, whereas moments from nuclei with less than the required quanta of energy yield to B_0 and align in the lower energy parallel state. Thus, samples that are thermally equilibrated at room temperature and subject to a strong magnetic field have an excess of moments in the parallel state. The effective number of parallel moments is given by the equation,

$$N_{effective} = N_{spin\text{-}down} - N_{spin\text{-}up} = N_T h\gamma f/(2kT)$$

Where N_T is the total number of moments in the sample, h is **Planck's constant** ($6.626x10^{-34}$ J s), f is the frequency of energy required for transition from the parallel to antiparallel state, k is **Boltzmann's constant** ($1.3805x10^{-23}$ J K^{-1}),and T is the absolute temperature of the sample. The result is a net magnetisation vector (NMV: see Westbrook and Kaut, 1993 for a description of the NMV), which is the sum of the effective moments ($N_{effective}$) times the magnetic moments, in the direction of B_0 (Figure 4.1).

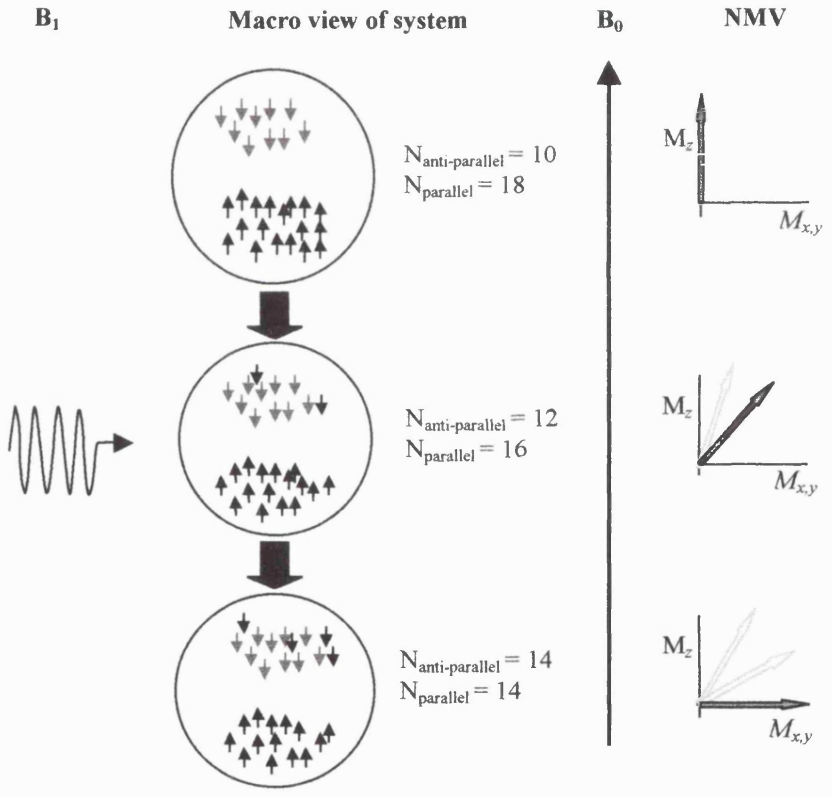

Figure 4.1. Diagrammatic representation of magnetic resonance. As the system is irradiated by RF energy (B_1) some of the excess moments in parallel alignment with B_0, which create the net magnetic vector (NMV) in the direction of B_0, gradually gain sufficient energy to move to the antiparallel state. In doing so, the position of the NMV gradually changes relative to B_0.

4.1.2 *Precession*

Parallel moments, which are already spinning about their own axes, also spin about the longitudinal axis of B_0. Hence, moments are often referred to as spins, though the former term is used here to differentiate it from other spin terminology. For the sake of simplicity, it can be imagined that the NMV is a large moment that also precesses about B_0 with a precessional path and frequency that is the same its constituent moments. The precessional frequency, known as the Larmor frequency (ω_o), is proportional to the frequency of energy required (f) for one moment contributing to the NMV to gain ΔE and move to the antiparallel state. It can be determined by,

$$\omega_o = B_0\gamma$$

From this it is possible to see that the precessional frequency of the moments, and hence the precessional frequency of the NMV, is proportional to the strength of the external magnetic field ($\omega_o \propto B_0$).

4.1.3 *Resonance*

Irradiating moments with frequencies that are similar to their Larmor frequency will, provided the energy is delivered perpendicular to NMV and B_0, increase the oscillatory amplitude of their spins i.e. the NMV begins to resonate. For a typical scanner (1-2 Tesla), frequencies in the radiofrequency (RF) range (42-84 MHz) are necessary to generate a state of 'excitation'. This state arises as some of the parallel moments gain sufficient energy (ΔE) to move into the antiparallel state, thereby causing the NMV to gradually move out of alignment with B_0 (Figure 4.1). The degree (θ) to which the NMV moves or 'flips' (angle of nutation) is determined

by the magnetic flux density produced by the RF pulse (B_1) and the duration of the pulse (t_p),

$$\theta = \gamma B_1 t_p$$

For MRI measurements B_1 and t_p are typically adjusted so that NMV moves into a plane perpendicular to B_0 and continues to precesses about B_0 at the Larmor frequency of its moments (N.B. other flip angles are often used during more complex procedures e.g. gradient echo sequences: see Hendrick and Osborn, 1988). In effect, there is now a larger component of moment magnetisation in a transverse plane (x,y) perpendicular to B_0 than in the longitudinal plane (z) parallel to B_0. An additional effect of excitation is that individual moments become displaced to the same location in their precessional paths and are said to be in **phase**. If a receiver coil is positioned across the transverse plane of coherent magnetisation (phased moments), a voltage will be induced in the coil with a similar frequency to that of the Larmor frequency of the moments.

4.1.4 *Relaxation: T1 recovery and T2 decay*

When the RF pulse ceases, the moments no longer gain energy and the transverse component of magnetisation ($M_{x,y}$) is gradually lost as excited moments relax back to their original parallel state. The recovery of the longitudinal component of magnetisation (M_z), i.e. moments re-aligning with B_0, is known as T_1 recovery or spin-lattice relaxation and is caused by moments losing energy to their surrounding environment or 'lattice'. Conversely, the reduction in the transverse component of magnetisation, known as T_2 decay or spin-spin relaxation, is due to moments exchanging energy and losing phase coherence.

As the voltage in the coil decreases with the loss of coherent magnetisation in the transverse plane, a characteristic **Free Induction Decay** (FID) signal is produced. The intensity and frequency of this signal describes the concentration and type of nuclei and its duration depends on the chemical environment of the moments. The rates of $\mathbf{T_1}$ **recovery** and $\mathbf{T_2}$ **decay** are exponential and the time taken for 1/exp. of the longitudinal magnetisation to be recovered and 1/exp. of the transverse component to be lost are known as the recovery time constant $\mathbf{T_1}$ and decay time constant $\mathbf{T_2}$, respectively.

In addition to T_1 and T_2 relaxation, there is a third relaxation process called T_2* decay. This is a combination of T_2 decay and dephasing caused by inhomogeneities in the magnetic field. Since the Larmor frequency is dependent on the size of the field ($\omega_o \propto B_0$), moments in regions of negative field inhomogeneity have lower precessional (Larmor) frequencies, whilst those in positive regions have higher precessional frequencies. This results in a loss of phase coherence across the field that also has an exponential decay rate denoted by T_2*.

4.2 Influences on proton (^{1}H) moments

4.2.1 *Chemical shift*

While all proton (^{1}H) moments resonate at about 200 MHz in a 4.7 Tesla field, the exact resonance frequency of each moment depends on the local electron distribution of the proton. This effect, known as chemical shift, arises because electrons (moving negatively charged particles) generate small magnetic fields in the opposite direction to B_0 and therefore partially shield (nuclear shielding) the proton moment against the external field B_0. Thus, moments belonging to protons

surrounded by a large number of electrons experience smaller external fields and exhibited slightly lower precessional frequencies than those moments belonging to protons surrounded by fewer electrons.

4.2.2 *Spin-spin coupling*

A further influence on the resonance frequency of proton moments is the presence of other non-zero spins (I>0) in the same molecule or sub-group. This effect, spin-spin coupling, can be caused by other proton moments with different spin directions (homonuclear couplings) or altogether different nuclei (heteronuclear couplings). Essentially, the extent of the external magnetic field experienced by a proton can be reduced or increased by the spin direction of the accompanying nuclei. For example, the proximity of ^{13}C (I= ½) in its spin-up state (+ ½) will shield a proton from the external magnetic field and cause its moment to resonate at a lower frequency. In contrast, the ^{13}C in its spin-down state (- ½) will deshield the proton and cause its moment to resonate at a higher frequency. The result is a splitting of the proton resonant frequency into two parts (a doublet). Other equivalent ($I_1=I_2$) and inequivalent ($I_1<>I_2$) couplings can yield more complex effects on the resonance frequency of the proton moment (e.g. triplet, quartet, or multiplet splitting).

4.2.3 *Motion*

In practice the transfer of energy in T_1 and T_2 relaxation is initiated by local fluctuations in the magnetic field caused by the movement of neighbouring nuclei and electrons with moments. The frequency of these fluctuations depends on the motion of the molecules: if the motion is unconstrained i.e. as in free water, the range will include high frequency fluctuations. If, on the other hand, the water

molecule is bound to a larger molecule, like a protein, its motion is constrained and low frequency field fluctuations are observed. In general, T_1 recovery and T_2 decay are sensitive to high frequency fluctuations close to the Larmor frequency while only T_2 decay is sensitive to lower frequency fluctuations close to zero. Thus, the T_1 and T_2 relaxation experienced is determined by the relative distance between the molecule containing the proton, typically water, and larger molecules. The overall observed relaxation times for a given tissue are determined by the proportion of water molecules in different positions relative to larger molecules (see Foster and Hutchison, 1987 for a more detailed description of water binding and its effects on relaxation times).

Since there are numerous permutations of chemical shift, spin-spin coupling, and especially water binding in the human body (e.g. lipid bound, protein bound, free etc.), the relaxation times for most tissues are characteristic and their signals are readily differentiated. This is the fundamental advantage of MRI in soft-tissue imaging.

4.3 Signal encoding

Before the information in the MR signal can be visualised it must be registered in three dimensions X,Y, and Z. Spatial encoding of the signal is achieved with three magnetic flux density gradients within the main field (see Figure 4.2). These are known as the slice selection, **frequency encoding** and **phase encoding** gradients and are positioned orthogonal to each other in the main field. When in operation, they have a gradual negative to positive effect on the value of B_0 in three-dimension, producing a characteristic magnetic field strength B_n for each point in

space. Since the magnetic field strength effects precession, the moments at different spatial locations, n, have specific Larmor frequencies, f_n, and phases, p_n. For the purpose of illustration, the gradients are defined here as G_z, G_x, and G_y, respectively. However, in practice the dimension in which each gradient is operated depends on the selected orientation of the image slice (sagittal, transverse, or coronal) and the frame of reference in the magnet.

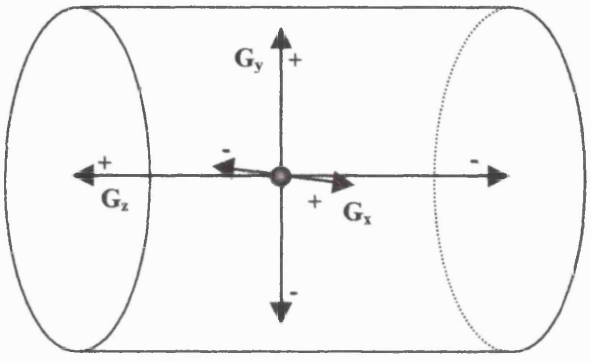

Figure 4.2. The slice selection (G_z), frequency encoding (G_x), and phase encoding (G_y) gradients negatively and positively vary the main magnetic field along their axes. The point at which the three gradients meet and where the effect on B_0 is zero is called the isocentre.

4.3.1 *Slice selection (G_Z)*

When the slice selection gradient is activated, the precessional frequency of moments along its axis is altered in a linear fashion. A slice is then selected by irradiating the sample with the correct range of frequencies that correspond to precessional frequency of moments at the predetermined slice location along the gradient. Only moments located within the slice, in a plane perpendicular to the gradient, are perturbed by the RF pulse such that the signal induced in the coil corresponds to only that slice. Slice thickness is determined by the range of RF frequencies applied (larger frequency ranges give thicker slices), and the size of the applied gradient (stronger gradients give larger frequency differences between adjacent points along the gradient direction). The spacing between slices is

determined by the position of the centre of the B_1 (RF) excitation envelope. In other words, interslice distance is determined by the proximity of subsequent RF pulse ranges.

4.3.2 *Frequency encoding (G_X)*

After slice selection, it only remains to locate the origin of signal in the two-dimensions of the slice. In one of these dimensions, frequency encoding is used. A gradient is applied perpendicular to the slice selection gradient during acquisition of the MR signal, which shifts the precessional frequency of moments in a linear fashion along its direction. Each point along the axis is then represented by its own unique frequency. Since this gradient is applied whilst the signal is being acquired it is also known as the readout gradient. Signal from the readout can be considered a function of time, in that signal sampling has a uniform duration (sampling time) and the interval between sampling is consistent. Eventually, each sampled frequency is allocated a position in the frequency column of K-space (see k-space filling).

4.3.2 *Phase Encoding (G_Y).*

It is now possible to map the signal in two dimensions (x,z), and it only remains to register the final dimension using phase encoding. Once again a gradient, orthogonal to the previous two, is applied and the moments lying along it experience different precessional frequencies. Since precessional speed is proportional to frequency, precessional frequency also varies linearly along the gradient and moments dephase along it in a linear fashion relative to the experienced increase or decrease in speed. Spatial position (y) can then be derived from the different phase steps.

4.4 Image formation

Before the three-dimensionally registered signal can be visualised as, for example a two dimensional x,y image of slice z, the data must be reconstructed. Initially, filtered backprojection methods, as applied in CT, were used (Lauterbur, 1973). More recently these have been superseded by Fourier Transform (FT) techniques (Bracewell, 1978). Typically, the signal information is collected in a 2D k-space **data matrix** (k-space filling) which then undergoes a two dimensional inverse Fourier transformation (2DFT) to map the data into an **image matrix** (this process in summarised in Figure 4.3). The number of element or **pixel** rows and columns in the image matrix is equal to the number of phase and frequency-encoding points analysed, respectively. As each slice has a given thickness, each pixel also represents a volume element or **voxel**.

During k-space filling a vector, k, is defined in relation to steps of the phase encoding gradient and the sampling time of the readout gradient. Signal is allowed to evolve as a function of sampling time (i.e. a FID signal) and is analysed at points k_n, giving $-k_{128}$ to $+k_{127}$. The phase encoding gradient is activated and the new FID at y_n is scanned at the same intervals k_n. This process is repeated for every phase encoding step $-y_{128}$ to $+y_{127}$, giving 65,536 signal collections in k-space. Since the amplitude of the phase encoding gradient changes but the duration remains the same, the data in k-space can be expressed as a function of real time (readout sampling time) and pseudo-time (phase encoding steps). A two-dimensional Fourier transform of the signal in relation to real and pseudo time produces an image.

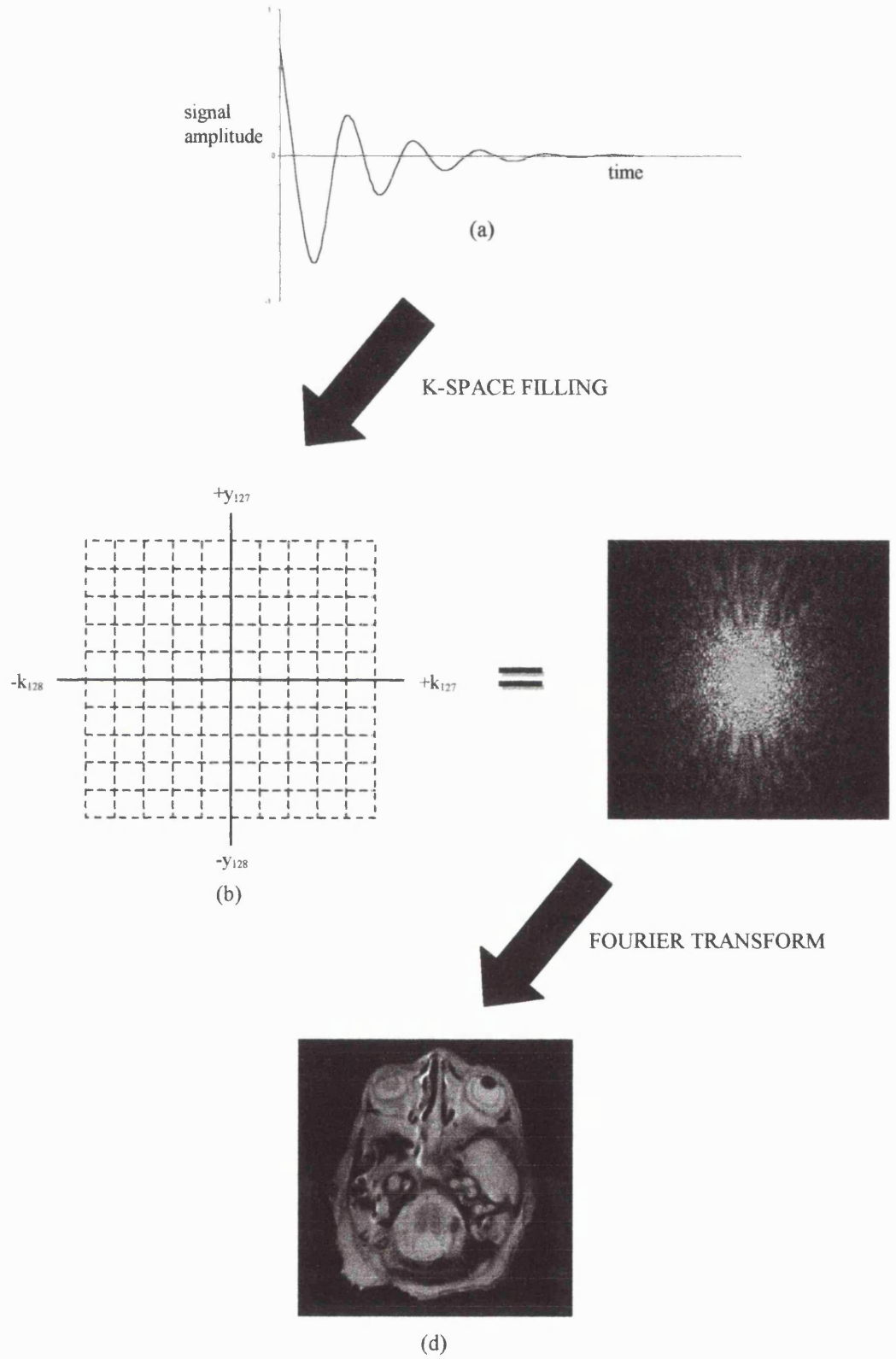

Figure 4.3. The FID (a) data from 256 phase and frequency encodings is mapped into k-space (b) and then undergoes an inverse Fourier transform to form an image (d).

The area of anatomy covered by the image, called the **Field Of View** (FOV), divided by the number of phase and frequency steps gives the **calculated spatial resolution** of the image. For example, with a FOV of 60x60mm and a data matrix of 256x256 (No. phase x No. frequency steps), the image matrix and resolution (size of each pixel) are 256x256 and 0.234x0.234 mm, respectively. Thus, decreasing the size of the FOV or increasing the number of phase and frequency encodings, or both, increases image resolution. Note, however, that the strength and stability of the magnetic field B_0 also limits observed resolution: Inhomogeneities in the magnetic field reduce image contrast and renders smaller objects unresolvable (Callaghan, 1993).

Each point in k-space may be sampled more than once to average out variable noise interference. The number of resamples, called the number of excitations (NEX), determines the amount of data that is average in k-space. The higher the NEX value the more data is collected and averaged in k-space, leading to a better signal to noise ratio (SNR). Note, however, that the improvement in SNR is proportional to the squared root of the number of averages (NEX). Consequently, more and more averages are needed for each subsequent increase in SNR and total imaging times become longer. Alternative techniques for improving SNR include reducing slice thickness and pixel resolution as this increases the number of protons being perturbed in each voxel or changing the imaging parameters to make better use of the protons available in each voxel. Unfortunately, larger voxels or image contrasts produced by changing the imaging parameters are not always desirable in quantitative studies of morphology.

4.4.1 *Contrast Mechanisms.*

Assuming equal proton concentrations, tissues with a large transverse component when the signal is sampled, produce larger signal amplitudes in the coil and the corresponding pixels in the image appear brighter. Conversely, tissues with a small transverse component when the signal is sampled, because the moments have mostly recovered, appear darker.

In general, water and fat provide these extremes of contrast in biological tissue. The hydrogen moments in water have a slightly different chemical environment to those fat, giving rise to different rates of T_1 recovery and T_2 decay: Fats have short T_1 and T_2 times whereas water has long T_1 and T_2 times (see Figures 4.4 and 4.5). Consequently, regions of fat appear dark and regions of water appear bright in images based on the T_2 mechanism, whereas images based on the T_1 mechanisms show the reverse. Tissues, which may also have characteristic relaxation times (see Bottomley *et al.*, 1984), containing intermediate concentrations of fat and water occupy the remaining grey values according to the mechanism analysed.

Proton density contrast is based on the differences in signal intensity observed from tissues containing different quantities of protons per unit volume. Tissues with a high proton density (e.g. grey matter) have a larger transverse component of magnetisation and appear brighter than tissues with progressively lower proton densities.

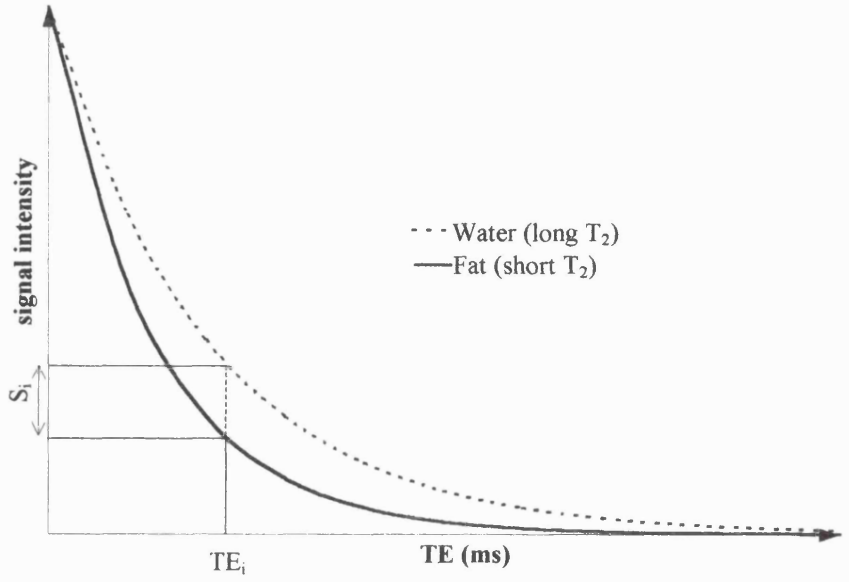

Figure 4.4. Graph showing the difference in signal intensity between fat and water as a function of TE. The intensity difference S_i is the contrast that appears with time TE_i.

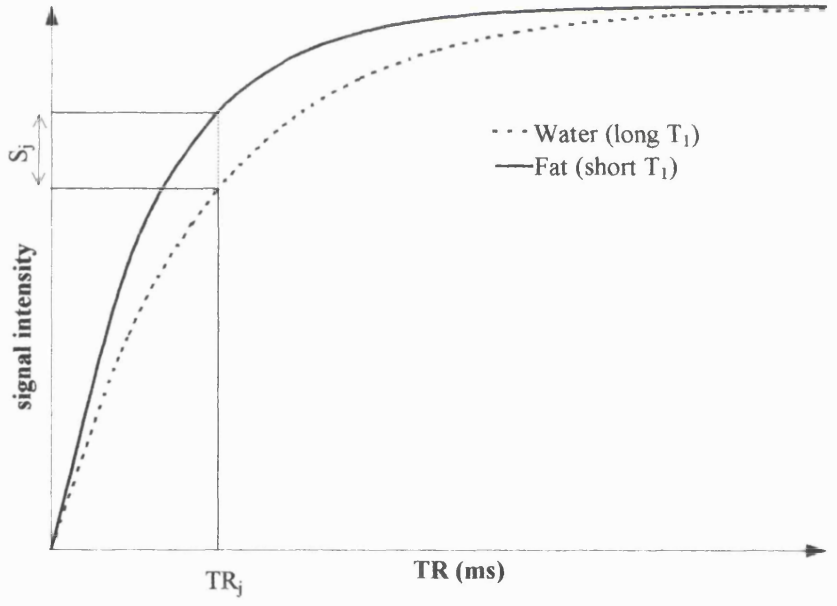

Figure 4.5. Graph showing the difference in signal intensity between fat and water as a function of TR. The intensity difference S_j is the contrast that appears with time TR_j.

4.4.2 *Weighting.*

To demonstrate useful contrast, images can be weighted to favour a particular mechanism by changing the acquisition parameters **TE** and **TR** in the pulse sequence. Following an initial RF excitation pulse in, for example, a spin-echo sequence (see later section), the component of magnetisation in the transverse plane (x,y) from fat moments rapidly diminishes (short T_1 and T_2) into a longitudinal component (z). Conversely, the water moments, which have long T_1 and T_2 times, maintain a transverse component for longer. Provided the time from the excitation pulse to sampling of the signal (time to echo, **TE**), is long enough to allow the moments time to decay at different rates without completely relaxing, there will be a greater contribution by water moments to the signal intensity received by the coil. Therefore, tissues containing larger amounts of water appear brighter in the image than those containing fats. This is known as **T_2 weighting**. The contrast between fat and water as a function of TE is illustrated in Figure 4.4.

If the above sequence is repeated, but the time between the first excitation pulse and the next (repetition time, **TR**) is short enough to allow the moments time to decay at different rates and differentiate without completely relaxing, the fat moments in the longitudinal component will be excited back into a transverse component while the transverse component of water is inverted to a longitudinal component (M_{-z}). Consequently, there is a larger contribution to the transverse component from fat moments than water moments and this is reflected in the signal from the coil. Tissues containing large amounts of fat appear brighter than those containing water in images produced with **T_1 weighting**. The signal differences i.e. contrast between fat and water as a function of TR is shown in Figure 4.5.

Proton density weighting is latently present somewhat in all images and is only expressed completely when T1 and T_2 contrast is suppressed. Increasing the TR time will reduce T_1 image weighting and shorter TE times will diminish T_2 weighting, allowing the proton density weighting to dominate.

4.4.3 *Artefacts*

In quantitative studies of morphology, it is important to be aware of artefacts that may degrade the qualitative (e.g. tissue contrast) or quantitative (e.g. pixel values and spatial positions) information of the image. This section provides a short description of some of the more common artefacts encountered (see Henkelman and Bronskill, 1987 for a review) that can be detrimental to image quality.

Chemical shift artefacts occur where fat and other tissues form borders (Szumowski, 1987). Since frequency is used for spatial encoding, significant difference between the resonant frequencies of tissues containing water and fat can be mistaken as a positional change. Therefore, fat-containing structures may shift in the frequency direction relative to water to form 'ghosting' within the image. This artefact is greater at higher field strengths and lesser at higher gradient strengths, but can be eliminated using fat suppression techniques.

RF overflow produces images with a non-uniform, zero contrast or 'washout' appearance and occurs when the signal received from the sample is too intense to be accurately measured. Decreasing the receiver gain can reduce this effect.

Susceptibility artefacts occur as the result of variations in the magnetic field strength that occur near the interfaces of regions with different bulk magnetic susceptibilities (Shizhe *et al.*, 1994). These cause the dephasing of moments and frequency shifts in the surrounding tissues, producing spatially distorted dark and light patches in the image. Large susceptibility artefacts are commonly seen surrounding ferromagnetic objects inside of diamagnetic materials (biological tissues). These artefacts are accentuated with long TE times and with gradient echo sequences.

Geometric distortion. Since k-space filling relies on linear variations in B_0 produced by the encoding gradients, any inhomogeneities in B_0 and or nonlinearity in the encoding gradients can distort the geometry of image space. For the purposes of morphological studies, there are usually two sources of encoding error, which are machine-dependent and sample-dependent (Michiels *et al.*, 1994). Machine-dependent distortions are caused by main field inhomogeneities, gradient field non-linearity's, and eddy currents induced by gradient switching. These can often be corrected for using phantom calibrations (Sumanaweera *et al.*, 1994). Sample-dependent factors, such as local magnetic field distortions caused by the magnetic properties of the sample (diamagnetism, paramagnetism, and ferromagnetism) are often unique to each particular sample, making it difficult to correct.

Wrap around. This occurs when the size of the specimen in the imaging plane is larger than the FOV. Signal from outside the FOV is folded and mapped onto the opposite side of the image. This can be avoided by increasing the size of the FOV or imaging in a more appropriate plane.

Cross talk and cross excitation. With small interslice separations, the range of slice selective frequencies generated by a pulse occasionally overlap into neighbouring slices. Remnants of signal from previous excitations in other slices may also leak into the target slice. These processes are known as cross-excitation and cross talk respectively and are detrimental to spatial and contrast information.

In multislice experiments interleaving can be used to reduce these problems by exciting slices alternatively rather than sequentially i.e. 1,3,5,7 and then 2,4,6 rather than 1,2,3,4 etc. This limits the amount of signal that can leak into the target slice and overlap by increasing the distance between successive slices.

Interference from preservative fluids. The relaxation characteristics of wet preserved tissues often change according to the type of solute, the amount of water in the solution, and how long tissue has been in solution (see Thickman *et al.*, 1983; Isobe *et al.*, 1994). This can lead to a reduction in image contrast, particularly with strong ethanol/methanol solutions: as the solute penetrates the tissue, the T_1 and T_2 times of different tissues tend towards those of the solute. Consequently, concentrated solutions should be avoided, especially with T_2 weightings. Often the process can be partially reversed by placing the specimen in a weaker solution, such as formalin (10% formaldehyde, 90% water).

4.5 Basic Spin-Echo sequence

The spin echo (Hahn, 1950) pulse is the basis for many imaging sequences and can be used to produce T_1, T_2 or proton weighted images. The sequence can be broken into four periods, as shown in Figure 4.6 (see Hendrick and Osborn, 1988).

Period A: The longitudinal component of magnetisation is flipped into a transverse component by exposing the sample to a 90° RF pulse in the presence of a slice selection gradient (rG_z).

Period B: The phase-encoding gradient(G_y) and two compensatory gradients are applied (cG_z and cG_x). The negative compensatory gradient (cG_z) rephases those moments dephased by the slice selection gradient during period A. Phase is further adjusted by a second compensatory gradient (cG_x) to maximise phase coherence during the sampling period D.

Period C: Moments which dephase due to inhomogeneities in the magnetic field are rephased by a 180° refocusing pulse. This is applied after time TE/2, flipping the slower moments that are furthest behind in the precessional path in front.

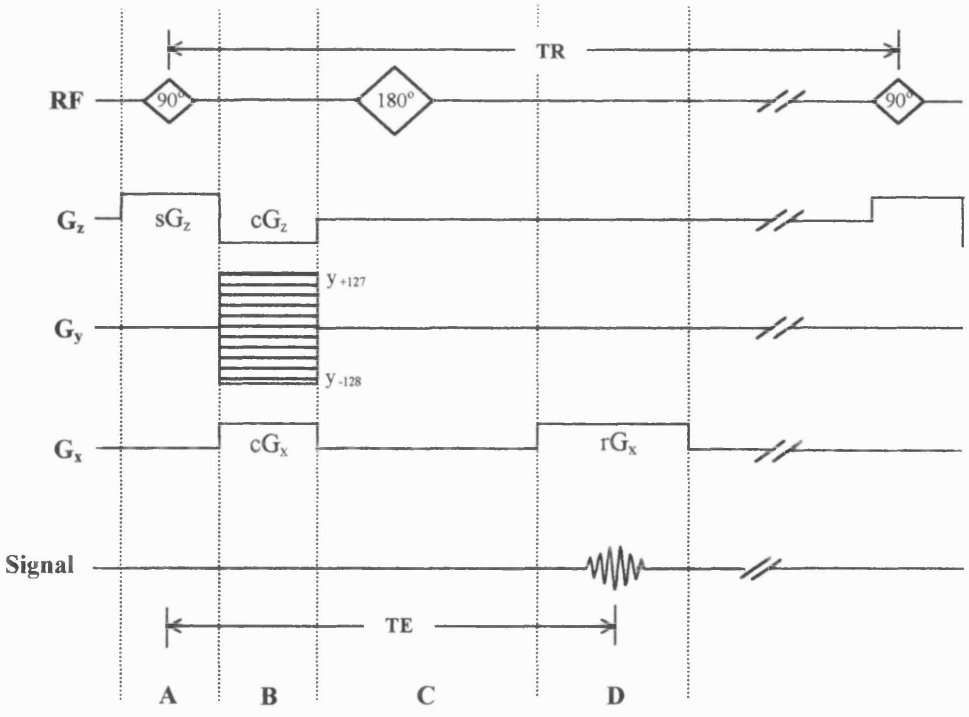

Figure 4.6. The spin echo sequence. Description and notation are given in the main text.

Period D: Phase coherence is regained an additional time period TE/2 after the 180° pulse as the faster moments catch up with the slower ones. The readout gradient (rG_x) is applied and the signal (echo) is sampled

T1 weighted images can be produce with the spin echo sequence using short TE and TR times. The short TE time ensures that the echo occurs before the T2 decay mechanism dominates and the short TR prevents water and fat fully recovering. Longer TE and TR can be used to provide T_2 weighted images. The longer TE used in T_2 weighting compared with T_1 weighting allows fat and water to differentiate between the transverse and longitudinal components without relaxing completely. A long TR is used to ensure all spins have completely recovered to the longitudinal component before the spin-echo is repeated, thereby diminishing the effect of underlying T_1 differences between tissues. Proton density images can be obtained with long TR and intermediate TE, which ensures the signal is sampled after the T_1 mechanism dominates and before the T_2 mechanism dominates. The relative TE and TR times for different spin echoes are shown in Table 4.1.

		TE	
		Short	Long
TR	Short	T_1 weighted TR = 500 TE = 11	
	Long	Proton weighted TR = 2700 TE = 20	T_2 weighted TR = 2700 TE = 90

Table 4.1. Typical TE and TR times in milliseconds for T_1, T_2, and proton image weightings

4.6 Volume imaging

Although previous sections have described MR in relation to the acquisition of discrete slices, the same principles can be applied to the acquisition of an entire volume. The RF pulse is used to excite moments throughout a specified volume and the acquired data can be subsequently re-sliced at will. Typically, spatial information is encoded along the slice direction (z) of the volume by applying a second, or supplementary, phase encoding gradient instead of the slice selection gradient G_z, though there are a number of other arrangements (see Foster and Hutchison, 1987). In effect, the compensatory slice selection gradient cG_z shown in Figure 1.39 is replaced by a similar gradient to the phase encoding gradient. As in two-dimensional acquisitions, the readout gradient is applied during sampling and the two phase encoding gradients are applied, usually simultaneously, during period B. After acquisition, the data can be divided into discrete voxels, slabs, or slices as required. The two main advantages of the technique are that image data can be resliced into almost any plane and SNR is greater because slice thickness is effectively the same as the z dimension, i.e. a greater number of moments are perturbed. The major drawback of the technique are that increments of each phase encoding gradient must be independent and consequently imaging times increase (see Foster and Hutchison, 1987; Westbrook and Kaut, 1993 for further details).

4.7 Instrumentation

4.7.1 *Magnets*

There are three basic types of magnet that are used to provide the magnetic flux B_0; resistive, permanent, and superconducting. Resistive magnets consist of

insulated wires, usually anodised aluminium or copper, wound around a central core. When a current is passed through the coil a magnetic field is induced along the z axis of the core and thermal energy is produced. Water cooling is essential to remove the thermal energy from the system and maintain a consistent state. The major drawbacks of this type of magnet are the low field strengths produced and its instability. Permanent magnets, on other hand, are constructed from materials exhibiting magnetic properties and as such do not require power or cooling. A simple cylindrical structure is formed from the material, producing a field along its central bore. Field strengths are limited to about 0.4T and consequently contrast levels are not always acceptable. Perhaps the commonest magnets used at present are superconducting magnets. These can produce large stable magnetic fields in excess of 2T. Typically, windings of low resistance materials like niobium-tin are cooled below their critical temperature range using liquid helium (4.2K) to maintain their superconducting properties. A second cryogenic jacket containing liquid nitrogen (77.4K) surrounds the helium tank to act as a thermal buffer between room temperature (about 293K) and the liquid helium. Once a field has been established with a current, it will persist until the temperature exceeds a critical value, at which point quenching occurs.

4.7.2 *Gradient Coils.*

The gradients coils used for spatial encoding are constructed around the central sample bore. The numerous different designs include the Maxwell pair, Golay set and the quadruple set. Typically, a Maxwell gradient is used for the long z axis (G_z) and four sets of Golay gradients are used for the x and y axis (G_x and G_y). In their basic form, field production is relatively inefficient and concentrates around

areas near the surface of the cylinder where the wires are in close proximity. Such non-linear field concentrations alter the electromagnetic properties of the coil, reducing the coils ability to switch rapidly and increasing the minimal value of the pulse sequence parameters TE and TR. These effects are minimised in modern gradients by distributing individual wires over the surface of the cylinder rather than bunching them.

4.7.3 *Shimming Coils*

In practice, it is almost impossible to create a completely homogenous magnetic field and shimming must be used. These are either metallic bars empirically fitted into the coil to compensate for static variations (passive shims), or windings that actively compensate for inhomogeneities.

4.7.4 *Radio-Frequency Coils.*

Perhaps the most critical component in MRI is the RF coil used for irradiating the sample and receiving the signal. While it is possible to use one coil for both RF operations, the complexities of the switching systems required at high frequencies can generate transient RF interference and consequently separate coils are often used for each operation.

The orientation of the field, B_1, produced by the RF coil relative to the main magnetic field is critical to the process of excitation. Coils are usually designed so that the RF field is formed perpendicular to B_0, thereby inducing moment excitation. The RF power (P) needed to excite moments is a function of the effective coil volume (V) and coil tuning quality (Q),

$$P = 2\omega B_{xy}^{2} V/ \mu_0 Q$$

Where μ_0 is the equilibrium state of the moments, and V and Q describe the filling and quality factors of the coil. The quality factor defines how sharply the coil is tuned and is dependent on the resistive properties of the coil and the sample. Large samples posses substantial eddy currents that degrade the Q-factor of the coil and lower SNR. Smaller samples provide greater Q-factors but produce lower signal intensities. Small coils have greater filling factors, because the sample takes up a greater proportion of the coil volume, and receive a greater signal intensity for a given number of proton moments. The four basic types of coil, the helmholtz, bird cage, surface, and saddle are shown in Figures 4.7

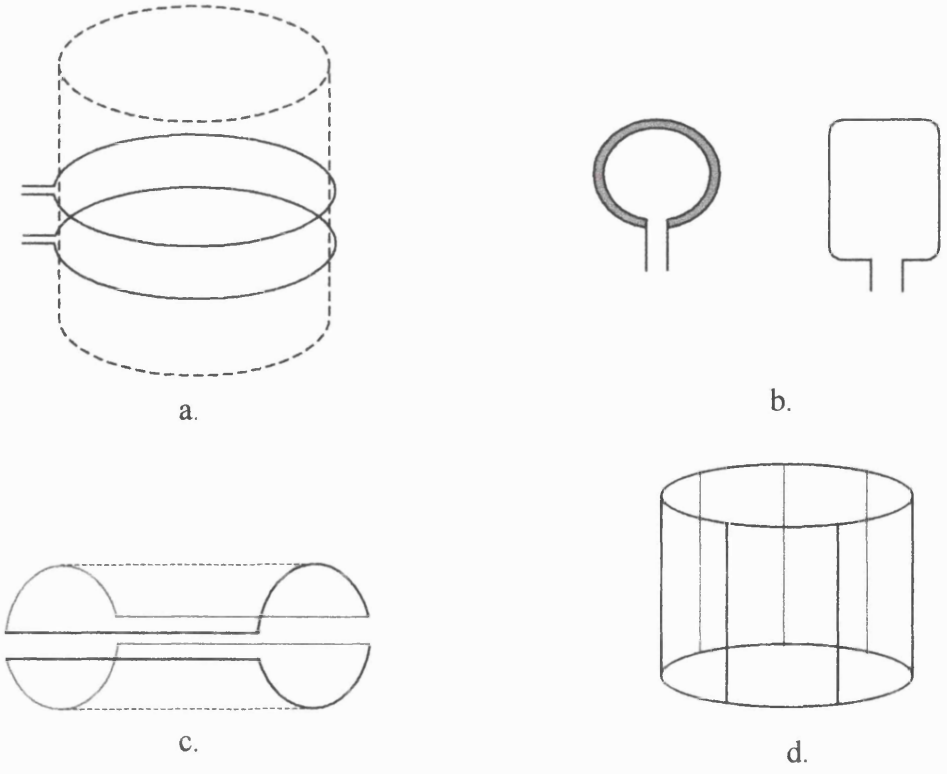

Figure 4.7. Illustrations of the RF coils often used MRI: (a) Helmholtz pair coil, (b) surface coils, (c) paired saddle coil, (d) bird cage coil.

CHAPTER 5. METHOD AND MATERIALS

5.1 Fetal sample

Hypotheses were tested with measurements from high-resolution magnetic resonance images of 42 formalin preserved humans fetuses of diverse age and undetermined sex (see Table 5.1 and Figure 5.1). Specimens were either natural or therapeutic abortuses and were obtained from the Department of Anatomy and Developmental Biology, University College London, and the Department of Anatomy, Queen Mary and Westfield College London. Fetal ages (weeks) were calculated using crown-rump length (Streeter, 1920), mean foot length (Streeter, 1920), and biparietal diameter (Campbell and Newman, 1971). Age estimates for partially dissected fetuses are based on the measurements available.

Although each specimen was carefully screened for signs of pathology before imaging, four specimens were excluded from the study based on abnormalities seen in hrMR images. The cranial vault and frontal bone was deformed in N55, the orbit was asymmetrically deformed in E9 (possibly an orbital encephalocele due to neurofibromatosis; see Bruwer, 1955), the cerebrum was pathologically convoluted in O11A, and basioccipital was warped in E84. Thus, the total number of fetuses studied was thirty-eight.

Table 5.1. Biparietal diameter (BP), crown-rump length (CRL), foot length (FL) in millimetres (mm), and calculated age (weeks) for the fetuses imaged.

I.D.	Source	CRL	FL	BP	Age: CRL[1]	Age: FL[1]	Age: BP[2]	Mean	Sample S.D.
10WM	UCL	53	7.7	15.9	11	11	N/A	11.0	0.0
NE20	UCL	70	10.0	20.5	13	12	N/A	12.5	0.7
QMWF49	QMW	70	10.5	18.8	13	13	N/A	13.0	0.0
N55†	UCL	90	13.2	24.3	14	14	13	13.7	0.6
QMWF7	QMW	90	14.0	24.0	14	14	13	13.7	0.6
QMWF34	QMW	87	13.7	25.5	14	14	14	14.0	0.0
12WM	UCL	95	16.0	28.0	15	14	14	14.3	0.6
E9†	UCL	N/A	17.2	27.3	N/A	15	14	14.5	0.7
011A†	UCL	100	16.0	31.8	15	15	15	15.0	0.0
14WM	UCL	104	20.0	33.9	15	16	15	15.3	0.6
E2	UCL	N/A	19.5	33.6	N/A	16	15	15.5	0.7
NS5	UCL	118	21.0	32.6	16	16	15	15.7	0.6
E4	UCL	120	24.0	36.2	16	17	16	16.3	0.6
E5	UCL	125	22.0	33.4	17	17	15	16.3	1.1
Z101	QMW	130	23.7	35.1	17	17	16	16.7	0.6
N6	UCL	145	24.0	36.3	18	17	16	17.0	1.0
QMW28	QMW	135	26.5	40.1	17	18	17	17.3	0.6
E147	UCL	148	26.0	39.9	18	18	17	17.7	0.6
E72	UCL	143	26.0	39.1	18	18	17	17.7	0.6
E93	UCL	145	30.0	36.9	18	19	16	17.7	1.5
QMW35	QMW	138	25.0	40.2	18	18	17	17.7	0.6
Z102	UCL	130	25.0	42.8	17	18	18	17.7	0.6
E84†	UCL	N/A	N/A	44.3	N/A	N/A	18	18.0	0.0
N50	UCL	143	32.0	40.8	18	20	17	18.3	1.5
E109	UCL	155	31.0	45.2	19	19	18	18.7	0.6
N22	UCL	160	31.0	41.0	20	19	17	18.7	1.5
E102	UCL	157	33.5	43.6	19	20	18	19.0	1.0
NS70	UCL	155	31.7	48.2	19	19	19	19.0	0.0
N30	UCL	160	32.0	44.4	20	20	18	19.3	1.1
NS71	UCL	160	33.0	42.7	20	20	18	19.3	1.1
ZN1	QMW	159	34.0	44.9	20	20	18	19.3	1.1
NS15	UCL	N/A	33.0	48.1	N/A	20	19	19.5	0.7
20WM	UCL	160	31.0	49.8	20	19	20	19.7	0.6
E20	UCL	180	34.0	49.0	21	20	20	20.3	0.6
E58	UCL	171	34.0	49.9	21	20	20	20.3	0.6
E6	UCL	N/A	36.5	50.9	N/A	21	20	20.5	0.7
E167	UCL	180	37.0	54.1	21	21	21	21.0	0.0
N12	UCL	180	40.0	50.4	21	22	20	21.0	1.0
NS92	UCL	185	39.0	53.0	22	22	21	21.7	0.6
N1	UCL	186	41.0	53.2	22	23	21	22.0	1.0
E90	UCL	193	41.0	55.4	23	23	22	22.6	0.6
E64	UCL	205	44.0	55.9	24	24	22	23.3	1.2

† Excluded from study on the basis of dysmorphology observed in the hrMR images.
UCL, University College London.
QMW, Queen Mary and Westfield College.
[1] Calculated with data published by Streeter (1920).
[2] Calculated with data published by Campbell and Newman (1971).

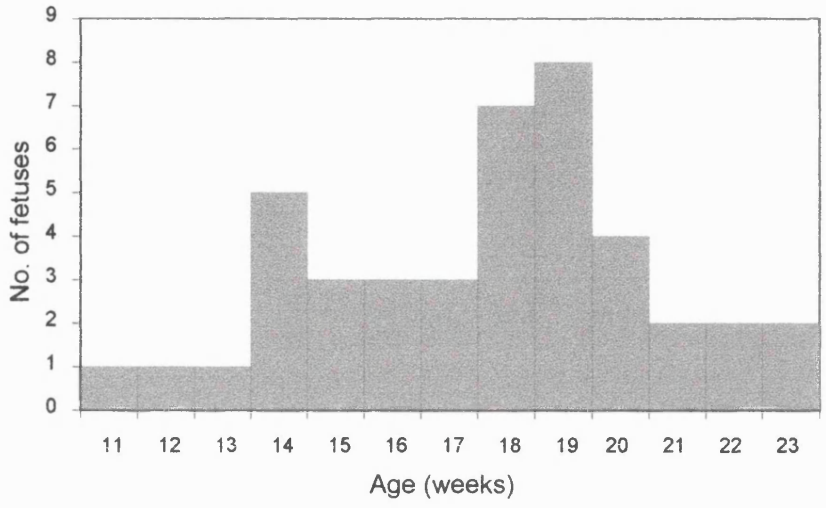

Figure 5.1. Bar graph showing the approximate age distribution of the fetuses imaged.

5.2 hrMRI Imaging

Fetal specimens were imaged using high-resolution magnetic resonance imaging (hrMRI). This technique uses magnetic fields in the region of 4 to 8 Tesla and gradient strengths of about 0.1 Tesla per metre (Tm^{-1}) (N.B. microimaging gradients can go up to $2Tm^{-1}$), as opposed to 2 Tesla and 0.01 Tm^{-1} in medical MRI. These provide better field homogeneity, and thus better magnetisation coherence and SNR, and better spatial sensitivity. Resolutions and slice thicknesses produced are in the order of tenths of a millimeter. While the instrumentation is similar to that used in MRI microscopy for the study of embryos (see Effman *et al.*, 1988; Johnson *et al.*, 1993; Smith *et al.*, 1994), hrMR images are less resolved because larger FOVs and coils are required to image fetuses as opposed to embryos.

A limitation, as with most high-resolution techniques like micro-CT, is that hrMRI requires long imaging times (typically 20hrs per fetus). Consequently,

the technique is not, at its current stage of development, suitable for the type of in vivo studies conducted with conventional MRI (Weinreb *et al.*, 1985; Powell *et al.*, 1988; Girard *et al.*, 1993; Colletti, 1996).

5.2.1 *Instrumentation*

The magnet used here was a 4.7 T, horizontal bore (Oxford 200/330 MkII), superconducting magnet developed by Oxford Instruments ltd (UK) for imaging and chemical spectroscopy. Resonance frequency of ^{1}H moments in this field is 200MHz ($B_0.\gamma$). The console used was an SISCO-200 (Varian-Siemens, Palo Alto, USA). Image data was acquired and processed using a Super Workstation 5 (SPARC 5 clone: Goss Scientific, UK) and Varian VnmrX_5.1a software. A fifteen channel active shimming coil was used (Oxford Instruments, Witney, UK) to correct for field inhomogeneities.

A high power 18 accessory gradient (hpag) coil insert was used rather than the standard gradient set (std33: 2 Gcm^{-1}), to provide higher gradient strengths. Performance and physical specifications of this gradient are as follows. Maximum gradient strength of 100mTm^{-1}; rise time (from zero to maximum strength) of 0.512 ms; bore size is 12cm (internal diameter); length is 189cm; and maximum duty cycles are 50%, 20%, and 10% at 3 mTm^{-1}, 4 mTm^{-1}, and 7 mTm^{-1} respectively.

Two ^{1}H RF coils were used according to specimen size. For larger fetuses, an 8.8cm (internal diameter) saddle coil, with an active volume of about 150 cm^3, was used. Smaller specimens were imaged using a 6.2cm (id) birdcage coil with an active volume of approximately 100 cm^3.

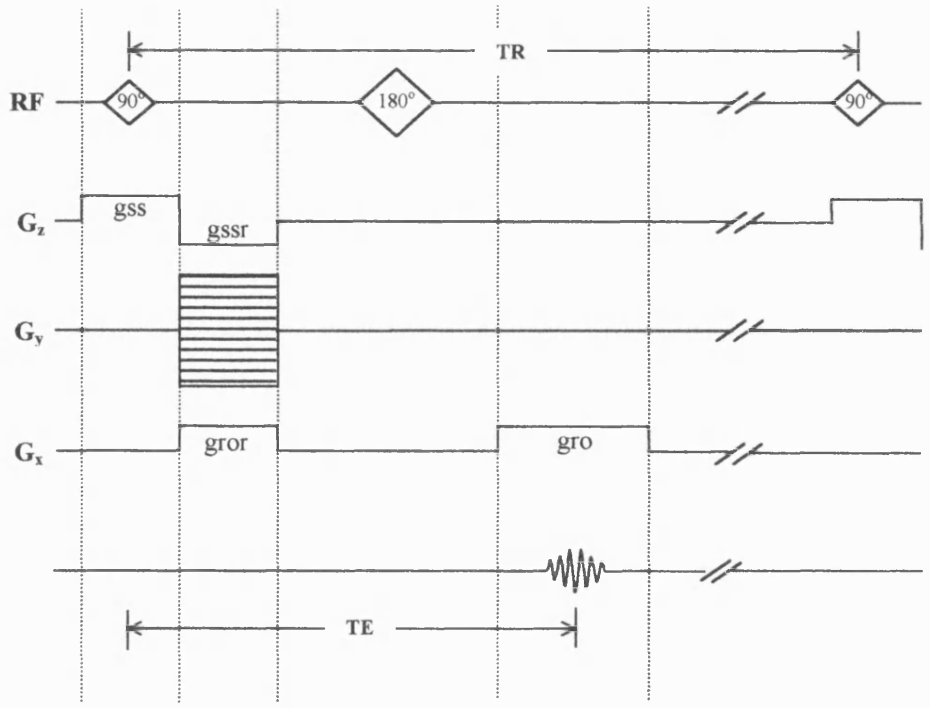

Figure 5.2 . Schematic of the multislice spin echo pulse sequence: *TE*, echo time; TR, repetition time = no. slices * inter-sequence timings; *gror*, readout compensation gradient; *gro*, readout gradient; *gss*, slice selection gradient; *gssr*, slice refocus gradient.

5.2.2 *Imaging protocol*

The pulse sequence used in this study was a Spin Echo Multislice Sequence (SEMS) (Figure 5.2). It was used to provide basic spin warp imaging (Edelstein *et al.*, 1980) with a 180° refocusing pulse and was T_2-weighted to maximise image contrast between the ossifying skull and formalin solution (>70% water) within the endocranial space. Preliminary experiments with different values of TE indicated that times in the region of 40msecs provided the most effective image contrast. Note that the time available on the instrumentation was limited and therefore TE was not adjusted for each subsequent specimen.

Each fetus was sealed into durable plastic and placed within a suitably sized RF coil, making sure it was probable centred and secured with foam blocks. Gradient strengths and FOVs were selected to maximise resolution whilst maintaining the

ratio between slice thickness and pixel size at 2:1. This ratio simplifies interpolation of the image data. The four different parameter set-ups used are presented in Table 5.2. Slice gradient offset (Hz) and transmitter frequency offset (Hz) were adjusted to ensure the longitudinal axis of the fetal head was covered by the selected number of slices and that the signal under the influence of the readout gradient was centred within the FOV. A pilot scan of 32 phase encodings was used to check the position of the sample and to give a preliminary indication of image contrast and SNR. Power levels for the 90^0 excitation and 180^0 refocusing pulse were calibrated. Typical values for the saddle and birdcage coil were in the region of 75 and 87, and 61 and 73 dB respectively.

Imaging was performed with 24 averages to maximise SNR and slices were taken from interleaved points to minimise cross talk and cross excitation. Resolutions and slice thickness achieved with the apparatus and FOVs are shown in Table 5.2. Calculated slice thickness was checked against the width of the slice selection frequency profile (Hz) to the nearest tenth of a millimetre.

Table 5.2. Parameters and resolutions achieved for each set-up .

FOV (mm)	COIL	Slice selection gradient (mTm^{-1})	Frequency bandwidth in read out dimension (Hz)	Phase encoding frequency bandwidth (Hz).	No. phase encoding steps.	No. frequency encoding steps.	In-plane resolution (mm)	Slice thickness (mm)
80x80	S	33.2	51085.6	851.5	256	256	0.31x0.31	0.62
64x64	S	42.5	40858.0	681.2	256	256	0.25x0.25	0.50
50x50	B	52.8	31923.4	532.2	256	256	0.20x0.20	0.40
40x40	B	66.4	25542.8	425.8	256	256	0.16x0.16	0.32

S = 88mm internal diameter saddle coil.
B = 62mm internal diameter bird-cage coil.

5.2.3 *Post-acquisition image processing*

Once data was acquired it was converted into image space with a two-dimensional Fourier Transform (2DFT) and stored sequentially in a raw 16bit format. Subsequently, pixel depth was reduced using Xdispimage (Dave Plummer, Middlesex Hospital, London) to 8bits (65536 to 256 greys) in order to reduce the computational load placed on the analysis software (AVS5: Advanced Visual Systems, USA). While reducing pixel depth destroys some of the quantitative information (i.e. pixel values), it had no effect on the visual cues required to identify landmarks or the spatial position of landmarks.

Further analysis was carried out using AVS5. In the first instance, images were interpolated (tri-linear interpolation) along the slice direction (x:y:z, 1:1:2) to produce an isometric block of image data consisting of 256x256x256 voxels. The block was passed through three transformations and three rotations (one for each dimension) to allow the frame of reference to be standardised. Landmark co-ordinates and volume measurements were taken from the orthogonally re-sliced images (transverse, sagittal, and coronal).

5.2.4 *Image measurement*

Prior to measuring, the image block was rotated (ip-rotate and translate modules) so that foramen caecum and sella were level in the sagittal plane and the petrous pyramids were level in the coronal plane. Landmarks and pixel areas for volume measurements were located by reslicing the image block orthogonally and examining the relevant planes. Regions of interest (ROI) for volume measurement were outlined manually using the ip-ROI module. The number of pixels in the ROIs were counted with the statistic module.

Three co-ordinates were taken for each landmark, two in plane and slice number. Since the AVS5 modules described only provide a two-dimensional frame of reference and slice number, each set of two-dimensional landmark co-ordinates and slice number were transformed into a standard three-dimensional frame of reference (x,y,z). The new transformed co-ordinates in this space are given according to the slice plane as,

$$x = y_{sagittal}/y_{coronal}/\text{slice no.}_{transverse}$$

$$y = \text{slice no.}_{sagittal}/x_{coronal}/x_{transverse}$$

$$z = x_{sagittal}/\text{slice no.}_{coronal}/y_{transverse}$$

Since individual landmarks were often identified in more than one slice, co-ordinates were taken from the slices best representing the landmark. These were averaged to produce a mean set of co-ordinates for each landmark. Mean landmark co-ordinates were used to calculate (co-ordinate geometrics) linear and angular measurements in three-dimensions. Often computation was simplified by collapsing the co-ordinates into two-dimensions. This was achieved by removing the dimension in which the difference between landmark co-ordinates was negligible and allows measures to be taken in a manner comparable to that used in key previous studies. A limitation with using co-ordinates as opposed to manual measurements is that lines fitted through landmarks can not be physically projected forwards or backwards to take angular measurements at their intersect. Consequently, the angle of intersect between two remote lines, each being defined by two landmarks, was calculated by mapping one line onto the other (target) to form the desired intersect.

This process is illustrated in Figure 5.3 and gives new co-ordinates (x',y',z') for the mapped landmark as,

$$x' = x_b + (x_c - x_a)$$

$$y' = y_b + (y_c - y_a)$$

$$z' = z_b + (z_c - z_a)$$

This new set co-ordinates, together with the co-ordinates describing the target line, were used to calculate the angle of intersect using, for example,

$$\phi = \cos^{-1}\left\{\frac{[(x_a-x_b)^2+(y_a-y_b)^2+(z_a-z_b)^2] + [(x_b-x')^2+(y_b-y')^2+(z_b-z')^2] - [(x_a-x')^2+(y_a-y')^2+(z_a-z')^2]}{2*\sqrt{[(x_a-x_b)^2+(y_a-y_b)^2+(z_a-z_b)^2]}*\sqrt{[(x'-x_b)^2+(y'-y_b)^2+(z'-z_b)^2]}}\right\}$$

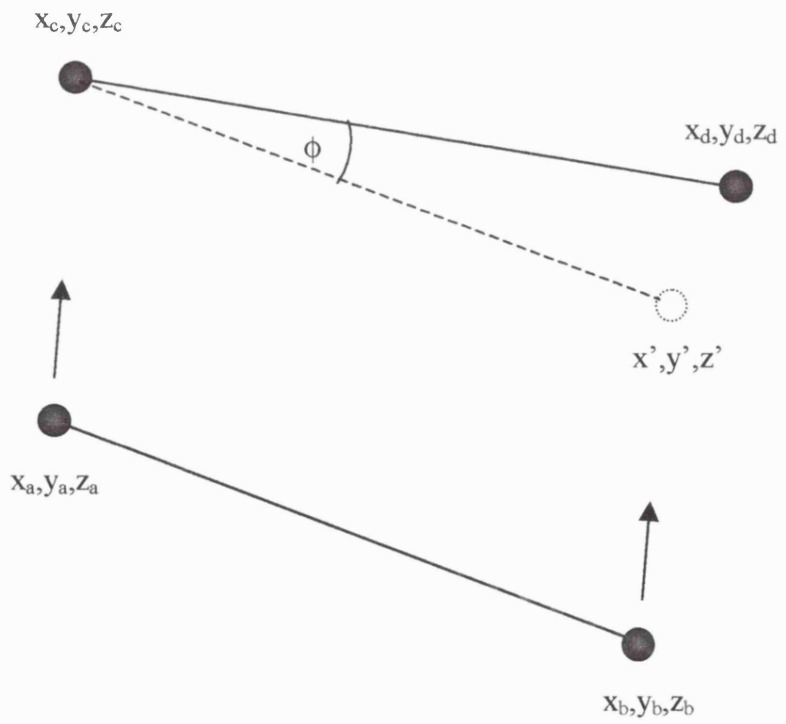

Figure 5.3. Sketch showing the geometric coordinate transformation process to determine the angle of intersect, ϕ, between two remote lines.

5.2.5 *Tests of measurement reliability and accuracy*

Repeatability and accuracy of the techniques used to take linear, angular, and volume measurements were tested by replicating each measure and with the test phantoms shown in Figures 5.4.

The reliability of taking volume measurements from every-other as opposed to every slice (see section 5.3.9) and the procedures used to take linear and angular measures were evaluated by replicating measurements in four randomly selected fetuses five times over five consecutive days. One observer made all replicated measurements. Note, however, that imaging system precision was not tested because it was impractical to re-image each fetus five times. Nonetheless, according to Varian NMR systems, normal system variation is in the region of 0.2% (A. Rath, imaging product manager, UK: pers. comm.) and is unlikely to be significant in the present study. Each group of replicated measures was tested with a one-way analysis of variance (ANOVA). These are presented in Table 5.3 and show that in comparison to the biological variation between individuals, the error incurred among repeated measurements is negligible. In other words, the null hypothesis that values for repeated measurements from one individual are the same is accepted ($P<0.05$).

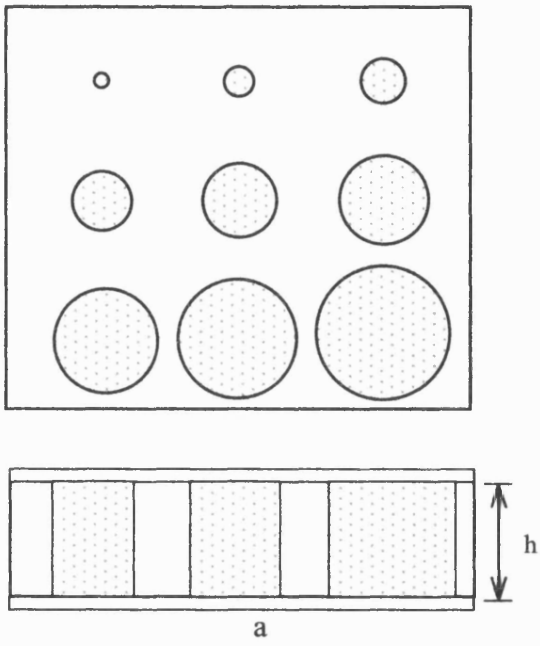

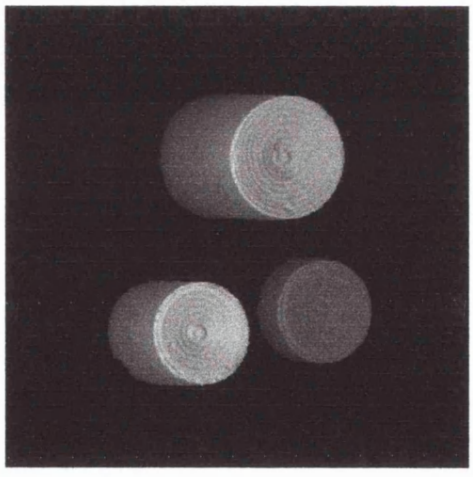
b

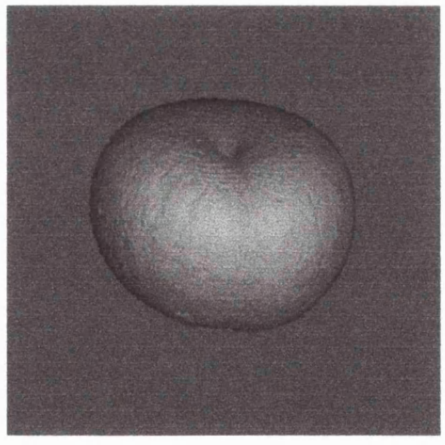
c

Figures 5.4. Phantoms used to test linear and volume accuracy: (a) superior and lateral diagrammatic representation of the phantom containing fluid filled chambers ranging from 1-9mm in diameter and 19.2mm high; (b) volume rendered construction of the syringes used to test volume accuracy; (c) volume reconstruction of the Victoria plum used to provide a more biologically analogous test of volume accuracy.

Table 5.3. Measurement error: results of one-way ANOVA of linear, angular and volume measurements (n=20, k=5; $F0.001_{[3,16]}$=9.0, $F0.01_{[3,16]}$ =5.29, $F0.05_{[3,16]}$=3.24)

Measurement	MS within groups	MS between groups	F	P
Anterior cranial base length	0.125	52.167	417.333	P<0.001
Posterior cranial base length	0.022	20.574	924.674	P<0.001
Total cranial base length	0.105	160.467	1531.908	P<0.001
Posterior cranial fossa length	0.135	77.831	576.523	P<0.001
Posterior cranial fossa width	1.189	114.901	96.636	P<0.001
Interorbital distance	0.041	3.344	81.561	P<0.001
Relative Interorbital distance	0.000	0.004	99.922	P<0.001
Maxillary height	0.098	29.693	302.985	P<0.001
Palate length	0.616	28.498	46.281	P<0.001
Cranial base angle	1.851	49.198	26.579	P<0.001
Spheno-occipital angle	3.385	216.068	63.826	P<0.001
Maxillary angle	3.455	26.407	7.643	P<0.01
Orbito-palatine angle	0.709	33.244	46.922	P<0.001
Palate orientation	1.444	57.123	39.566	P<0.001
Orbital axes orientation	0.677	113.565	167.686	P<0.001
Orbital rim orientation	1.457	57.230	39.286	P<0.001
Interorbital angle	2.927	229.023	78.238	P<0.001
Tentorial angle	0.319	6.822	21.385	P<0.001
Petrous pyramid orientation	3.520	62.721	17.817	P<0.001
Endocranial volume ($x10^{-3}$)	0.608	3265.894	5367.342	P<0.001
Supratentorial volume ($x10^{-3}$)	0.479	2669.377	5571.894	P<0.001
Infratentorial volume ($x10^{-3}$)	0.057	30.148	524.501	P<0.001
Midline area ($x10^{-2}$)	4.061	14458.750	35.606	P<0.001

Accuracy of linear measures taken from hrMRI images were tested using a phantom (Figure 5.4a) similar to those used in previous MRI accuracy studies (Zhu *et al.*, 1986; Clifford *et al.*, 1988; Clifford *et al.*, 1990; Prott *et al.*, 1995). It is constructed from a clear acrylic block (rapid T_1 and T_2 relaxation) with nine chambers ranging from approximately 1 to 9 millimetres in diameter and 19.2mm ± 0.1 high. These chambers were filled with a 5mM solution of copper (II) sulphate pentahydrate ($CuSO_4.5H_2O$), with a formula weight of 249.68. Typical relaxation times for this solution are in the region of 160ms for T_1 and 100ms for T_2 at a frequency ~10Mhz (Zhu *et al.*, 1986). The smallest linear measure in this study is in the region of 5mm (interorbital distance) and thus linear accuracy was assessed with

chambers 5 to 9 and height. Diameter measurements were taken four times at 90-degree intervals around each chamber. Mean diameters measured from the hrMR images for each FOV are compared with micrometer readings in Table 5.4.

Table 5.4. Linear errors determined using the box phantom for each FOV.

FOV (mm)	hrMRI error	Micrometer readings † 5.1	6.2	7.2	8.2	9.2	19.2
40x40	Diameter	5.2	5.9	7.1	8.4		
	Error	+0.1	-0.3	-0.1	+0.2		
	%Error	2.0	4.8	1.4	2.4		
50x50	Diameter	4.8	5.8	7.2	8.4		
	Error	-0.3	-0.4	0.0	+0.2		
	%Error	5.9	6.5	0.0	2.4		
64x64	Diameter			6.9	7.6	9.7	18.8
	Error			-0.3	-0.6	+0.5	-0.4
	%Error			4.2	7.3	5.4	2.1
80x80	Diameter			7.8	8.4	8.5	18.7
	Error			+0.6	+0.2	-0.7	-0.5
	%Error			8.3	2.4	7.6	2.6

† Means of five micrometer readings (± 0.1)
Diameters were taken as the mean of four measurements to the nearest tenth of millimetre.

Volume accuracy was assessed in two stages. In the first instance, accuracy was evaluated using 10ml syringes containing 1,2,4,6 and 8ml of copper (II) sulphate pentahydrate solution (5Mm), see Figure 5.4b. Non-uniform pixel areas were formed by reslicing data obliquely, approximately 15 degrees relative to the longitudinal axes of each syringe. Real and measured volumes are compared in Table 5.5.

A second limited, but more biologically analogous evaluation of volume accuracy and a validation of the every-other slice method as opposed to every slice was made using a Victoria plum (*Prunus domestica*; see Figure 5.4c) and the brain of a formalin preserved sheep fetus (*Ovis aries).* Volumes calculated using every slice and every-other slice for both the brain and plum are compared with measured values (water displacement in a high-grade cylinder) in Table 5.6.

Table 5.5. Volume errors determined using the syringe phantom for each FOV. Volume measurements given in cubic millimetres.

FOV (mm)	hrMRI error	Syringe volumes 1000	2000	4000	6000	8000
40x40	Volume	1020	2030	4160		
	Error	+20	+30	+160		
	%Error	2.0	1.3	3.9		
50x50	Volume	1030	2030	4160		
	Error	+30	+30	+160		
	%Error	2.8	1.4	4.1		
64x64	Volume			3900	5990	8010
	Error			-100	-10	+10
	%Error			2.6	0.2	0.1
80x80	Volume			4060	5950	8050
	Error			+60	-50	+50
	%Error			1.4	0.9	0.7

Table 5.6. Biological validation of every other slice method for calculating volumes and evaluation of accuracy. All volume measurements are in cubic millimetres.

Phantom	FOV	Volume # 1	Volume # 2 every slice	Volume # 3 every other slice	Difference #2 -#3	Error for every other (#1-#2)	% Error for every other
Plum	80x80	44890	43810	43710	100	-1180	2.6
Brain	64x64	7050	6900	6940	40	-110	1.6

These comparisons show that linear and volume errors are in the region of 0.0 to 0.7mm (mean of 0.34mm) and 10 to 1180mm^3 (mean of 136.4mm^3), respectively. Errors are determined by the FOV used and the size of the phantom. In general, linear errors are in the region of one to three times pixel resolution and both linear and volume errors are variable enough to make any significant compounding unlikely. While linear errors seem high, it should be noted that the phantom measurements made are smaller than most taken during this study, measurements from younger specimens are taken using the smaller FOV , and that the ANOVA study indicates that such errors are insignificant compared with differences between

individuals. Mean squares between groups are considerable greater than the errors reported here (see Table 5.3). These tests also reveal that the difference between the every-other and every slice method of estimating endocranial volume is in the region of 40-100mm^3 or 0.2 - 0.5% and is therefore negligible. These findings demonstrate that the imprecisions and inaccuracies encountered in this study are unlikely to have any significant effect on the results reported.

5.3 Morphometry

In order to test the hypotheses outlined in the introduction, suitable measures of basicranial morphology, brain volumes, and sagittal orientation of the tentorium cerebelli were selected. In the past, basicranial architecture has typically been quantified with either line segments fitted to bone surfaces (e.g. Moss, 1958; Flügel *et al.*, 1993), discrete landmarks (e.g. Burdi, 1969; Dean and Wood, 1981), or a combination of lines and landmarks (e.g. Ross and Ravosa, 1993; Spoor, 1997). Here landmarks are used to define cranial base architecture and tentorial orientation to keep this study comparable with previous key studies and to utilise the co-ordinated frame of reference, consisting of pixels, intrinsic to hrMRI. Measurements were taken in units of weeks, degrees, and millimetres unless otherwise stated.

When selecting points to represent morphology it is important to note that landmarks, which traditionally have been used, may be inappropriate for the present study. For example, a number of landmarks previously used to study the cranial base and face, have been defined inconsistently in the past and consequently the results are difficult to interpret (Gould, 1977). In addition, some traditional landmarks, such as nasion are no longer considered meaningful in the study of basicranial morphology (Scott, 1956, 1958).

The following section describes the concept of landmark homology, the landmarks used in this study, and the method used to determine brain volumes. In each case only the commonest alternatives to the selected landmarks are described (see Lieberman and McCarthy, 1999; McCarthy, submitted, for descriptions of more

esoteric landmarks). A summary of the landmarks and measurements used are presented in Tables 5.7 and 5.8.

5.3.1 *Landmark Homology*

Homology, defined as the morphological equivalence of two subjects due to the inheritance of features from a common ancestor (Marcus *et al.*, 1996), is an essential concept in any quantitative study of morphology, but its significance is easily overlooked. Without it characters (or measures) are, by definition, unrelated and thus inferences can not be made about a population or comparative group under investigation. To take an obvious example, there is little, or no, homology between the sphenoid bone of a modern human and the occipital bone of a chimpanzee and though there may be some evolutionary relationship between these two species, no inferences to this effect can be made upon such a comparison. Comparisons of the orbits, on the other hand, would be more informative since the phylogenetic and ontogenetic mechanisms by which the orbits form are similar, thereby instating a certain degree of homology in orbital landmarks between the two species.

The exact meaning of the term 'homology' remains equivocal, having been in the past integrated with analogy (similarities arising through independent evolution) and redefined on a number of occasions to meet the specific requirements of different research fields (e.g. in molecular biology, homology is the degree of similarity between DNA sequences rather than resulting morphology). Without wishing to enter into the semantic arguments surrounding the terminology (see Nieuwenhuys and Bodenheimer, 1966; Moyers and Bookstein, 1979; Roth, 1984; Bookstein, 1991; Cartmill, 1994), homology and analogy can be thought of in terms of morphometrics as the similarity of anatomical or geometric points (homologies)

on structures that are common to individuals within a sample and have a shared evolutionary origin, developmental origin, or are functional equivalents (analogies) (see O'Higgins and Dryden, 1992; Marcus *et al* , 1996; O'Higgins and Jones, 1998).

In developmental studies such as this one, there are a number of problems associated with homology arising from temporal and cross-sectional variations. Firstly, individual landmarks used to measure ontogenetic changes in, for example, base flexion, may introduce variations that are unrelated to the feature under investigation. Secondly, the growth processes (e.g. chondrification and ossification) that normally define adult homologies (e.g. sutures and foramen) are portrayed at different stages of development in a fetal age series. Thus, consideration must be given as to whether landmarks are discernible in each individual of the sample and homologous between different developmental stages. For example, is a landmark on the midline condensation of mesenchyme rostral to the embryonic notochord homologous with a similar point on the cartilaginous sphenoid of a first trimester fetus? For that matter, is the latter homologous with a point on the ossifying sphenoid bone in a third trimester fetus? After what age can it be safely assumed a point is developmentally homologous? There is unlikely to be a straightforward answer since different structures within the head develop and mature at different rates, though it is logical to assume that more robust homologies are available towards the end of gestation than at the beginning.

The problem of homology is compounded in the present study by the preservation of material and the imaging technique used. Soft tissues, particularly the brain, tend to shrink or expand during wet (e.g. formalin) preservation (Small and Peterson, 1982), causing the spatial position of soft tissue landmarks to shift in relation to hard tissue landmarks. Factors determining this effect include differences

in the preservative used (formalin or ethanol) and how long the specimens have been preserved. The result is often non-uniform and consequently difficult to adjust for (Kretschmann *et al.*, 1982). Fetuses used in this study were preserved in formalin twenty years or more ago and the brains exhibit a considerable degree of shrinkage that precludes the use of neuroanatomical landmarks.

An additional consideration is that while hrMRI is superior in many respects to plain film radiography, CT and conventional MRI, interpreting the anatomy as it is shown and locating landmarks remains troublesome. This is exacerbated by variations in the contrast and grey levels representative of a landmark in one image and subsequent images of the same individual due to magnetic field inhomogeneities. Small variations also occur among individuals due to differences in the imaging setup (e.g. position of the fetus in the coil), preservation (see Thickman *et al.*, 1983), and stage of development (e.g. cartilage gives a medium signal whilst bone gives none). For example, in a MR image a landmark in the sulcus of the transverse sinus is readily discerned in the early part of gestation because the signal from the occipital cartilage is contrasted against the signal void of the sinus (desoxyhaemoglobin is a paramagnetic compound which disturbs the local magnetic field, thereby reducing spin coherence and signal intensity). Following ossification, however, the occipital bone also appears as a signal void (very rapid T_1 and T_2 relaxation) and the landmark is no longer so readily discerned.

Despite the problems of homology associated with the present study, the large size increases exhibited by most cranial structures during fetal development are likely to negate most errors introduced by more pragmatic landmarks. Thus, less than ideal anatomical or geometric homologies can be selected provided there is sufficient evidence (e.g. ANOVA study) to show that the errors incurred are insignificant in

comparison with the shape or size changes in the feature under investigation, as has already been proven in the previous section.

5.3.2 *Cranial base length and angle*

Landmarks traditionally used to mark the anterior border of the cranial base in the midsagittal plane (see review in Lieberman and McCarthy, 1999) include nasion (e.g. Björk, 1955; Levihn, 1967; Johnston, 1974; Sirianni and Newell-Morris, 1980; Diewert, 1983), foramen caecum (e.g. Ford, 1958; Lynch *et al.*, 1996; Spoor, 1997; Jeffery and Spoor, 1999; Lieberman and McCarthy, 1999), and the anterior border of planum sphenoideum (e.g. Moss, 1958; Ross and Ravosa, 1993; Ross and Henneberg, 1995) (Figure 5.5).

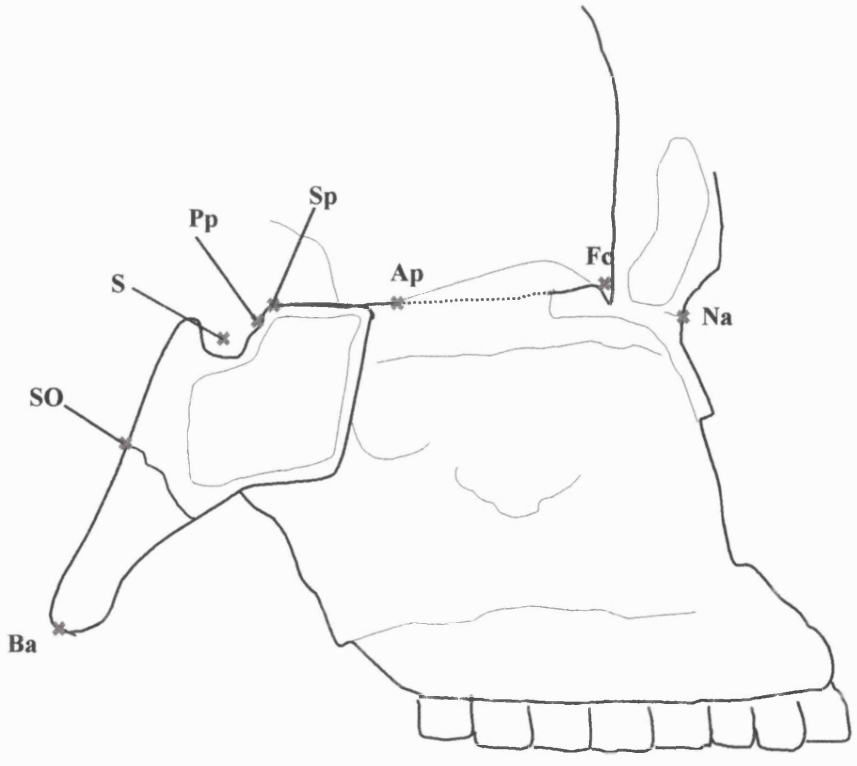

Figure 5.5. Midsagittal view of the skull showing the landmarks most often used to define the cranial base: spheno-occpital synchondrosis (SO); nasion (Na), foramen caecum (Fc), anterior border of planum sphenoideum (Ap), sphenoidale (Sp; referred to as the posterior point of planum sphenoideum [Pps] by Ross and Ravosa, 1993), the pituitary point (Pp), sella (S), and basion (ba).

Nasion, which is the preferred landmark in many developmental studies (Levihn, 1967; Burdi, 1969; Houpt, 1970; Johnston, 1974; Kvinnsland, 1971; Sirianni and Newell-Morris, 1980; Diewert, 1983; van den Eynde, 1992; Eriksen, 1995), was not selected here for two reasons: Firstly, the biological significance of this landmark between species and more importantly between different ages of the same species remains equivocal (Keith and Campion, 1922; Scott, 1956, 1958). Secondly, nasion is a facial not a basicranial landmark and may introduce additional variation from facial growth processes to the analysis of CBA (Enlow and Moyers, 1971; Lieberman and McCarthy, 1999). Points along the planum sphenoideum (see review in Lieberman and McCarthy, 1999) are also unsuitable for the present study since they exclude the contribution of the cribriform plate to the length of the cranial base in human fetuses and many anthropoids (with the exception of some prosimians; see McCarthy, submitted). While the ethmoid region, which includes the cribriform plate, can be justifiably grouped with the face in terms of adult functional morphology (Moss and Young, 1960), it is ontogenetically recognised as part of the cartilaginous base plate and thus part of the cranial base (De Beer, 1937). In modern humans it partially supports the load of the developing frontal and prefrontal lobes of the brain. Hence, the remaining landmark, foramen caecum (Fc), seems the most appropriate for the present study and was used to defined the anterior border of the anterior cranial base. It was defined as the endocranial opening of the foramen along the fronto-ethmoidal suture, seen as a pit on the cribriform plate between the fetal crista galli and the endocranial wall of the frontal bone. In fetal specimens it is therefore similar to the landmark 'criblé antériur' or cribriform anterior (Cousin, 1969; Pellerin, 1983).

The anatomical landmarks most often used to define the intersect between the anterior and posterior cranial base and the point at which base flexion is measured include sella (e.g. George, 1978; Houpt, 1978; Sirianni and Van Ness, 1978; Moore, 1978; Sirianni and Newell-Morris, 1980), the pituitary point (e.g. Zuckerman, 1955; Ross and Ravosa, 1993; Ross and Henneberg, 1995; Strait, 1999), sphenoidale (e.g. George, 1978; Anton, 1989; Lieberman and McCarthy, 1999), and prosphenion (e.g. Huxley, 1867; Cameron, 1924) (Figure 5.5). Note that in contrast to the references cited earlier, Ford (1956) defines the pituitary point as the central point of the arc describing the floor of the pituitary fossa as opposed to the midline point on the raised tuberculum sella.

Ideally, cranial base angulation should be measured where base flexion occurs, or points approximating these locations. It is generally accepted that flexion occurs in human and non-human primates at the synchondroses along the cranial base, namely the spheno-ethmoidal, mid-sphenoidal, and spheno-occipital synchondrosis (Figure 5.6) (Scott, 1958; Williams *et al.*, 1995; Lieberman and McCarthy, 1999). However, it remains unclear which of these represents the major centre of flexion during human development (see review in Lieberman and McCarthy, 1999) and it is difficult to formulate a single representative angle that is

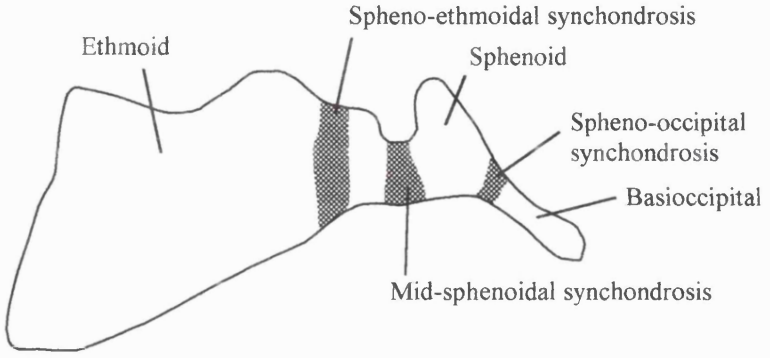

Figure 5.6. Midline sketch of the cranial base illustrating the prenatal position of the spheno-ethmoidal, mid-sphendoidal, and spheno-occipital synchondroses.

biological meaningful using all three. Moreover, only the spheno-occipital synchondrosis can be discerned reliably in preliminary hrMR images (Figures 5.7) at the junction between the basioccipital ossification centre, which appears early in fetal life (51mm CRL: De Beer, 1937), and the mostly cartilaginous basisphenoid. Since this synchondrosis is located along the posterior cranial base as opposed to the junction between the anterior and posterior cranial base it is not a particularly suitable intersect for measuring CBA and base lengths in relation to foramen caecum.

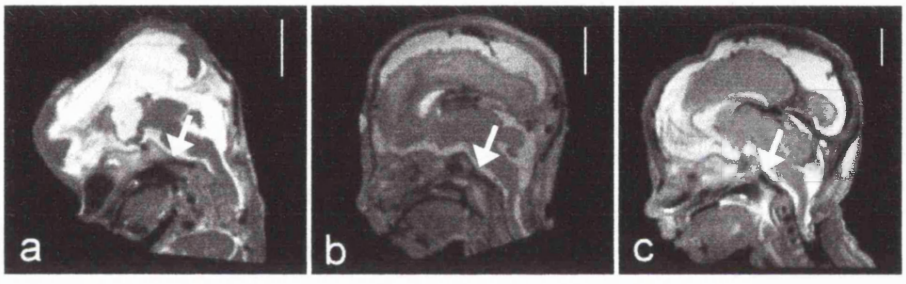

Figure 5.7. Midsagittal T_2 weighted hrMR images of human fetuses. a. 14 week old , b. 18 week old, and c. 23 week old. Only the spheno-occipital synchondrosis (white arrows) is clearly visible in all three images. Scale bar are 10mm.

Despite concerns as to the effects of bone remodelling in the region of sella (e.g. Baume, 1957; Ford, 1958; Latham, 1972; Moore, 1978), it has been used perhaps more than any other landmark to measure the point of base flexion in a wide variety of studies covering both extant and extinct species and growth series (e.g. Björk, 1951, 1955; Levihn, 1967; Melsen, 1971; Fields *et al.*, 1978; Diewert, 1983, 1985 Anagnostopoulou *et al.*, 1988; Spoor, 1997; Jeffery and Spoor, 1999). It also seems appropriately positioned near the two more likely sites of flexion, i.e. the spheno-occipital and mid-sphenoidal synchondroses (spheno-ethmoidal is primarily a site for anterior base elongation: Diewert, 1985; Hoyte, 1991), and is considered by Inoue (1961) the region of angular change in human fetuses. Here sella (S) was used

to mark the boundary between the anterior and posterior cranial base and the point of base flexion. It was defined as the centre point of sella turcica (Figure 5.5).

Finally, the majority of workers employ basion to mark the posterior point of the posterior cranial base (e.g. Moss, 1958; Johnston, 1974; Baer, 1976; Diewert, 1983; Lavelle, 1987; Eriksen, 1995; Lynch *et al.*, 1996; O'Higgins and Dryden, 1992; Spoor, 1997), though there are a few alternatives such as the Bolton point (see Levihn, 1967; Houpt, 1970). Basion (Ba) was used here to mark the posterior end of the posterior cranial base to keep this study comparable with the majority of previous work. It is defined as the tip or point of greatest curvature of the basioccipital on the anterior margin of foramen magnum in the midsagittal plane. Cranial base angle (CBA) was therefore measured as the angle of foramen caecum (Fc) - sella (S) - basion (Ba) and base lengths were calculated as the distances between these landmarks (Figure 5.8).

A second measure of CBA, the spheno-occipital angle (SOA) (Figure 5.9), was also used to evaluate possible differences between angular values taken to basion and those taken to the spheno-occipital synchondrosis. Here, the spheno-occipital synchondrosis (SO) was defined as the midpoint of the junction between the fetal sphenoid and the ossified basioccipital (Figure 5.9). The spheno-occipital angle (SOA) was therefore measured as Fc-S-SO (Figure 5.9).

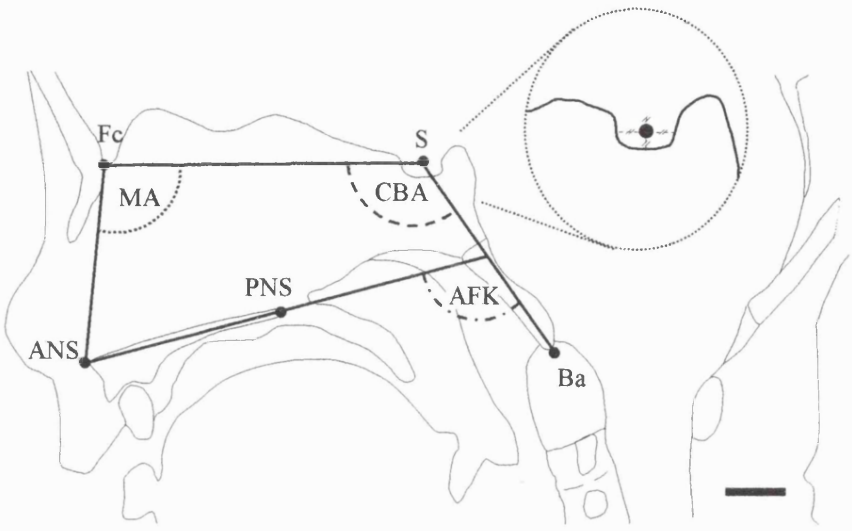

Figure 5.8. Midsagittal view of the fetal skull showing the landmarks used to measure cranial base angle (CBA), palate orientation (AFK), and the maxillary angle (MA): foramen caecum (Fc), sella (S), basion (Ba), anterior nasal spine (ANS) and posterior nasal spine (PNS). Scale bar 5mm.

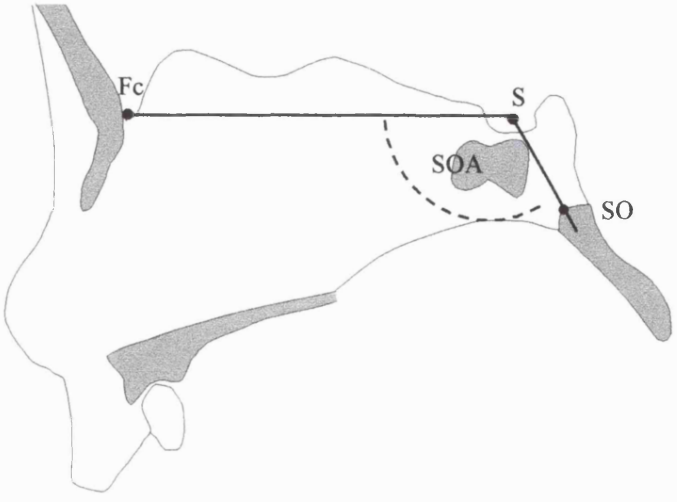

Figure 5.9 Midsagittal view of the fetal skull showing the landmarks used to measure spheno-occipital angle (SOA): foramen caecum (Fc), sella (S), and spheno-occipital synchondrosis (SO).

5.3.3 *Tentorium cerebelli*

Both Hochstetter (1939) and Moss *et al.* (1956) describe the orientation of the tentorium cerebelli in the midsagittal plane in relation to its attachment on the endocranial surface of the calvarium. Here, the angle was measured with a point on the endocranial surface of the calvarium (Ct) positioned perpendicular to and equidistant along the posterior border of the confluence of sinuses (see Figure 5.10). A line was subsequently projected through the calvarial point to the postero-superior surface of dorsum sellae (Ds), which approximates the anterior attachment of the tentorium to the posterior and anterior clinoid processes. The sagittal tentorial angle (STA) was measured at the intersect with a line passing through foramen caecum and sella (Figure 5.10). This method was selected in preference to the more obvious approach of using points along the attachment of the falx to the tentorium (e.g. Bull, 1969) because within the endocranial space the tentorium was frequently distorted

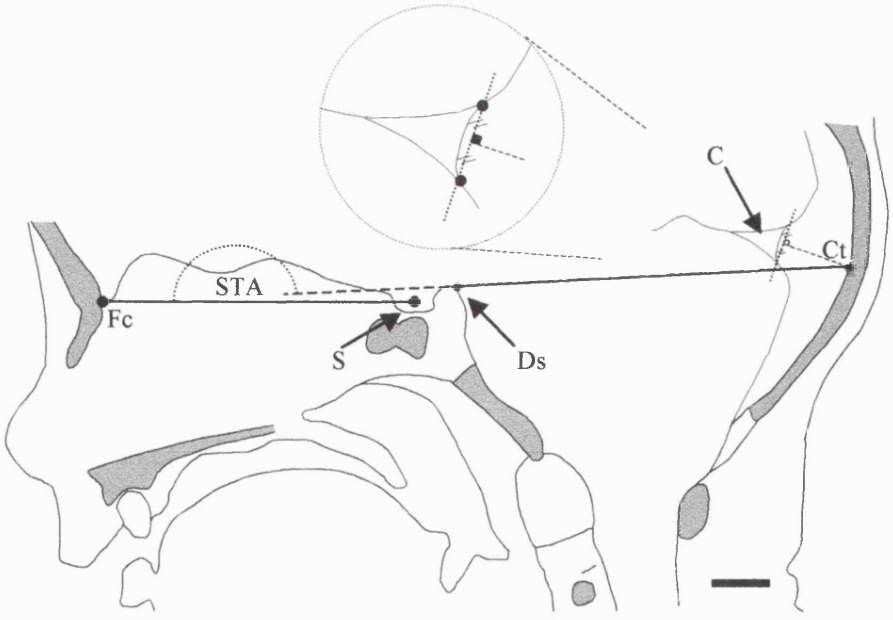

Figure 5.10. Midsagittal view of the fetal head showing the sagittal tentorial angle (STA). This is measured between the anterior cranial base (Fc-S) and a line drawn through dorsum sellae (Ds) and the calvarial attachment of the tentorium (Ct). The latter is defined as the intersect between the endocranial surface and a line drawn perpendicular to and equidistant along the plane of the posterior wall of the confluence of sinuses (C). Scale bar 5mm.

by brain shrinkage, particularly towards the tentorial incisure, or masked by the signal void of the straight sinus.

5.3.4 *Posterior cranial fossa*

The basin shaped posterior fossa is defined by the basioccipital, temporal, and occipital structures and covered superiorly by the tentorium cerebelli. Here, the posterior fossa width was defined as the greatest width between the lateral-most points (Wfs_1 and Wfs_2) of both sigmoid sulci (sinuses) and the length was defined as the greatest distance from sella to a mean co-ordinate representing the dural lining on the occipital (Pfs) (Figure 5.11). The mean co-ordinate, Pfs, is calculated from two landmarks taken either side of the falx cerebelli in parasagittal images marking the most posterior extent of the dural lining of the occipital, below the level of the tentorium cerebelli.

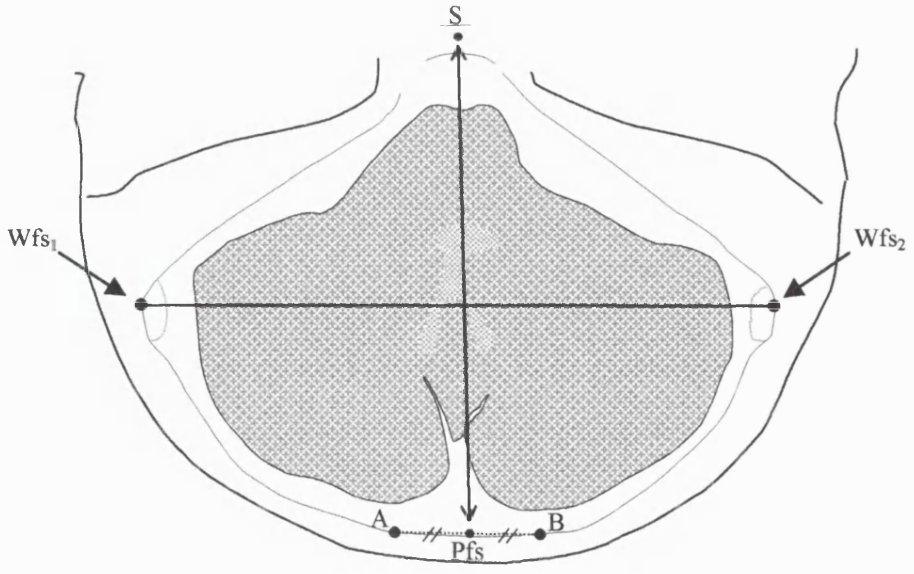

Figure 5.11. Transverse schematic of the fetal skull at the level of the cerebellum (grey stippled area). Posterior fossa width was measured as the greatest distance between the walls of the sigmoid sulci (Wfs_1 and Wfs_2) and posterior fossa length was measured from sella to the mean co-ordinate Pfs. The latter was calculated from the co-ordinates of two landmarks (A and B) marking the posterior extent of the dural lining below the level of the tentorium. In practice these points were taken on either side of the falx cerebelli in parasagittal images.

5.3.5 *Petrous pyramid orientation*

A number of studies have measured petrous temporal orientation using exocranial landmarks (e.g. Dean and Wood, 1981, 1984), radiographs (Putz, 1974), and landmarks on the posterior petrosal surface (Spoor, 1997; Spoor and Zonneveld, 1995,1998). These do not, however, take into account Moss's (1958) contention that the dura contribute to the formation of the cranial base during human ontogeny. The tentorium is said to influence the orientation of the petrosal surface as the force from the developing cerebrum is dissipated via the tentorium to the skull base (Bull, 1969). It follows that the tentorial attachment along the petrous temporal is likely to provide a more informative indication of changes in the competing forces of supratentorial (cerebrum) and infratentorial (cerebellum and brain stem) parts of the brain and the effect on petrous pyramid orientation.

Petrous pyramid orientation (PPO) in the transverse plane was measured here from the lateral most to the medial most attachment of the tentorium on the petrous temporal (Figure 5.12). In practice the landmarks were taken from coronal images.

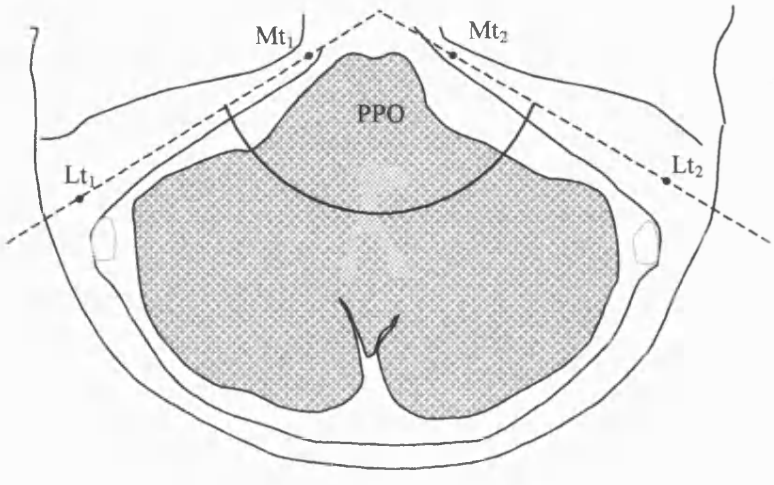

Figure 5.12. Transverse schematic of the posterior fossa showing the medial (Mt_1 and Mt_2) and lateral (Lt_1 and Lt_2) attachments of the tentorium to the petrous portion of the temporal bone. The transverse angle of the petrous pyramids (PPO) was measured at the intersect of two lines drawn through the attachment points. In practice the landmarks were taken in coronal images (see Figures 5.13a-b).

Landmarks used to define the medial most part of each pyramid (Mt_1 and Mt_2) were positioned between the attachments of the tentorium cerebelli to the margins of the superior petrosal sinus at the apex of each petrous bone (*apex partis petrosae*), close to the trigeminal cave (Figure 5.13a). Laterally, landmarks (Lt_1 and Lt_2) were positioned between the attachments of the tentorium cerebelli to the margins of the superior petrosal sinus in coronal images showing the apex of the posterior semicircular canal (Figure 5.13b). After collecting these landmarks, the co-ordinates were transformed into the transverse plane and the angle at the intersect between Lt_1-Mt_1 and Lt_2-Mt_2, petrous pyramid orientation (PPO), was computed (Figure 5.12).

5.3.6 *Maxilla and palate*

The two landmarks most often used to measure palate orientation (facial kyphosis) and palate length are the anterior and posterior nasal spines (e.g. Ford, 1956; Inoue, 1961; Burdi, 1969; Houpt, 1970; Kvinnsland, 1971; Johnston, 1974; Ross and Ravosa, 1993; Ross and Henneberg, 1995), although other landmarks have been used (e.g. Huxley, 1863, 1867; Sirianni and Newell-Morris, 1980; Anagostopoulou *et al.*, 1988). The palate, maxilla and 'premaxilla' ossify early in life (25,15,and 26mm crown-rump length respectively [De Beer, 1937]) and consequently the ossified nasal spines are easily differentiated from the surrounding soft-tissues with hrMRI throughout the fetal period.

Palate orientation is usually measured at the intersect between a line drawn through the nasal spines and a line fitted along the clivus (Ross and Ravosa, 1993; Ross and Henneberg, 1995) or a line connecting sella and basion (Kvinnsland, 1971; Johnston, 1974). Since the line sella to basion has already been defined for the

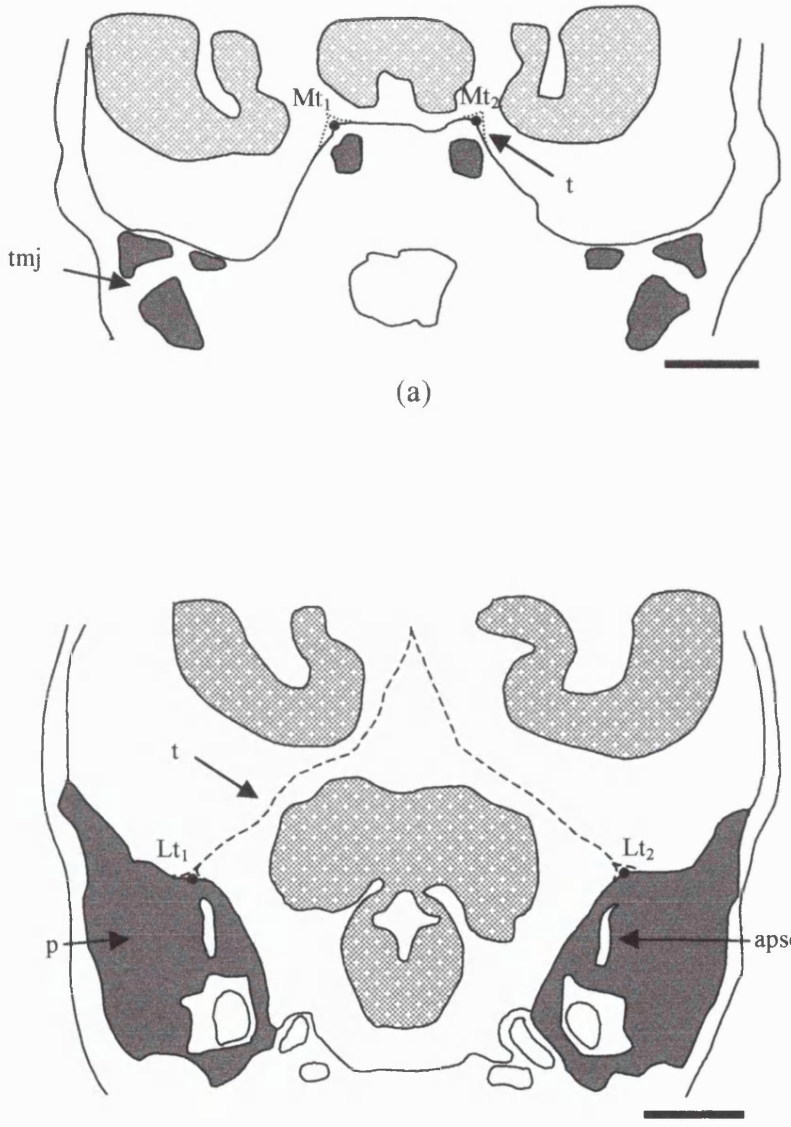

Figure 5.13. Coronal sketches of the fetal skull showing (a) the left and right medial attachments of the tentorium (Mt_1 and Mt_2) to the apex of each petrous pyramid and (b) the left and right lateral attachments of the tentorium (Lt_1 and Lt_2) at the level of the apex of the posterior semicircular canal (apsc). Also shown are the tentorium cerebelli (t), petrous temporal bone (p), and the temporomandibular jont (tmj). Scale bars 10mm.

posterior cranial base, palate orientation was measured as the angle of intersect of the sella-basion line and a line drawn through the anterior and posterior nasal spines (ANS and PNS) (Figure 5.8). Palate length was measured as the distance from ANS to PNS (Figure 5.8). Following previous studies (e.g. Burdi, 1965; Levihn, 1967; Johnston, 1974; Lynch *et al.*, 1996), the vertical maxillary angle (MA) was measured here as the angle of intersect between foramen caecum - sella and foramen caecum - anterior nasal spine (Figure 5.8). Maxillary height was measured as the distance from foramen caecum to the anterior nasal spine.

5.3.7 *Orbital axis orientation and frontation*

Changes in the orientation of the orbital axes have been measured directly from dry skulls (Cartmill, 1970) and lateral radiographs (Ross and Ravosa, 1993; Ross and Henneberg, 1995). Both radiographic studies use measures developed by Ravosa (1988) and define the orbital axis according to lines projected from the optical canal to the roof and floor of the orbit (see Figure 5.14). The point on the roof of the orbit is positioned where the orbital roof and anterior cranial base cross in lateral radiographs (see Ross and Henneberg, 1995). Such points, which are positioned at the intersect of superimposed structures as observed in plain film radiographs but are not discernible as discrete points on the specimen itself, can have little biological meaning. The dimension perpendicular to the plane of the radiographic film is not quantified and unless the point is distinct (e.g. supra-orbital foramen) its location along the same dimension in real space, i.e. the specimen, remains indeterminable. Posteriorly, the apex of the orbital cavity is placed by Ravosa (1988) at the optical canal, but in modern humans at least the recti muscles, which to some exent influence the orbital apex, attach to a tubercle on the lower

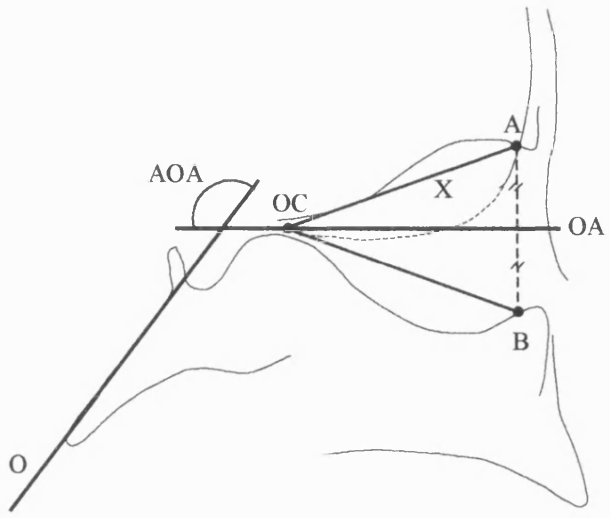

Figure 5.14. Midline diagram of the skull showing the measure used by Ross (1988) to determine the angle of orbital axis orientation (AOA): A line is drawn from the optical canal (OC) to the overlap between the orbital roof and anterior cranial fossa (A) distance X. This distance is reflected onto the orbital floor (B). The midpoint between A and B, the orbital axis (OA), is projected through OC to the plane of the occipital (O) to determine the angle AOA. (from Ross and Henneberg, 1995).

margin of the medial part of the superior orbital fissure (Williams *et al.*, 1995) as well as around the optical canal by way of a common tendinous ring (Figure 5.15). In order to account for the origin of the recti muscles, the apex of the orbit was defined here by a mean co-ordinated (AP) calculated from a point at the centre of the opening of the optical canal (OC) and a point (SOF) equidistant from the tubercle on the lower margin of the superior orbital fissure and the superior margin of the superior orbital fissure. Here the axis of each orbit (OA) was defined as the midpoint between the inferior and superior orbital margins (Iom and Som) in parasagittal images positioned equidistant from the medial and lateral orbital walls. A line was subsequently projected from the orbital axis (OA) through the mean co-ordinate (AP) to the posterior cranial base (S-Ba) and the angle of orbital axis orientation (AOA) was measured at the intersect of these two lines (Figure 5.16). The degree of lateral orbital frontation, referred to here as orbital rim orientation (ORO), was measured as the angle between the anterior cranial base (Fc-S) and a line drawn

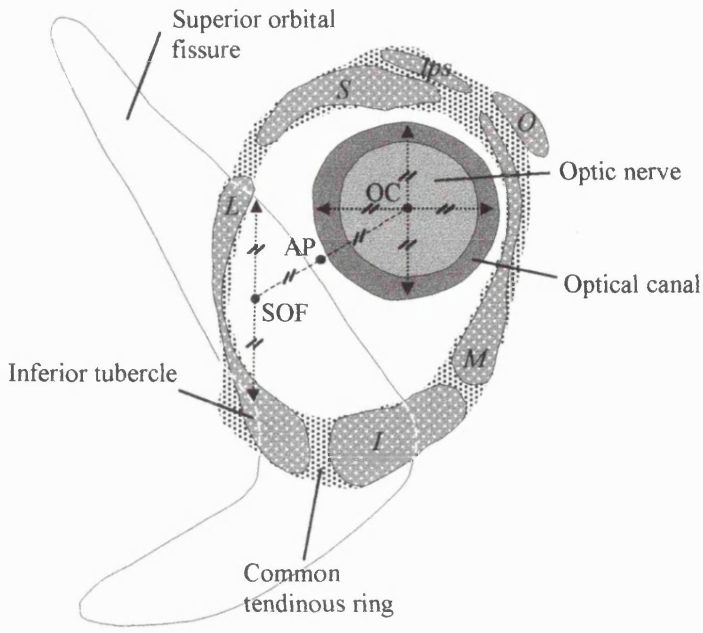

Figure 5.15. Schematic illustration of the recti muscles (*levator palpebrae superioris*, *lps*; superior oblique, *O*; medial rectus, *M*; inferior rectus, *I*; lateral rectus, *L*; superior rectus, *S*). These originate from the common tendinous ring, which attaches to the skull around the optical canal and a tubercle on the inferior margin of the superior orbital fissure (figure and information from Williams *et al.*, 1995). To take into account these attachments, the orbital apex (AP) was defined as the mean co-ordinate from two points marking the centre of the optical canal (OC) and the midpoint (SOF) between the inferior tubercle and the superior margin of the superior orbital fissure. In practice OC and SOF were taken from parasagittal images along the two vertical planes shown.

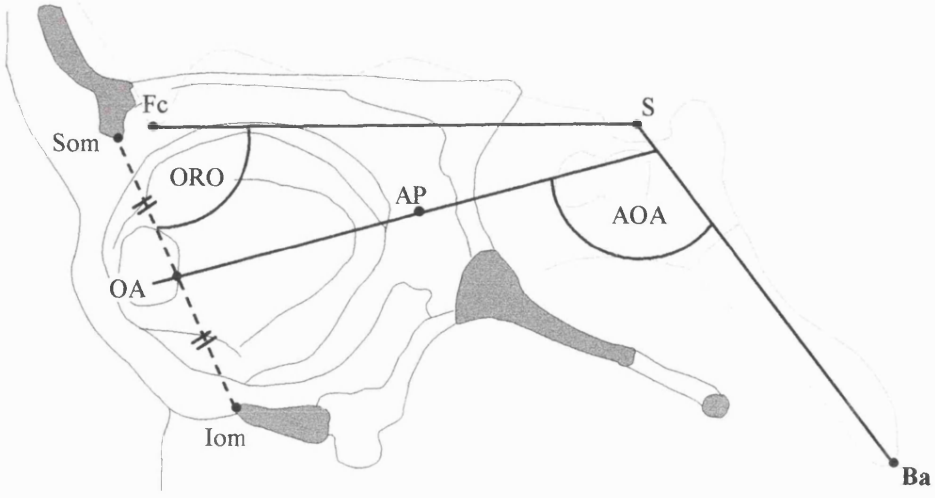

Figure 5.16. Midline view of the cranial base (grey) overlaid with a parasagittal view of the orbit (black). The angle of orbital axis orientation (AOA) was measured as the angle from a plane drawn from the orbital axis (OA), the midpoint between the superior (Som) and inferior (Iom) orbital margins, through the orbital apex (AP) to the posterior cranial base (Ba-S). Orbital rim orientation (ORO) was measured as the angle between a line drawn through Iom and Som and the anterior cranial base (Fc-S). Both Iom and Som were located in parasagittal images equidistant from the medial and lateral orbital walls. The final values of ORO and AOA were calculated as means from the results for each orbit.

through the inferior and superior orbital margins (Figure 5.16). Final values for AOA and ORO were calculated as means from the results for each orbit.

A limitation with the measures used here to define palate and orbital axes orientation is that both are taken relative to the same plane, i.e. the posterior cranial base. The hypotheses predict a correlation between these two measures and CBA, which also includes the posterior cranial base. Thus, it will be difficult to determine whether resulting correlations amongst these angles are biologically meaningful or are associated with the topographical relationship between the anatomical landmarks selected (see Solow, 1966; van den Eynde et al., 1992). In other words, variations in the position of the posterior cranial base may realise a somewhat artificial correlation between measures referenced to it. To clarify the situation, a fourth angle was also taken directly between the palate and orbital axes (Figure 5.17). This measure, the

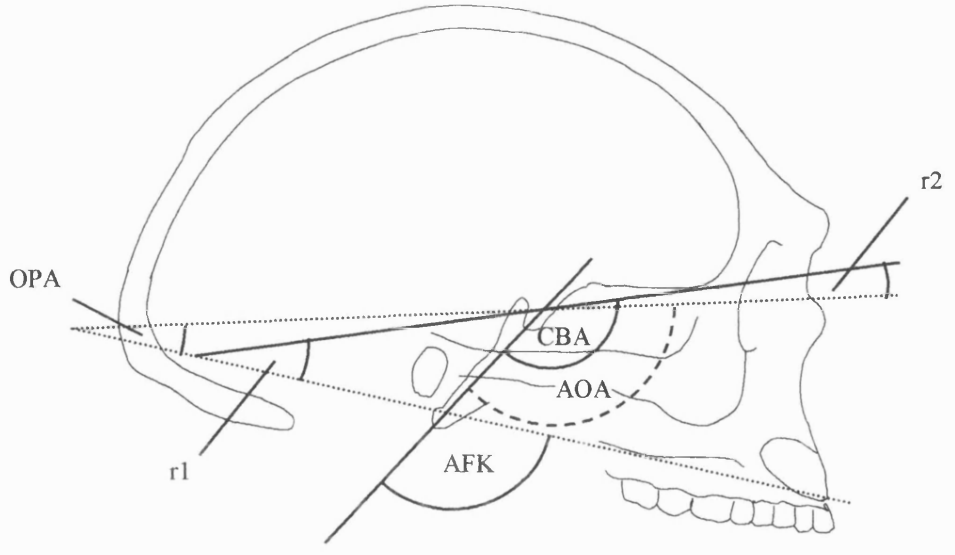

Figure 5.17. Lateral view of a hominid skull showing the angle of orbital axis orientation (AOA), cranial base angle (CBA) and palate orientation (AFK). All of these angles are measured relative to the posterior cranial base and consequently the topographical correlations between these angles can not be considered significant unless the residual angle between the orbital axes and palate, the orbito-palatine angle (OPA), also shows a significant correlation with CBA. Two additional residual angles (r1 and r2) were computed to further investigate the relationship between the anterior cranial base and face. These were calculated as CBA minus AFK and CBA minus AOA, respectively.

orbito-palatine angle (OPA), was defined as the angle of intersect between lines fitted along the palate (ANS-PNS) and orbital axes (OA-AP) and was computed as orbital axis orientation minus palate orientation. It can be used to test the biological usefulness of correlations observed amongst orbital axes orientation, palate orientation, and cranial base angle by comparing it directly to the cranial base angle. In this way, the correlations observed amongst the three angles can only be considered biologically meaningful if there is also a significant correlation between OPA and CBA.

In order to further elucidate whether the face and anterior cranial base form a block and that the angles therein covary, two additional residual angles were also taken between the palate and the anterior cranial base (r1) and the orbital axes and anterior cranial base (r2). These angles, which are shown in Figure 5.17, were computed as cranial base angle minus the angle of facial kyphosis and cranial base angle minus orbital axes orientation, respectively.

5.3.8 *Interorbital angle and convergence*

Cartmill (1970) and Enlow and McNamara (1973) considered orbital orientation in the transverse plane, but only Cartmill (1970) defines an angle to quantify this. He reports a measure of convergence as the dihedral angle between the mid-sagittal plane and the plane of the orbital margin. Here landmarks were taken at the lateral (Lom) and medial (Mom) margins of each orbit at its widest point in transverse images positioned equidistant from the roof and floor of the orbit. The transverse angle of orbital orientation, referred to here as the interorbital angle (IOA) to differentiate from Cartmill's measurement, was measured as the angle of intersect

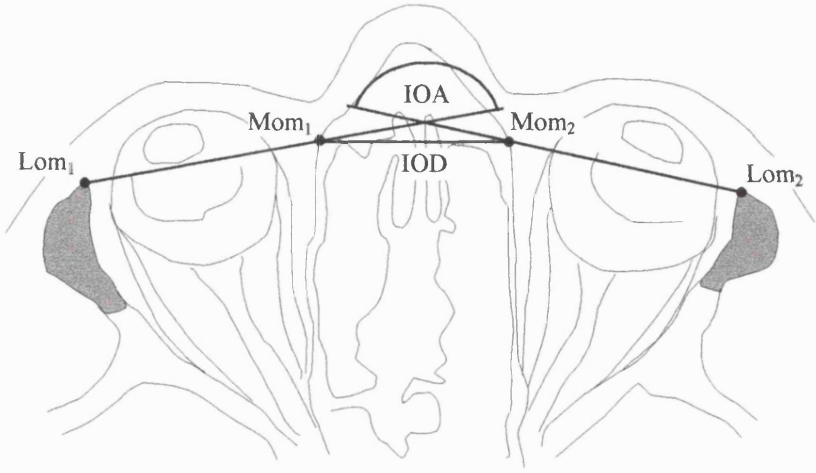

Figure 5.18. Transverse view of the orbits. The degree of orbital convergence was measured as the interorbital angle (IOA) between lines fitted to the lateral and medial orbital margins (Lom and Mom). Interorbital distance (IOD) was measured as the distance between the medial margins (Mom-Mom). Both lateral and medial margins were located in transverse slices located equidistant from the floor and roof of the orbit.

between lines drawn through these landmarks on either side of the fetal head (Figure 5.18). The interorbital distance (IOD) was measured as the distance between the medial orbital margins (Figure 5.18). To correct for size, interorbital distance was divided by mean foot length (see sample) to give values of relative interorbital distance. Note that this combination of measures gives an indication of both convergence and frontation.

5.3.9 *Volume measurement with hrMRI*

To consider relative and partial brain sizes and their interactions with the tentorium cerebelli and cranial base morphology, whole endocranial, infratentorial, and supratentorial volumes were measured.

Numerous workers have used MR imaging to measure brain volumes (e.g. Jack *et al.*, 1988a; Jack *et al.*, 1988b; Filipek *et al.*, 1989; Jack *et al.*, 1989; Cook *et al.*, 1992; Gilmore *et al.*, 1995; Becker *et al.*, 1996; Aylward *et al.*, 1997; Julin *et al.*, 1997; Semendeferi *et al.*, 1997; Doherty *et al.*, 1999; Lee *et al.*, 1999). In particular,

MRI has recently been used to measure fetal brain volumes in *utero* (Baker *et al.*, 1995; Garden and Roberts, 1996; Gong *et al.*, 1998). The basic approach used in many of these studies is the same and relies on the fact that MRI images have depth, i.e. slice thickness. Consequently, image pixels represent volume elements or voxels that can be counted in a region of interest (ROI) to obtain a volume measurement.

The three approaches most often used to segment ROI's from the rest of the image are thresholding, boundary algorithms, and manual tracing (see Ostergaard, 1997; Thatcher *et al.*, 1997). Thresholding has traditionally been used with CT to isolate anatomical structures with characteristic ranges of Hounsfield numbers (CT numbers) for three-dimensional reconstruction (see Spoor *et al.*, in press, for a review of thresholding). Volume measurements can either be taken from thresholded 2D images or three-dimensional reconstructions (e.g. Conroy *et al.*, 1990; Conroy *et al.*, 1998). The second approach is to trace ROI boundaries with an interactive, semi-automated, or fully automated algorithm (e.g Udupa, 1982; Kennedy *et al.*, 1987; Chuang *et al.*, 1989; Filipek *et al.*, 1989; Kennedy *et al.*, 1989; Clark *et al.*, 1998; Heinon *et al.*, 1998). Typically, a mathematical histogram function is applied across the image, defining contours on the basis of gradient shifts in pixel values (e.g. Byrum *et al.*, 1997; Joshi *et al.*, 1999). The third and perhaps the most pragmatic approach, is to trace boundaries by hand, i.e. the operator uses their own visual skills to outline the ROI (see Ostergaard, 1997, for a comparison of automated and manual segmentation). The limited contrast differentiation of the human eye, which can distinguish less than 256 greys, compared with more computational approaches is outweighed by the eye's higher qualitative acuity. Being more adaptive, the human eye can perceive features regardless of variations in pixel value across the slice and among different slices, tissues, individuals, or developmental stages. This is an

important consideration in this study, since hrMRI pixel values are influenced by numerous interrelated and often variable factors. Thresholding approaches to segmenting ROI's are unlikely to be sensitive enough to deal with the variation in pixel values seen in hrMRI and an algorithm has yet to be created with sufficient biological insight to be capable of differentiating (Zollikofer *et al.*, 1998), for example, infra- and supratentorial parts of the brain. Consequently, manual tracing was used here to measure endocranial volumes as ROI areas in sagittal slices multiplied by slice thickness. Here slices were interpolated in the slice direction by a factor of 1:2 to form cubic voxels (see hrMRI section), thereby providing spatially uniform pixels in orthogonally re-sliced images. Nonetheless, original slice thickness must be considered the limiting factor in volume measurements. Thus, area measurements were taken from every other slice as opposed to every slice and multiplied by the original slice thickness. This also had the advantage of reducing the time required to measure each individual.

Volumes were measured by outlining the endocranial region in every-other sagittal image, taking care not to include normal dural structures such as the confluence of sinus, falx cerebelli, and tentorium cerebelli (see Figure 5.19), and multiplying the sum by original slice thickness. This gave an endocranial volume that approximates brain volume. Infratentorial volumes were measured by outlining the endocranial area below the tentorium cerebelli and supratentorial volumes were calculated by subtracting infratentorial volume from whole endocranial volume. Area measurements were taken as the number of pixels in the outlined ROI of the endocranial space seen in midline sagittal images (see Figure 5.19), excluding normal dural structures, multiplied by pixel area.

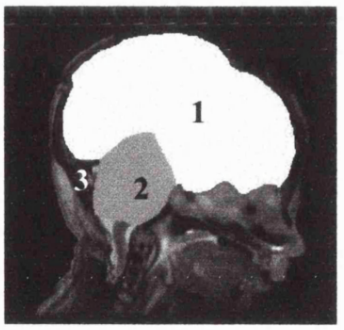

Figure 5.19. Pixel areas for calculating endocranial volume (1 and 2), infratentorial volume (2), and supratentorial volume (1). Note that the space (3) formed by the tentorium cerebelli, confluence of sinuses, and falx cerebelli is not included in the pixel area measurement. Area measurements were taken as the number of pixels in regions 1 and 2 in midline images multiplied by pixel area.

Table 5.7. Summary of landmarks used in the present study.

Abbr.	Name	†Plane	Figure(s) 5.	Definition
ANS	Anterior nasal spine	S	8	Tip of the anterior nasal spine.
AP	Orbital apex	PS	15, 16	Mean co-ordinate calculated from the position of the optical canal (OC) and the centre of the medial part of the superior orbital fissure (SOF).
Ba	Basion	S	5, 8, 16	Point on the tip of the basioccipital at the anterior boundary of the foramen magnum.
Ct	Calvarial attachment of tentorium	S	10	Point on the endocranial surface of the calvarium indicating the distal end of a line drawn perpendicular to and half along a plane fitted to the back of the confluence of sinuses.
DS	Dorsum sellae	S	10	Point on the posterosuperior edge of the dorsum sellae.
Fc	Foramen caecum	S	5, 8, 9, 10, 16	Estimated centre of the endocranial opening of foramen caecum along the fronto-ethmoidal suture, seen as a pit between the cribriform plate and the wall of the frontal bone.
Iom	Inferior orbital margin	PS	16	Tip of the inferior orbital rim in a plane estimated to be equidistant from the medial (ethmoid) and lateral (zygomatic) orbital walls.
Lom	Lateral orbital margin.	T	18	Tip of the lateral orbital rim on the zygomatic process of the frontal bone in a transverse plane equidistant from the floor and roof of the orbit.
Lt	Lateral tentorial attachment.	C	12, 13	Point between the attachments of the tentorium cerebelli to the margins of the superior petrosal sinus at the base of the petrous part of the temporal bone. Taken in a plane where the apex of the posterior semicircular canal is visible.
Mom	Medial orbital margin.	T	18	Tip of the medial orbital rim on the frontal process of the maxilla in a transverse plane estimated to be equidistant from the floor and roof of the orbit.
Mt	Medial tentorial attachment.	C	12, 13	Point between the attachments of the tentorium cerebelli to the margins of the superior petrosal sinus at the apex of the petrous part of the temporal bone, near the trigeminal cave.
OA	Orbital axis	PS	16	Midpoint between the inferior and superior orbital margins (Iom and Som).
OC	Optical canal	PS	15	Centre of the optical canal as it opens into the orbit.
Pfs	Posterior margin of the posterior cranial fossa.	PS	11	Mean point calculated from two landmarks taken either side of the falx cerebelli, marking the most posterior part of the dura lining the posterior wall of the posterior fossa below the level of the tentorium cerebelli.
PNS	Posterior nasal spine.	S	8	Tip of posterior nasal spine.
S	Sella.	S	5, 8, 9, 10, 11	Estimated centre of sella turcica.
SO	Spheno-occipital synchondrosis	S	9	The midpoint of the junction between the fetal sphenoid and the ossified basioccipital.

Table 5.7. Summary of landmarks used in the present study (contd.).

SOF	Centre of the medial part of the superior orbital fissure.	PS	15	Midpoint of a line drawn vertically from the tubercle on the inferior margin of the superior orbital fissure to the superior margin of the superior orbital fissure.
Som	Superior orbital margin.	PS	16	Tip of the superior orbital rim in a plane estimated to be equidistant from the medial (ethmoid) and lateral (zygomatic) internal walls of the orbit.
Wfss	left and right margins of the posterior cranial fossa.	T	11	Two landmarks on the lateral edge of the sigmoid sulci (sinuses) describing the greatest width of the posterior cranial fossa below the level of the tentorium.

† Slice planes in which landmarks were taken: coronal, C; parasagittal, PS; sagittal, S; Transverse

Table 5.8. Summary of measurements (mm, mm^3, and degrees).

Name	Landmarks	‡Plane	Definition
Anterior cranial base length	*Fc-S*	S	Distance from foramen caecum to sella.
Angle of orbital axes orientation (AOA)	*OA-AP^S-Ba*	S	Angle between the posterior cranial base and a line projected through the orbital axis and orbital apex. Calculated as the mean of the bilateral results.
Endocranial ratio	-	-	Infratentorial volume / Supratentorial volume
Endocranial volume	-	S	Volume of the endocranial space, excluding normal dural and venous structures.
Cranial base angle (CBA)	*Fc-$\hat{S}$-Ba*	S	Angle between the anterior and posterior parts of the basicranium.
Total cranial base length (BL)	*Fc-S-Ba*	S	Distance from the foramen caecum to sella and sella to basion.
Infratentorial volume	-	S	Endocranial volume below the tentorium cerebelli.
Interorbital angle (IOA)	*Lom-Mom^Mom-Lom*	T	Angle between lines projected through the lateral and medial orbital margins.
Interorbital distance (IOD)	*Mom-Mom*	T	Distance between the medial margins of the orbits.
Cube root endocranial volume	-	-	$\sqrt[3]{}$endocranial volume
Maxillary Angle (MA)	*ANS-$\hat{S}$-FC*	S	Angle between the anterior cranial base and the anterior nasal spine.

Table 5.8. Summary of measurements (contd.)

Maxillary height	ANS-Fc	S	Distance from the anterior nasal spine to foramen caecum.
Midline area	-	S	Area of the endocranial space in midsagittal images.
Orbital rim angle (ORO)	*S-Fc^Som-Iom*	S	Angle between the anterior cranial base and a line projected through the superior and inferior orbital margins. Calculated as the mean of the bilateral results.
Orbito-palatine angle (OPA)	*OA-OP^PNS-ANS*	S	Angle of intersect between a line fitted through the anterior and posterior nasal spines and a line fitted through the orbital axes and orbital apexes. Computed as orbital axes orientation minus palate orientation.
Orbital width	*Iom-Mom*	T	Distance from the lateral to medial orbital margin.
Palate length	*ANS-PNS*	S	Distance from the anterior nasal spine to the posterior nasal spine.
Palate orientation (AFK)	*ANS-PNS^S-Ba*	S	Angle between the palate and posterior cranial base.
Posterior cranial base length	*S-Ba*	S	Distance from sella to basion.
Posterior cranial fossa length	*S-Pfs*	T	Greatest distance from sella to posterior wall of posterior fossa , below the tentorium.
Posterior cranial fossa width	*Wfs-Wfs*	T	Greatest distance between left and right margins of the posterior fossa , below the tentorium.
Posterior fossa index	-	-	$\frac{\text{Posterior fossa width}}{\text{Posterior fossa length}}$
Relative interorbital distance	-	-	$\frac{\text{Interorbital distance}}{\text{mean foot length}}$
Relative endocranial size (IRE)	-	-	$\frac{\sqrt[3]{\text{Endocranial volume}}}{\text{total base length}}$
Relative infratentorial size (IRE2)	-	-	$\frac{\sqrt[3]{\text{infratentorial volume}}}{\text{posterior cranial base length}}$
Relative midline area	-	S	$\frac{\sqrt[2]{\text{midsagittal area}}}{\text{total base length}}$
Relative supratentorial size (IRE3)	-	-	$\frac{\sqrt[3]{\text{Supratentorial volume}}}{\text{Anterior cranial base length}}$
Residual angle 1 (r1)	*Fc-S^ANS-PNS*	S	Angle between anterior cranial base and palate.
Residual angle 2 (r2)	*Fc-S^OA-AP*	S	Angle between anterior cranial base and orbital axes.
Sagittal tentorial angle (STA)	*Fc-S^Ds-Ct*	S	Angle between the anterior cranial base and a line from the calvarial attachment of the tentorium (Ct) to dorsum sellae (Ds).
Supratentorial volume	-	S	Endocranial volume above the tentorium cerebelli.

‡ Plane in which measurement is taken.
^ Point where angle was taken.

5.4 Statistical analysis

In this study the number of decimal places that results should be reported to varies between individuals according to pixel size and therefore the imaging field of view (FOV) used. For convenience and to simplify the analyses of the data, measures were taken to the mean pixel size (0.2mm). Hence, linear and angular measurements were taken to the nearest two-tenths of a millimetre and degree, respectively. Others were taken to the nearest ten cubic millimetres, one square millimetre, and a tenth of a week. Indices, ratios and relative sizes were reported to two decimal places. Obviously, this leads to some information being lost on fetuses imaged using the smaller FOV and spurious information being gained on fetuses imaged using the larger FOV. Nonetheless, these changes are negligible in comparison with the differences between individuals.

Results from the present study were analysed using Excel 97 (Microsoft) and SPSS 6.1.3 (SPSS Inc.). Hypotheses outlined in the introductory chapter were mostly evaluated with Spearman rank correlation coefficients (r_{rank}) and Model II reduced major axis regressions (RMA). In all significance tests, a level of $P<0.05$ was used to reject null hypotheses.

The association between variables was evaluated with Spearman's rank correlation as it is non-parametric (i.e. independent of data distribution) as opposed to product-moment correlations which assume a normal data distribution. Samples representing growth series are not normally distributed and rank correlation is the more appropriate method of determining bivariate association.

Sokal and Rohlf (1995) report two methods for computing Spearman's rank correlation (pages 598 and 600, respectively). The first computes the correlation directly from the rank order of variables *x* and *y* with,

$$r_{rank} = 1 - \frac{6\sum(R_x - R_y)^2}{n(n^2 - 1)}$$

Where n is the number of paired datum points and R_x and R_y are the rank orders of variables *x* and *y*, respectively. The alternative method, which is applied by many statistical programs (e.g. SPSS 6.1.3), is to compute r_{rank} as the product-moment correlation coefficient of the *x* and *y* rank orders. While there is little in the literature on the subject, initial evaluations with test data have revealed a limitation with the latter method. For reasons requiring further statistical assessment, the value and therefore significance of rank correlation computed as a product-moment correlation deviates from that directly computed from rank orders and product-moment correlation (see examples in Figures 5.20). These deviations appear to be associated with the degree of variable variation relative to sample noise introduced by cross-sectional and intraspecific variations (see Figures 5.21) and whether or not variables increase or decrease in relation to one another. The differences between the correlation coefficient of the degree observed in the examples could have serious implications for the interpretations of results. Since rank correlation computed with product-moment correlation assumes a normal distribution of ranks and is therefore not appropriate, the equation shown earlier was used. It should be noted, therefore, that the rank correlations reported in this study will not always agree with those computed by individuals of software using the alternative approach.

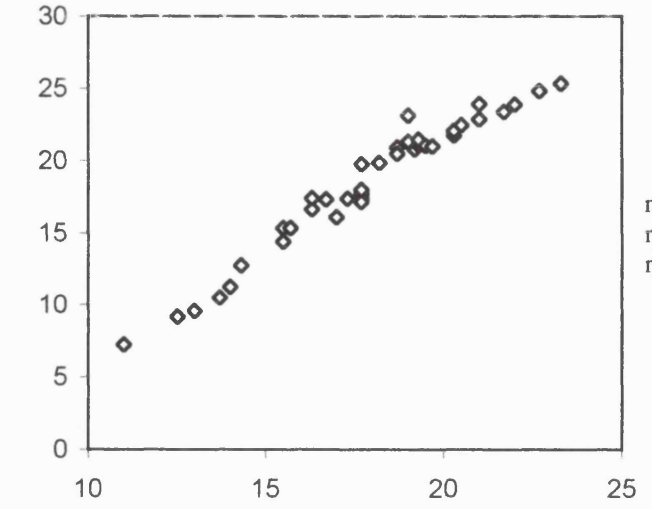

$r_{rank1} = 0.972$, $P<0.001$
$r_{prctm} = 0.975$, $P<0.001$
$r_{rank2} = 0.978$, $P<0.001$

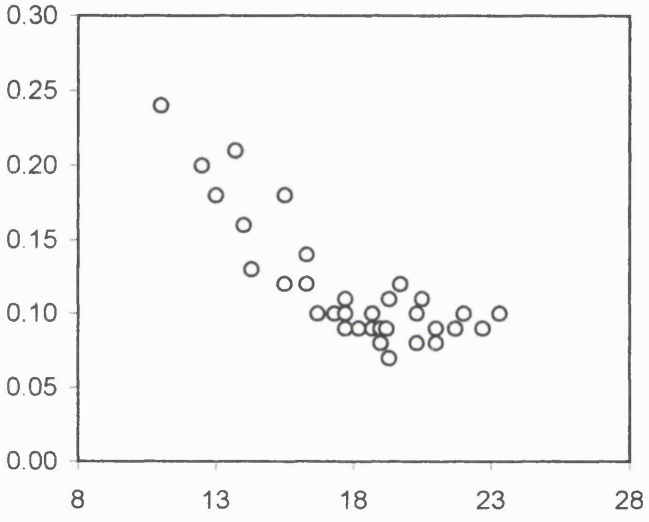

$r_{rank1} = -0.846$, $P<0.001$
$r_{prctm} = -0.808$, $P<0.001$
$r_{rank2} = -0.686$, $P<0.001$

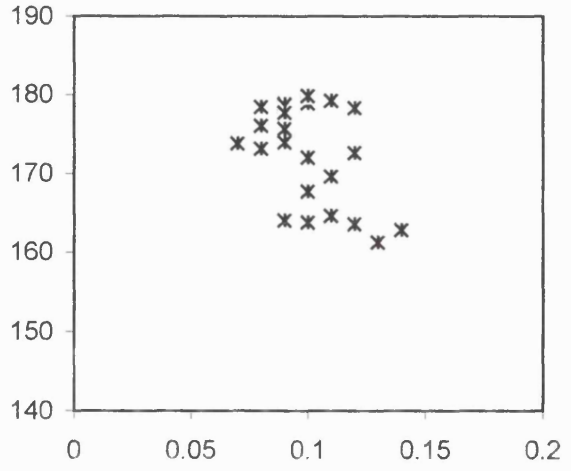

$r_{rank1} = -0.489$, $P<0.01$
$r_{prctm} = -0.509$, $P<0.01$
$r_{rank2} = -0.336$, $P>0.05$, ns

Figure 5.20. Bivariate plots illustrating that values of rank correlation computed as the product-moment correlation of rank orders (r_{rank2}) varies from that computed directly from the rank orders of datum points (r_{rank1}) and product-moment correlation (r_{prctm}). This effect appears to be related to reduced variation in relation to sample noise and whether variables are positively or negatively associated (r_{rank2} was computed using SPSS 6.1.3; Raw data for these plots is taken from anterior base length vs. age, endocranial ratio vs. age, and tentorial angle vs. endocranial ratio).

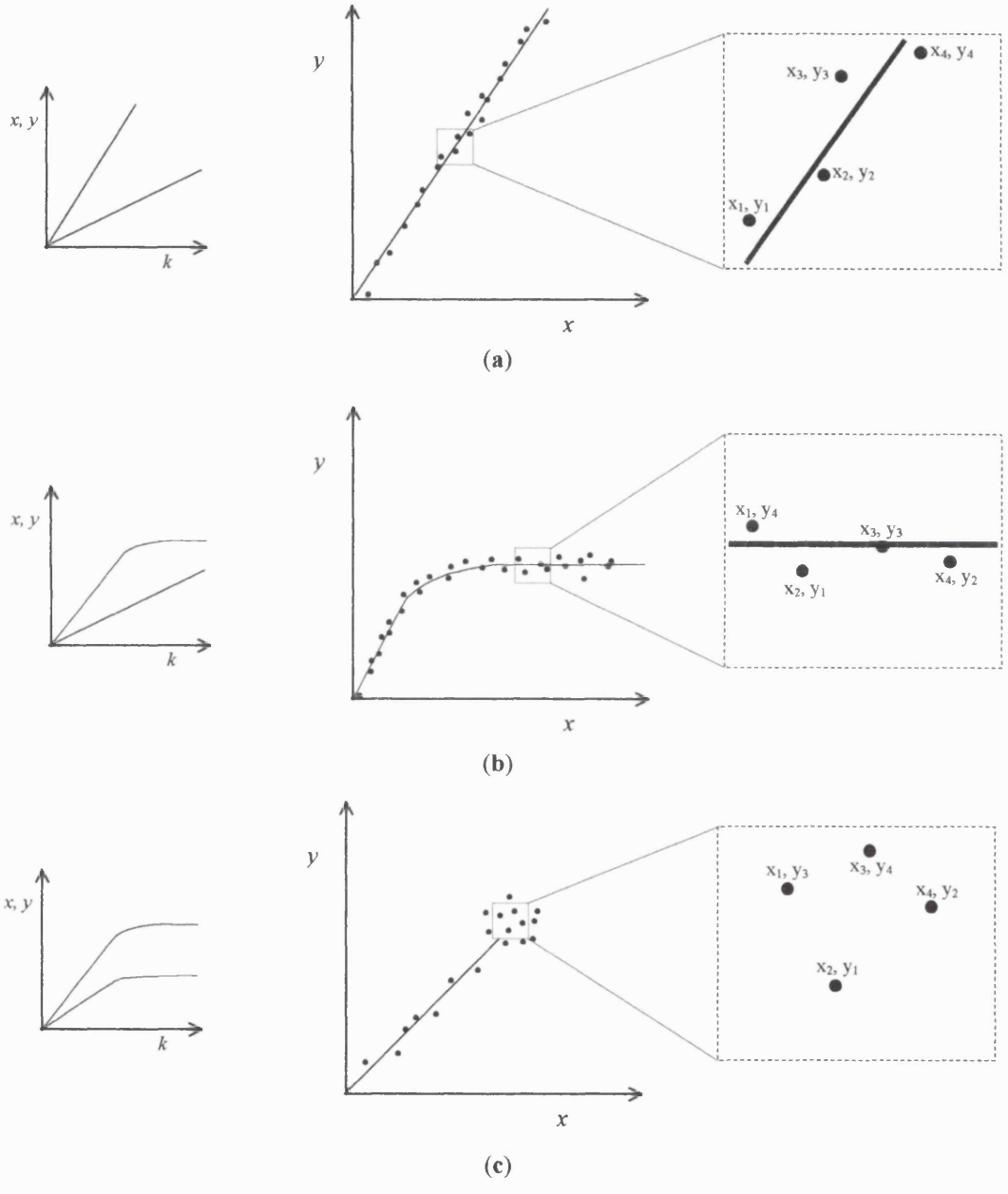

Figure 5.21. Illustrations showing how variations in x and y in relation to another variable k (e.g. age) or each other can effect rank correlations. As the effective change in x, y, or x and y decreases towards changes due to sample noise, the rank order of datum points is gradually lost. In figure (a) changes in x and y are greater than sample noise in x and y respectively across the sample, producing a rank of $x_1=y_1$, $x_2=y_2$, $x_3=y_3$, $x_4=y_4$; (b) initially changes in both x and y are greater than noise, but as y plateau's the proportion of noise in y increases. Consequently, most of the rank order of datum points is lost along the y axis, producing a rank of $x_1\neq y_1$, $x_2\neq y_2$, $x_3=y_3$, $x_4\neq y_4$; (c) initially changes in both x and y are greater than noise, but as y and x plateau the proportion of noise in both variables increases and all rank order is lost. This gives a rank of $x_1\neq y_1$, $x_2\neq y_2$, $x_3\neq y_3$, $x_4\neq y_4$.

The Model II RMA approach to line fitting was employed in preference to the Model I least squares (LSR) method because the data in the present study should not be considered asymmetrical (i.e. one variable dependent and independent). In such cases, it is considered more pertinent to use Model II regressions (e.g. RMA and major axis [MA]) for investigating trends within the data and the relationships between variables (see Martin, 1980; Hofman, 1988; Aiello, 1992; Hartwig-Sherer and Martin, 1992). Both RMA and MA assume that variation is symmetrical between x and y, i.e. variation occurs in both variables (Aiello, 1992). Although there is some disagreement as to which Model II regression is the most appropriate, RMA was selected in preference to MA in the present study for two reasons. Firstly, it has been shown that the slope produced by MA can be affected by changes in the value of the correlation coefficient (Aiello, 1992). Secondly, while the result of RMA regressions are unaffected by changes in the scale of either the x or y variable, MA regressions can alter with scale changes (see Rayner, 1985; Pagel and Harvey, 1988; Aiello, 1992). RMA regression statistics (e.g. slope, intercept, 95% conf. int. of slope) were calculated using the methods reported by Sokal and Rohlf (1995:pp 541-548).

Log-log transforms and polynomial regressions were used when straightforward RMA regressions were insufficient to describe the observed data trend. Log-log transforms enable the allometric equation, $y = bx^k$, as proposed by Huxley (1932), to be simplified to logy = logb + klogx, thereby making the analyses of proportionalities and the interpretation of results more convenient. However, it is not always possible to say with any certainty the circumstances in which log-log transforms are warranted since untransformed data often works just as well (Smith,

1980). It is also difficult to interpret the RMA statistics for complex variables (e.g. relative brain size) back into biologically meaningful terms once transformed. Thus, to reduce the complexity of testing certain hypotheses and the risk of misinterpreting RMA results, log-log transforms were used as little as possible for analysing normal variables and not at all for analysing complex variables such as ratios or indices. Instead, curvilinear trends were described with polynomial equations and two-step RMAs.

Provided the variances (s^2) of two groups were not too dissimilar the significance of the difference between means (null hypothesis: parametric $mean_{group1}$ - parametric $mean_{group2} = 0$) was estimated with the t-test for unequal but large (30>) samples reported by Sokal and Rohlf (1995;224; expression 9.4). The significance of differences between variances was calculated with the F-test described by Sokal and Rohlf (1995;189, Box 8.1).

CHAPTER 6. RESULTS

The raw measurement data for each individual specimen are given in Appendix 3. The temporal trends of the angles, volumes and other measurements are investigated by analysing their relationship with estimated age. Given that fetal age is calculated from crown rump length, biparietal diameter, and foot length, it can also be considered an adjunct to overall size. However, it must be remembered that age is a non-linear description of size that is subject to noise and the analyses of the temporal trends must therefore be interpreted with caution. Relevant tables and figures are given at the end of each section.

6.1 Basicranial architecture: 'spatial-packing' hypothesis

The descriptive statistics of the measurements that are used to test the different versions of the spatial-packing hypothesis are listed in Table 6.1. In Figure 6.1, the cranial base angle CBA is plotted against the spheno-occipital angle to compare these two different measures of base angulation. The slope is not significantly different from one ($P>0.05$) and there is no significant difference between the variances of the two angles (17.54 for spheno-occipital angle, 11.93 for CBA; null hypothesis $s^2_1 \neq s^2_2$ rejected, $P>0.1$). Thus, there is no notable difference in the variance or trajectory between these two measures and further analysis of basicranial angulation presented here focuses on CBA (i.e. Fc-S-Ba).

Figure 6.2 plots CBA against age. No significant correlations were observed for the whole (r_{rank} = 0.137, ns) or the second half of the period studied (18 to 23 weeks, r_{rank} = -0.068 [ns]). However, a comparison covering the first half of the period studied reveals a significant positive correlation (11-18 weeks, Table 6.2). This suggests that the basicranium initially retroflexes, i.e. the cranial base angle increases from about 127 to 136 degrees, but remains essentially unchanged during the latter half of the second trimester.

Increases of endocranial volume arise from both midline and lateral expansion of the brain. This realises a potential problem with the spatial packing model: lateral expansion can lead to increases of cube root volume relative to base length without necessarily influencing the midline cranial base associated with base flexion. The null hypothesis that endocranial enlargement arises mostly through lateral expansion was assessed with a direct comparison between square root midline endocranial area and cube root endocranial volume (Figure 6.3, Table 6.2). The slope of this plot is significantly greater than one ($P<0.01$), indicating that medial endocranial enlargement along the cranial base occurs more rapidly than lateral growth. These results show that proposed model of spatial-packing is suitable for testing in a developmental context.

Figure 6.4 plots the endocranial volume, and its two subsets supratentorial and infratentorial volume, against age. This graph reveals a much greater increase of supratentorial volume than the infratentorial volume. At the end of the period studied, measured values of absolute endocranial, supratentorial, and infratentorial volume are approximately 46, 53, and 21 times larger than at the beginning, respectively (Table 6.1). To quantify the infratentorial and supratentorial contributions to overall enlargement of the endocranial space, cube root endocranial,

supratentorial, and infratentorial volume are plotted against age (Figures 6.5, Table 6.2). The slope of cube root supratentorial volume against age is almost three times larger than that of cube root infratentorial volume against age, showing that the supratentorial volume makes a much greater contribution to overall increases of endocranial size. In other words, it is cerebral enlargement, as opposed to growth of the cerebellum and brain stem, that predominately results in overall increases of endocranial size.

To assess midline basicranial growth the total, anterior and posterior base lengths are plotted against age (Figure 6.6, Table 6.2). At the end of the period studied measured values are approximately 3 to 4 times larger than at the beginning (Table 6.1). The slope of anterior base length against age is two times that of the posterior base length (Table 6.2), which shows that the former contributes almost twice as much as the posterior cranial base to increases of total base length.

The observations so far, which are summarised in Figure 6.7, demonstrate that the growth of the antero-superior parts of the brain and the basicranium is clearly distinct from their postero-inferior counterparts. Essentially, it appears that there are two regions within the skull with separate growth trajectories for both endocranial enlargement and cranial base elongation. The tentorium, which traverses the endocranial space and attaches to the basicranium near the junction between the anterior and posterior cranial base (clinoid processes), acts as a boundary between these regions. Components antero-superior to the tentorium not only make the greatest contributions to increases of total cranial base length and endocranial size, but also show a more significant degree of differential growth (Figure 6.7). Linear increases of the supratentorial volume (i.e. cube root) in relation to age are almost two and half times greater than that of the anterior cranial base length. In contrast,

linear increases of infratentorial volume in relation to age are under one and half times that of the posterior cranial base length. Consequently, increases of relative supratentorial size should exceed that of relative infratentorial size.

To investigate the extent of increases in relative endocranial size, cube root endocranial, supratentorial, and infratentorial volume were plotted against total, anterior, and posterior base length, respectively (Figure 6.8). Table 6.2 lists the RMA and correlation statistics for these plots, all of which show significant correlations (Table 6.2, $P<0.001$). The slopes for all three bivariate comparisons are significantly greater than one (Table 6.2, $P<0.001$). These results show that relative endocranial, supratentorial, and infratentorial size increase significantly across the sample. The slope depicting relative supratentorial size is steeper than that for relative infratentorial size, suggesting that differential growth between the anterior cranial base and supratentorial volume is the major factor behind increases of relative endocranial size.

Bivariate comparisons of relative endocranial sizes against age were used to assess their temporal trends. There is a small increase of relative endocranial size with age, (Figure 6.9, Table 6.2), but no correlated increase of relative infratentorial or relative supratentorial size (r_{rank} = 0.033[ns] and 0.292[ns], respectively) despite that the slope of cube root supratentorial volume against anterior base length is steeper.

Since relative endocranial, supratentorial, and infratentorial sizes increase across the sample and relative endocranial size increases with age the spatial-packing hypothesis predicts a correlated decrease in cranial base angle. However, no significant correlations were observed between the increases of relative endocranial, infratentorial or supratentorial size and CBA (r_{rank} = 0.088 [ns], 0.021 [ns], and -

0.049 [ns], respectively). Figure 6.10 shows the plot for relative endocranial size and CBA. Alternative comparisons, using the midline area rather than endocranial volume, the spheno-occipital angle rather than CBA, and by considering only the first half of the period studied failed to reveal any significant correlation (Table 6.3). The first half of the period studied was included separately because earlier results show that CBA increases during this period. These results suggests that increases of relative endocranial size are not accommodated during fetal development by isometric extension or flexion of the cranial base and therefore fail to support the spatial packing hypothesis in a developmental context.

Table 6.1. Descriptive statistics for fetal age, cranial base angle, endocranial volumes, and base lengths.

	N	Mean	S.D.	Min.	Max.
Age (weeks)	38	17.9	2.9	11	23
Cranial base angle (deg.)	38	133.52	3.56	127.0	139.4
Spheno-occipital angle (deg.)	37	129.48	4.20	121.2	139.0
Endocranial volume $x10^{-3}$ (mm^3)	36	39.979	24.433	1.87	87.44
Supratentorial volume $x10^{-3}$ (mm^3)	35	36.870	22.597	1.51	79.14
Infratentorial volume $x10^{-3}$ (mm^3)	35	3.655	2.028	0.36	8.30
Midline endocranial area $x10^{-2}$ (mm^2)	34	12.959	5.949	1.66	23.64
Total base length (mm)	38	30.87	7.10	12.6	41.2
Anterior base length (mm)	38	18.48	4.65	7.2	25.4
Posterior base length (mm)	38	12.38	2.50	5.4	16.2

Table 6.2. RMA and correlation statistics for cranial base angle, endocranial volumes, and base lengths with age (* , P<0.05; ** , P<0.01; *** P<0.001).

	n	r_{rank}	P	Slope	95% conf. int for slope	Intercept
Cranial base angle x spheno-occipital angle	37	0.732	***	0.82	0.65,1.00	26.95
Cranial base angle x age (11 to 18wks)	19	0.686	***	1.89	1.24, 2.52	104.04
Sqrt midline endocranial area x qrt endocranial volume	34	0.980	***	1.09	1.03, 1.16	-0.92
Qrt endocranial volume x age	36	0.977	***	2.86	2.68, 3.04	-19.03
Qrt supratentorial volume x age	35	0.977	***	2.83	2.64, 3.00	-19.38
Qrt infratentorial volume x age	35	0.959	***	1.07	0.98, 1.15	-4.36
Total base length x age	38	0.965	***	2.46	2.28, 2.64	-13.30
Anterior base length x age	38	0.971	***	1.61	1.50, 1.73	-10.45
Posterior base length x age	38	0.929	***	0.87	0.78, 0.96	-3.19
Qrt endocranial volume x total base length	36	0.969	***	1.16	1.09, 1.24	-3.59
Qrt supratentorial volume x anterior cranial base length	35	0.978	***	1.75	1.65, 1.86	-1.14
Qrt infratentorial volume x posterior cranial base length	35	0.907	***	1.23	1.09, 1.38	-0.48
Relative endocranial size x age	36	0.620	***	0.02	0.01, 0.02	0.72

Qrt, cube root; Sqrt, square root

Table 6.3. Rank correlation matrix for relative sizes, cranial base angle, and spheno-occipital angle for the whole and first half of the period studied. None of these correlations are significant (P>0.05).

	Cranial base angle (11-23 wks)	Cranial base angle (11-18 wks)	Spheno-occipital angle (11-23 wks)	Spheno-occipital angle (11-18 wks)
Relative endocranial size	0.088	0.075	0.239	0.014
Relative supratentorial size	-0.049	-0.271	0.021	-0.261
Relative infratentorial size	0.021	0.046	0.210	0.069
Relative midline size†	0.086	-0.054	0.132	-0.010

† square root midline area over base length.

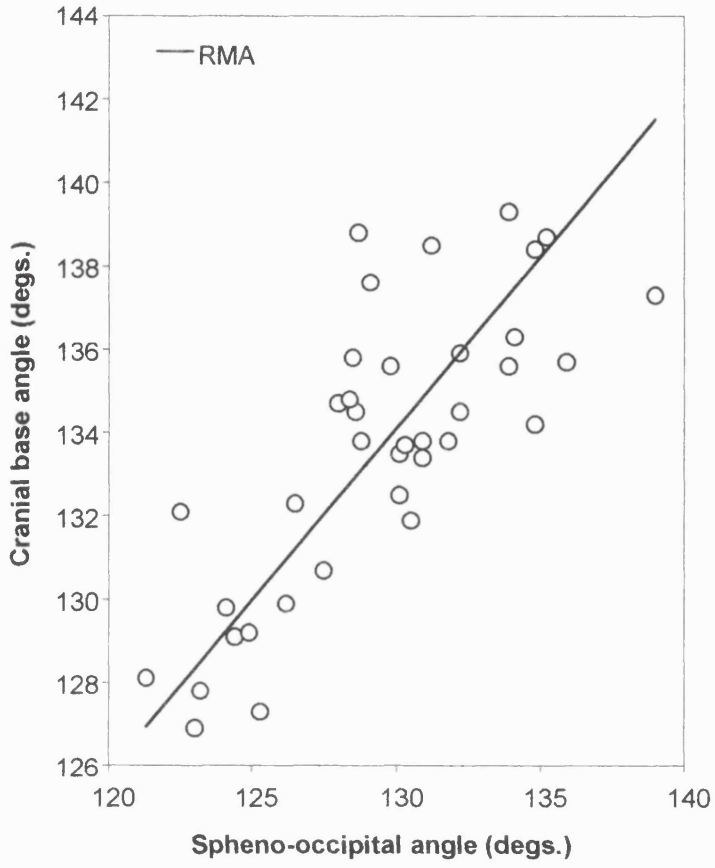

Figure 6.1. Bivariate comparison of cranial base angle and spheno-occipital angle

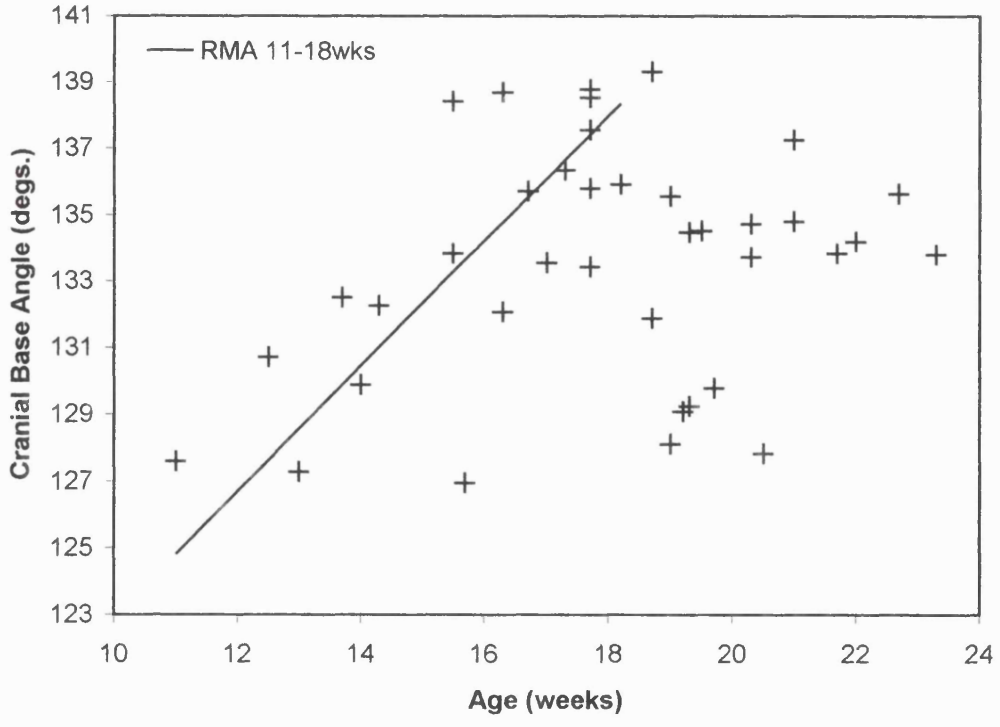

Figure 6.2. Bivariate comparison of cranial base angle and age

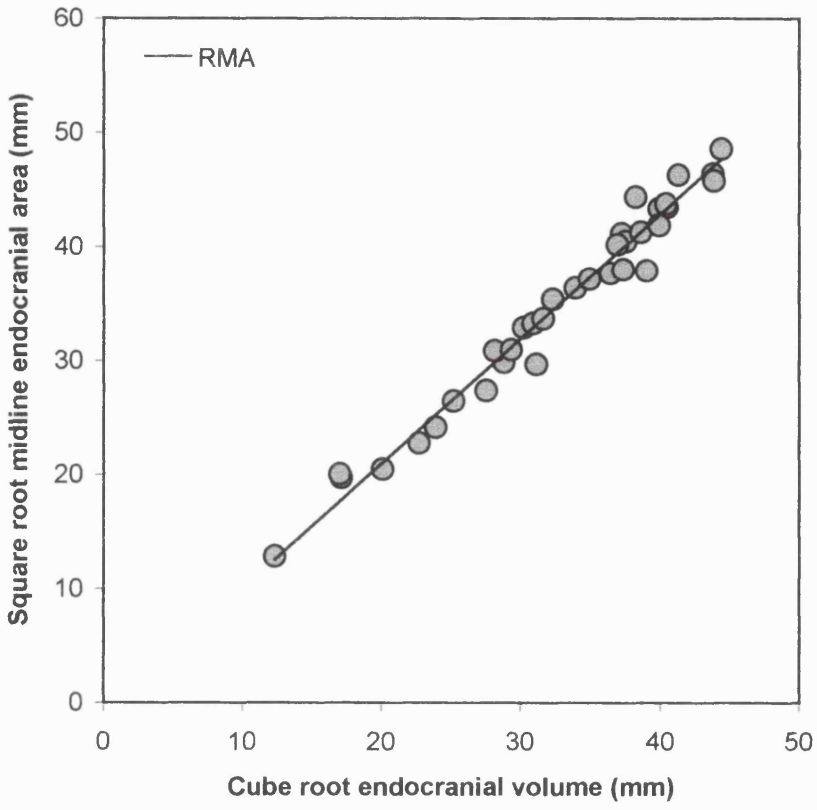

Figure 6.3. Bivariate plot of square root midline endocranial area against cube root endocranial volume.

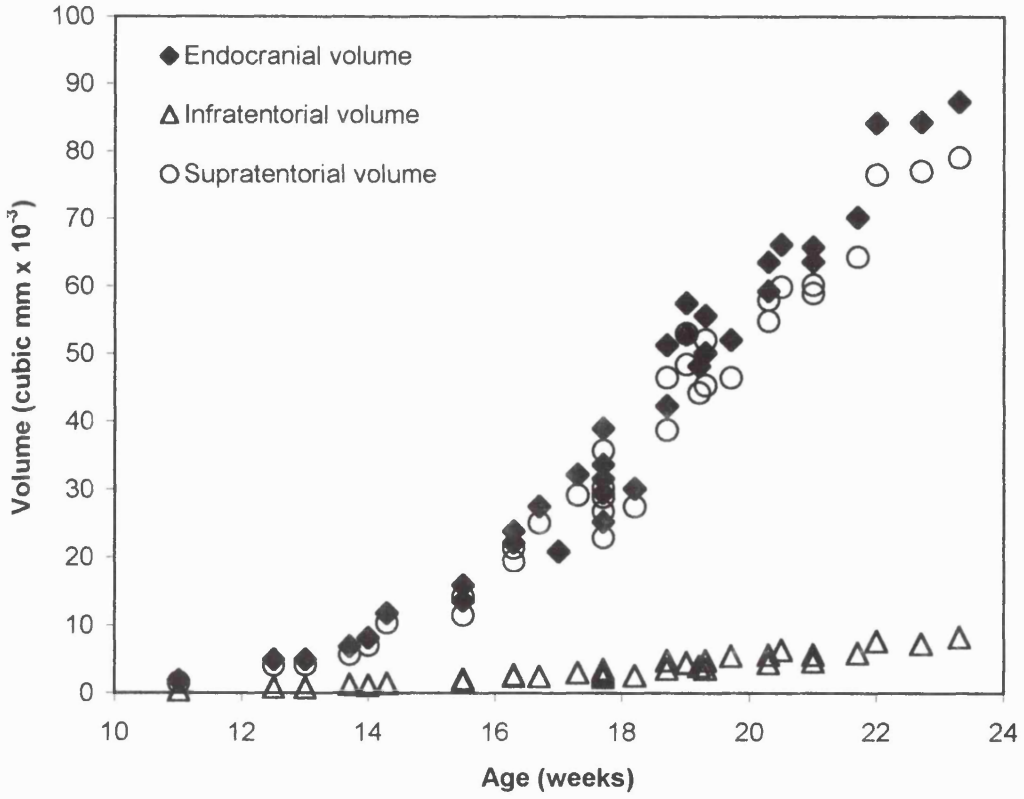

Figure 6.4. Bivariate plot of endocranial volume, supratentorial volume, and infratentorial volume against age.

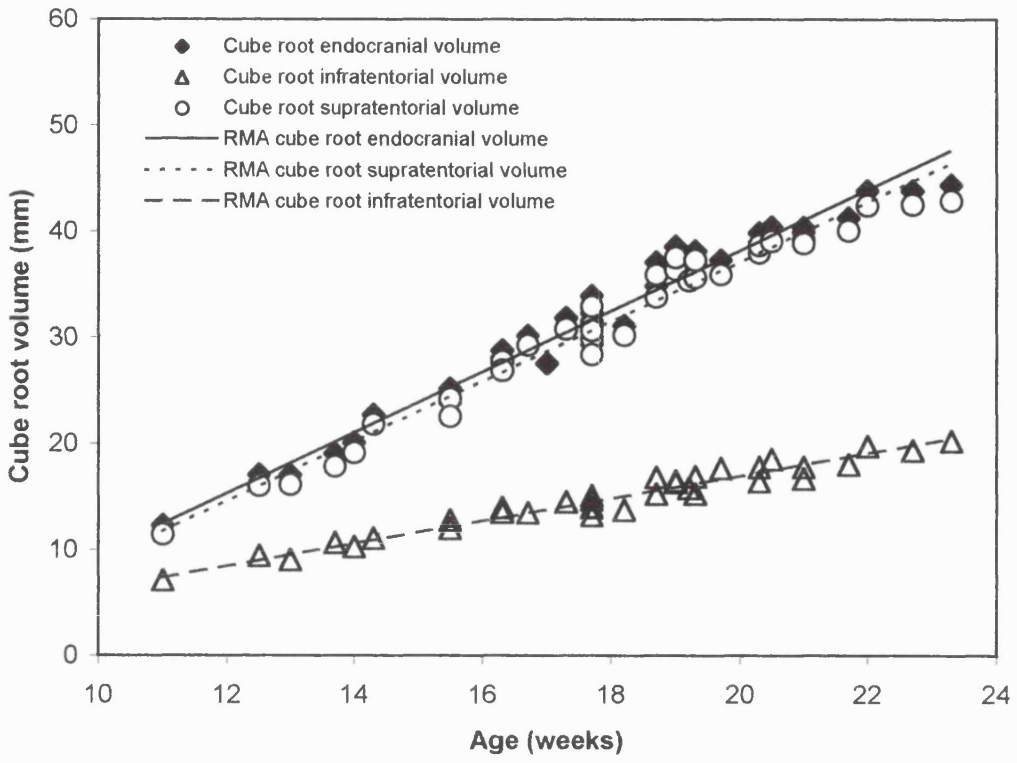

Figure 6.5. Bivariate plot of cube root endocranial volume, cube root supratentorial volume, and cube root infratentorial volume against age.

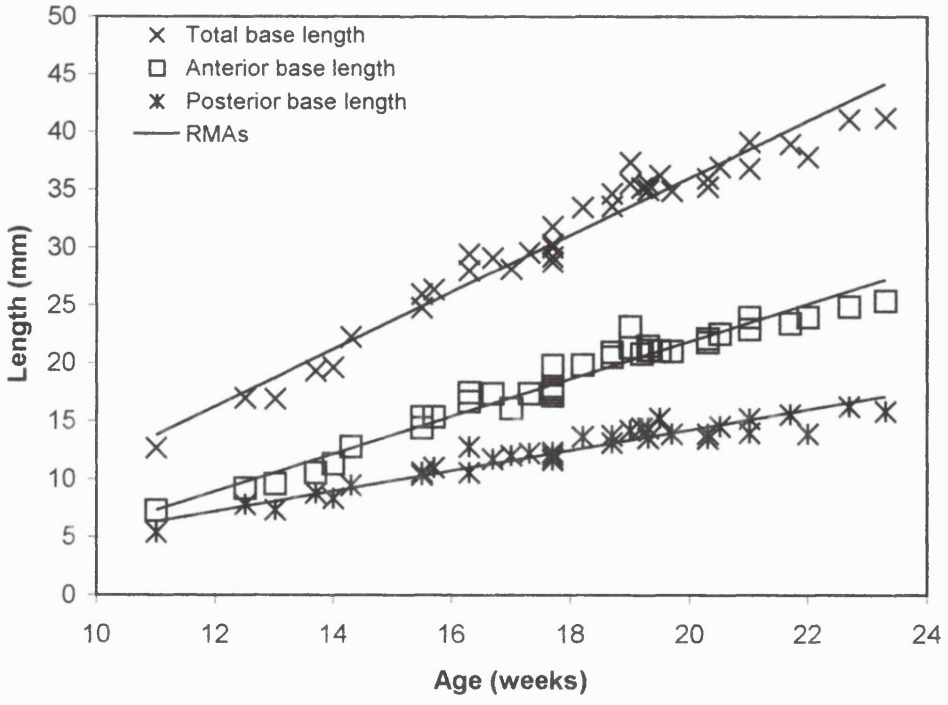

Figure 6.6. Bivariate plot of total, anterior, and posterior base lengths against age. The RMA is shown for each length.

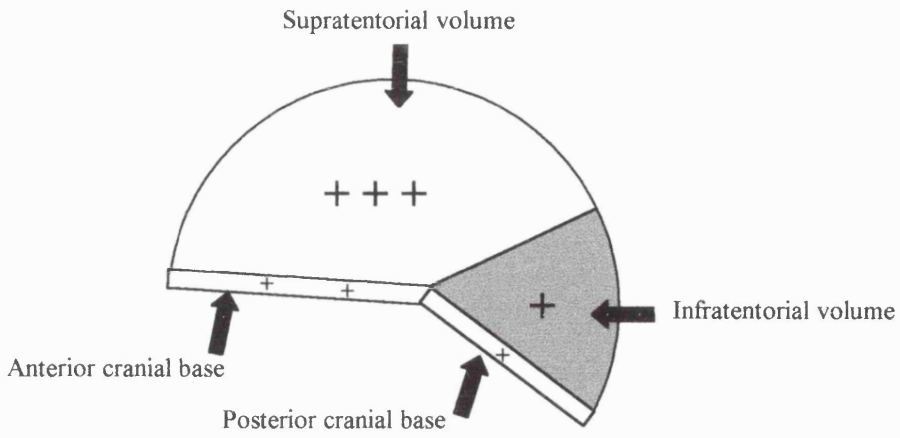

Figure 6.7. Schematic illustration of the relative contributions (+) of the supratentorial and infratentorial volumes to overall increases of endocranial volume and anterior and posterior cranial base lengths to increases of total base length. Supratentorial volume and anterior cranial base contribute the most. It is interesting to note that there is a greater difference in growth between supratentorial volume and anterior base length than between infratentorial volume and posterior base length.

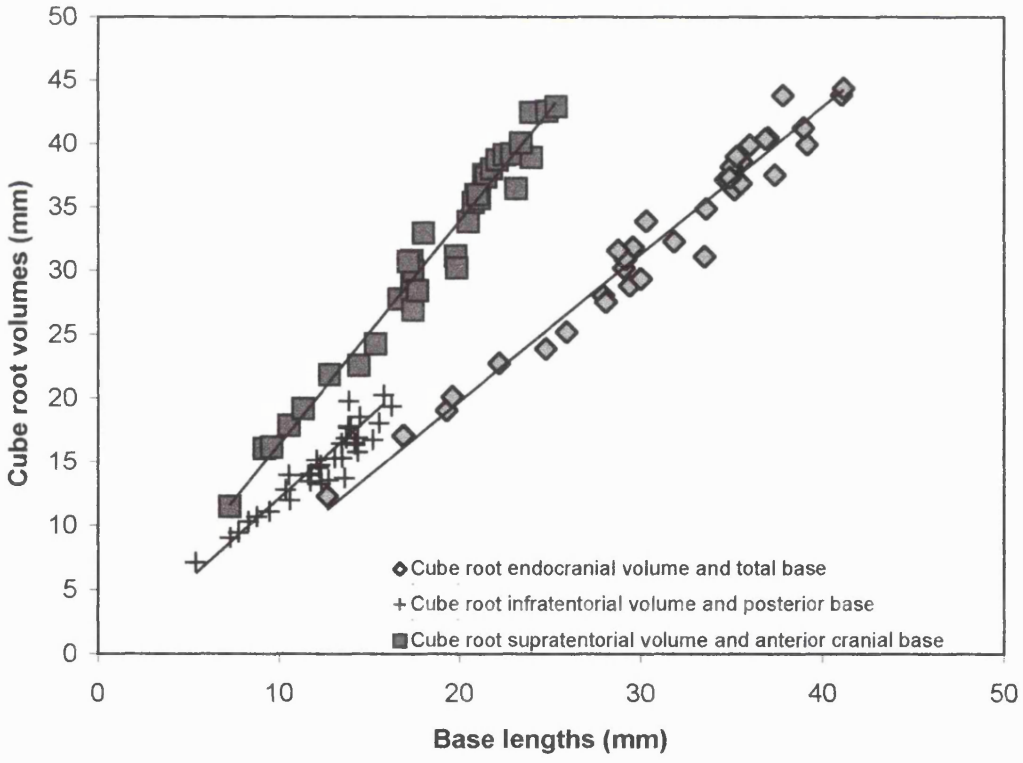

Figure 6.8. Bivariate plots of cube root endocranial volume, cube root supratentorial volume, and cube root infratentorial volumes against total, anterior, and posterior base length, respectively. The RMAs are shown for each plot (Note that $\sqrt[3]{A} + \sqrt[3]{B} \neq \sqrt[3]{A+B}$).

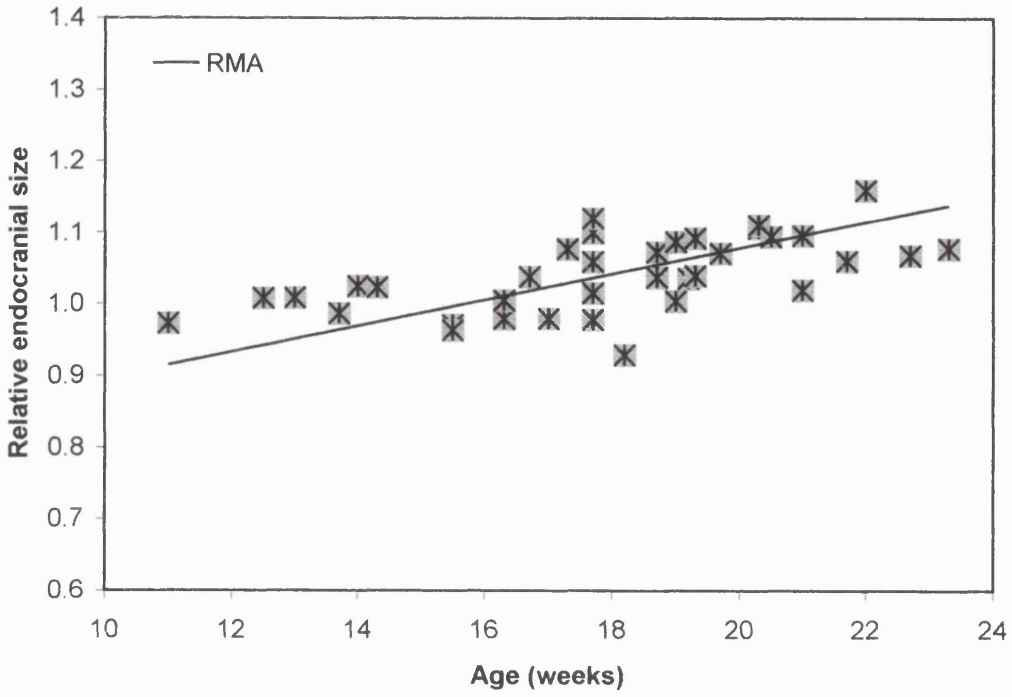

Figure 6.9. Bivariate comparison of relative endocranial size and age

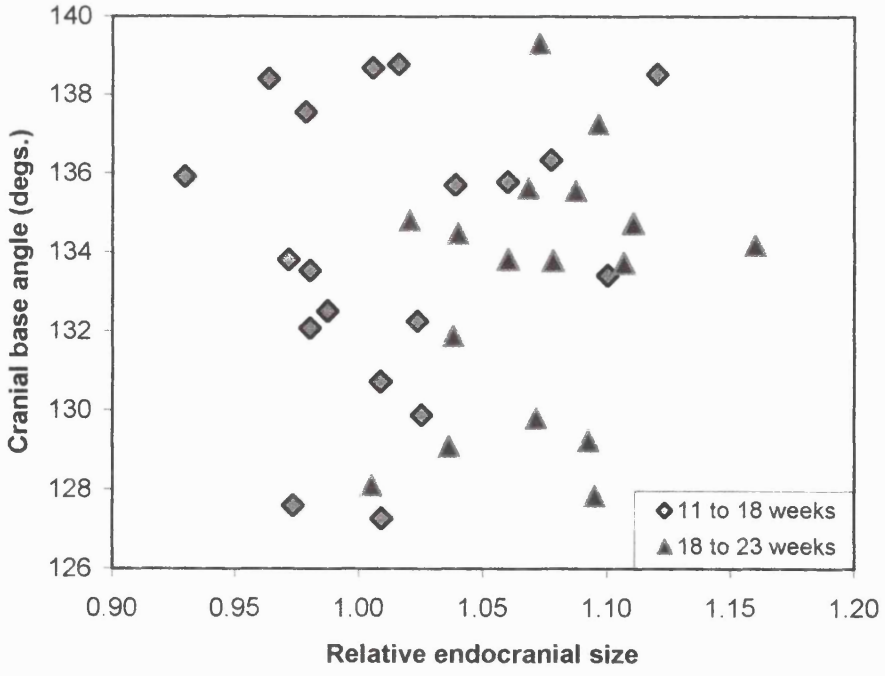

Figure 6.10. Bivariate plot of cranial base angle against relative endocranial size.

6.2 Basicranial architecture: posterior cranial fossa

The descriptive statistics of measurements that were used to evaluate associations amongst variations of brain topography, sagittal tentorial orientation, cranial base angulation and posterior cranial fossa morphology are listed in Table 6.4. Contemporaneous variations of brain topography and tentorial orientation were investigated with bivariate plots of the endocranial ratio (infra/supratentorial volume) and the sagittal tentorial angle against age (Figure 6.11a-b). Figure 6.11a illustrates temporal variations of endocranial ratio and tentorial angle with second order polynomials. These reveal that endocranial ratio decreases and tentorial angle increases during early fetal development. However, it is also shown that these variables plateau during the latter half of the period studied. To assess these temporal shifts in variations two-step RMAs are fitted in Figure 6.11b for the periods 11 to 18 and 18 to 23 weeks. The first steps reveal that endocranial ratio and tentorial angle negatively and positively correlate with age, respectively (Table 6.5). In contrast, no significant correlations were observed between either endocranial ratio or tentorial angle and age over the second step from 18 to 23 weeks (r_{rank} = 0.044 [ns] and 0.351 [ns], respectively). These results indicate that the tentorium cerebelli rotates backwards, towards the foramen magnum by about 25 degrees during early fetal life and that this is contemporaneous with an increase of the supratentorial volume relative to the infratentorial volume.

Figure 6.12 plots the tentorial angle directly against the endocranial ratio, distinguishing the 11 to 18 week and 18 to 23 week periods. The points appear discontinuous because one or the other measure, particular tentorial angle, is absent for some individuals from the first half of the second trimester. This graph reveals that tentorial angle negatively correlates with endocranial ratio with and without the

isolated group of points representing younger individuals (Table 6.5). Furthermore, the RMA slope computed with all available datum points is not significantly different from that computed without the isolated group of points (null hypothesis $slope_1 \neq slope_2$ rejected, $P>0.05$). These findings suggest that differential growth between supratentorial, i.e. the cerebrum, and infratentorial parts of the brain during early fetal life is associated with posterior rotation of the tentorium. Angles and ratios from the 18-23 week period cluster with mean values of 175.6 degrees (SD = 4.24 degs.) and 0.09 (SD = 0.003), respectively. This indicates that after eighteen weeks the cerebrum and subtentorial parts of the brain reach their topographical proportions within the endocranial space (90% and 10%, respectively) and variations of tentorial orientation are markedly smaller (Figure 6.13).

To investigate temporal variations of posterior cranial fossa morphology, petrous pyramid orientation and the proportions of the posterior fossa were plotted against age. No significant correlations were observed between petrous pyramid orientation and age across the whole, first half, or second half of the period studied (r_{rank} = 0.133 [ns], -0.442 [ns], and 0.372[ns], respectively).This suggests that there is no temporal change in the angle between the petrous pyramids. Figure 6.14 plots posterior fossa width and length against age. This graph reveals a greater increase of width than length in relation to age. At the end of the period studied, measured values of width and length are three and half and three times that at the beginning, respectively. Figure 6.15 plots posterior fossa width directly against length (Table 6.5). The slope of this graph is significantly greater than one ($P<0.001$), showing that there are direct increases of width in relation to length. In other words, posterior cranial fossae are more ellipsoidal amongst older fetuses.

A Bivariate comparison of endocranial ratio and cranial base angle was made to investigate their combined action upon the posterior cranial fossa and its contents. No significant correlation was observed over the whole period studied (r_{rank}= -0.324, ns). However, a comparison covering the first half of the period studied reveals a significant negative correlation (Figure 6.16, Table 6.5). This suggests that increases of supratentorial relative to infratentorial volume are associated with basicranial retroflexion. Thus, variations of brain topography and cranial base angulation have an associated action that converges upon the contents of the posterior cranial fossa during early fetal development. Consequently, the hypotheses predict that variations of basicranial angulation and endocranial ratio correlate with changes of posterior fossa morphology during early fetal life. Given that endocranial ratio and cranial base angle vary mostly during early fetal development, all of the following comparisons are made with individuals from the first half and the whole period studied.

To investigate the extent to which variations of brain topography influence posterior fossa morphology, posterior fossa proportions (width/length) and petrous pyramid orientation were plotted against endocranial ratio. No significant correlations were observed between petrous pyramid orientation and endocranial ratio over the whole or first half of the period studied (r_{rank} = 0.069 [ns] and 0.374 [ns], respectively). Figure 6.17 plots the index of proportions against endocranial ratio. There is a significant negative correlation between these variables across the whole but not the first half of the period studied (Table 6.5 and r_{rank} = -0.100 [ns], respectively). This reveals that increases of supratentorial relative to infratentorial volume are associated with increases of posterior fossa width in relation to length. These results are therefore consistent with the hypothesis that changes in brain

topography influence the proportions of the posterior fossa. However, there is no support for the hypothesis that brain topography influences petrous pyramid orientation during fetal development.

To investigate the extent to which variations of basicranial angulation influence posterior fossa morphology, the posterior fossa proportions (width/length) and petrous pyramid orientation were plotted against cranial base angle. No significant correlations were observed between the index of proportions and cranial base angle over the whole or first half of the period studied (r_{rank} = 0.047 [ns] and 0.232 [ns], respectively). In addition, no significant correlation was observed between petrous pyramid orientation and CBA over the whole period studied (r_{rank} = -0.089, ns). However, a significant negative correlation was observed between petrous pyramid orientation and CBA over the first half of the period studied (Figure 6.18, Table 6.5), i.e. increases of CBA are associated with decreases of petrous pyramid angle during early fetal development. Thus, the posterior attachments of the tentorium shift medially in relation to the anterior attachments as the base retroflexes. In other words, increases of cranial base angle (retroflexion) are associated with more sagittally orientated petrous pyramids.

Bivariate comparisons of the posterior cranial fossa proportions and petrous pyramid orientation against relative infratentorial size were used to assess the hypothesis that increases of infratentorial size relative to posterior cranial base length are associated with variations of petrous pyramid orientation and posterior fossa width in relation to length. No significant correlations were observed between the proportions and relative infratentorial size over the whole or first half of the period studied (r_{rank} = -0.226 [ns] and 0.213 [ns], respectively). In addition, no correlations were observed between petrous pyramid orientation and relative infratentorial size

over the whole or first half of the period studied (r_{rank} = 0.110 [ns] and -0.393 [ns], respectively). Thus, these findings suggest that increases of infratentorial size relative to posterior base length are not accommodated within the posterior fossa by rotation of the petrous pyramids or increases of posterior fossa width in relation to length.

These observations, which are summarised in Figure 6.19, indicate that: posterior fossa width increases in relation to length with increases of supratentorial relative to infratentorial volume; sagittal orientation of the petrous pyramids increases with increases of cranial base angle during early fetal development; neither petrous pyramid orientation or the proportions of the posterior fossa vary in relation to increases of relative infratentorial size. Thus, changes of posterior cranial fossa morphology are associated more with variations of brain topography and base angulation than with the spatial-packing problem caused by enlargement of the cerebellum and brain stem relative to the length of the posterior cranial base.

Table 6.4. Descriptive statistics for the ratio between infra tentorial and supratentorial volumes, sagittal tentorial angle, the proportions of the posterior fossa, and petrous pyramid orientation.

	N	Mean	S.D.	Min.	Max.
Endocranial ratio (infra/supra)	35	0.116	0.041	0.07	0.24
Sagittal tentorial angle (deg.)	31	169.91	10.95	139.8	179.8
Posterior fossa width (mm)	38	29.83	7.35	11.0	40.8
Posterior fossa length (mm)	38	22.87	5.24	10.4	32.4
Petrous pyramids orientation (deg.)	31	66.63	5.47	56.4	77.2

Table 6.5. RMA and correlation statistics for tentorial angle, endocranial ratio, posterior fossa proportions, and petrous pyramid orientation (* , P<0.05; ** , P<0.01; *** P<0.001).

	n	r_{rank}	P	Slope	95% conf. int for slope	Intercept
Tentorial angle x age, 11 to 18 weeks	13	0.854	***	6.70	4.44, 8.95	56.27
Endocranial angle x age, 11 to 18 weeks	18	-0.861	***	-0.02	-0.03, -0.02	0.48
Tentorial angle x endocranial ratio	30	-0.679	***	-326.50	-389.78, -263.22	205.80
Tentorial angle x endocranial ratio, points omitted	27	-0.465	*	-380.49	-515.72, -245.26	211.00
Posterior fossa width x age	38	0.979	***	2.55	2.39, 2.72	-15.90
Posterior fossa length x age	38	0.931	***	1.82	1.65, 2.00	-9.69
Posterior fossa width x length	38	0.910	***	1.40	1.25, 1.56	-2.22
Cranial base angle x endocranial ratio, 11 to 18 weeks	18	-0.625	**	-79.55	-112.52, -46.59	145.06
Posterior fossa width/length x endocranial ratio	35	-0.474	**	-2.79	-3.73, -1.85	1.62
Petrous pyramid orientation x cranial base angle, 11 to 18 weeks	13	-0.501	*	-1.49	-2.24, -0.73	264.35

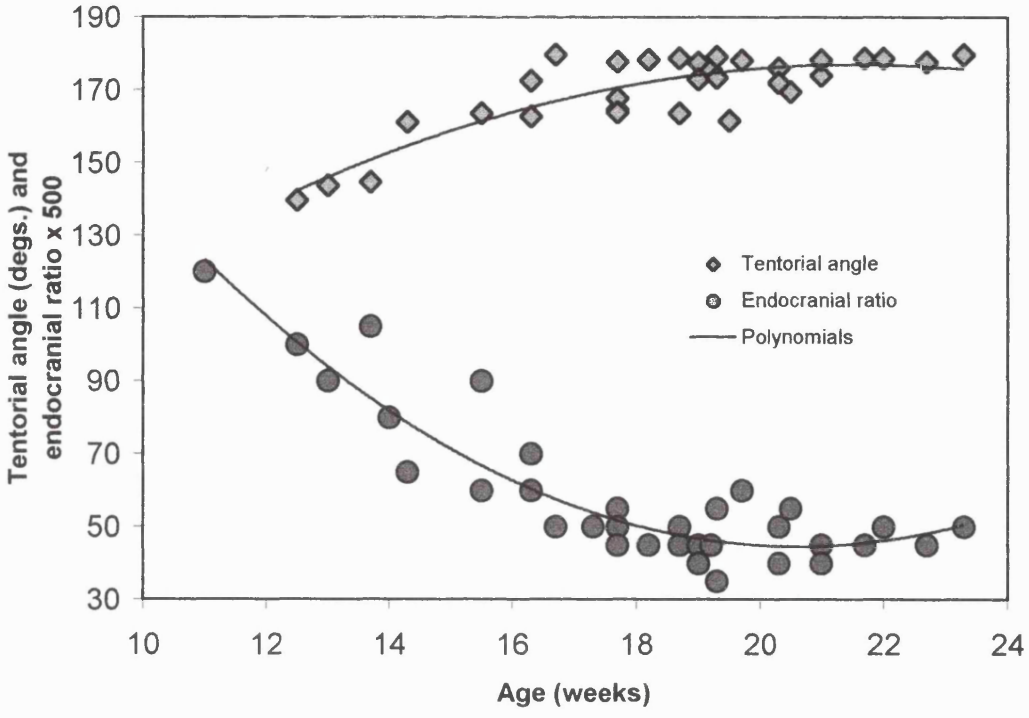

(a)

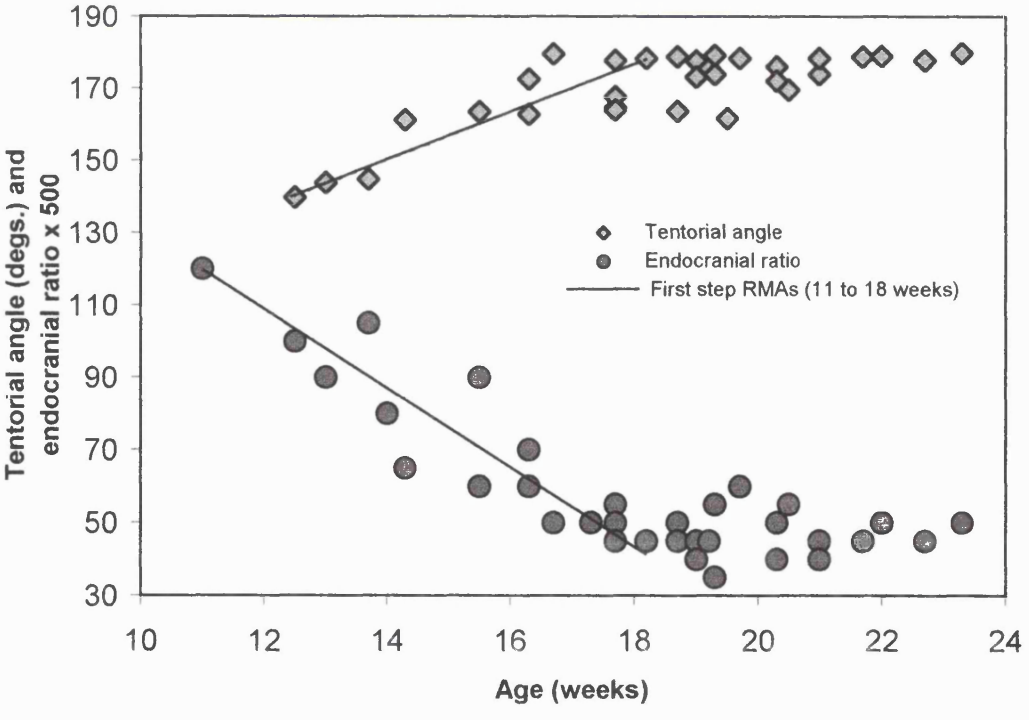

(b)

Figure 6.11a & b. Bivariate plots of endocranial ratio and tentorial angle against age: (a) 2nd order polynomials for endocranial ratio against age ($y = 0.0017x^2 - 0.0702x + 0.8128$, $R^2 = 0.846$) and tentorial angle against age ($y = -0.4251x^2 + 18.314x - 20.272$, $R^2 = 0.73$); (b) RMA regressions for endocranial ratio and tentorial angle against age for 11 to 18 weeks (Table 5).

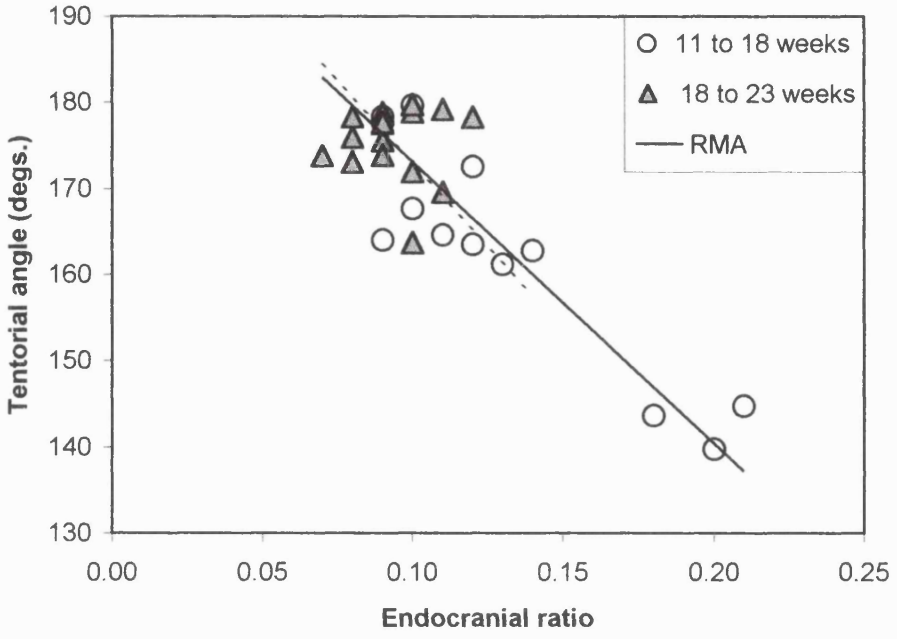

Figure 6.12. Bivariate plot of tentorial angle against endocranial ratio. A second RMA (broken line) is shown, omitting the three right most points (see Table 5).

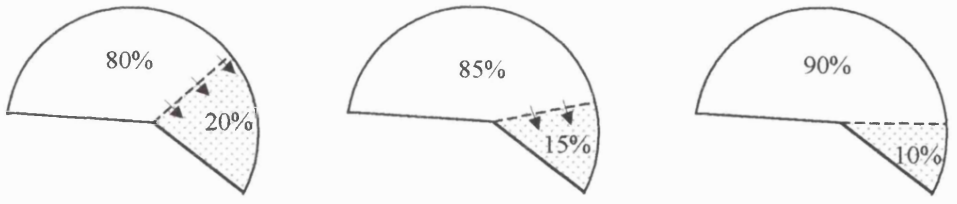

Figure 6.13. Schematic representation of tentorial rotation in relation to changes of supratentorial (white area) and infratentorial (shaded area) proportions of the endocranial space. During early fetal life, the supratentorial parts of the brain increase in relation to the infratentorial parts and the tentorium, which separates these brain segments, rotates posteriorly. After eighteen weeks, the topographically proportions of the endocranial space are reached, consisting of 90% supratentorial and 10% infratentorial parts, and tentorial rotation is markedly reduced.

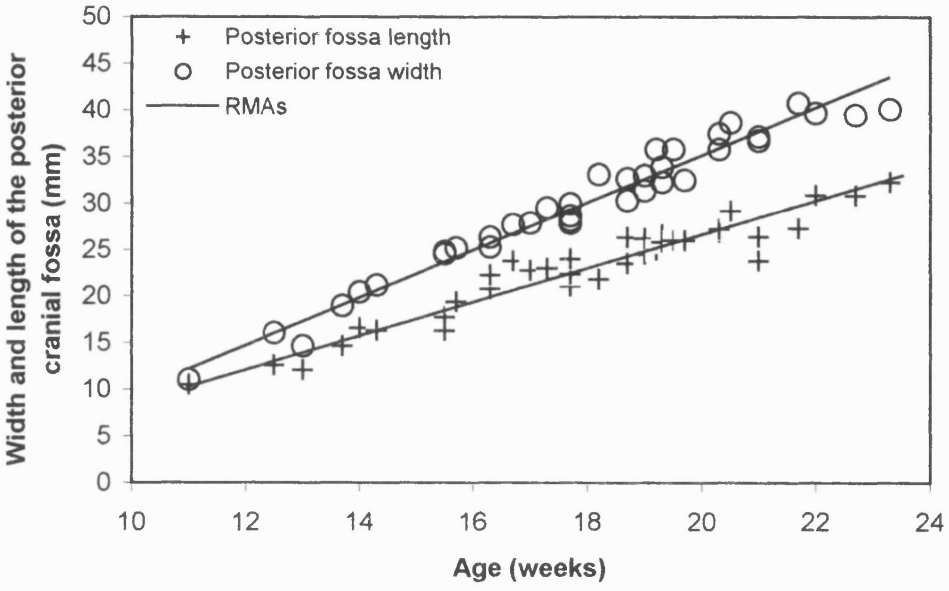

Figure 6.14. Bivariate plots of posterior cranial fossa width and length against age.

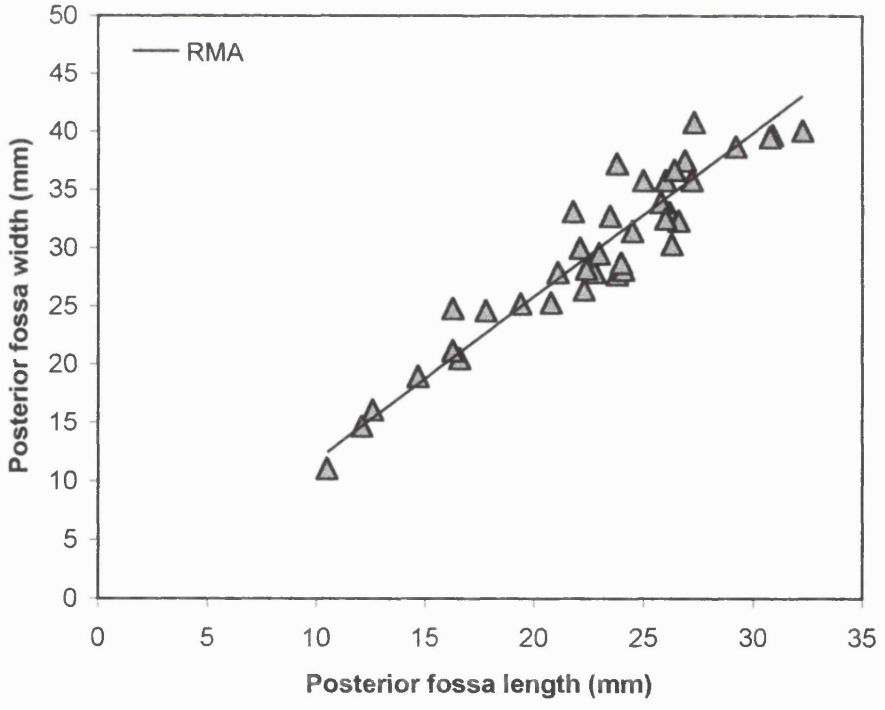

Figure 6.15. Bivariate comparison of posterior fossa width against length.

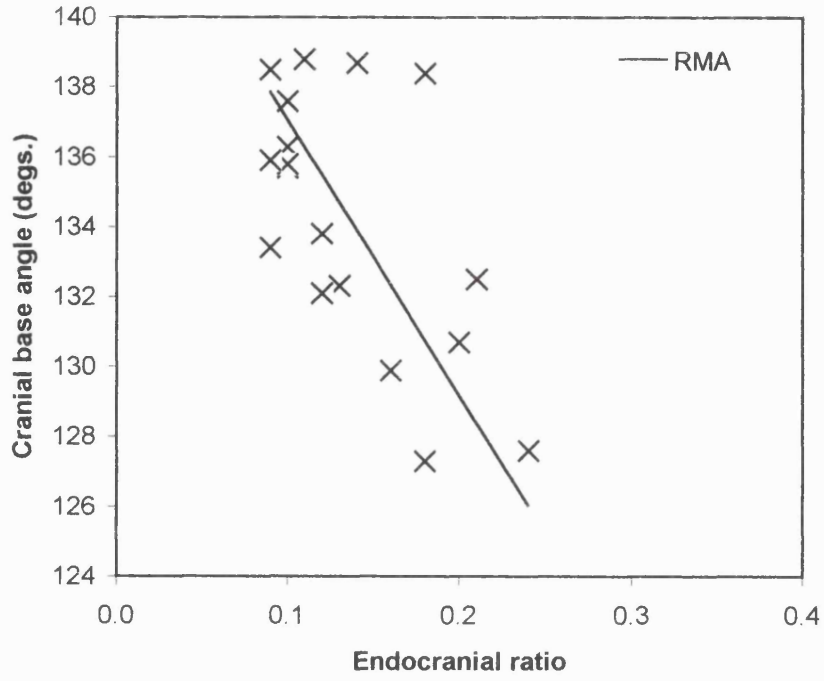

Figure 6.16. Bivariate plot of cranial base angle against endocranial ratio from 11 to 18 weeks.

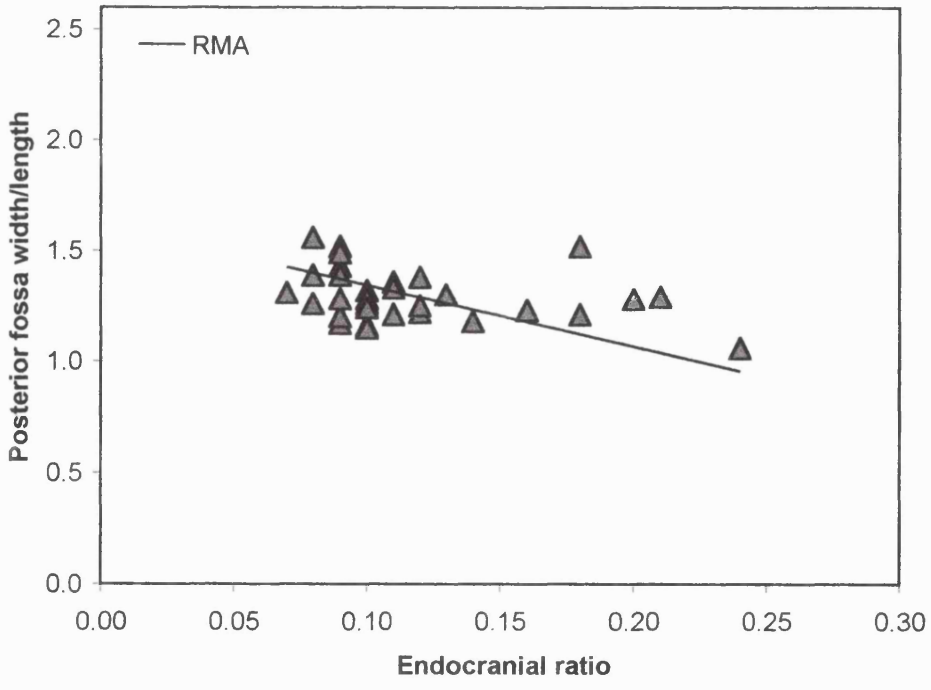

Figure 6.17. Bivariate plot of posterior fossa width/length against endocranial ratio.

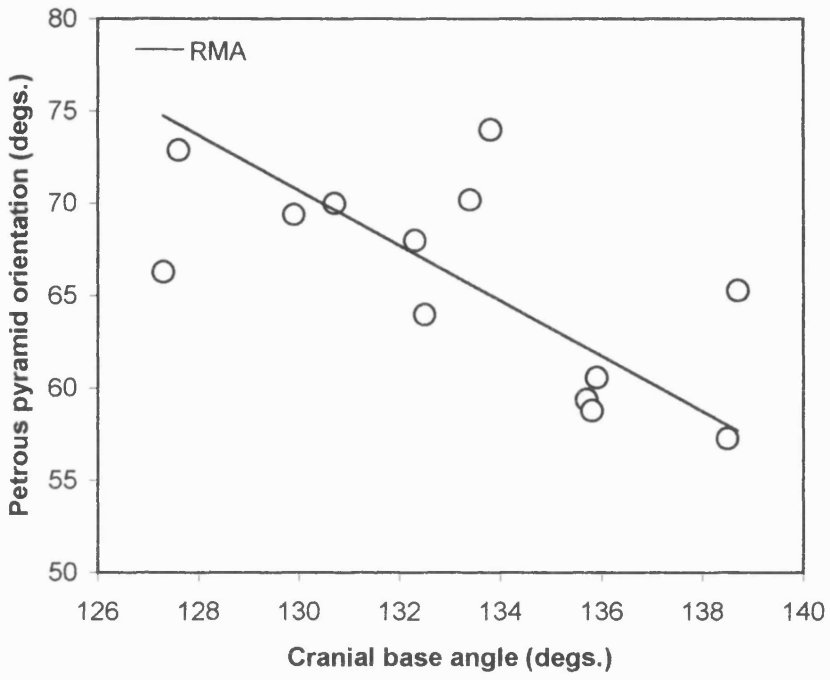

Figure 6.18. Bivariate comparison of petrous pyramid orientation and cranial base angle from 11 to 18 weeks.

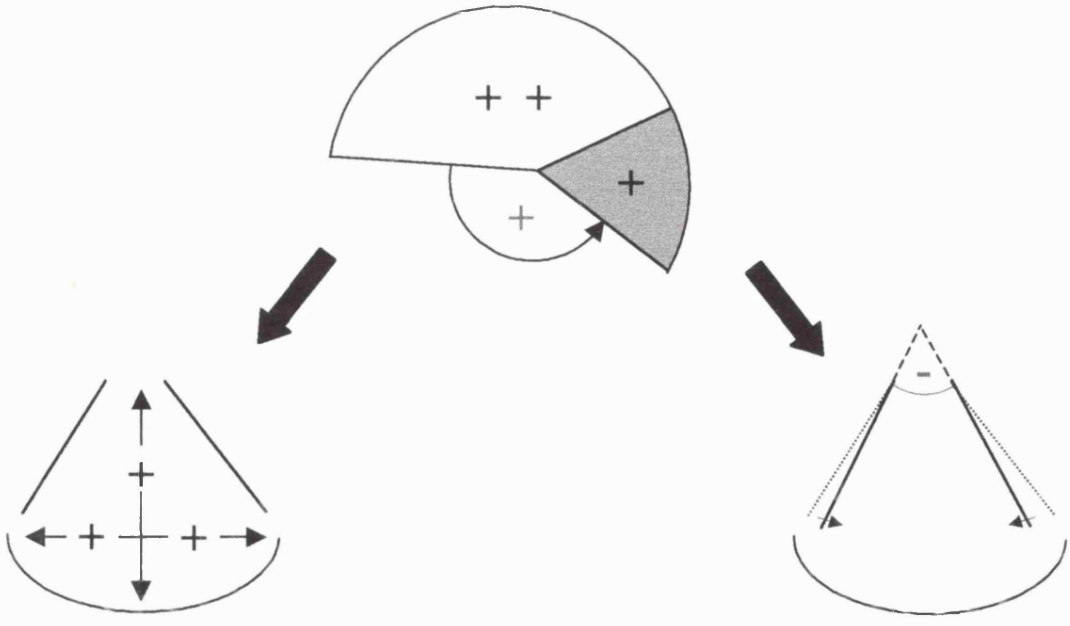

Figure 6.19. Schematic illustrations of the relationship between increases of supratentorial size relative to infratentorial size and increases of posterior cranial fossa width in relation to length (dark signs). Also shown is the relationship between increases of cranial base angle, which is associated with increases of supratentorial size relative to infratentorial size, and decreases of petrous pyramid orientation (grey signs).

6.3 Basicranial and facial complex: facial kyphosis and maxillary prognathism

The descriptive statistics of the measurements used to test hypotheses relating to facial morphology are listed in Table 6.6. To assess temporal variations in facial morphology, palate length, maxillary height, palate orientation, and maxillary angle are plotted against age. All of these measures are significantly correlated with age (Table 6.7). Figure 6.20 plots maxillary height and palate length against age. The slope of palate length against age is significantly steeper than that for maxillary height against age ($P<0.001$), signifying a one third greater increase of the former. The slope of palate length against age is significantly greater than one ($P<0.01$) while that of maxillary height is not ($P>0.05$, ns). Figure 6.21 plots palate length directly against maxillary height (Table 6.7). The slope of this graph is significantly greater than one ($P<0.01$), showing that palate length directly increases relative to maxillary height. These findings indicate that facial height develops in proportion with age while facial length increases in relation to age. Thus, facial height is comparatively the same in both young and old fetuses while facial depth is comparatively longer in older fetuses.

Figure 6.22 plots maxillary angle and palate orientation against age. This graph shows that both maxillary angle and palate orientation increase with age. The slope of maxillary angle against age is not significantly greater than that of palate orientation and age ($P>0.05$, ns), indicating that there is little increase of maxillary angle in relation to palate orientation. These results illustrate maxillary prognathism and facial retroflexion, as opposed to kyphosis, during second trimester human development. The maxilla rotates anteriorly from a retrognathic position of 86 degrees relative to the anterior cranial base to a more prognathic position of 96

degrees. Palate orientation opens out superiorly from 113 degrees to 121 degrees relative to the posterior cranial base. Thus, the palate is more superiorly orientated relative to the posterior cranial base and the maxilla is more anteriorly orientated relative to the anterior cranial base in older fetuses. Direct comparisons fail to reveal a significant association between maxillary prognathism and palate rotation over the whole or first half of the period studied (r_{rank} = 0.248 [ns] and 0.104 [ns], respectively).

To investigate the extent to which changes of facial morphology are associated with variations in basicranial angulation, maxillary angle and palate orientation were compared with cranial base angle. No significant correlations were observed between maxillary angle and cranial base angle with individuals from the whole or first half of the period studied (r_{rank} = -0.155 [ns] and -0.026 [ns], respectively). There was, however, a significant positive correlation between palate orientation and cranial base angle over the whole period studied with a slope that is not significantly different to one (Figure 6.23, Table 6.7). This graph reveals that superior rotation of the palate relative to the posterior cranial base is associated with cranial base retroflexion, i.e. increases of CBA. However, this association may be due to both measures containing the line segment sella to basion that describes the posterior cranial base.

Bivariate comparisons of maxillary angle and palate orientation against relative endocranial size were used to assess the notion that increases of endocranial size relative to base length are associated with variations of facial morphology. No significant correlations were observed between relative endocranial size and palate orientation with individuals from the whole and first half of the period studied (r_{rank} = 0.289 [ns] and 0.033 [ns], respectively). Figure 6.24 plots maxillary angle against

relative endocranial size (Table 6.7). This plot reveals a significant positive correlation, indicating that maxillary prognathism is associated with increases of endocranial size relative to total base length. These observations, which are summarised in Figure 6.25, show that maxillary prognathism and facial retroflexion increase with age and are associated with relative endocranial size and cranial base angulation, respectively.

Table 6.6. Descriptive statistics for palate length, maxillary height, palate orientation, and maxillary angle.

	N	Mean	S.D.	Min.	Max.
Palate length (mm)	36	13.19	4.01	5.4	20.0
Maxillary height (mm)	36	10.94	3.08	4.6	18.0
Palate orientation (degs.)	36	118.21	3.43	110.6	125.0
Maxillary angle (degs.)	36	91.81	4.77	84.4	102.0

Table 6.7. RMA and correlation statistics for palate length, maxillary height, palate orientation, and maxillary angle (* , P<0.05; ** , P<0.01; *** P<0.001).

	n	r_{rank}	P	Slope	95% conf. int for slope	Intercept
Palate length x age	36	0.963	***	1.36	1.23, 1.50	-11.27
Maxillary height x age	36	0.881	***	1.04	0.88, 1.21	-7.83
Palate length x maxillary height	36	0.894	***	1.30	1.12, 1.48	-1.07
Palate orientation x age	36	0.425	**	1.16	0.81, 1.51	97.29
Maxillary angle x age	36	0.548	***	1.62	1.14, 2.10	62.68
Palate orientation x cranial base angle	36	0.606	***	0.95	0.69, 1.21	-8.41
Maxillary angle and relative endocranial size	34	0.566	***	89.33	62.38, 116.28	-1.02

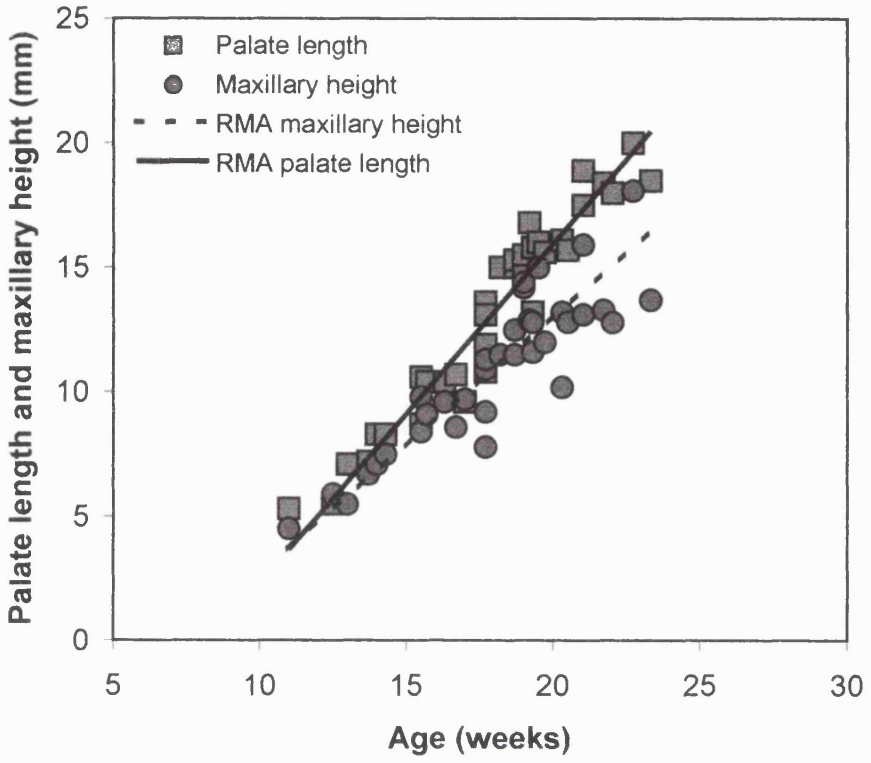

Figure 6.20. Bivariate plots of maxillary height and palate length against age.

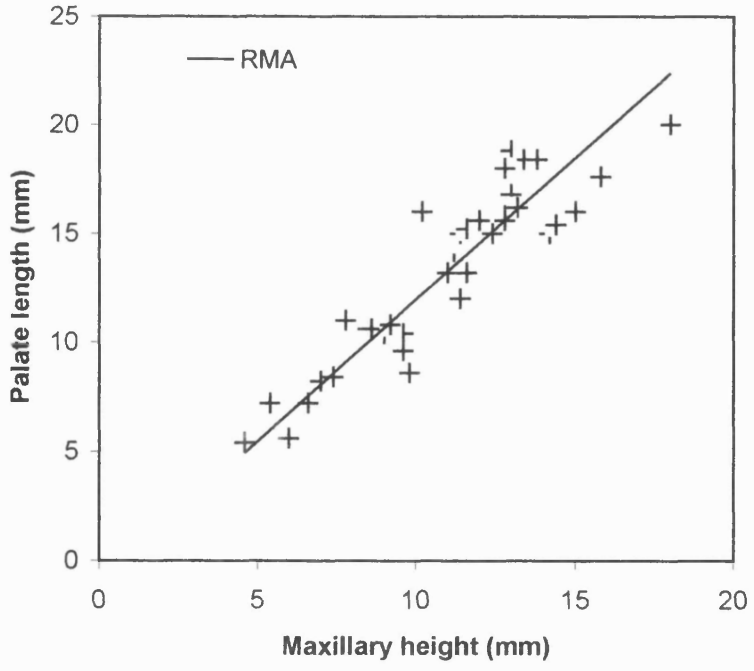

Figure 6.21. Bivariate plot of palate length against maxillary height.

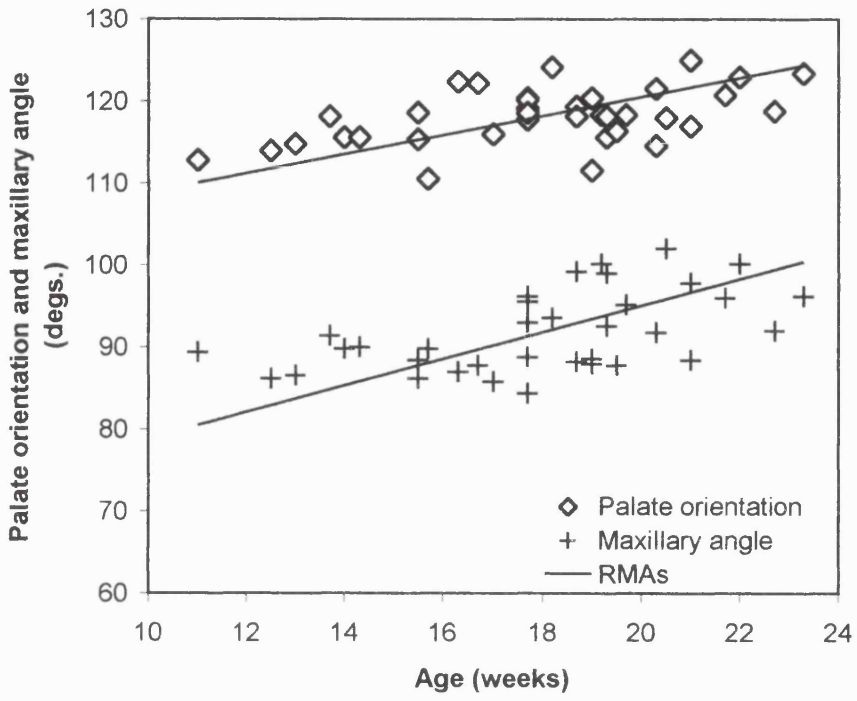

Figure 6.22. Bivariate plot of maxillary angle and palate orientation against age.

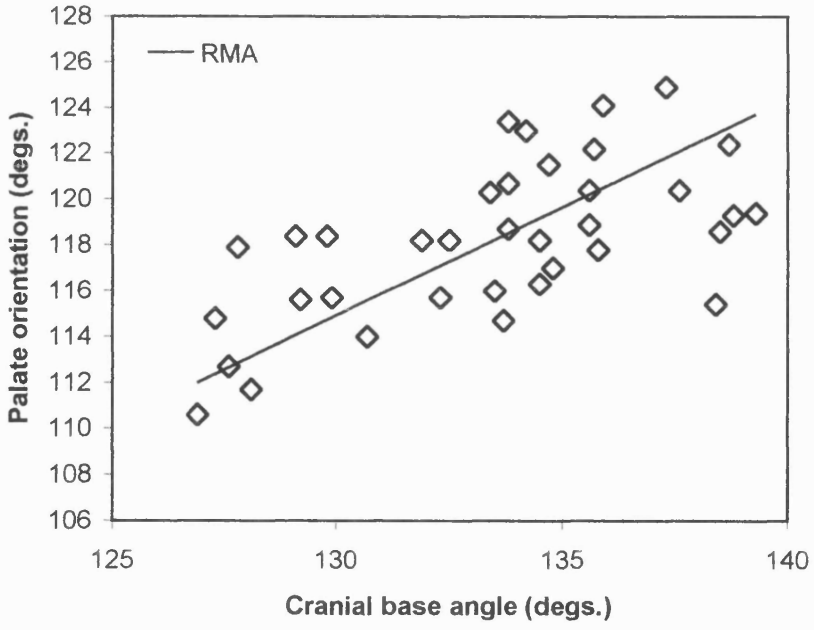

Figure 6.23. Bivariate plot of palate orientation against cranial base angle.

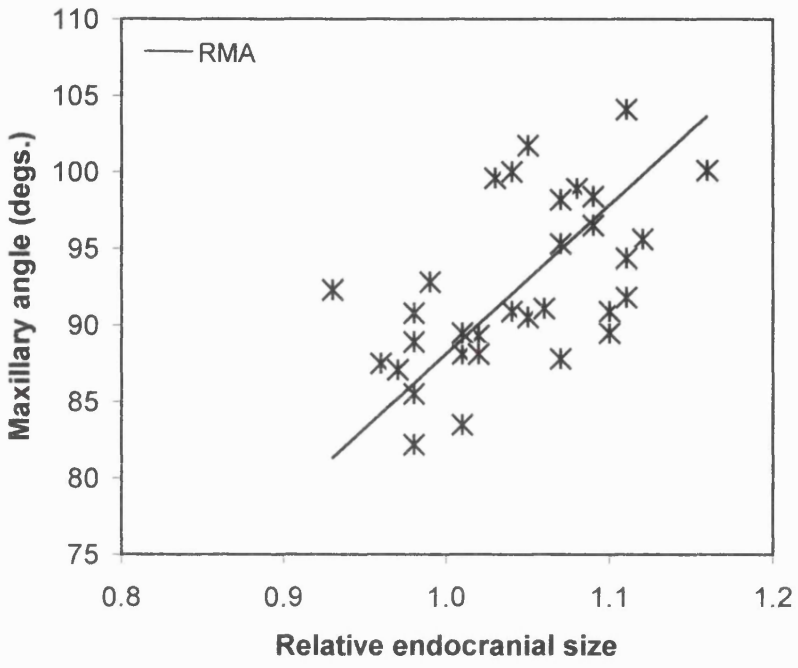

Figure 6.24. Bivariate plot of maxillary angle against relative endocranial size.

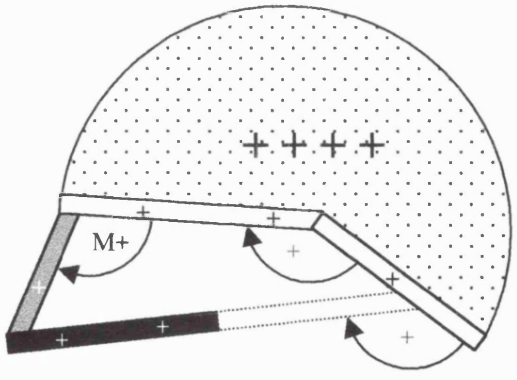

Figure 6.25. Schematic illustration of variations in facial morphology. The study indicates that palate length (white plus signs on black) increases in relation to maxillary height (white plus sign on grey). It is also shown that maxillary prognathism (M+) is associated with increases of endocranial size relative to base length and that increases of the angle between the palate and posterior cranial base are associated with increases of cranial base angle (grey plus signs). Notice that both palate orientation and cranial base angle are measured relative to the posterior cranial base.

6.4 Basicranial and facial complex: orbital convergence and frontation

The descriptive statistics for the measurements that are used to quantify orbital morphology are listed in Table 6.8. Temporal variations of orbital morphology were evaluated with bivariate plots of orbital axes orientation, orbital rim orientation, interorbital angle, and relative interorbital distance against age. No significant correlations were observed between orbital axes orientation or orbital rim orientation and age over the whole period studied (r_{rank} = -0.137 [ns] and 0.270 [ns], respectively). However, plots for these variables from 11 to 18 weeks yield significant positive correlations (Figures 6.26 and 27, Table 6.9). These graphs reveal increases of 18 degrees between the orbital axes and the posterior cranial base and 10 degrees between the orbital rims and the anterior cranial base.

Figures 6.28 and 29 show bivariate comparisons of interorbital angle and relative interorbital distance against age over the whole period studied. Relative interorbital distance negatively correlates with age while interorbital angle positively correlates with age (Table 6.9). Thus, interorbital angle increases by about thirty degrees and relative interorbital distance is almost halved across the second trimester.

These findings indicate a number of temporally associated changes in orbital morphology. Firstly, that during early fetal development the orbital axes rotate superiorly relative to the posterior cranial base and that the inferior orbital rims rotate anteriorly in relation to the superior orbital rims and the anterior cranial base (sagittal orbital frontation). Secondly, the temporal trends over the whole period studied suggest that the lateral orbital rims rotate anteriorly in relation to the medial orbital rims (transverse orbital frontation) and the relative size of the interorbital

distance decreases (orbital convergence). Thus, older fetuses have more frontated and convergent orbits and more superiorly orientated orbital axes relative to the posterior cranial base.

Relationships between these variations of orbital morphology and basicranial architecture were assessed with bivariate comparisons against cranial base angle. Given that CBA varies during early fetal life, these comparisons were made with individuals from the whole and first half of the period studied. No significant correlations were observed between CBA and orbital rim orientation or relative interorbital distance over the whole period studied (r_{rank} = 0.034 [ns] and -0.109 [ns], respectively). In addition, no significant correlation was observed with orbital rim orientation over the first half of the period studied (r_{rank} = 0.096, ns).

Figure 6.30 plots relative interorbital distance against CBA over the first half of the period studied, revealing a significant negative correlation (Table 6.9). Comparisons of CBA with orbital axes orientation and interorbital angle yield significant positive correlations (Figures 6.31 and 32, Table 6.9). These findings reveal a number of associations. Firstly, orbital convergence is associated with the increase of CBA observed during early fetal life. Secondly, that transverse orbital frontation and superior rotation of the orbital axes relative to the posterior cranial base are associated with CBA across the whole period studied.

Bivariate plots of the orbital axes orientation, orbital rim orientation, interorbital angle, and relative interorbital distance against relative endocranial size were used to investigate relationships between orbital morphology and variations of endocranial size relative to base length. No significant correlations were observed between relative endocranial size and orbital axes orientation or orbital rim orientation over the whole (r_{rank} = 0.031 [ns] and 0.262 [ns], respectively) or first half

of the period studied (r_{rank} = 0.173 [ns] and 0.094 [ns], respectively). Figures 6.33 and 6.34 plot interorbital angle and relative interorbital distance against relative endocranial size over the whole period studied (Table 6.9). These graphs reveal that transverse orbital frontation and orbital convergence are associated with increases of brain size relative to base length.

These observations, some of which are illustrated in Figure 6.35, indicate that: increases of CBA are associated with orbital convergence during early fetal development, transverse orbital frontation, and superior rotation of the orbital axes; increases of endocranial size relative to base length are also associated with orbital convergence and transverse orbital frontation.

Table 6.8. Descriptive statistics for orbital axes orientation, orbito-palatine angle, orbital rim orientation, interorbital angle, and relative interorbital distance.

	N	Mean	S.D.	Min.	Max.
Orbital axes orientation (degs.)	36	122.92	6.08	108.4	133.4
Orbital rim orientation (degs.)	37	63.66	5.84	50.2	72.2
Interorbital angle (degs.)	37	129.90	8.84	106.4	144.2
Relative interorbital distance	37	0.331	0.057	0.25	0.50

Table 6.9. RMA and correlation statistics for orbital axes orientation, orbito-palatine angle, orbital rim orientation, interorbital angle, and relative interorbital distance (* , $P<0.05$; ** , $P<0.01$; *** $P<0.001$).

	n	r_{rank}	P	Slope	95% conf. int for slope	Intercept
Orbital axes orientation x age, 11 to 18 weeks	19	0.790	***	3.27	2.41, 4.13	72.88
Orbital rim orientation x age, 11 to 18 weeks.	20	0.480	*	2.90	1.74, 4.07	17.08
Interorbital angle x age	37	0.698	***	3.04	2.41, 3.67	75.61
Relative interorbital distance x age	37	-0.893	***	-0.020	-0.023, -0.016	0.682
Relative interorbital distance x cranial base angle, 11 to 18 weeks	20	-0.511	*	-0.012	-0.017, -0.007	1.981
Orbital axes orientation x cranial base angle	36	0.691	***	7.71	1.29, 2.13	-104.93
Interorbital angle x cranial base angle	37	0.456	**	2.45	1.72, 3.19	-197.66
Interorbital angle x relative endocranial size	35	0.504	**	159.04	110.39, 207.70	-35.38
Relative interorbital distance x relative endocranial size	35	-0.517	**	-1.04	-1.37, -0.71	1.42

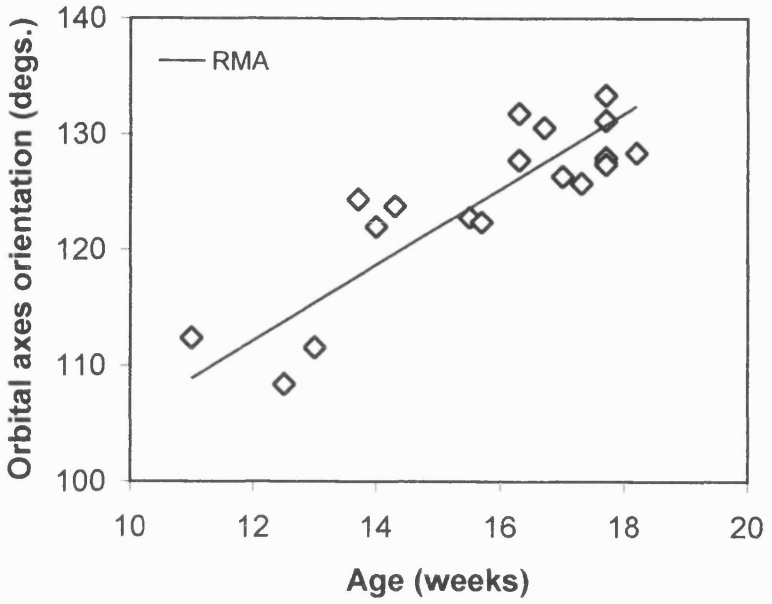

Figure 6.26. Bivariate plot of orbital axes orientation and age from 11 to 18 weeks.

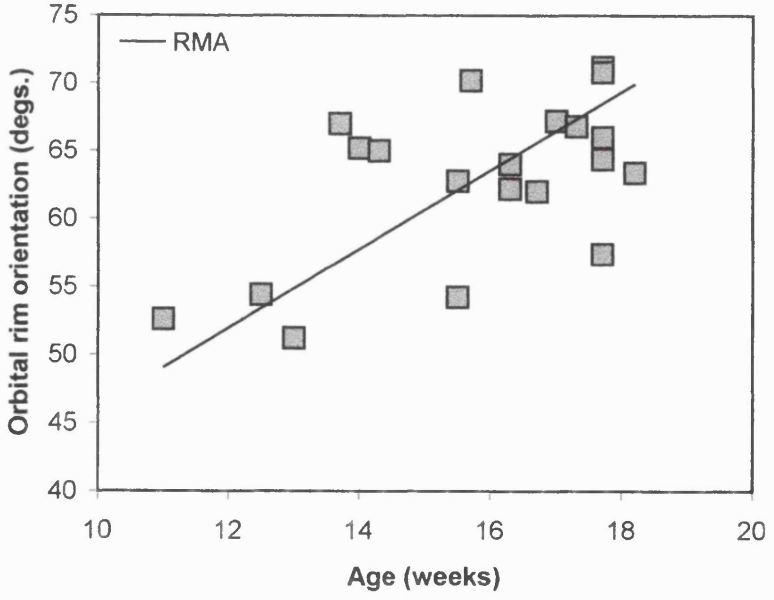

Figure 6.27. Bivariate plot of orbital rim orientation against age from 11 to 18 weeks

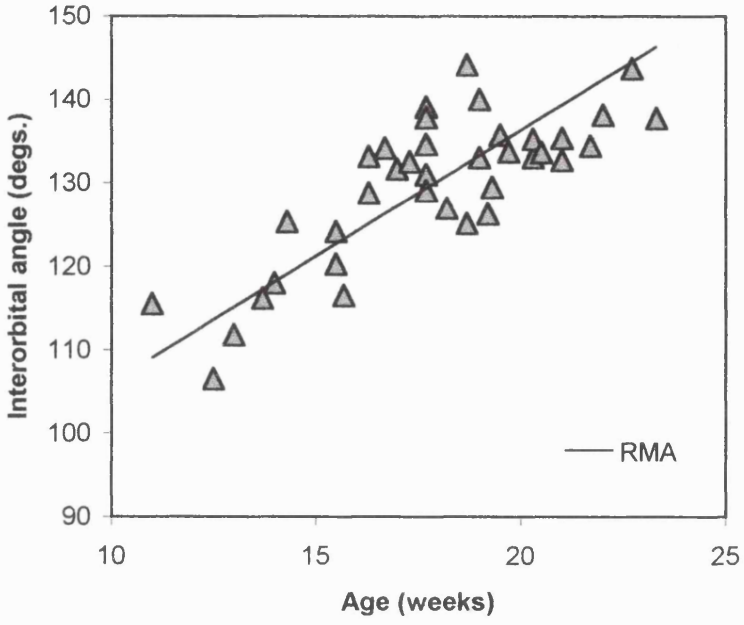

Figure 6.28. Bivariate plot of interorbital angle and age.

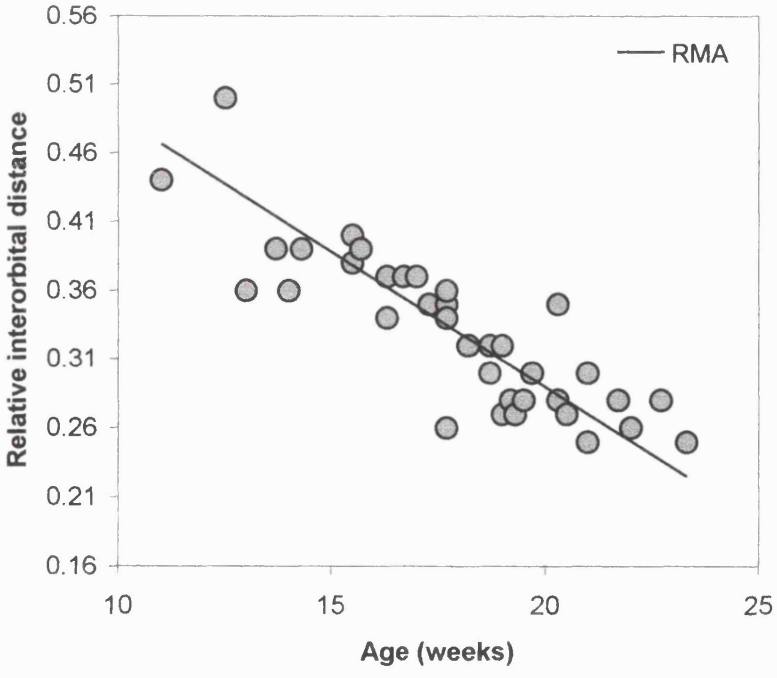

Figure 6.29. Bivariate plot of relative interorbital distance against age.

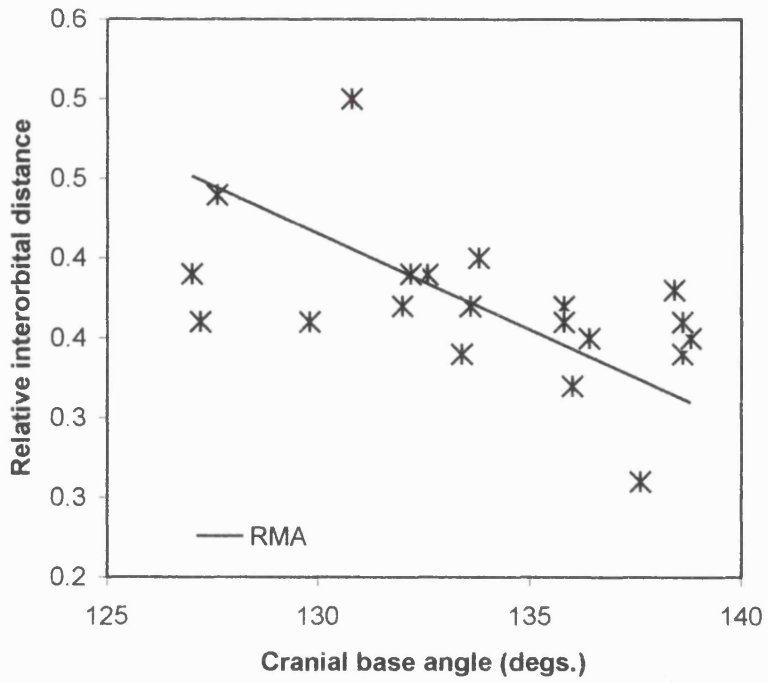

Figure 6.30. Bivariate plot of relative interorbital distance against cranial base angle from 11 to 18 weeks.

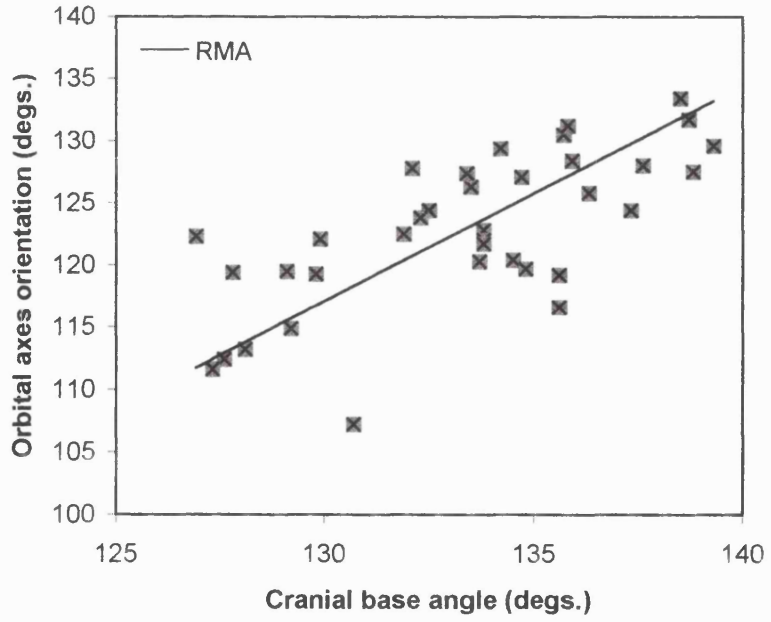

Figure 6.31. Bivariate plot of orbital axes orientation and cranial base angle.

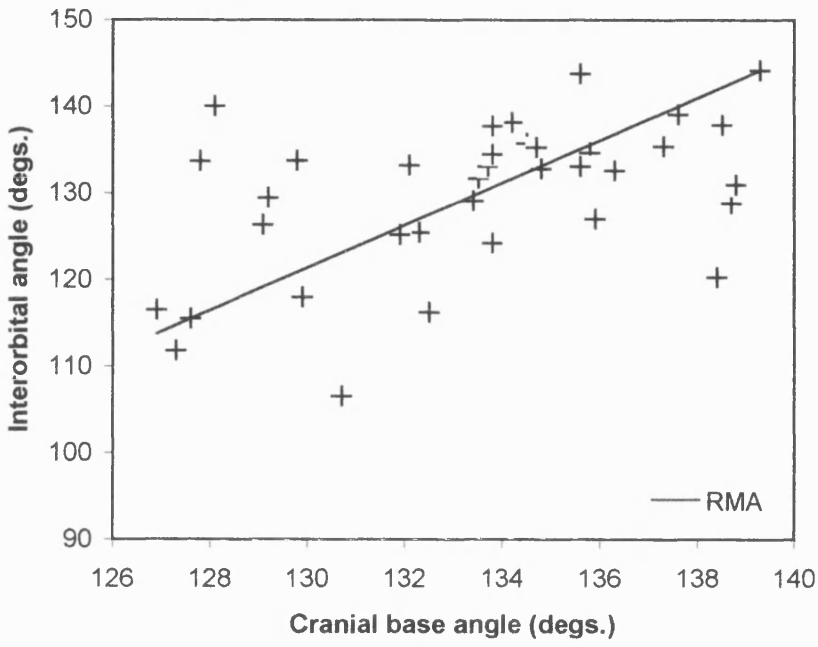

Figure 6.32. Bivariate plot of interorbital angle and cranial base angle.

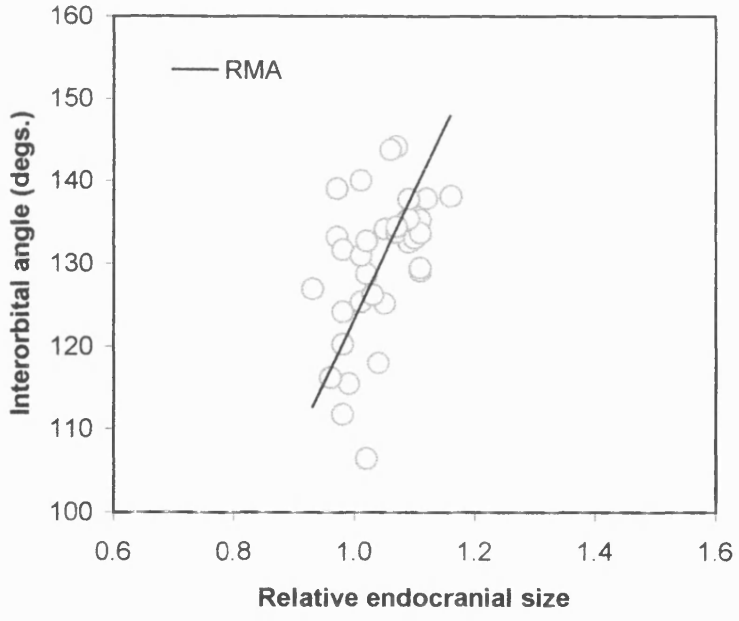

Figure 6.33. Bivariate plot of interorbital angle and relative endocranial size.

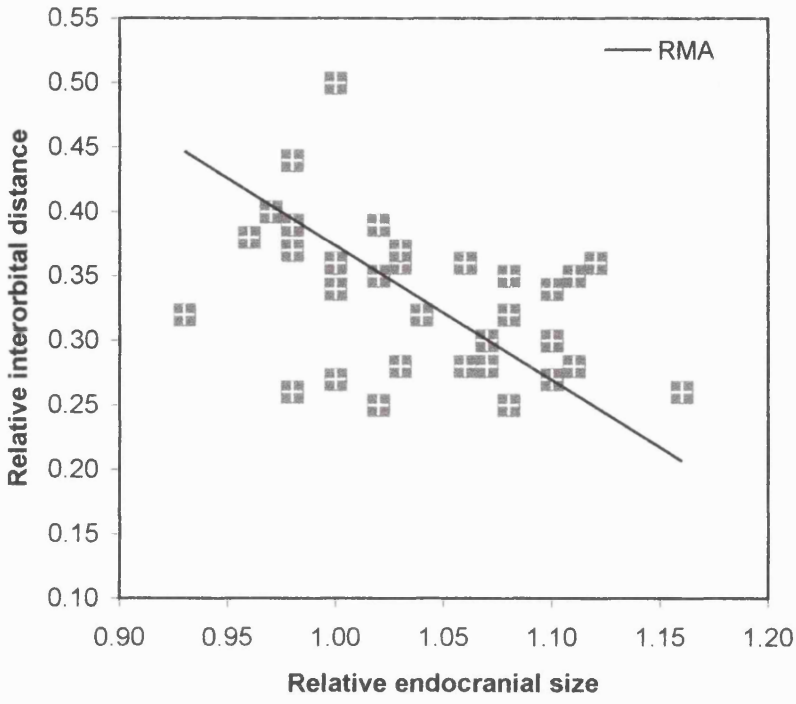

Figure 6.34. Bivariate plot of relative interorbital distance and relative endocranial size.

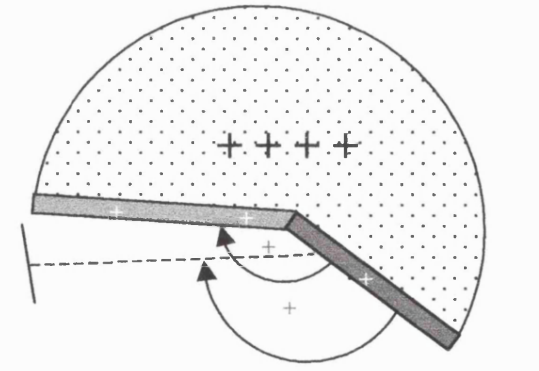

(a)

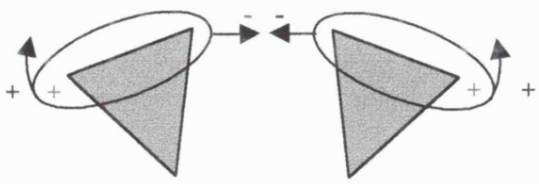

(b)

Figure 6.35. Schematic illustrations of (a) superior orbital axes rotation relative to the posterior cranial base and its association with cranial base angulation; (b) orbital convergence and transverse orbital frontation and their associations with cranial base angulation and increases of endocranial size relative to base length.

6.5 Basicranial and facial complex: synthesis

The descriptive statistics for the additional measurements (orbito-palatine angle and residual angles) that are used to quantify the relationship between the cranial base and face are listed in Table 6.10. Temporal variations of these measures were evaluated with plots of orbito-palatine angle, residual angle 1 (angle between anterior cranial base and palate), and residual angle 2 (angle between anterior cranial base and orbital axis) against age.

There is no significantly correlated change of the angle between the anterior cranial base and palate (r1) with age over the whole or first half of the period studied (r_{rank} = -0.308 [ns] and 0.215 [ns], respectively). Furthermore, there is no significant correlation of age with the angle between the anterior cranial base and orbital axes over the whole or first half of the period studied (r_{rank} = 0.218 [ns] and -0.328 [ns], respectively). There is, nonetheless, a correlated variation of orbito-palatine angle with age across the whole period studied (Figure 6.36; Table 6.11) indicating that the orbital axes and palate diverge during earlier fetal life, but converge again after about the 17^{th} to 18^{th} week of gestation. To clarify this trend and focus on the apparent acute change at around 17 weeks, two-step RMAs were computed for the periods 11 to 18 weeks and 17 to 23 weeks. Notice that these are periods not the same as those used in earlier sections and include one weeks overlap. This produced significant negative and positive correlations, respectively (Figure 6.36; Table 6.11), showing that there is a process of divergence then convergence back to an almost parallel position during the period studied.

In order to evaluate whether or not palate orientation relative to the posterior cranial base (AFK) and orbital axes orientation relative to the posterior cranial base

(AOA) correlate with CBA because of the shared segment line sella to basion, orbito-palatine angle and residual angles 1 and 2 were compared with CBA. Figure 6.37 plots orbito-palatine angle against CBA (Table 6.11). This plot reveals a significant association between CBA and orbito-palatine angle with a slope that is not significantly different from one. Since the orbito-palatine angle excludes the line segment describing the posterior cranial base it appears that correlations of palate orientation and orbital axes orientation against CBA represent more than the shared topographical reference plane sella to basion. A bivariate comparison of the angle between the anterior cranial base and palate (r1) against CBA also reveals a significant correlation and a slope that is not significantly different from one (Figure 6.38; Table 6.11). However, the angle between the anterior cranial base and orbital axes does not significantly correlate with CBA over the whole or first half of the period studied (r_{rank} = -0.119 [ns] and -0.026 [ns], respectively). This suggests that that the correlation between orbital axes orientation relative to the posterior cranial with CBA is the result of the shared line segment.

Bivariate comparisons of orbital axes orientation, orbital rim orientation, interorbital angle, relative interorbital distance against maxillary angle and palate orientation were used to evaluate relationships within the facial structure. No significant correlations were observed from comparisons of orbital axes orientation against maxillary angle, orbital rim orientation against palate orientation, and interorbital angle against maxillary angle over the whole (r_{rank} = 0.048 [ns], 0.181 [ns], and 0.269 [ns], respectively) or first half of the period studied (r_{rank} = 0.378 [ns], 0.127 [ns], and 0.203 [ns], respectively). All other comparisons yielded significant correlations over the whole period studied (Table 6.11). Figure 6.39 plots orbital axes orientation and interorbital angle against palate orientation. This graph

reveals that superior rotation of the orbital axes relative to the posterior cranial base and transverse orbital frontation are associated with superior rotation of the palate relative to the posterior cranial base. Both slopes are significantly greater than one ($P<0.01$ and $P<0.001$, respectively), indicating that transverse orbital frontation and orbital axes orientation increase in relation to palate orientation. Figure 6.40 plots orbital rim orientation against maxillary angle. The slope of this plot is not significantly greater than one ($P>0.05$, ns), suggesting that increases of maxillary prognathism and sagittal orbital frontation are almost equal. This finding indicates that the orientation of the orbits relative to the anterior cranial base, is associated with a more prognathic face. In Figure 6.41, relative interorbital distance is plotted against palate orientation and maxillary angle. Both comparisons yield significant negative correlations (Table 6.11). This graph reveals that orbital convergence during fetal development is associated with increases of maxillary prognathism relative to the anterior cranial base and superior rotation of the palate relative to the posterior cranial base. These findings show that variations of orbital morphology are associated with maxillary prognathism and changes in the orientation of the palate.

To evaluate whether changes within the sagittal plane of the facial structure are associated with increases of palate length in relation to anterior cranial base length, orbital rim orientation, orbital axes orientation, palate orientation, and maxillary angle were compared with palate length divided by anterior cranial base length. Temporal variation of the latter variable was assessed with a comparison against age (Figure 6.42; Table 6.11) which revealed a significant positive correlation. This suggests that palate length increases in relation to anterior cranial base length across the period studied. No correlations were found over the whole or first half of the period studied between palate length/anterior base length and orbital

rim orientation (r_{rank} = 0.054 [ns] and 0.068 [ns], respectively), orbital axes orientation (r_{rank} = -0.296 [ns] and -0.134 [ns], respectively), or palate orientation (r_{rank} = 0.171 [ns] and -0.018 [ns], respectively). However, a significant positive correlation was observed with maxillary angle (Figure 6.43; Table 6.11).

These findings indicate a number of associations during fetal development, which are summarised in Figure 6.44. Firstly, changes of facial profile as defined anteriorly by maxillary prognathism and inferiorly by palate orientation are closely associated with cranial base flexion and differential growth between the anterior cranial base and palate. However, within the sagittal plane of the face orbital morphology is associated with that of the facial profile as opposed to the cranial base. The lack of correlation between r2 (angle between orbital axes and anterior cranial base) and CBA shows that the correlation between AOA and CBA is probably due to the shared line segment. Lastly, orbital morphology within the transverse plane of the face is associated with both changes to the facial profile and cranial base flexion.

Table 6.10. Descriptive statistics for orbito-palatine angle and residual angles r1 and r2.

	N	Mean	S.D.	Min.	Max.
Orbito-palatine angle* (deg.)	34	4.41	4.97	-5.6	14.8
Residual angle 1** (deg.)	36	15.28	3.13	9.8	23.0
Residual angle 2*** (deg.)	36	10.43	4.37	4.2	22.4

* computed as orbital axes orientation minus palate orientation
** computed as cranial base angle minus palate orientation.
*** computed as cranial base angle minus orbital axis orientation

Table 6.11. RMA and correlation statistics for comparisons of residual angles and other angles within the face and cranial base (* , P<0.05; ** , P<0.01; *** P<0.001).

	n	r_{rank}	P	Slope	95% conf. int for slope	Intercept
Orbito-palatine angle x age	34	-0.346	*	-1.66	-2.25, -1.07	34.27
Orbito-palatine angle x age (11-18wks)	16	0.791	***	2.58	1.66, 3.50	-33.33
Orbito-palatine angle x age (17-23wks)	23	-0.831	***	-2.78	-3.76, -1.80	58.85
Orbito-palatine angle x CBA	34	0.399	*	1.37	0.93, 1.82	-178.71
Residual angle 1 x CBA	36	0.455	**	0.87	0.60, 1.13	-100.21
Orbital axes orientation x palate orientation	34	0.563	***	1.77	1.25, 2.28	-86.17
Interorbital angle x palate orientation	35	0.478	**	2.61	1.79, 3.42	-178.25
Orbital rim orientation x maxillary angle	35	0.454	**	1.25	0.86, 1.69	-53.54
Relative interorbital distance x palate orientation	35	-0.351	*	-0.017	-0.022, -0.011	2.313
Relative interorbital distance x maxillary angle.	35	-0.479	**	-0.012	-0.016, -0.009	1.472
Palate length/anterior base length x age	36	0.508	**	0.022	0.015, 0.029	0.308
Palate length/anterior cranial base length x maxillary angle	36	0.448	**	73.50	50.00, 97.00	40.03

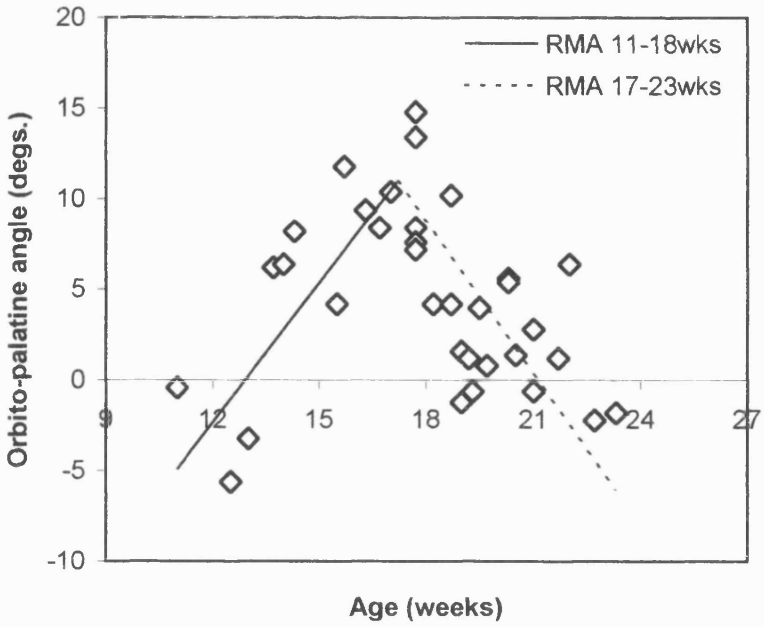

Figure 6.36. Bivariate plot of orbito-palatine angle against age. Two-step RMAs are shown.

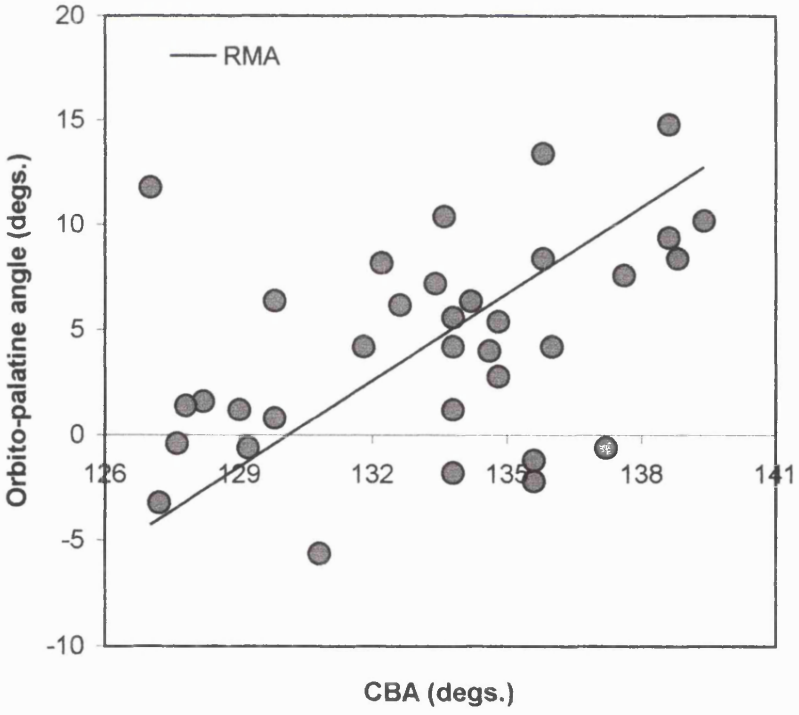

Figure 6.37. Bivariate plot of orbito-palatine angle against cranial base angle (CBA).

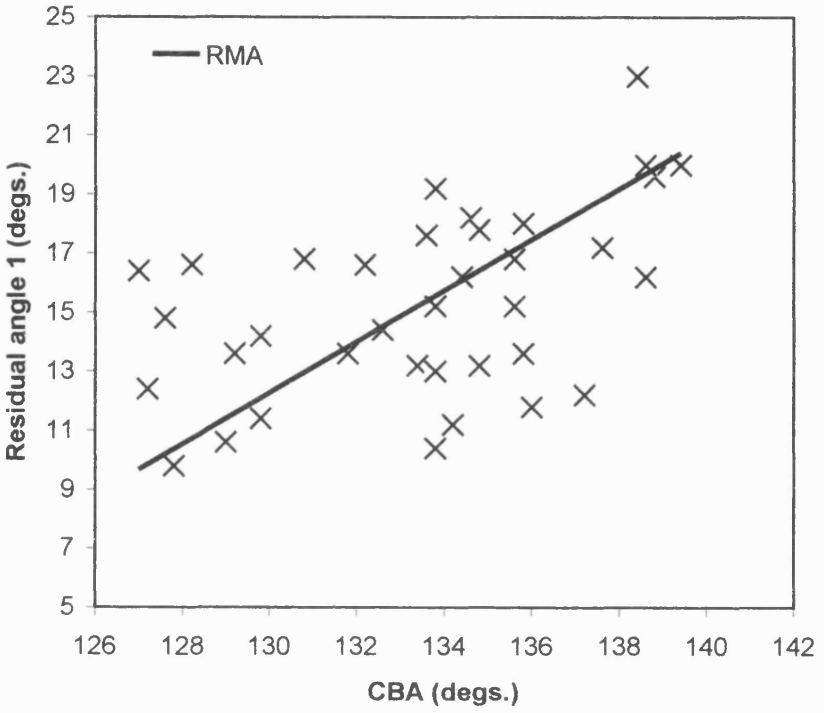

Figure 6.38. Bivariate plot of residual angle 1 (angle between anterior cranial base and palate) against cranial base angle.

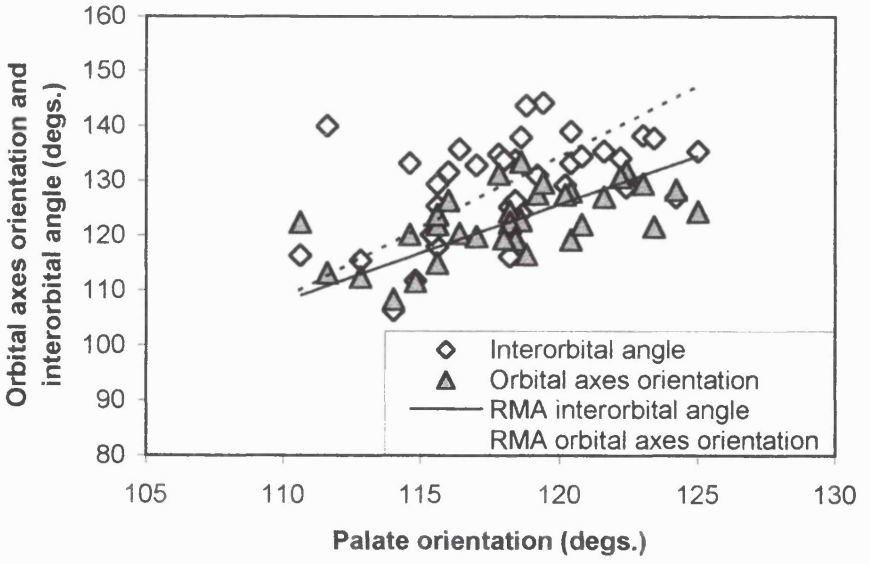

Figure 6.39. Bivariate plots of orbital axes orientation and interorbital angle against palate orientation.

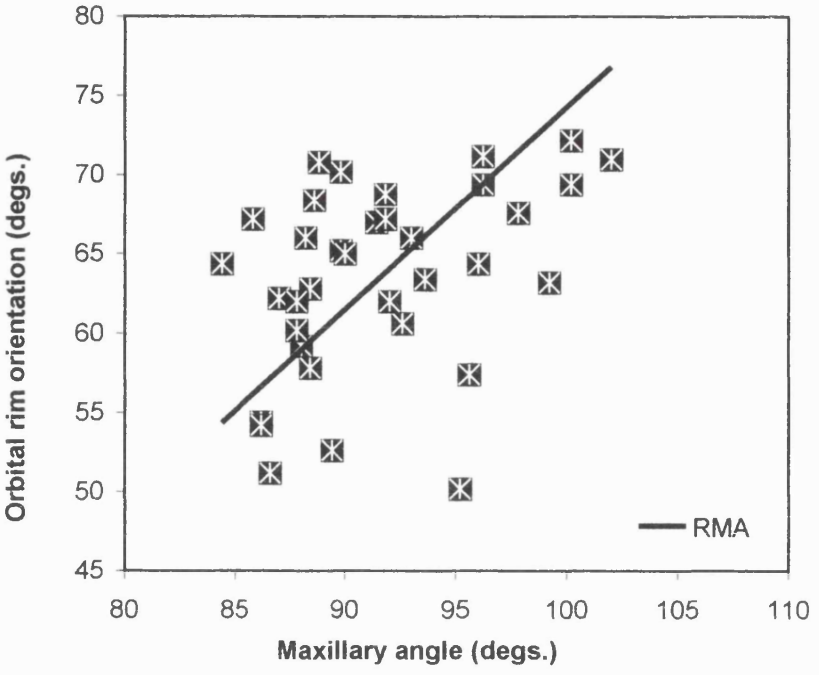

Figure 6.40. Bivariate plot of orbital rim orientation and maxillary angle.

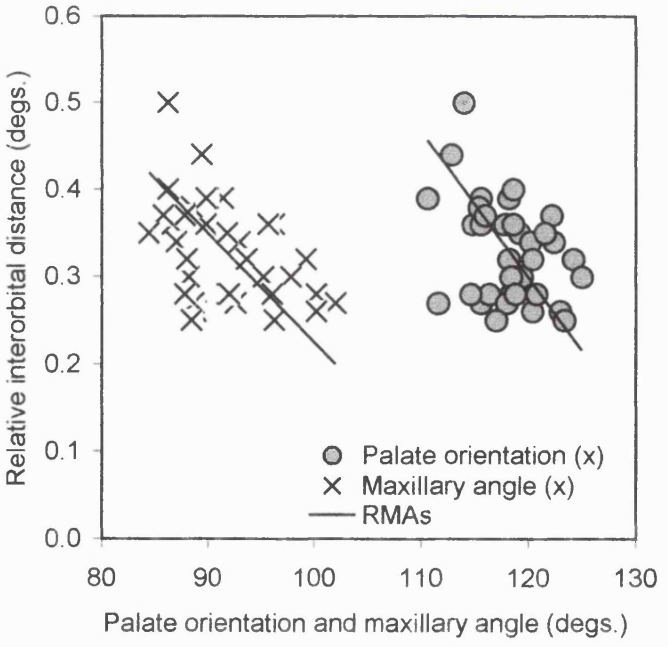

Figure 6.41. Bivariate plots of relative interorbital distance against palate orientation and maxillary angle.

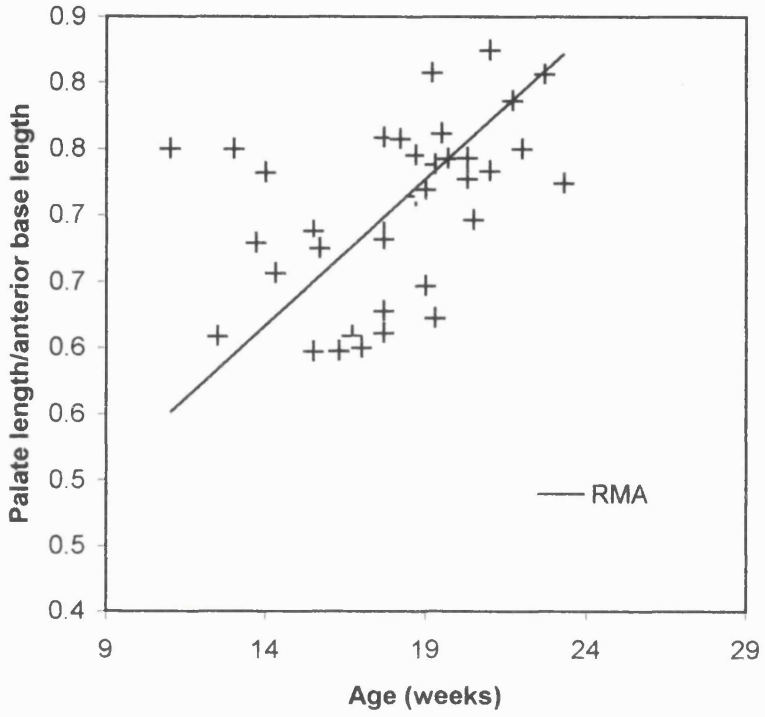

Figure 6.42. Bivariate plot of palate length/ anterior base length against age.

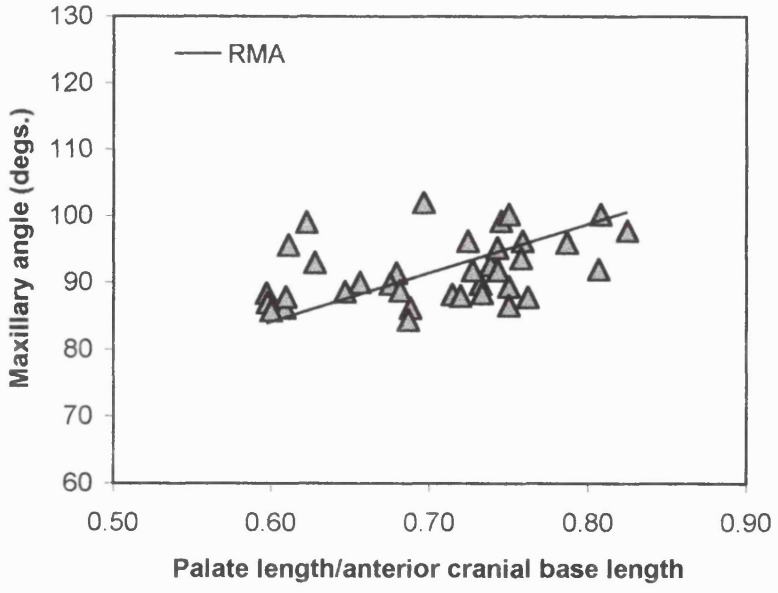

Figure 6.43. Bivariate plot of maxillary angle against palate length/anterior cranial base length.

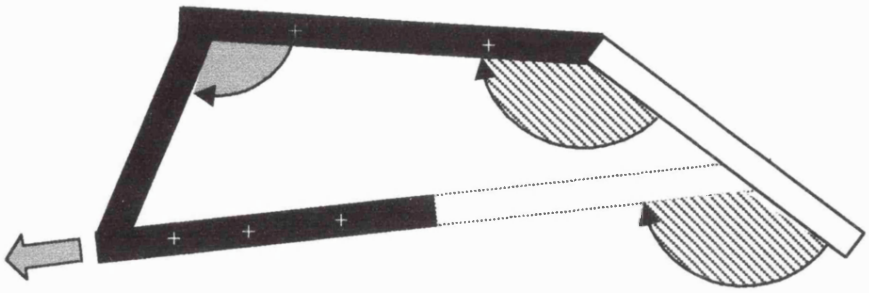

(a)

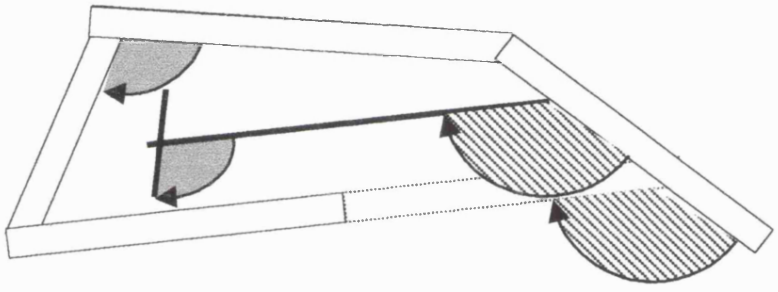

(b)

Figure 6.44. Schematic illustration showing that (a) the profile of the face (black) as represented by the maxillary angle and palate orientation is associated with differential growth between the anterior cranial base and palate (white arrows) and cranial base flexion. Within the sagittal plane of the face (b) orbital axes orientation and orbital rim orientation are associated with the facial profile as opposed to the cranial base.

6.6 Summary of findings

1) Basicranial architecture: spatial-packing hypothesis

Increases of brain size occur mainly along the midline as opposed to laterally and there is no biological difference between angular measures of CBA taken to the spheno-occipital synchondrosis and basion. The human fetal cranial base initially retroflexes and then remains essentially unchanged during the remainder of the second trimester. There are large increases of endocranial, supratentorial, and infratentorial volume and the anterior cranial base grows at a faster rate than the posterior cranial base. Endocranial sizes also increase in relation to base lengths, showing that relative brain size increases. Thus, the spatial-packing hypothesis predicts a correlated decrease of CBA. No correlation was observed between CBA and relative brain size during the period studied. These findings fail to support the spatial-packing hypothesis.

2) Fetalization

Since no postnatal specimens were measured in this study the fetalization hypothesis will be considered further in the discussion section by making comparisons with CBA values reported for adults and juveniles in the literature. Mean CBA for the fetal period studied is 133.52 (SD = 3.56).

3 & 4) Basicranial architecture: posterior cranial fossa

Changes of brain topography, i.e. increases of supratentorial relative to infratentorial volume, are associated with posterior rotation of tentorium cerebelli and cranial base angulation during early fetal development. The posterior fossa

becomes more ovate in shape as its width increases in relation to length with age. This proportional change is associated with increases of supratentorial relative to infratentorial volume but not CBA. Petrous pyramids become more sagittally orientated with cranial base retroflexion during early fetal life but in a manner that is not correlated with age. Thus, the hypothesis that variations of brain topography and CBA influence posterior fossa morphology is partially supported. Neither petrous orientation or proportional changes correlate with increases of infratentorial size relative to posterior base length. These findings therefore fail to support the second version of the spatial-packing hypothesis.

5) Basicranial and facial complex: facial kyphosis and maxillary prognathism

The human fetal palate becomes more dorsally kyphotic relative to the posterior cranial base with age. The maxilla becomes more prognathic with age. Facial kyphosis is associated with CBA but not increases of relative brain size. In contrast, maxillary prognathism is associated with increases of relative endocranial size as opposed to CBA. These results only partially supports the notion that the cranial base and face form a single unit that reacts to increases of relative brain size.

6 & 7) Basicranial and facial complex: orbital convergence and frontation

The orbits become progressively more frontated and convergent with age in both sagittal and transverse planes. Orbital axes shift dorsally with age relative to the posterior cranial base. This variation of orbital axes orientation is correlated with CBA. Transverse orbital frontation is associated with both CBA and increases of relative endocranial size while sagittal orbital frontation is not associated with either of these. Orbital convergence is associated with CBA during early fetal life and

relative endocranial size over the whole period studied. Thus, the hypothesis that variations of orbital morphology are associated with cranial base angulation and spatial-packing is in many respects supported.

8) Basicranial and facial complex: synthesis

The orbital axes and palate diverge during early fetal development and subsequently converge back to an almost parallel position. There is no significant change in the angle between the anterior cranial base and orbital axes with age or the angle between the anterior cranial base and palate with age. Both the orbito-palatine angle and the angle between the anterior cranial base and palate correlate with CBA. However, there is no significant variation of the angle between the anterior cranial base and orbital axes with CBA. Thus, correlations of orbital axes orientation and CBA are probably due to the shared line segment.

Within the facial structure orbital axes orientation correlates with palate orientation, orbital rim orientation correlates with maxillary angle, relative interorbital distance correlates with palate orientation and maxillary angle. The length of the palate increases in relation to the anterior cranial base with age and this increase is correlated with maxillary angle.

These findings indicate that the facial profile as defined by maxillary prognathism and palate orientation is closely related to the cranial base, particularly the anterior cranial base. This supports the notion of the cranial base and face as a single unit. However, within the facial structure morphologies are mostly influenced by changes to the facial profile as opposed to directly by changes in the architecture of the cranial base.

CHAPTER 7. DISCUSSION

This study set out to provide an ontogenetic framework for the interpretation of evolutionary hypotheses using basic quantitative descriptions of basicranial development in relation to the face and the brain. In general, these aims have been met. Quantitative descriptions of the midline cranial base, posterior cranial fossa, face, and absolute and relative brain sizes during human fetal development are documented. These data was subsequently used to test predictions from a number of evolutionary hypotheses, yielding comparisons between ontogenetic mechanisms of morphological development and their proposed phylogenetic counterparts.

7.1 Limitations of the present study

Data from the present study suffer from several limitations that prevents the categorical falsification or generalised support of any hypothesis for the whole of the prenatal period. Firstly, the period studied only constitutes one third of human gestation and most of the hypotheses discussed have yet to be tested with material from the first and third trimesters. According to the polyphasic model of cranial base development advocated here, it is likely that support for hypotheses depends on the temporal period investigated. The second problem is the cross-sectional nature of the material. For example, the observed increase of relative endocranial size is small and the equivalently small predicted decrease of CBA may remain undetectable amongst individual variations within the sample. Future developments in MRI may enable the acquisition of longitudinal data by imaging fetuses *in utero* (e.g. Weinreb *et al.*,

1985; Powell *et al.*, 1988; Girard *et al.*, 1993; Colletti, 1996), but at present the images obtained in these experiments are too poorly resolved to identify key landmarks.

As previously described, shrinkage is also a major limitation of the present study. While it is unlikely that the anatomical landmarks selected for this study were significantly affected by shrinkage, it precluded the use of neuroanatomical landmarks. It would be desirable to conduct a more in-depth investigation on the effects of different parts of the brain on facial and basicranial morphology, particularly enlargement of the neocortical regions in relation to the brain stem. A Recent MRI study of living non-human primate material has been able to assess enlargement of the neocortex, revealing that the neocortex in humans is no greater than that expected for the anthropoid brain (Rilling and Insel, 1999). It would be interesting to investigate the effects of differential enlargement of the brain using fresh fetal material, though ethico-legal considerations make this unlikely. Nonetheless, such hypotheses could be tested with fresh non-human primate material.

7.2 Imaging

The two-dimensional spin-echo multislice sequence and spatial encoding gradients provided sufficient contrast and resolution to visualise most structures of the prenatal head. The T_2 weighting, though nosier than T_1 weighting, gave better contrast between the membranous, cartilaginous, and ossified structures of the chondrocranium, splanchnocranium, and neurocranium and the high signal of the preservative fluid within the endocranial cavity. It also allowed the visualisation of such details as the semicircular canals against the ossified mass of the petrous

temporal bone. Over all, the imaging approach used was more than satisfactory for the requirements of the present study and considerably better than more traditional techniques. There are, however, a number of improvements that could have been made if time permitted and the equipment was available. Firstly, it would have been desirable, for the purposes of improving SNR (signal-to-noise ratio) and therefore reducing the number of averages used, to image volumes rather than slices. The second improvement would be to invest more time in tailoring the pulse timing parameters to each individual fetus and maximise image quality as a result. It would have also been preferable to conduct a more rigorous test of imaging repeatability and accuracy. Although the tests carried out in this study are more than sufficient for the measures undertaken, future work on the semicircular canals for example would require a more in-depth assessment. It also seems likely that more powerful equipment, similar to that used in MRI microscopy (e.g. Effman *et al.*, 1988; Johnson *et al.*, 1993; Smith *et al.*, 1994), will be required if the sample is to include embryonic material.

7.3 Spatial-packing hypotheses

In contrast to a number of previous reports (e.g. Ford, 1958; Burdi, 1965, 1969; Johnston, 1974) results from the present study indicate that the cranial base angulation shown in the early fetal period is not essentially the same as that shown later in the second trimester. Table 7.1 lists values of CBA taken and computed from the literature. The mean value of CBA from these studies covering 11 to 24 weeks is approximately 133.0 degrees (n, 31; SD, 12.37) and is not, therefore, significantly different to the mean reported here ($P>0.05$). The initial increase of about 6 to 9

degrees reported here for the first half of the second trimester is in agreement with a number of studies documenting basicranial retroflexion during the second trimester (e.g. Kvinnsland, 1971; Lemire, 1986; Dimitriadis *et al.*, 1995). In particular, Kvinnsland (1971) found comparable increases in midsagittally sectioned fetal heads using the measure nasion-sella-basion. He reports that the mean CBA for two samples increases from 121.7 and 124.7 degrees in the early fetal period (HL = 20mm) to 134.7 and 139.7 degrees respectively towards the middle of the second trimester (HL = 150mm). Lemire (1986) also reports that the cranial base angle increases from the late embryonic to early fetal period. Dimitriadis *et al.* (1995) examined cranial base angulation in midline CT sections of 26 fetuses aged from 15 to 25 weeks gestation and found the minimum CBA at 19 weeks to be approximately 12 degrees greater than that at 15 weeks. Results reported here also show that the cranial base angle remains essentially unchanged during the second half of the period studied are not therefore consistent with reports of continued retroflexion (e.g. Kvinnsland, 1971; Dimitriadis *et al.*, 1995) or flexion (e.g. Erdoglija, 1989; van den Eynde *et al.*, 1992). Note however, that while the correlation for the second half of the period studied was shown to be insignificant the distribution of datum points shown Figure 6.2 (Chapter 6, Results) could be interpreted as retroflexion and therefore needs further clarification with a larger sample. Inconsistencies within the literature are probably due to differences of technique (e.g. plain radiographs, CT, and sections) and the anatomical landmarks used to measure CBA. It is also interesting to note that Ford's (1956) results are questionable in the sense that they are inconsistent with those calculated using his published data (Figure 7.1). Although the author reports that in terms of variance (ANOVA) there is a significant regression for each angle with age

Table 7.1. Values of CBA computed from and reported in the literature.

Age (weeks)	CBA	n	measure of CBA (examination technique)	Reported size or age variable	Reference
19.9-25.3	*132.0*	32	na-s-ba (hs)	26-70mm HL	Johnston (1974)
12.5-16.5	*135.9*	10	na-s-ba (rdg & hst)	70-110mm CRL	van den Eynde *et al.* (1992)
16.5-20.5	*131.5*	7	na-s-ba (rdg & hst)	110-150mm CRL	van den Eynde *et al.* (1992)
20.5-24.5	*126.6*	12	na-s-ba (rdg & hst)	150-190mm CRL	van den Eynde *et al.* (1992)
20-24	*147*	1	ca-s-ba (rdg)	5-6 months IU	Cousin (1969)
24.5-28.5	123.7	11	na-s-ba (rdg & hst)	190-230mm CRL	van den Eynde *et al.* (1992)
20-24	*144.5*	13	na-s-bo (rdg)	20-24 weeks	Levihn (1967)
12-15	*149.5*	4	na-s-bo (rdg)	12-15 weeks	Levihn (1967)
16-19	*148.0*	13	na-s-bo (rdg)	16-19 weeks	Levihn (1967)
25-28	148.0	5	na-s-bo (rdg)	25-28 weeks	Levihn (1967)
28-32	140.3	3	ca-s-ba (rdg)	7-8 months IU	Cousin (1969)
29-32	154.5	6	na-s-bo (rdg)	29-32 weeks	Levihn (1967)
32-36	148	1	ca-s-ba (rdg)	8-9months IU	Cousin (1969)
33-36	153.5	4	na-s-bo (rdg)	33-36 weeks	Levihn (1967)
37-40	153.0	4	na-s-bo (rdg)	37-40 weeks	Levihn (1967)
7.3	117.0	10	na-s-ba (hst)	18.1mm CRL	Diewert (1983)
7.6	126.0	9	na-s-ba (hst)	21.2mm CRL	Diewert (1983)
7.8	127.0	7	na-s-ba (hst)	22.8mm CRL	Diewert (1983)
8.1	127.0	7	na-s-ba (hst)	25.5mm CRL	Diewert (1983)
8.4	125.0	4	na-s-ba (hst)	29.3mm CRL	Diewert (1983)
8.9	130.0	6	na-s-ba (hst)	34.4mm CRL	Diewert (1983)
9.4	131.0	4	na-s-ba (hst)	39.0mm CRL	Diewert (1983)
10.0	[b]126.8	2	na-pt-ba (hst & sct)	10 weeks	Ford (1956)
10.4	127.0	6	na-s-ba (hst)	49.0mm CRL	Diewert (1983)
10.6	[a]*127.6*	-	na-s-ba (hst & sct)	105mm CRL	Burdi (1969)
11.0	[b]*109.6*	2	na-pt-ba (hst & sct)	11 weeks	Ford (1956)
12.0	[b]*111.8*	1	na-pt-ba (hst & sct)	12 weeks	Ford (1956)
12.5	[a]*126.4*	-	na-s-ba (hst & sct)	70mm CRL	Burdi (1969)
13.0	[b]*134.1*	2	na-pt-ba (hst & sct)	13 weeks	Ford (1956)
14.0	[b]*154.7*	1	na-pt-ba (hst & sct)	14 weeks	Ford (1956)
15.0	*109.3*	3	na-s-ba (CT)	15 weeks	Dimitriadis *et al.* (1995)
15.0	[b]*147.0*	3	na-pt-ba (hst & sct)	15 weeks	Ford (1956)
16.0	*116.5*	2	na-s-ba (CT)	16 weeks	Dimitriadis *et al.* (1995)
16.0	[b]*135.4*	3	na-pt-ba (hst & sct)	16 weeks	Ford (1956)
17.0	*119.3*	3	na-s-ba (CT)	17 weeks	Dimitriadis *et al.* (1995)
17.0	[b]*127.7*	1	na-pt-ba (hst & sct)	17 weeks	Ford (1956)
18.0	[b]*149.3*	2	na-pt-ba (hst & sct)	18 weeks	Ford (1956)
19.0	*121.0*	3	na-s-ba (CT)	19 weeks	Dimitriadis *et al.* (1995)
19.0	[b]*148.5*	2	na-pt-ba (hst & sct)	19 weeks	Ford (1956)
19.5	[a]*128.9*	-	na-s-ba (hst & sct)	140mm CRL	Burdi (1969)
20.0	[b]*140.6*	1	na-pt-ba (hst & sct)	20 weeks	Ford (1956)
21.0	[b]*145.7*	1	na-pt-ba (hst & sct)	21 weeks	Ford (1956)
22.0	*128.5*	6	na-s-ba (CT)	22 weeks	Dimitriadis *et al.* (1995)
22.0	[b]*130.5*	2	na-pt-ba (hst & sct)	22 weeks	Ford (1956)
23.0	*132.0*	3	na-s-ba (CT)	23 weeks	Dimitriadis *et al.* (1995)
23.0	[a]*130.1*	-	na-s-ba (hst & sct)	175mm CRL	Burdi (1969)
24.0	*133.6*	5	na-s-ba (CT)	24 weeks	Dimitriadis *et al.* (1995)
24.0	[b]154.3	2	na-pt-ba (hst & sct)	24 weeks	Ford (1956)
25.0	134.0	1	na-s-ba (CT)	25 weeks	Dimitriadis *et al.* (1995)
26.0	[b]155.1	3	na-pt-ba (hst & sct)	26 weeks	Ford (1956)
26.5	[a]131.3	-	na-s-ba (hst & sct)	210mm CRL	Burdi (1969)
28.0	146	1	ca-s-ba (rdg)	7 months IU	Cousin (1969)
28.0	[b]131.5	2	na-pt-ba (hst & sct)	28 weeks	Ford (1956)
30.0	[a]132.5	-	na-s-ba (hst & sct)	245 mm CRL	Burdi (1969)
30.0	[b]127.6	3	na-pt-ba (hst & sct)	30 weeks	Ford (1956)
32.0	[b]143.4	7	na-pt-ba (hst & sct)	32 weeks	Ford (1956)
33.5	[a]133.7	-	na-s-ba (hst & sct)	280 mm CRL	Burdi (1969)
34.0	[b]140.6	8	na-pt-ba (hst & sct)	34 weeks	Ford (1956)
36.0	[b]140.8	4	na-pt-ba (hst & sct)	36 weeks	Ford (1956)
37.0	[a]135.0	-	na-s-ba (hst & sct)	315 mm CRL	Burdi (1969)
38.0	[b]144.4	13	na-pt-ba (hst & sct)	38 weeks	Ford (1956)
40.0	[b]145.8	11	na-pt-ba (hst & sct)	40 weeks	Ford (1956)
40.5	[a]136.2	-	na-s-ba (hst & sct)	350 mm CRL	Burdi (1969)
44.0	[a]137.4	-	na-s-ba (hst & sct)	385 mm CRL	Burdi (1969)
47.5	[a]138.7	-	na-s-ba (hst & sct)	420 mm CRL	Burdi (1969)

Abbreviations: hst, histological sections; sct, gross sections; CT, computed tomography; rdg, plain film radiography; HL, head length; CRL, crown-rump length; pt, pituitary point (centre of the floor of the pituitary fossa); bo, bolton point (the highest point in the upward curvature of the retrondylar fossa);ca, cribriform anterior (see Cousin , 1969); [a], CBA values calculated from the equation y = 123.591 + (0.035*CRL) for 70 to 420mm CRL (Burdi, 1969); [b], CBA values calculated from linear measures of na-pt, pt-ba, and ba-na (Ford, 1956). CBA values in italics are for comparable ages to the present study.

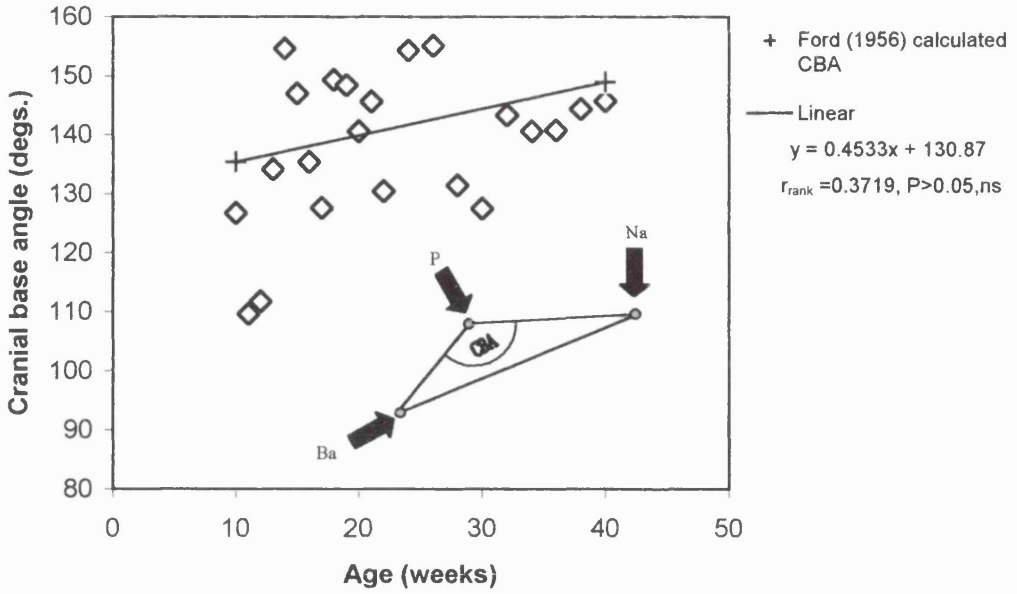

Figure 7.1. Graph showing the cranial base angles calculated from pituitary-nasion (P-Na), basion-nasion (Ba-Na), and pituitary-basion (P-Ba) distances published by Ford (1956) for fetuses ranging from 10 - 40 weeks gestation. The line represents the regression probably used by Ford (1956) to calculate CBA values for 10 and 40 weeks.

($P<0.001$), it appears his values for cranial base angle at 10 weeks and 40 weeks are computed from a linear regression model of data that is not significantly correlated (rank correlation coefficient $r_{rank} = 0.317$; $P>0.05$,ns). Consequently, his results for CBA may not be reliable.

Numerous authors propose that the degree of flexion observed in adult modern humans is a fetalized character (Zuckerman, 1955; Schultz, 1955; Ford, 1956). Studies of adult modern humans using the same measure of CBA (Luboga, 1986; Spoor, 1997; Lieberman and McCarthy, 1999) are compared with the second trimester fetal mean reported here and the third trimester mean reported by Cousin (1969) in Table 7.2. Although Cousin used cribriform anterior (criblé antériur) as opposed to foramen caecum, both landmarks are spatially concurrent during most of fetal development. Foramen caecum, however, gradually shifts superiorly to form a separate landmark following growth around the fronto-ethmoidal suture and the anterior part of the crista galli.

Table 7.2. Comparison of differences between adult and fetal means for CBA as reported by Cousin (1969), Luboga (1986), Spoor (1997), and Lieberman and McCarthy (1999).

	n	mean CBA	SD	Luboga	Spoor	Lieberman and McCarthy	Cousin	Present study
Luboga	240	130	5.7		H_{lt}, (P<0.001)	H_{lt}, (P<0.01)	H_{lt}, (P<0.001)	H_{lt}, (P<0.001)
Spoor	48	137	4.9			H_{gt}, (P<0.05)	H_{eq}, (P>0.05)	H_{gt}, (P<0.001)
Lieberman and McCarthy	16	134.22	3.10				H_{lt}, (P<0.001)	H_{eq}, (P>0.05)
Cousin	6	141.1	4.7					H_{gt}, (P<0.05)
Present study	38	133.52	3.54					

Null hypotheses: H_{lt}, $\mu_1 <= \mu_2$; H_{gt}, $\mu_1 >= \mu_2$; H_{eq}, $\mu_1 = \mu_2$.

The comparison of the means given in Table 7.2 shows that the fetal mean reported here is not significantly different to that reported by Lieberman and McCarthy for adult modern humans. In addition, the fetal mean reported by Cousin is not significantly different from the adult mean observed by Spoor. Notice, however, that the adult mean reported by Luboga is less than all other values and that there are significant differences between the two other adult means and between the two fetal means. One possible reason for these differences is the diverse geographic origin of the samples. Values for geographic subsets in Spoor (1993) vary from 134 to 140 degrees, and in Pellerin (1983), for example, population means of cranial base angles (Ba-S-Crib. Ant.) vary by as much as 10 degrees. The data in Table 7.2 could thus be seen as indicative of stasis in CBA from fetal to adult stages, but another interpretation seems more likely when the early postnatal period is considered as well. Lieberman and McCarthy (1999) have shown that the base flexes from 143 degrees at one postnatal month to 134 degrees at seventeen years of age, with the majority of flexion occurring within the first postnatal year. Although the CBA value at seventeen years is not significantly different from the fetal mean as shown in Table 7.2, values of CBA for the postnatal periods imply that the base retroflexes during the third trimester from 133 in the second trimester (mean reported here) to

143 degrees and subsequently flexes again following birth to 134 degrees. This is consistent with Cousin's (1986) result of 141 degrees for the third trimester. Thus, base flexion is not retained , i.e. remains unchanged, from fetuses or juveniles into adulthood, though it remains equivocal whether similarities of CBA arise from the repetition of the prenatal mechanism after birth. Nonetheless, these findings fail to directly support the hypothesis of human fetalization and are as such consistent with early challenges to the notion of human paedomorphosis based on studies of base flexion (see review in Gould, 1977, p. 379).

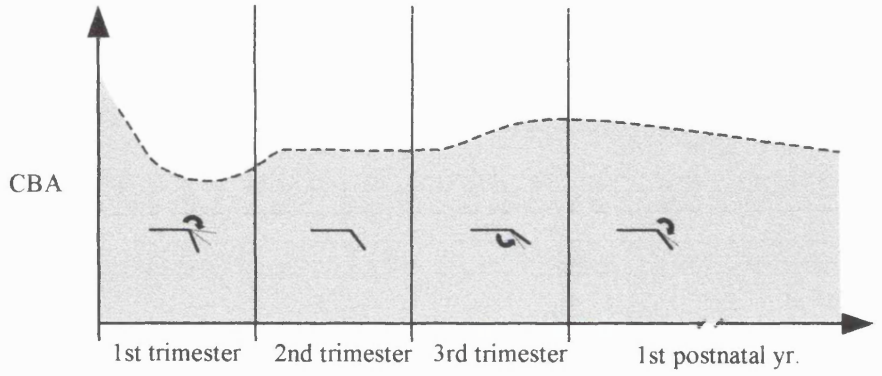

Figure 7.2. Graphic illustration of the polyphasic model of human base flexion from the first trimester of fetal development through to the first postnatal year. Based on the results from this study and the literature cited in the text.

Studies covering other prenatal periods, suggest the cranial base flexes during the first trimester (Müller and O'Rahilly, 1980; Diewert, 1983) and retroflexes during the third trimester (Ford, 1956; Burdi, 1969). These together with reported values for the third trimester and the early postnatal period (Cousin, 1986; Lieberman and McCarthy, 1999) are consistent with a polyphasic model of human base flexion. As such the cranial base initially flexes, then retroflexes slightly during the late embryonic and early fetal period, remains essentially unchanged during the rest of the second trimester, retroflexes during the third trimester, and finally flexes again postnatally (Figure 7.2).

The results of this study show that growth of the anterior cranial base is almost twice that of the posterior cranial base. This is in close agreement with a number of previous studies reporting similar findings for both non-human and human development (Ortiz and Brodie, 1949; Mestre, 1959; Burdi, 1965, 1969; Levihn, 1967; Houpt, 1970; Johnston, 1974; Eriksen *et al* , 1995). According to Ford (1956, 1958) such differences are due to the fact that the anterior base exhibits a similar growth rate to the brain while the posterior base has a skeletal rate of growth. However, amongst non-human primates it is reported that growth of the anterior cranial base relates to that of the face rather than the brain (Sirianni and Swindler,1979). It is likely, as Lavelle (1987) suggests, that the growth pattern defined for the anterior cranial base depends on the anatomical landmarks selected. Differences in growth of the anterior and posterior cranial base may also be associated with the presence of extra growth centres and ossification of the basioccipital. The anterior cranial base can extend from both the fronto-ethmoidal suture and sphenoethmoidal synchondrosis while the posterior cranial base has only one major growth centre, the spheno-occipital synchondrosis. In addition, ossification of the basioccipital, which appears before any of the centres along the anterior cranial base, probably limits the more rapid interstitial growth found in cartilage (Johnston, 1974).

Values of absolute endocranial volume reported here are consistent with brain volumes reported in previous studies (Jenkins, 1921; Koop *et al.* 1986). In particular Jenkins observed an increase from 0.603cm^3 at 11 weeks to 54.290 cm^3 at 26 weeks and 489.970cm^3 at 40 weeks. Koop *et al.* (1986) studied 10 fetuses ranging from 63 to 176 days after conception (9 to 25 weeks) and observed an increase in total brain volume from 2.34 to 67.75cm^3 during this period. Both studies also

observed an increase of infratentorial volume of 0.002 to 34.18cm^3 from 4 to 40 weeks and 0.24 to 4.69cm^3 from 63 to 176 days, respectively. These observations are comparable, but consistently smaller than those reported here especially towards the end of the period studied (compare Table 7.3 with the results found here). These differences probably reflect differences of technique. In contrast to the present study, both Jenkins and Koop *et al.* use projections of sectioned material to take volume measurements by outlining regions of interest. This technique has a number of drawbacks. These include shrinkage during the embedding process prior to sectioning (see Jenkins, 1921) and that the ventricular system is often excluded from volume measurements.

Table 7.3. Total, infratentorial, supratentorial volumes (cm^3), excluding the ventricular system, reported by Jenkins (1921) and Koop *et al.* (1986).

Weeks	Total brain volume (ref.)	Present study, total brain volume.	Infratentorial volume† (ref.)	Present study, infratentorial volume
4	0.003 (J)	-	0.002 (J)	-
7	0.041 (J)	-	0.019 (J)	-
8	0.126 (J)	-	0.046 (J)	-
9	2.340 (K)	-	0.240 (K)	-
9.7	2.230 (K)	-	0.220 (K)	-
10.1	3.770 (K)	-	0.250 (K)	-
10.9	4.540 (K)	-	0.320 (K)	-
11	0.603 (J)	1.870	0.077 (J)	0.360
12.5	1.977 (J)	4.970	0.201 (J)	0.840
13.5	1.503 (J)	5.925	0.100 (J)	0.980
14.1	9.500 (K)	9.930	0.750 (K)	1.225
15	16.240 (K)	14.770	1.050 (K)	1.905
16	8.750 (J)	23.900	0.527 (J)	2.470
16	24.130 (K)	22.190	0.880 (K)	2.720
19	13.120 (J)	52.886	0.645 (J)	4.298
21.3	19.210 (K)	66.580	2.620 (K)	5.383
25.1	67.750 (K)	-	4.690 (K)	-
26	54.290 (J)	-	2.860 (J)	-
40	489.970 (J)	-	34.180 (J)	-

†Infratentorial volumes computed from values of Rhombencephalon + cerebellum.
(K) Koop *et al.* (1986), (J) Jenkins (1921).

The results of this study reveal an increase of endocranial size relative to base length across the sample and with age. Increases were also observed for relative

infra- and supratentorial size and accordingly a small correlated decrease in CBA was predicted. However, no significant correlations were revealed between increases of any of the relative endocranial sizes and CBA during the whole or either half of the period studied. In fact, it has been shown here that the base retroflexes during early fetal development despite increases of relative brain size. These findings therefore fail to support the notion that increases in brain size relative to base length directly and mechanically drive base flexion during human fetal ontogeny, at least during the period studied. However, it remains unclear whether first trimester flexion and third trimester retroflexion reported by other workers relate to variations of relative brain size.

It seems possible that early first trimester flexion relates to the formation of the brain flexures due to increased growth of the telencephalon. Moreover, third trimester retroflexion could well be associated with changes in the rate of brain growth towards birth which drops from 26 grams per week at 35 weeks to 20 grams per week at 40 weeks (Guihard-Costa and Larroche, 1992). This may be a safeguard against difficult births of large headed infants (see Leutenegger, 1987 for a discussion of cephalo-pelvic constraints). The effect of this change in the rate of brain growth is probably expedited by fusion of the midsphenoidal synchondrosis late in fetal life and perhaps development of the pharynx (Ford, 1958; Scott, 1958; Hoyte, 1975). Fusion of the midsphenoidal synchondrosis reduces the plasticity between the anterior and posterior cranial base and causes the base to hinge at the spheno-ethmoidal and spheno-occipital synchondroses through either differential cartilage growth or bone re-modelling (see Hoyte, 1971; Michejda, 1971, 1972; Giles *et al.*, 1981; Sirianni, 1985). Both synchondroses remain patent throughout fetal life and into sub-adulthood (fusion occurs at around six and twenty-five

postnatal years, respectively: Brash, 1953; Scott, 1958). The spheno-occipital and spheno-ethmodial synchondroses contribute to the lengths of the anterior and posterior cranial base, respectively and ultimately, therefore, influence values of relative brain size. Their importance is further illustrated by the fact that in third-trimester anencephalic fetuses, were the midsphenoidal synchondrosis fuses earlier than normal, the base is flexed despite the absence of the brain (Abd-El-Malek, 1957; Marin-Padilla, 1965; Fields *et al.*, 1978). Although care must taken before reading too much into these results since pathologies may also be manifested within the base itself, it indicates that the cranial base has a certain degree of autonomy from brain enlargement arising from differential fusion of the synchondroses that may be regulated by genes.

The correlation observed between increases of supratentorial size in relation to infratentorial size and increases of cranial base angulation during early fetal life requires further discussion. Although the mechanism underlying this relationship is not clear it indicates an association between base angulation and variations of brain topography. Based on the results reported here, a hypothesis can be formulated that more conservative growth of the cerebellum and brain stem compared with that of the cerebrum leads to cranial base retroflexion. Conversely, increases in growth of the cerebellum and brain stem relative to the cerebrum leads to flexion. As such, late fetal retroflexion may be associated with a reduction in the size of the cerebellum and brain stem relative to the cerebrum. Moreover, postnatal flexion would associate with increases in the size of the cerebellum and brain stem in relation to the cerebrum. Perhaps this increase relates to improved manual dexterity or other cognitive functions essential for exploring the environment and the attainment of a bipedal posture during neonatal development (see review in Eccles, 1989). During

the first postnatal year, the weight of the cerebellum as a percentage of its adult value increases from below that of the forebrain as a percentage of its adult value to exceed the forebrain percentage within twelve months (see Figure 10 in Dobbing and Sands, 1973). In other words, compared with growth of the forebrain there is a growth spurt in the weight of the cerebellum during the first twelve months of postnatal life that is contemporaneous with postnatal base flexion.

The value of endocranial ratio computed from Stephan *et al.*'s (1986) data for adult humans (n=1) is approximately 0.130 while that computed from volumes measured using MRI (n=7) by Filipek *et al.* (1989) is 0.137, giving a mean of about 0.133. Thus, according to the RMA equation reported here for cranial base angle against endocranial ratio during early fetal development (y = -79.55x + 145.06) adult modern human CBA should be 134.5 degrees. This is almost identical to the mean CBA for adult modern humans reported by Lieberman and McCarthy (1999) (mean of 134.22, S.D. 3.10). Interestingly, an association of basicranial flexion with an

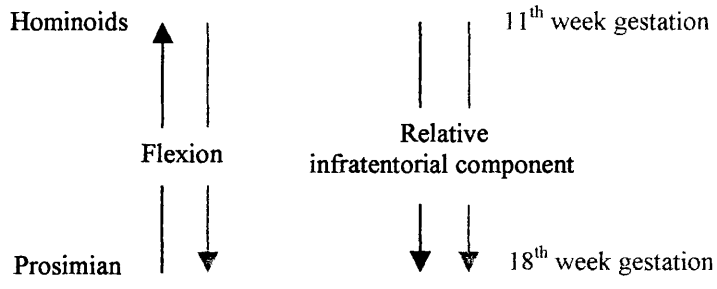

Figure 7.3. Illustration showing that the interspecific trend amongst primates (black lines) base on data published by Stephen *et al.* (1986) and Ross and Ravosa (1993) is the opposite to that observed here during human fetal development (grey lines) in that it appears flexion is interspecifically associated with an increase of the supratentorial component.

increase of infratentorial size relative to supratentorial size during human development is the opposite to what appears to be the case interspecifically amongst primates. Prosimians with the least flexed bases have the relatively largest infratentorial volume (Figure 7.3). However, across primates there is no significant

correlation between the decrease in endocranial ratio and the CBA values reported by Ross and Ravosa (1993) ($r_{rank} = 0.217$, ns).

That during at least part of human prenatal ontogeny CBA is dissociated from increases of relative brain size is consistent with results for the end result of growth, i.e. adult human morphology (Ross and Henneberg, 1995), but not with those from interspecific studies of adult nonhuman primates (Ross and Ravosa, 1993; Spoor, 1997). This suggests that the mechanism(s) underlying the highly flexed modern human basicranium may be different to those operating amongst non-human primates, thereby corroborating findings from previous studies of postnatal development (Zuckerman, 1955; Sirianni and Swindler, 1979). The pattern of angulation seen during late prenatal and early postnatal human development appears distinct from that observed for non-human primates during equivalent periods. During most of the fetal period the cranial base of *Macaca nemestrina* remains essentially unchanged at around 153 degrees, but after birth it gradually opens out from 160 to 164 degrees in adulthood (Ashton, 1957; Sirianni and Van Ness, 1978; Sirianni and Newell-Morris, 1980). Moore (1978), on the other hand, has shown that the fetal *Macaca nemestrina* cranial base retro-flexes from 156.7 degrees at 121-130 days to 160.6 degrees at 141-150 days and subsequently flexes again to 155.1 degrees at 161-171 days. This overall period of activity is roughly equivalent to the third human trimester and indicates that while the macaque base flexes prior to birth and retroflexes after birth, the human base continues to flex into the first postnatal year. It could be argued therefore, that the period over which retroflexion and flexion occur in humans has, in comparison with non-human primates, been extended into the postnatal period (Figure 7.4). If corroborated, this would illustrate the slowing of human ontogeny relative to macaque ontogeny, i.e. human paedomorphosis by

somatic retardation otherwise referred to as neoteny (Gould, 1977; Godfrey and Sutherland, 1995). With this hypothesis, the smaller CBA exhibited by humans compared with non-human primates can be attributed to the extension of prenatal flexion and the forgoing of the retroflexion seen in postnatal non-human primates. This conjecture could partly explain the aberration of humans from the non-human primate trend between CBA and relative brain size.

At present there is insufficient data available to determine whether these non-human primate trends are in any way associated with changes in brain development, i.e. rates of brain growth, relative to base length. Nonetheless, the relationship with activity within the synchondroses and possible implications for differential patterns of flexion between humans and non-human primates can be explored. As previously mentioned the midsphenoidal fuses late in the third human trimester, while in non-human primates it fuses in the second postnatal year (Ford, 1958; Michejda, 1971, 1972; Hoyte, 1975; Kodama, 1976; Shapiro and Robinson, 1980; Sirianni, 1985) . The spheno-ethmoidal, on the other hand, fuses at the time of birth in non-human primates, but remains patent in humans for six postnatal years (Scott, 1958;

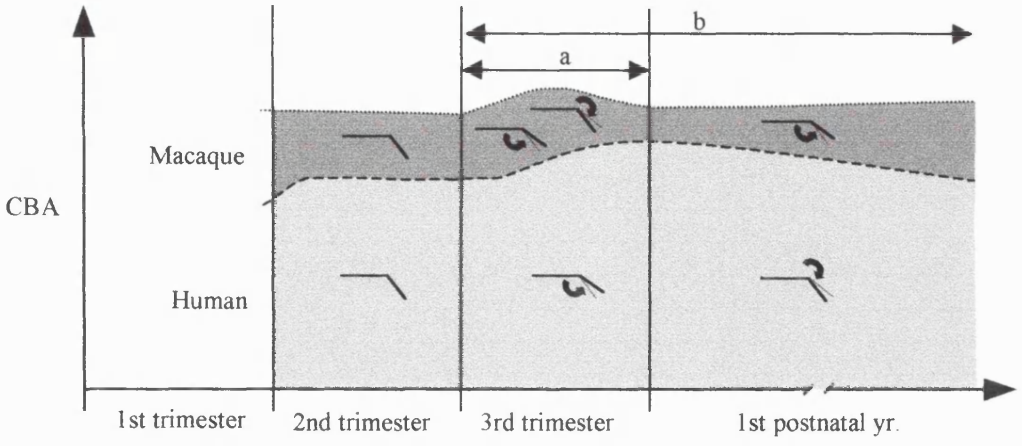

Figure 7.4. Graphic comparison of the pattern of flexion seen in humans and macaques. The human equivalent to the macaque pattern (a) is extended into the postnatal period (b), thereby forgoing postnatal retroflexion.

Michejda and Lamey, 1971). In both groups, the spheno-occipital synchondrosis fuses in adulthood (Brash, 1953; Scott, 1958; Melsen, 1969; Sirianni, 1985). This reveals that while the synchondroses in non-human primates fuse sequentially from the anterior to the posterior part of the basicranium, the sequence of spheno-ethmoidal and mid-sphenoidal fusion is reversed in humans (Figure 7.5). This would seem to suggest that postnatal retroflexion in non-human primates is facilitated by sequential fusion of the synchondroses but prevented in humans by the early fusion of the midsphenoidal synchondrosis. Thus, human base flexion would seem to be determined by a number of interdependent factors which include irregular fusion of the synchondroses, development of the pharynx, as well as increases of relative brain size, though the exact nature of these relationships remain to be investigated.

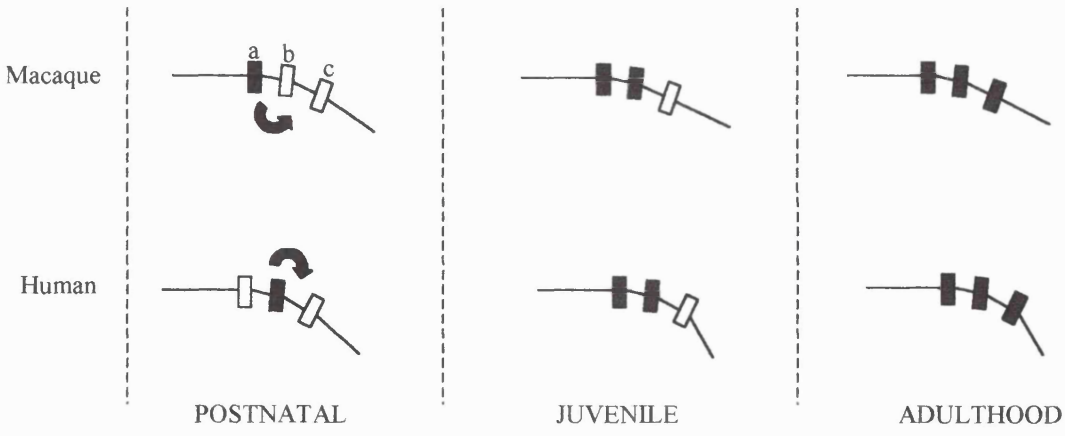

Figure 7.5. Schematic illustration of the different sequence of fusion of the spheno-ethmoidal (a), mid-sphenoidal (b), and spheno-occipital synchondroses in humans and macaques. Areas of black indicate fusion of the synchondrosis. Note that the major difference in flexion (arrows) corresponds to the postnatal period when the sequence of fusion is also different.

7.4 Posterior cranial fossa morphology

The increase of supratentorial relative infratentorial volume (endocranial ratio) observed in the present study is consistent with the results reported by Guihard-Costa and Larroche (1990) for brain mass and Jenkins (1921) and Koop *et al.* (1986) for brain volumes. Studies have also shown that parts of the brain anterior to sella increase more rapidly than posterior parts during the second trimester (Blechschmidt, 1977; Friede, 1981). This is in close agreement with the present findings which show that linearised supratentorial growth is more than double that of the infratentorial region. Guihard-Costa and Larroche (1990) show that infratentorial mass decreases as a percentage of overall brain mass from 6 to 4 ½ % over the second trimester. Interestingly, their results also show an increase of the infratentorial percentage of overall brain mass from 4 ½ to 7% , which is mainly due to a growth of the cerebellum, during the third trimester. However, it is difficult to interpret variations of mass in terms of physical brain enlargement because ventricular growth and differential densities of neural tissue are not taken into account. Variations of infratentorial size relative to supratentorial size computed from the human fetal brain volumes published by Jenkins (1921) and Koop *et al.* (1986) are also in close agreement with those reported here (refer to Table 7.3, section 7.3). Endocranial ratios range from 0.15 at 11 weeks to 0.05 at 19 weeks while those reported here range from 0.23 to 0.05 during the same period. Values from the present study are in general higher due to differences of technique (see section 7.3). Nonetheless, both show a general increase of supratentorial size relative to infratentorial size as a decrease of the endocranial ratio during early fetal development. In contrast to the mass percentages (Guihard-Costa and Larroche, 1990), there is very little change in the values computed from the data of Jenkins

(1921) and Koop *et al.* (1986) during the third trimester indicating that the proportions remain virtually constant during this period. There is a small increase of 0.02 between 19 and 40 weeks and sharp rise to 0.15 at around 21 weeks, though the latter is probably due to error. Adult human values of endocranial ratio based on direct measurements and MRI studies are in the region of 0.130-0.137 (Stephen *et al.*, 1986; Filipek *et al.*, 1989). This is some 0.05-0.06 (90%) higher than that observed during the second half of the second trimester, indicating that infratentorial size increases in relation to supratentorial size during the third trimester, postnatally, or both. Thus, it appears that the cerebrum increases relative to the cerebellum and pons during early fetal development (endocranial ratio decreases) and that this process is reversed either later in fetal life, i.e. third trimester, or during postnatal development. Perhaps tissue density increases by foliation of the cerebellum during the third trimester while volumetric increases occur postnatally. Although volumetric proportions have yet to be investigated for these periods, studies show that the base flexes postnatally. Thus, a result showing that the increase of infratentorial size occurs postnatally would be consistent with the apparent relationship between brain topography and cranial base angulation discussed earlier (see section 7.1.).

Results from the present study show that the tentorium cerebelli rotates towards foramen magnum during early fetal life and that this rotation slows towards the end of the second trimester. The angle between the tentorium and anterior cranial base increases by about 35 degrees from 11 to 18 weeks gestation. This is consistent with the observations of Hotchstetter (1939) who notes a rotation of approximately 38 degrees during the same period (measured from Abb. 42, Hotchstetter [1939]: 48-144mm CRL; Figure 7.6). Hotchstetter also shows that after this period the rotation slows with a total increase of about 8 degrees from 18-23 weeks (144-200mm CRL).

This is similar to the 5-10 degree increase observed here during the same period. There are no studies of tentorial rotations relative to the anterior cranial base during the third trimester, postnatally, or adulthood. However, data published by Bull (1969) on the orientation of the tentorium relative to foramen magnum indicates that the adult value of tentorial orientation relative to the anterior cranial base is not that dissimilar to that observed at the end of the second trimester. Thus, it would appear that tentorial rotation is not reversed or substantially increased in adulthood from the fetal condition.

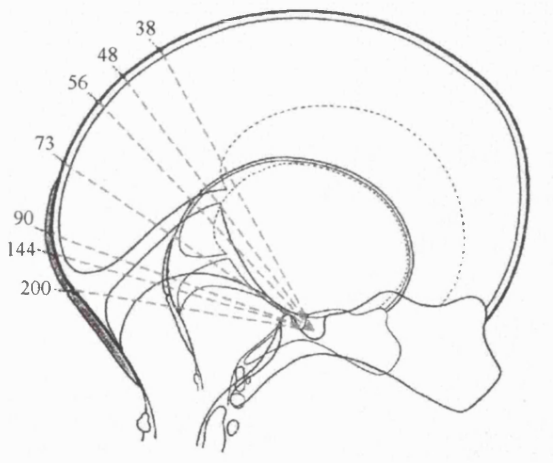

Figure 7.6. Midline sagittal sketch of the fetal head showing posterior rotations of the tentorium cerebelli from 38 to 200mm crown-rump length (from Hotchstetter, 1939).

Previous studies of the cranial base do not provide quantitative data on the proportions of the posterior cranial fossa during human fetal development. The findings of the present study show large increases of both fossa length and width with age which are greater than that expected for generalised scaling with size, assuming that age is a suitable adjunct to size. In addition to the positive allometry of overall size, posterior fossa width increases in relation to its length. Consequently, the posterior fossa, which is circular-shaped in the early fetus, becomes progressively more ovate with age, i.e. wider than it is long. This is consistent with

Ford's (1956) observation that the posterior fossa becomes progressively broader. Although there are no studies of the proportions of the posterior fossa in adulthood, Dean and Wood's (1981) exocranial measures of basicranial morphology show that the bitympanic width of the posterior fossa is almost 40% larger than the distance from the spheno-occipital synchondrosis to the opisthion. While these measures are not exactly equivalent to the endocranial dimensions of the fossa the large difference is consistent with the findings of the present study.

In contrast to the Lee *et al.*'s (1996) study of otic capsule orientation, the results from the present study show no correlated change in the orientation of the petrous pyramids with age. Lee *et al.* observed a rapid decrease of about 10 degrees in the angle between the petrosal ridges of the otic capsules from 16 to 30 weeks gestation. This almost plateaus during later fetal development. Third trimester fetuses therefore have more sagittally orientated otic capsules than second trimester fetuses. Such a decrease was not evident in the present study. It is possible that a decrease in the order of 10 degrees was masked in the present study by cross-sectional noise in both the measure and age variable. There are no values of petrous orientation in adulthood using the measure used here, but measures of the petrous temporal axis and posterior petrosal surface relative to the midline give adult values of about 44 and 55 degrees, respectively (Dean and Wood, 1981 [90-α]; Spoor, 1997 [180-PPip to sagittal]). These represent inter-petrous angles of 88 and 110 degrees, respectively.

The results from this study also show that tentorial rotation ceases at around eighteen weeks gestation once the brain portions have reached their second trimester topographical relations with one another. These findings are in close agreement with Moss *et al.* (1956) who state that there are only minor changes in the orientation of

the tentorium once the portions of the brain have assumed their topographical relations at around 90mm crown-rump length. Thus, it appears that increases in the size of the cerebrum relative to the cerebellum and pons drives tentorial rotation towards the foramen magnum during early fetal development. The relative proportions of the brain and the position of the tentorium has also been shown to vary across anthropoids (Klintworth, 1968; Bull, 1969; Stephan *et al.* 1986), indicating that a similar mechanism occurs interspecifically amongst primates. According to a number of authors the tentorium has also played an important role in human evolution, dissipating the increased load of the cerebrum brought about by upright posture and cerebral expansion (e.g. Bull, 1969; Aiello and Dean, 1992). In most primates the tentorium cerebelli attaches to the occipital, petrous crests and the clinoid processes and thus isolates the spheno-occipital synchondrosis, which is considered a major centre of postnatal flexion amongst humans, from the direct influence of cerebral enlargement. Although the tentorium has been shown here to shift with cerebral enlargement during fetal development and has probably done so during human evolution, its influence should not be overlooked as it still provides a degree of resistance to the momentum of cerebral expansion. It is interesting to note, therefore, that very few evolutionary hypotheses relating to human brain enlargement (e.g. the spatial-packing hypothesis) take into account the support provided by the tentorium for occipital lobe enlargement and its rotations, preferring instead to treat the supratentorial and infratentorial parts of the brain, which have distinct fetal growth rates, as a single unit. A more complex interpretation of brain enlargement involving the tentorium and differential growth between supratentorial and infratentorial parts may prove informative in future studies.

There is no evidence from the present study to indicate that increases of infratentorial size relative to posterior cranial base length underlies the change in the proportions of the posterior fossa or variations of petrous pyramid orientation. Rather the results suggest that cranial base angulation and variation of brain topography, which converge upon the contents of the posterior cranial fossa, are the major determinants of posterior fossa morphology during fetal development. Increases of supratentorial size relative to infratentorial size, thereby limiting superior growth of the contents of the posterior cranial fossa, were found to be associated with increases of posterior fossa width in relation to length. It appears, therefore, that the restriction place on superior growth of the cerebellum by cerebral enlargement leads to lateral expansion, thereby increasing the width of the posterior fossa.

Increases of cranial base angle were found to correlate with decreases of petrous pyramid orientation during early fetal life. This correlation is also observed whilst holding relative brain size constant ($r_{partial} = 0.611$ [$P<0.05$]) and is consistent with Du Brul and Laskin's (1961) rat experiments. These showed that excision of the spheno-occipital synchondrosis leads to cranial base kyphosis and more coronally orientated petrous bones. Moreover, Du Brul (1977) has linked coronal rotation of the petrous bones with cranial base angulation as adaptive requirements for bipedalism during human evolution. The findings reported here are not consistent with Dean's (1988) hypothesis which suggests the petrous bones are more coronally orientated in humans compared with great apes because of size increases of the cerebellum and brain stem in relation to the posterior cranial base. Dean's hypothesis is partly supported by Spoor' s results (1997) which show that petrous pyramid orientation amongst primates is significantly correlated with relative brain size but

not CBA. As with base flexion and relative brain size, it appears that the process of petrous reorientation evident during prenatal development is distinct from the interspecific primate trend.

7.5 Facial morphology

The results of this study show that palate length increases in relation to maxillary height during human prenatal development. This finding is consistent with other studies showing that facial length (depth) increases in relation to facial height during prenatal ontogeny (Scammon and Calkins, 1929; Birch, 1968; Houpt, 1970). However, Ford (1956) and Inoue (1961) indicate that facial height increases in relation to length, though this is probably due to differences in the anatomical landmarks used to measure facial length. For example, Ford defines facial depth as the length of the nasal septum as opposed to the palate. The increase of facial length reported here is possibly due to lengthening of the maxillary arch in both posterior and anterior directions in conjunction with the development of the tooth buds (Enlow and Hans, 1996).

The results from the present study also indicate that the maxilla becomes progressively less retrognathic with age. The angle between the maxilla and anterior cranial base increases from approximately 84 to 96 degrees over the period studied. These results are therefore in close agreement with other prenatal studies showing increases of maxillary angle with age (Levihn, 1967; Diewert, 1983; Erdoglija, 1990; van den Eynde *et al.*, 1992). In particular, Levihn observed an increase from 76.5 to 91.5 degrees during fetal life and an increase from 76.5 to 89 degrees during the second trimester. Eynde *et al.* also observed an increase of maxillary prognathism from 82.8 to 93.9 during from 12 to 40 weeks. Although these values are different to

those reported here, probably because Levihn and Eynde *et al.* use nasion as opposed to foramen caecum, overall increases in maxillary prognathism are similar. Ford (1956) found no change of maxillary angle except for a slight increase during the last 10 weeks of gestation which he suggests is due to alveolar development.

Results from this study also show a small increase of 8 degrees in the orientation of the palate. There are no other fetal studies with which to compare this result, but suffice as to say that the orientation differs across primates by some 40 degrees with a 20 degree decrease (i.e. ventral rotation) from great apes to modern humans (Ross and Ravosa, 1993; Ross and Henneberg, 1995). Thus, results from the present study show increases of facial length in relation to height, maxillary prognathism, and dorsal facial kyphosis (bending of the palate upwards). These do not, therefore, corroborate reports that the facial profile (shape) remains essentially unchanged with ontogenetic size increases (e.g. Ford, 1956; Inoue, 1961; Burdi, 1969; Johnston, 1974; Anagnostopoulou, 1988).

A number of authors have noted that the orbits move to a more frontal position on the head during development, particularly during the embryonic period (e.g. Keith, 1948; Sperber, 1981; Moore, 1982). This is consistent with the findings of the present study. These show that during early fetal life the orbital axes rotate superiorly by some 20 degrees relative to the posterior cranial base and the orbital rims become more vertically orientated relative to the anterior cranial base. The results also indicate that orbital convergence and frontation occurs in the transverse plane throughout the period studied. Once again it is interesting to note that while there are no comparable fetal studies, the trend from African apes to modern adult humans represents a decrease of orbital axes orientation rather than an increase as observed in the fetal sample (Ross and Henneberg, 1995). The process of frontation

and convergence, on the other hand, does appear to be similar to that observed in Cartmill's (1970) study of primate evolution.

Significant correlations were observed between orbital axes orientation, palate orientation, and cranial base angle, supporting the notion that changes of the face are associated with cranial base morphology (Enlow, 1976; Sperber, 1981; Ross and Ravosa, 1993; Ross and Henneberg, 1995). Although changes in the orientation of the palate were not shown to correlate with relative brain size, the results support the notion of an almost isometric relationship between base flexion and palate orientation during human fetal development. This is consistent with results from studies of adult non-human primates (Ross and Ravosa, 1993) and normal and abnormal human development (Björk, 1955; Burtson, 1959; Kvinnsland, 1971; Latham, 1976). Moreover, correlations of orbito-palatine angle and the angle between the anterior cranial base and palate with cranial base angle show that the association between CBA and palate orientation is not just the consequence of the shared line segment. However, the residual angle between the anterior cranial base and orbital axes was not correlated with CBA, suggesting that orbital axes orientation relative to the posterior cranial base is only correlated with CBA because of the shared line segment sella to basion. Results from the present study also indicate that maxillary prognathism is associated with differential growth between the palate and anterior cranial base. As such growth of the anterior cranial base is retarded in relation to that of the palate. Hence, anterior increases of the palate, whether through growth in the palate itself or the vomer (see McCollum, 1999), exceeds that of the anterior cranial base, thereby resulting in maxillary prognathism (Figure 7.7). These findings show that the facial profile in the sagittal plane, which is

defined by the degree of maxillary prognathism and facial kyphosis, is closely integrated with changes to the cranial base (e.g. flexion and differential growth).

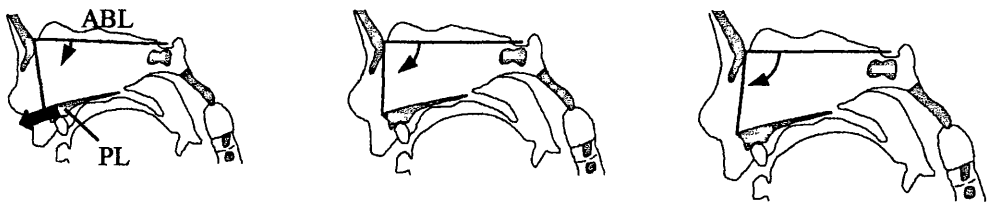

Figure 7.7. Illustration of the midline fetal head showing that anterior growth of the palate (PL) in relation to the anterior cranial base (ABL) leads to maxillary prognathism.

The findings of this study also reveal a number of other associations. Firstly, that more forward facing and convergent orbits in the transverse plane are associated with dorsal facial kyphosis, base retroflexion, and relative brain size. Secondly, maxillary prognathism is associated with sagittal orbital frontation and orbital convergence. Thus, in the sagittal plane orbital morphologies are associated with changes of the facial profile while in the transverse plane associations exist with the cranial base, relative endocranial size, and the facial profile. These findings are in many respects consistent with hypothesis relating to primate and human evolution (Enlow, 1976). In particular, the observed associations of maxillary prognathism with sagittal frontation and of relative endocranial size with transverse frontation are consistent with the evolutionary propositions of Enlow and McNamara (1973) and Enlow (1976), respectively. However, there is little evidence to support Enlow and McNamara's notion that the orbits become more vertically orientated relative to the anterior cranial base with enlargement of the brain. Nonetheless, the findings from the present study do suggest that transverse orbital frontation and orbital convergence are associated with brain enlargement.

The results reported here reveal a number of correlations of facial morphology with relative brain size. In particular, there appears to be evidence supporting Enlow and McNamara's (1973) notion that increases of brain size are associated with orbital convergence. However, because the cranial base separates the face from the brain such correlations can not represent a direct physical relationship. One possible intermediary process is a chain of events that links brain enlargement to basicranial architecture and from basicranial architecture to facial profile which in turn influences inter-facial morphology. Alternatively, the correlations could be the result of comparatively slower growth along the midline cranial base causing changes of facial morphology (e.g. maxillary prognathism) and an unrelated increase of relative brain size at the same time. A recent interspecific study indicates that the spatial-packing problem in non-human primates arises from an evolutionary reduction in base length rather than an increase in brain size (Strait, 1999). The argument being that because brain size scales against body size with negative allometry, base length must scale against size with extreme negative allometry to account for the increase in relative brain size and the subsequent reduced value of CBA seen in larger bodied anthropoids.

While this hypothesis is not directly applicable to the special case of humans, which possess uniquely enlarged brains, and merely changes the evolutionary interpretation of the spatial-packing hypothesis among non-human primates, it raises the question as to the role of growth along the anterior cranial base in correlations of maxillary prognathism, transverse orbital frontation, and orbital convergence with relative endocranial size. It seems pertinent to suggest that these correlations arise due to retarded growth along the midline anterior cranial base compared with general size increases and growth of the palate, lateral orbital rims, and endocranial size.

This implies that increases of palate length in relation to anterior base length lead to maxillary prognathism, as has already been shown, and that this is indirectly correlated with relative endocranial size because growth of the cranial base is also retarded in relation to linearised brain size. Similarly, retarded anterior growth of the medial orbital rims, which are closely related to the anterior cranial base, compared with that of their lateral zygomatic counterparts could lead to transverse orbital frontation in association with increases of endocranial size relative to cranial base length. This chord or ligament of growth resistance along the anterior cranial base reflects the position of embryonic bands of retensive mesenchyme. These provide biomechanical ligaments of resistance or retension between the embryonic organs of the head and converge into the mesenchyma of the supranasal furrow (Blechschmidt, 1976). Moreover, growth retension along the midline basicranium limits growth of closely related portions of the brain. Consequently, basal parts of the brain are associated with growth in thickness as opposed to surface area. Thus, the midline anterior cranial base may act as a ligamental force that limits growth of closely associated parts of the face in relation to more distal parts, thereby causing the more distal parts to flex anteriorly (Figure 7.8). Partial correlations of the results reported here would seem to support this notion. Comparisons of interorbital angle and relative interorbital distance against relative endocranial size fail to produce significant partial correlation coefficients while keeping base length constant ($r_{partial}$ = 0.143 [P>0.42] and 0.001 [P>0.99], respectively). In addition, comparisons of maxillary angle against relative endocranial size also fails to produce a significant correlation while controlling for increases of palate length in relation to base length, i.e. palate length over base length ($r_{partial}$ = 0.139, P>0.43). There is, however, a significant partial correlation between maxillary angle and relative endocranial size

whilst keeping just base length constant ($r_{partial} = 0.380$, $P<0.05$), indicating that some other relationship between these variables is also involved. Nonetheless, in general these coefficients indicate that growth along the midline cranial base and growth of the midline cranial base in relation to palate length accounts for the associations observed. This may explain, for example, why large bodied anthropoids possess highly frontated orbits (Cartmill, 1970; Ross and Ravosa, 1993). By approaching the question in terms of differences of basicranial and orbital growth rather than a spatial-packing problem, it can be suggested that large bodied anthropoids possess highly frontated orbits because the cranial base length scales with very strong negative allometry in relation to body mass (Strait, 1999).

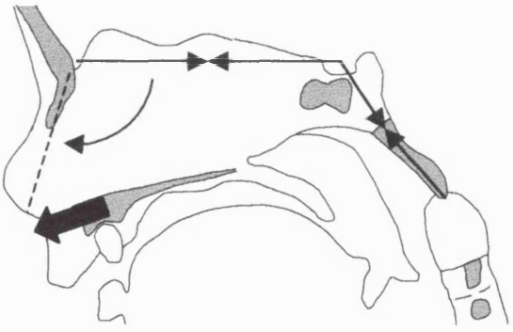

(a)

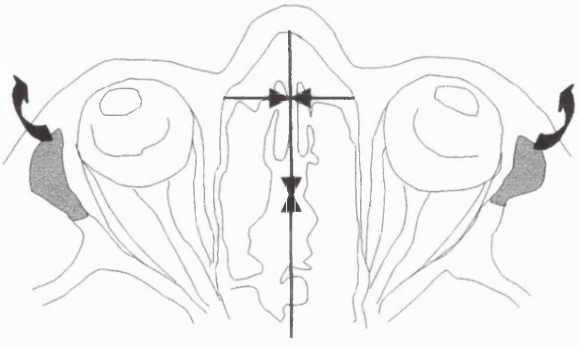

(b)

Figure 7.8. Illustrations of the ligamental hypothesis that suggests retarded growth of the cranial base, particularly the anterior cranial base, in comparison with (a) palate growth and (b) growth of lateral aspects of the orbits leads to maxillary prognathism, transverse orbital frontation, and orbital convergence during fetal development. Given that brain size also increases in relation to base length, the hypothesis indicates that correlations of orbital and facial morphology with relative endocranial size are due to retension in the cranial base rather than directly due to brain enlargement.

7.6 Concluding remarks and evolutionary interpretations

The findings of this study show that there is a complex matrix of associations amongst facial, and basicranial morphologies together with variations of relative brain size and changes in brain topography. These relationships are both spatially and temporally variable, giving rise to polyphasic patterns of association. As such the nature of interactions amongst ontogenetic enlargement of the brain, both in terms of relative brain size and topography, facial morphology, and basicranial morphology varies with fetal age. Consequently, generalised conclusions covering the whole prenatal period are not forthcoming. Regardless, the present study provides a unique insight into the developmental mechanism that may underlie certain characters of interest to evolutionary studies of modern humans. A number of hypotheses have been formulated upon the evidence presented here that warrant further study. Most are unlikely to yield profound debate, but a few may form the basis from which to elucidate the evolution of certain, uniquely, modern human features.

There is also evidence to suggest that developmental variations of the morphologies studied are to a certain degree influenced by intrinsic growth potentials of the synchondroses, midline cranial base, and brain. In other words, the activation of conserved genes regulating the rate of brain and basicranial growth would also seem to indirectly influence the heterochrony of skull determination by epigenetic factors. This is illustrated by the extended period of ontogenetic base flexion observed in humans compared with that seen in non-human primates. Whether this is due to a particular gene remains to be investigated. Nonetheless, it appears that skull formation, and perhaps therefore evolution of the modern human

skull, is both a genetic and epigenetic construct. Thus, both absolute epigenetic and genetic theses of skull formation are rejected in favour of a combined thesis in which genes indirectly and epigenetics directly affect facial and cranial base morphology during human fetal development.

Direct evolutionary interpretations of the findings reported here are difficult to draw because there is still a long way to go before the developmental mechanisms are fully understood and can therefore be compared with their proposed phylogenetic counterparts. What is clear, however, is that many interspecific trends observed amongst extant primates are not reflected in the findings of the present study. For example the associations of relative brain size with base flexion and between increases of relative brain size and petrous orientation. Furthermore, general trends from the fetal sample appear to be the opposite to those seen across primates: the pattern of fetal base flexion is polyphasic as opposed to linear; petrous bones reorientate sagittally rather than coronally despite increases of relative infratentorial size; large infratentorial relative to supratentorial size is accompanied by flexion not a comparatively flatter base; the sequence of fusion of the synchondroses is different; the palate moves dorsally as opposed to ventrally; and the maxilla becomes progressively less retronagthic as opposed to prognathic. The list goes on and ultimately shows that human fetal ontogeny does not reflect interspecific primate trends and *vice versa*. In fact, in many respects the associations are so distinct as to call into question the validity of , for example, comparisons between base flexion in humans with that across extant primates.

If extant primates are considered surrogates for human ancestors it would be tempting at this point to conclude that these findings show that human ontogeny does not parallel phylogeny. This would have implications for the concept of

heterochrony, though strictly speaking comparisons of primate fetal development would be required since heterochrony relates to differences between ontogenies not between adults and fetuses. Moreover, stating that ontogeny does not reflect phylogeny based on the evidence presented here assumes that the interspecific trends are the better models of human evolution. The alternate interpretation is that the mechanisms underlying prenatal human development would be more informative equivalents to evolutionary processes and that the trends observed amongst adult extant primates are unduly influenced by specialised adaptation. From the ontogenetic stance and based on the evidence reported here, evolution of human features such as cranial base angulation would be considered polyphasic in nature. Moreover, each phase would relate to a number of factors which in the case of CBA may include increases of brain size (both relative and general topography), pharyngeal enlargement for speech, bipedalism, and masticatory adaptations. In this light, simple cause and effect hypotheses of human evolution involving a single proactive component no longer seem appropriate. Furthermore, it can no longer be taken for granted that trends observed across extant adult primates are the best representations of the evolutionary mechanisms that underlie human morphology.

7.7 Summary of conclusions

1. There is little evidence from the present study to indicate that increases of brain size relative to base length drives cranial base flexion, at least during the period studied. It seems likely that cranial base angulation is associated with a number of mutually dependent and dynamic variables that included variations in the rate of brain growth, fusion of the synchondrosis, brain topography, and pharyngeal development. These relationships have still to be investigated fully.

2. The nature of prenatal base angulation appears polyphasic with embryonic flexion, early fetal retroflexion, second trimester stabilisation, and third trimester retroflexion.
3. There is little support for the notion that adult modern human cranial base flexion is due to fetalization (paedomorphosis), though there is some evidence of somatic retardation in comparison with the late non-human fetal pattern of base flexion.
4. Differential patterns of base angulation between humans and non human primates are probably the result of differences in: (a) the sequence of the fusion of the synchondroses; (b) negative allometries of brain size and base length with size; (c) neural growth patterns; (d) facial growth patterns; and (e) pharyngeal development.
5. Changes of brain topography influence the orientation of the tentorium and the proportions of the posterior cranial fossa.
6. Results are inconsistent with the hypothesis that increases of relative infratentorial size are associated with more coronally orientated petrous bones and base flexion. In fact the findings indicate that the petrous pyramids become more sagittally orientated with increases of cranial base angle during early fetal development.
7. The findings of this study show that maxillary prognathism increases across the period studied in relation to age and is associated with increases of relative brain size.
8. There are a number of close associations of facial morphologies with basicranial architecture throughout the second trimester of human development. Variations of orbital morphology, which include orbital frontation and convergence with

age, are associated with cranial base angulation, maxillary prognathism, and increases of relative brain size.

9. The facial profile, as defined by maxillary prognathism and facial kyphosis, is closely related to basicranial architecture. In turn, inter-facial morphologies are associated with the facial profile. Thus, the face and cranial base appear to be structurally integrated during fetal development.
10. Interspecific trends across extant adult primates are not evident during the process of human fetal development. This calls into question the validity of using only interspecific models to investigate possible mechanisms of human evolution.

Appendix 1a. Approximation of age in weeks from crown-rump length (CRL), stage, and greatest length (GL).

	Age (weeks)	CRL (mm)	Stage	GL (mm)
Embryonic period	1	0.0-0.1	1-4	0.0-0.1
	2	0.1-0.3	5-6	0.1-0.3
	3	0.4-2.5	7-9	0.4-2.5
	4	3.5-6	10-13	3-6
	5	5-9	14-15	5.5-9
	6	11-14	16-17	7-14.2
	7	16-18	18-19	
	8	20-31	20-23	
Fetal period	9	31		
	10	40		
	11	50		
	12	61		
	13	74		
	14	87		
	15	101		
	16	116		
	17	130		
	18	142		
	19	153		
	20	164		
	21	175		
	22	186		
	23	197		
	24	208		
	25	218		
	26	228		
	27	238		
	28	247		
	29	256		
	30	265		
	31	274		
	32	283		
	33	293		
	34	302		
	35	311		
	36	321		
	37	331		
	38	341		
	39	352		
	40	362		

Data based on reported by Streeter (1921), O'Rahilly and Müller (1971), Moore (1982).

Appendix 1b. Details of some of the synonyms encountered in the literature.

Name	Synonyms (reference)
Cephalic flexure	mesencephalic flexure (O'Rahilly and Gardner, 1971) cranial flexure (O'Rahilly and Gardner, 1971) anterior flexure (Keith, 1948) midbrain flexure (Moore, 1982)
Cervical flexure	nuchal flexure (Keith, 1948)
Alisphenoid	greater wing of sphenoid (De Beer, 1937) ala magna (Noback and Robertson, 1951) ala temporalis (Noback and Robertson, 1951) alapostsphenoid (Noback and Robertson, 1951)
Orbitosphenoid	ala orbitalis (Gasser, 1976) lesser wing of sphenoid (De Beer, 1937) ala parva (Noback and Robertson, 1951) alipresphenoid (Noback and Robertson, 1951)
Basisphenoid	postsphenoid (Kodama, 1976a-c) medial postsphenoid (Noback and Robertson, 1951) median centres (Noback and Robertson, 1951) basipostsphenoid (Noback and Robertson, 1951)
Lingula	lateral basisphenoid (Noback and Robertson, 1951) alar process (Noback and Robertson, 1951)
Presphenoid	basipresphenoid (Noback and Robertson, 1951)
Lacrimal	lachrymal (De Beer, 1937)
Neural folds	medullary plates (Keith, 1948)
Condylar part of occipital	exoccipital (De Beer, 1937)
Interparietal part of occipital	Supranuchal part of occipital (De Beer, 1937)
Supraoccipital part of occipital	Infranuchal part of occipital (De Beer, 1937)
Trabecula cartilages	trabeculae cranii (Keith, 1948; Moore, 1982)
Otic vesicle	otocyst (Moore, 1982)

Appendix 2. Glossary of MRI terms.

Angular momentum. The moment of the linear momentum of a particle about an axis. In atomic physics, the angular momentum of particles with spin energy is quantized by multiplies of half Dirac constant (Planck's constant/2π).

Bit. A single digit of the binary numbers (0 or 1) used by computers. A combination of eight bits can express 2^8 or 256 different values, 12 bits 4096 values and 16 bits 65536 values.

Bit range. See pixel depth.

Byte. computer memory used to store a group of eight bits.

Boltzmann's constant. Derived from the theory of statistical distribution of particles subject to thermal, electric, or magnetic energy. Given by $k = R/N = 1.3805 \times 10^{-23}$ JK^{-1}, where R is the ideal gas constant and N is the Avogadro constant (6.02252×10^{23} mol^{-1}).

Data matrix. Columns and Rows of data stored in k-space, determined by the number of phase and frequency encodings.

Dipole. Two equal and opposite charges separated by a small distance e.g. bar magnet.

Electromagnetic induction. Faraday's law of induction states that the movement of charged induces a magnetic field and vice versa.

Electron. Negatively charged atomic particle (1.602×10^{-19} coulombs) around the nucleus. The distribution of electrons in the shells surrounding the nucleus determines the chemical properties of the atom.

Field of view (FOV). The area of the scanned object that is represented in the reconstructed image.

Free induction decay signal (FID). The electrical current induced in the MRI receiver coil by the relaxing spins. It gradually decreases as more and more spins return to their unexcited state.

Frequency encoding. The introduction of spatial information using a magnetic gradient to produce characteristic frequencies along one dimension of the magnet.

Gyromagnetic ratio. The ratio between the magnetic moment of a spin and its angular momentum.

Image matrix. The square two-dimensional array of pixels that makes up an image.

Magnetic flux. The distribution of a magnetic field.

Moment. the vector product of two force or vector components e.g. a 0^{o} component and a 180^{o} component of the same magnitude produces a 90^{o} moment perpendicular to the line $0\text{-}180^{0}$.

Neutron. Atomic particle contained within the nucleus with no charge. Mass is approximately equal to that of a proton.

Nyquist theorem. This theory dictates that a signal frequency must be sampled at least twice in order to reproduce it reliably.

Phase. The position (or angle) of the spin in its rotational path.

Phase encoding. The introduction of spatial information using a magnetic gradient to produce characteristic phases along one dimension of the magnet.

Pixel. Abbreviation of "picture element" representing the (two-dimensional) building blocks of the matrix of a MR image.

Pixel depth. The range of possible values (CT or MR numbers) assigned to a pixel, given in bits.

Pixel size. The size of the imaged area represented by one pixel, calculated by dividing the field of view by the matrix size.

Planck's constant (h). Action of an object, usually a photon, described in dimensions of energy x time ($6.626\text{x}10^{-34}$ Js).

Proton. Positively charged atomic particle contained within the nucleus. The number of protons in a nucleus is equal to the atomic number of the atom.

Quantum. Term for indivisible i.e. discrete units of energy.

Signal to Noise Ratio (SNR). The ratio between a signal and the background signal.

Spatial resolution. A quantitative measure of the ability to resolve small details, ie. to visualize to small details separately. It is not the smallest isolated detail that can be visualized.

T_1. The time taken for 1/exp. of spins to return a state of alignment with the magnetic field.

T_1 recovery. The restoration of spins to a state of alignment with the magnetic field, also called spin-lattice relaxation.

T_1 weighting. A method for showing differences in T1 times between tissues as image contrast.

T_2. The time taken for 1/exp. of the excited spins to decay.

T_2 decay. The loss of spins from the excited state, also called spin-spin relaxation.

T_2 weighting. A method for showing differences in T2 times between tissues as image contrast.

TE. Time to Echo; the time between the excitation pulse and the echo.

Tesla. SI unit of magnetic flux.

TR. Repetition Time; the time between excitation pulses.

Uncertainty principle. There is a fundamental limit to the precision with which a position co-ordinate of a particle and its momentum in that direction can be known simultaneously.

Voxel. Abbreviation of "volume element". The (three-dimensional) volume represented by a (two-dimensional) pixel. In volume it therefore equals the squared pixel size times the slice thickness.

Appendix 3. Raw measurement data for each individual specimen (mm, degrees, mm^3, and mm^2)

CODE	Age (weeks)	Anterior cranial base length	Posterior cranial base length	Total cranial base length	Posterior cranial fossa length	Posterior cranial fossa width	Palate length	Maxillary height	Interorbital distance	Relative interorbital distance	Cranial base angle
10WM	11.0	7.2	5.4	12.6	10.4	11.0	5.4	4.6	3.4	0.44	127.6
NE20	12.5	9.2	7.8	17.0	12.6	16.0	5.6	6.0	5.0	0.50	130.8
QMWF49	13.0	9.6	7.4	17.0	12.2	14.8	7.2	5.4	3.8	0.36	127.2
QMWF7	13.7	10.6	8.8	19.4	14.8	19.0	7.2	6.6	5.4	0.39	132.6
QMWF34	14.0	11.2	8.4	19.6	16.6	20.6	8.2	7.0	5.0	0.36	129.8
12WM	14.3	12.8	9.4	22.2	16.2	21.2	8.4	7.4	6.2	0.39	132.2
14WM	15.3	15.4	10.6	26.0	17.8	24.6	10.6	8.4	8.0	0.40	133.8
E2	15.5	14.4	10.4	24.8	16.2	24.8	8.6	9.8	7.4	0.38	138.4
NS5	15.7	15.4	11.0	26.4	19.4	25.2	10.4	9.0	8.2	0.39	127.0
E5	16.3	16.6	12.8	29.4	20.8	25.2	N/A	N/A	8.2	0.37	132.0
E4	16.3	17.4	10.6	28.0	22.2	26.4	10.4	9.6	8.2	0.34	138.6
Z101	16.7	17.4	11.8	29.2	23.8	27.8	10.6	8.6	8.8	0.37	135.8
N6	17.0	16.0	12.0	28.0	22.8	28.0	9.6	9.6	8.8	0.37	133.6
QMW28	17.3	17.4	12.2	29.6	23.0	29.4	N/A	N/A	9.2	0.35	136.4
E147	17.7	19.8	12.0	31.8	22.0	30.0	13.6	11.2	9.0	0.35	138.8
E72	17.7	17.4	11.8	29.2	21.2	27.8	13.2	11.0	9.4	0.36	135.8
E93	17.7	17.6	12.2	29.8	22.4	28.2	12.0	11.4	7.8	0.26	137.6
QMW35	17.7	17.2	11.6	28.8	24.0	28.0	10.8	9.2	8.4	0.34	133.4
Z102	17.7	18.0	12.2	30.2	24.0	28.6	11.0	7.8	9.0	0.36	138.6
N50	18.3	19.8	13.6	33.4	21.8	33.0	15.0	11.4	10.2	0.32	136.0
E109	18.7	21.0	13.8	34.8	26.4	30.2	15.0	12.4	9.4	0.30	139.4
N22	18.7	20.4	13.0	33.4	23.4	32.8	15.2	11.6	9.8	0.32	131.8
E102	19.0	23.2	14.2	37.4	24.6	31.4	15.0	14.2	9.2	0.27	128.2
NS70	19.0	21.4	14.2	35.6	26.2	33.0	15.4	14.4	10.0	0.32	135.6
N30	19.3	20.8	14.4	35.2	25.0	35.8	16.8	13.0	8.8	0.28	129.0
ZN1	19.3	21.2	14.4	35.6	26.6	32.4	13.2	11.6	N/A	N/A	134.4
NS71	19.3	21.4	13.4	34.8	25.8	33.8	15.8	12.8	9.0	0.27	129.2
NS15	19.5	21.0	15.2	36.2	26.0	35.8	16.0	15.0	9.2	0.28	134.6
20WM	19.7	21.0	13.8	34.8	26.0	32.6	15.6	12.0	9.4	0.30	129.8
E58	20.3	21.8	13.4	35.2	26.8	37.4	16.2	13.2	9.6	0.28	133.8
E20	20.3	22.0	13.8	35.8	27.2	35.8	16.0	10.2	12.0	0.35	134.8
E6	20.5	22.4	14.4	36.8	29.2	38.6	15.6	12.8	9.8	0.27	127.8
N12	21.0	22.8	14.0	36.8	26.4	36.6	18.8	13.0	11.2	0.30	137.2
E167	21.0	24.0	15.2	39.2	23.8	37.2	17.6	15.8	9.8	0.25	134.8
NS92	21.7	23.4	15.6	39.0	27.2	40.8	18.4	13.4	10.8	0.28	133.8
N1	22.0	24.0	13.8	37.8	31.0	39.8	18.0	12.8	10.6	0.26	134.2
E90	22.6	24.8	16.2	41.0	30.8	39.6	20.0	18.0	11.4	0.28	135.6
E64	23.3	25.4	15.8	41.2	32.4	40.2	18.4	13.8	10.8	0.25	133.8

Appendix 3 (contd.)

CODE	Flexion of the synchondrosis	Palate orientation	Maxillary Angle	Orbital axes orientation	Orbito-palatine angle	Orbital rim orientation	Interorbital angle	Sagittal angle of tentorium	Petrous pyramid orientation	Endocranial volume	Infratentorial volume	Supratentorial volume	Midline area
10WM	N/A	112.8	89.4	112.4	3.4	52.6	115.4	N/A	73.0	1870	360	1510	166
NE20	127.6	114.0	86.2	108.4	5.6	54.4	106.4	139.8	70.0	4970	840	4130	393
QMWF49	125.4	114.8	86.6	111.6	3.2	51.2	111.8	143.8	66.4	4940	740	4200	405
QMWF7	130.0	118.2	91.4	124.4	6.2	67.0	116.2	144.8	64.0	6910	1220	5690	N/A
QMWF34	126.2	115.6	89.8	122.0	6.4	65.2	118.0	N/A	69.4	8120	1090	7030	421
12WM	126.4	115.6	90.0	123.8	8.0	65.0	125.4	161.2	68.0	11740	1360	10380	522
14WM	130.8	118.6	86.2	122.8	4.2	54.2	124.2	163.6	74.0	15950	1720	14230	701
E2	134.8	115.4	88.4	N/A	N/A	62.8	120.2	N/A	N/A	13590	2090	11500	585
NS5	123.0	110.6	89.8	122.4	12.0	70.2	116.4	N/A	N/A	N/A	N/A	N/A	N/A
E5	122.4	N/A	N/A	127.8	N/A	64.0	133.2	172.6	N/A	23900	2470	21430	892
E4	135.2	122.4	87.0	131.8	9.4	62.2	128.8	162.8	65.4	22190	2720	19470	952
Z101	136.0	122.2	87.8	130.6	8.2	62.0	134.2	179.8	59.4	27530	2440	25090	1082
N6	130.0	116.0	85.8	126.4	10.4	67.2	131.6	N/A	N/A	20890	N/A	N/A	751
QMW28	134.0	N/A	N/A	125.8	N/A	66.8	132.6	N/A	N/A	32260	3050	29210	N/A
E147	128.8	119.2	84.4	127.6	8.2	64.4	131.0	164.6	N/A	33720	3450	30270	1251
E72	128.4	117.8	96.2	131.2	13.4	71.2	134.8	167.8	58.8	29550	2750	26800	1109
E93	129.2	120.4	88.8	128.0	7.6	70.8	139.0	N/A	N/A	25270	2330	22940	963
QMW35	130.8	120.2	93.0	127.4	7.2	66.0	129.2	177.8	70.2	31620	2720	28900	1135
Z102	131.2	118.6	95.6	133.4	14.8	57.4	138.0	164.0	57.2	38990	3180	35810	1326
N50	132.2	124.2	93.6	128.4	4.4	63.4	127.0	178.4	60.6	30130	2580	27550	885
E109	134.0	119.4	88.2	129.6	10.2	66.0	144.2	163.6	68.0	51310	4780	46530	1698
N22	130.6	118.2	99.2	122.4	4.4	63.2	125.2	178.8	65.0	42340	3550	38790	1387
E102	121.2	111.6	88.6	113.2	1.6	68.4	140.0	177.6	60.8	52860	4380	48480	1638
NS70	134.0	120.4	88.0	119.2	1.2	59.2	133.2	173.0	69.8	57520	4480	53040	1707
N30	124.4	118.4	100.2	119.6	1.2	69.4	126.4	175.6	58.8	48200	3940	44260	1425
ZN1	128.6	118.2	99.0	N/A	N/A	N/A	N/A	179.2	68.8	50180	4820	45360	1618
NS71	125.0	115.6	92.6	115.0	0.8	60.6	129.4	173.4	64.2	55670	3570	52100	1971
NS15	132.2	116.4	87.8	120.4	4.2	60.2	135.8	161.6	71.2	N/A	N/A	N/A	N/A
20WM	124.0	118.4	95.2	119.2	2.2	50.2	133.8	178.2	67.4	52070	5510	46560	1441
E58	130.4	114.6	91.8	120.2	5.6	67.2	133.2	176.0	69.8	59310	4430	54880	1435
E20	128.0	121.6	91.8	127.0	5.6	68.8	135.4	172.0	59.8	63600	5630	57970	1885
E6	123.2	118.0	102.0	119.4	1.6	71.0	133.8	169.6	67.8	66250	6360	59890	1888
N12	139.0	125.0	97.8	124.4	1.4	67.6	135.4	174.0	70.4	65820	5620	60200	1917
E167	128.4	117.0	88.4	119.8	2.6	57.8	132.8	178.4	56.4	63670	4670	59000	1752
NS92	128.8	120.8	96.0	122.0	1.2	64.4	134.4	178.8	70.6	70250	5850	64400	2147
N1	134.8	123.0	100.2	129.4	6.4	72.2	138.2	178.8	77.2	84260	7680	76580	2151
E90	129.8	118.8	92.0	116.6	2.4	62.0	143.8	177.8	75.2	84360	7240	77120	2096
E64	131.8	123.4	96.2	121.6	1.8	69.4	137.8	179.8	67.8	87440	8300	79140	2364

BIBLIOGRAPHY

Abd-El-Malek S. (1957). The anencephalic skull and a vascular theory of causation. *Egyptian Medical Association* **40**: 216-224.

Adrias-Mendoza K., Martinez I., Aristi G., Garcia-Cavazos R., Koffman-Alfaro S., Garcia-Pelaez I., Arteaga M., Madroza M., and Madrazo I. (1991). Magnetic resonance imaging (MRI) application to the study of embryo-fetal development. *Proceedings of the 8th International Congress on Human Genetics* **49**: 172.

Aiello L. and Dean C. (1990). *Human Evolutionary Anatomy*. London: Academic Press.

Aiello L. C. (1992). Allometry and the analysis of size and shape in human evolution. *Journal of Human Evolution* **22**: 127-147.

Akam, M. (1989). Hox and HOM: Homologous gene clusters in insects and vertebrates. *Cell* **57**: 347-349.

Anagnostopoulou S., Karamalika D. D., and Spyropoulos M. N. (1988). Observations on the growth and orientation of the anterior cranial base in the human foetus. *European Journal of Orthodontics* **10**: 143-148.

Anton S. C. (1989). Intentional cranial vault deformation and induced changes in the cranial base and face. *American Journal of Physical Anthropology* **79**: 253-267.

Arey L. B. (1965). *Developmental anatomy: a textbook and laboratory manual of embryology* (7th ed). Philadelphia: W.B. Saunders and Co.

Ashton E.H. (1957). Age changes in the basicranial axis of the Anthropoidae. *Proceedings of the Zoological Society of London* **129**: 61-64.

Avis V. (1959). The relation of the temporal muscle to the form of the coronoid process. *American Journal of Physical Anthropology* **17**: 99-104.

Aylward E. H., Augustine A., Li Q., Barta P. E., and Pearlson G. D. (1997). Measurement of frontal lobe volume on magnetic resonance imaging scans. *Psychiatry Research* **75**: 23-30.

Bach-Petersen S. and Kjaer I. (1993). Ossification of lateral components in the human prenatal cranial base. *Journal of Craniofacial Genetics and Developmental Biology* **13**: 76-82.

Baer M. J. and Nanda S. K. (1976). A commentary on the growth and form of the cranial base. In (Bosma J. F. Ed) *Symposium on Development of the Basicranium*, pp. 127-189. Bethesda: U.S. Government D.H.E.W. Publications No. (NIH) 76-989.

Bailey W. J. J. (1986). Genes that affect morphogenesis of the murine mandible. *Journal of Heredity* **77**: 17-25.

Baker L. W. (1941). The influence of the formative dental organs on the growth of bones and the face. *American Journal of Orthodontics* **27**: 489-506.

Baker P. N., Johnson I. R., Gowland P. A., Hykin J., Adams V., Mansfield P., Worthington B. S. (1995). Measurement of fetal liver, brain and placental volumes with echo-planar magnetic resonance imaging. *British Journal of Obstetrics and Gynaecology* **102**: 35-39.

Balling R., Mutter G., Gruss P., and Kessel M. (1989). Craniofacial abnormalities induced by ectopic expression of the homeobox gene Hox-1.1 in transgenic mice. *Cell* **56**: 337-347.

Baron D. (1950). An experimental analysis of some factors involved in the development of the tissue pattern of the cerebral cortex. *Journal of Experimental Zoology* **113**: 553-558.

Bartelmez G. W. and Blount M. P. (1954). The formation of the neural crest from the primary optic vesicle in man. *Contributions to Embryology* **35**: 55-71.

Bartelmez G. W. and Dekaban A. S. (1962). The early development of the human brain. *Contributions to Embryology* **37**: 15-31.

Bast T. H. (1930). Ossification of the otic capsule in human fetuses. *Contributions to Embryology* **21**: 55-82.

Bateson W. (1909). *Mendel's Principles of Heredity*. Cambridge: Cambridge University Press.

Baume L. J. (1957). A biologist looks at the sella point. *Transactions of the European Orthodontics Society* 150-169.

Becker T., Elmer K., Schneider F., Schneider M., Grodd W., Bartels M., Heckers S., and Beckmann H. (1996). Confirmation of reduced temporal limbic structure volume on magnetic resonance imaging in male patients with schizophrenia. *Psychiatry Research* **67**: 135-143.

Behrents R. G. and Johnston L. E. (1984). The influence of the trigeminal nerve on facial growth and development. *American Journal of Orthodontics* **85**: 199-206.

Bergerhoff W. and Martin A. (1954). Messung von Winkeln and Strecken am Röntgenbild des Schädels von Säuglingen und kleinkindern. *Fortschritte auf dem Gebiete der Rontgenstrahlen.* **80**: 741-749.

Berkovitz B. K. B. and Moxham B. J. (1988). *Head and neck anatomy.* London: Wolfe Medical Publications Limited.

Biegert J. (1964). The evaluation of characteristics of the skull, hands, and feet for primate taxonomy. In (Washburn S. L., Ed) *Classification and human evolution* pp 116-145. London: Methuen.

Birch R. H. (1968). Foetal retrognathia and cranial base. *Angle Orthodontist* **38**: 231-235.

Björk A. (1951). The significance of growth changes in facial patterns and their relationship to changes in occlusion. *Dental Record* **71**: 197-208.

Björk A. (1955). Cranial base development. *American Journal of Orthodontics* **41**: 198-225.

Blechschmidt M. (1976). The biokinetics of the basicranium. In (Bosma J. F. Ed) *Symposium on Development of the Basicranium*, pp 44-53. Bethesda: U.S. Government D.H.E.W. Publications No. (NIH) 76-989.

Blechschmidt M. (1977). *The beginnings of human life.* New York: Spinger-Verlag.

Bloch F., Hansen W. W, and Packard M. E. (1946). Nuclear induction. *Physics Review* **69**:127.

Bolk L. (1926). La récapitulation ontogenetique comme phénomène harmonique. *Archives d Anatomie, d Histologie et d Embryologie* **5**: 85-98.

Bonnet C. (1769). La palingénésie philosophique. tr. Philibert C. and Chirol B.

Bookstein F. L. (1991). *Morphometric tools for landmark data.* Cambridge University Press: Cambridge.

Bottomley P. A., Foster T. H., Argersinger R. E., and Pfeifer I. M. (1984). A review of normal tissue hydrogen NMR relaxation times and relaxation mechanisms from 1-100MHz: Dependence on tissue type, NMR frequency, temperature, species, excision and age. *Medical Physics* **11**: 425-448.

Bracewell R. N. (1978). *The Fourier Transform and its Applications* (2nd ed). New York: McGraw-Hill.

Bradley O. C. (1903). On the development and homology of mammalian cerebellar fissure. *Journal of Anatomy and Physiology* **17**: 130-70.

Brash J. C. (1953). *Cunningham's text-book of anatomy* (9th ed). London: Oxford University Press.

Brown J. and Glazier E. V. D. (1974). *Telecommunications* (2nd ed). London: Chapman and Hall.

Bruwer A. (1955). Neurofibromatosis and congenital unilateral pulsating and nonpulsating exophthalmos. *Archives of Ophthalmology* **53**: 2-12.

Bull J. W. D. (1969). Tentorium cerebelli. *Proceedings of the Royal Society of Medicine* **62**: 1301-1310.

Burdi A. R. (1965). Sagittal growth of the nasomaxillary complex during the second trimester of human prenatal development. *Journal of Dental Research* **44**: 112-125.

Burdi A. R. (1969). Cephalometric growth analyses of the human upper face region during the last two trimesters of gestation. *American Journal of Anatomy* **125**: 113-22.

Burdi A. R. (1976). Early development of the human basicranium: its morphogenic controls, growth patterns, and relations. In (Bosma J. F. Ed) *Symposium on*

Development of the Basicranium, pp 81-90. Bethesda: U.S. Government D. H. E. W. Publications No. (NIH) 76-989.

Burston W. R. (1959). The development of cleft lip and palate. *Annals of the Royal College of Surgeons* **25**: 225-253.

Byrum C. E., MacFall J. R., Charles H. C., Chitilla V. R., Boyko O. B., Upchurch L., Smith J. S., Rajagopalan P., Passe T., Kim D., Xanthakos S., Ranga K., and Krishnan R. (1996). Accuracy and reproducibility of brain and tissue volumes using a magnetic resonance segmentation method. *Psychiatry Research* **67**: 215-234.

Callaghan P. T. (1993). *Principles of Nuclear Magnetic Resonance Microscopy.* Oxford: Clarendon Press.

Cameron J. (1924). The cranio-facial axis of Huxley. Part I. Embryological considerations. *Transactions of the Royal Society* **19**: 115-123.

Cameron J. (1930). The human and comparative anatomy of Cameron's craniofacial axis. *Journal of Anatomy* **64**: 324

Campbell S. and Newman G. B. (1971). Growth of the fetal biparietal diameter during normal pregnancy. *The Journal of Obstetrics and Gynaecology of the British Commonwealth* **78**: 513-519.

Cartmill M. (1970). *The orbits of arboreal mammals: a reassessment of the arboreal theory of primate evolution.* Ph.D dissertation, the University of Chicago.

Cartmill M. (1994). A critique of homology as a morphological concept. *American Journal of Physical Anthropology* **94**: 115-123.

Chaung K. S., and Udupa J. K. (1989). Boundary detection in grey level scenes. In *Proceedings of the tenth annual conference and exposition of the national computer graphics association.* NCGA, Fairfax; vol. **I**: 112-117.

Chitty L. S., Altman D. G., Henderson A., and Campbell S. (1994). Charts of fetal size:2. Head measurements. *British Journal of Obstetrics and Gynaecology* **101**: 35-43.

Clark M. C., Hall L. O., Goldgof D. B., Velthuzian R., Murtagh F. R., Silbiger M. S. (1998). Automatic tumor segmentation using knowledge-based techniques. *IEEE Transactions in Medical Imaging* **17**: 187-201.

Clifford R .J., Gerhring D. G., Sharbrough F. W., Felmlee J. P. (1988). Temporal lobe volume measurement from MR images: Accuracy and left-right asymmetry in normal persons. *Journal of Computer Assisted Tomography* **12**: 21-29

Clifford R. J., Bentley M. D., Twomey C. K., and Zinsmeister A. R. (1990). MR imaging-based volume measurements of the hippocampal formation and anterior temporal lobe: validation studies. *Radiology* **176**: 205-209.

Colleti P. M. (1996). Computer-assisted imaging of the fetus with magnetic resonance imaging. *Computers in Medical Imaging and Graphics.* **20**: 491-496.

Conroy G. C., Vannier M. W., Tobias P. V. (1990). Endocranial features of Austropithecus africanus revealed by 2-D and 3-D computed tomography. *Science* **247**: 838-841.

Conroy G. C., Weber G. W., Seidler H., Tobias P. V., Kane A., Brunsden B. (1998). Endocranial capacity in an early hominid cranium from Sterkfontein, South Africa. *Science* **280**: 1730-1731.

Cook M. J., Fish D. R., Shorvon S. D., Straughan K., and Stevens J. M. (1992). Hippocampal volumetric and morphometric studies in frontal and temporal lobe epilepsy. *Brain* **115**: 1001-1015.

Copray J. C. V. M. (1986). Growth of the nasal septal cartilage of the rat in vitro. *Journal of Anatomy* **144**: 99-111.

Correns C. G. (1900). Mendel's Regel über das Verhalten der Nachkommenschaft der Rassenbastarde. *Berichte der deutschen botanischen Gesellschaft* **18**.

Cousin R. P. (1969). *Etude en projection sagittale de cranes d'emfants orientes dans les axes vestibulaires.* PhD Thesis. Faculty of Medicine, Paris.

De Beer G. R. (1937). *The development of the vertebrate skull.* Oxford: Clarendon Press.

De Beer G. R. (1940). *Embryos and ancestors.* Oxford: Clarendon Press.

Dean M. C. (1988). Growth processes in the cranial base of hominoids and their bearing on morphological similarities that exist in the cranial base of Homo and Paranthropus. In (Grine F. E., Ed) *Evolutionary history of the "robust" Australopithecines*, pp 107-112. New York: Aldine de Gruyter.

Dean M. C. and Wood B. A. (1981). Metrical analysis of the basicranium of extant hominoids and *Australopithecus*. *American Journal of Physical Anthropology* **54**: 63-71.

Dean M. C. and Wood B. A. (1984). Phylogeny, neoteny and growth of the cranial base in Hominids. *Folia Primatologica.* **43**: 157-180.

Desmond M. E. and Jacobson A. G. (1977). Embryonic brain enlargement requires cerebrospinal fluid pressure. *Developmental Biology* **57**: 188-198.

Diewert V. M. (1983). A morphometric analysis of craniofacial growth and changes in spatial relations during secondary palatal development in human embryos and fetuses. *American Journal of Anatomy* **167**: 495-522.

Diewert V. M. (1985). Development of human craniofacial morphology during the late embryonic and early fetal periods. *American Journal of Orthodontics* **88**: 64-76.

Dimitriadis A. S., Haritanti-Kouridou A., Antoniadis K., and Ekononmou L. (1995). The human skull base angle during the second trimester of gestation. *Neuroradiology* **37**: 68-71.

Dobbing J. and Sands J. (1973). Quantitative growth and development of human brain. *Archives of Diseases in Childhood* **48**: 757-767.

Doherty C. P., Meredith G. E., Farrell M., Toland J., and Stauton H. (1999). Radiological determination of posterior limits of the temporal lobe for volumetric analysis. *Brain Research: Brain Research Protocols* **4**: 1-10.

Dorenbos J. (1972). In vivo cerebral implantation of the anterior and posterior halves of the spheno-occipital synchondrosis in rats. *Archives of Oral Biology* **17**: 1067-1072.

Dorovini-Zis K. and Dolman C. L. (1977). Gestational development of brain. *Archives of Pathology and Laboratory Medicine* **101**: 192-195.

Du Brul E. L. and Laskin D. M. (1961). Preadaptive potentialities of the mammalian skull: an experiment in growth and form. *American Journal of Anatomy* **109**: 117-132.

Du Brul E. L. (1977). Early hominid feeding mechanisms. *American Journal of Physical Anthropology* **47**: 305-320.

Duckworth W. L. H. (1915). *Morphology and anthropology* (2nd ed). Cambridge: Cambridge University Press.

Duterloo H. S. and Enlow D. H. (1970). A comparative study of cranial growth in *Homo* and *Macaca*. *American Journal of Anatomy* **127**: 357-368.

Eccles J. C. (1989). *Evolution of the brain, creation of self.* London: Routledge.

Ede D. A. (1983). Cellular condensations and chondrogenesis. In (Hall B. K., Ed) *Cartilage Vol.2*, pp 143-185. New York: Academic Press.

Edelstein, W. A., Hutchinson, J. M. S., Johnson, G. and Redpath, T. (1980). Spin warp NMR imaging and applications to human whole-body imaging. *Physics in Medicine and Biology* **25**: 751-756.

Effmann E. L., Johnson G. A. (1988). Magnetic resonance microscopy of chick embryos in ovo. *Teratology* **38**: 59-65.

Enlow D.H. and Bang S. (1965). Growth and remodelling of the human maxilla. *American Journal of Orthodontics* **51**: 446-450.

Enlow D. H. (1968). *The human face.* New York: Harper and Row.

Enlow D. H., and Hunter W. S. (1968). The growth of the face in relation to the cranial base. *Report of the Congress of the European Orthodontic Society* **44**: 321-335.

Enlow D. H. and Moyers R. E. (1971). Growth and architecture of the face. *Journal of the American Dental Association* **82**: 763-774.

Enlow D. H. and McNamara J. A. (1973). The neurocranial basis for facial form and pattern. *Angle Orthodontist* **43**: 256-270.

Enlow D. H. (1975). *Facial Growth.* London: W. B. Saunders Company.

Enlow D. H. (1976). The prenatal and postnatal growth of the human basicranium. In (Bosma J. F. Ed) *Symposium on Development of the Basicranium*, pp 192-205. Bethesda: U.S. Government D.H.E.W. Publications No. (NIH) 76-989.

Enlow D. H. and Hans M. G. (1996). *Essentials of facial growth.* London: W. B. Saunders Company.

Erdoglija L. J. (1989). Dynamics of the cranial base angle changes during the second trimester of the normal intrauterine growth and development. *Bilten Udruzenja Ortodonata Jugoslavije* **22**: 7-14.

Erdoglija L. J. (1990). Dynamics of changes of anteroposterior jaw positions relative to the cranial base during the second trimester of normal intrauterine growth. *Bilten Udruzenja Ortodonata Jugoslavije* **23**: 59-68.

Eriksen E., Bach-Petersen S., van den Eynde B., Solow B. and Kjaer I. (1995). Midsagittal dimensions of the prenatal human cranium. *Journal of Craniofacial Genetics and Developmental Biology* **15**: 44-50.

Feess-Higgins A. and Larroche J. (1987). *Development of the human foetal brain.* Paris: INSERM CNRS, MASSON.

Fenart R. (1953). Ontogenese cranio-faciale chex l'Homme. *Revue Scientifique* **91**: 101-115.

Fields H. W., Metzner L., Garol J. D., and Kokich V. C. (1978). The craniofacial skeleton in anencephalic human fetuses, I. cranial floor. *Teratology* **17**: 57-66.

Filipek P. A., Kennedy D. N., Caviness V. S., Rossnick S. L., Spraggins T. A. Starewicz P. M. (1989). Magnetic resonance imaging based brain morphometry: development and application to normal subjects. *Annals of Neurology* **25**: 61-67.

Flügel C. Schram K. and Rohen J. W. (1993). Postnatal development of the skull base, neuro- and viscerocranium in man and monkey: morphometric evaluation of CT scans and radiograms. *Acta Anatomica* **146**: 71-80.

Ford E. H. R. (1956). The growth of the foetal skull. *Journal of Anatomy* **90**: 63-72.

Ford E. H. R. (1958). Growth of the human cranial base. *American Journal of Orthodontics* **44**: 498-506.

Foster M. A. and Hutchinson J. M. S. (1987). *Practical NMR imaging*. Oxford: IRL press.

Foster M. A., Knight C. H., Rimmington J. E., Mallard J. R. (1983). Fetal imaging by nuclear magnetic resonance: a study in goats. *Radiology* **149**: 193-195.

Friede H. (1981). Normal development and growth of the human neurocranium and cranial base. *Scandinavian Journal of Plastic and Reconstructive Surgery* **15**: 163-169.

Froham M. A., Boyle M. and Martin G. R. (1990). Isolation of the mouse Hox 2.9 gene: Analysis of embryonic expression suggests that positional information along the anterior-posterior axis is specified by mesoderm. *Development* **110**: 589-607.

Garden A. S. and Roberts N. (1996). Fetal and fetal organ estimations with magnetic resonance imaging. *American Journal of Obstetrics and Gynecology* **175**: 442-448.

Gasser R. F. (1976). Early formation of the basicranium in man. In (Bosma J. F. Ed) *Symposium on Development of the Basicranium*, pp 29-43. Bethesda: U. S. Government D. H. E. W. Publications No. (NIH) 76-989.

George S. L. (1978). A longitudinal and cross-sectional analysis of the growth of the postnatal cranial base angle. *American Journal of Physical Anthropology* **49**: 171-178.

George W. C. (1942). A presomite human embryo with chorda canal and prechordal plate. *Contributions to Human Embryology* **30**: 1-7.

Giles W. B., Philips C. L. and Joondeph D. R. (1981). Growth in the basicranial synchondroses of adolescent *Macaca macaca*. *Anatomical Record* **199**: 259-266.

Gilmore R. L., Childress M.D., Leonard C., Quisling R., Roper S., Eisenschenk S., Mahoney M. (1995). Hippocampal volumetrics differentiate patients with temporal lobe epilepsy and extratemporal lobe epilepsy. *Archives of Neurology* **52**: 819-824.

Girard N., Raybaud C., Dercole C., Boubli L., Chau C., Cahen S., Potier A., and Gamerre M. (1993). In vivo MRI of the fetal brain. *Neuroradiology* **35**: 431-436.

Gluecksohn-Waelsch, S., Hagedora, S. D., and Sisken, B. F. (1956). Genetics and morphology of a recessive mutation in the house mouse affecting head and limb skeleton. *Journal of Morphology* **99**: 465-479.

Godfrey L. R. and Sutherland M. R. (1995). What's growth got to do with it? Process and product in the evolution of ontogeny. *Journal of Human Evolution* **29**: 405-431.

Gong Q. Y., Roberts N., Garden A. S., and Whitehouse G. H. (1998). Fetal and fetal brain volumes in the third trimester of human pregnancy using gradient echo MR imaging. *Magnetic Resonance Imaging* **16**: 235-240.

Gopinathan K. (1992). A rare anomaly of 5 ossicles in the preinterparietal part of the squamous occipital bone in the north Indians. *Journal of Anatomy* **180**: 210-202.

Gould S. J. (1977). *Ontogeny and phylogeny*. London: Harvard University Press.

Green M. C. (1951). Further morphological effects of the short ear gene in the house mouse. *Journal of Morphology* **88**: 1-21.

Grüneberg H. (1963). *The pathology of development.* Oxford: Blackwell.

Grüneberg H. (1975). How do genes affect the skeleton?. In (Neuberg, D. and Meker, H. J., Eds) *New Approaches to the Evaluation of Abnormal Embryonic Development*, pp 354-359. Stuttgart: Georg Thieme.

Guihard-Costa A. and Larroche J. (1990). Differential growth between the fetal brain and its infratentorial part. *Early Human Development* **23**: 27-40.

Guihard-Costa A. M. and Larroche J. C. (1992). Growth velocity of some fetal parameters. *Biology of the Neonate* **62**: 309-316.

Haeckel E. (1879). *The evolution of man.* (McCabe J., trans). London: Watts, 1907.

Hahn E. (1950). Spin echoes. *Physical Review* **80**: 580-594.

Hall B. K. (1970). Cellular differentiation in skeletal tissues. *Biological Reviews* **45**: 455-484.

Hall B. K. (1983). Epigenetic control of development and evolution. In (Goodwin B. C., Ed) *Development and Evolution*, pp 353-379. Cambridge: Cambridge University Press.

Hall B. K. (1984). Developmental processes underlying the evolution of cartilage and bone. *Symposium of the Zoological Society of London* **52**: 155-176.

Hansen P. E., Ballsteros M. C., Soila K., Garcia L., and Howard J. M. (1993). MR imaging of the developing human brain. *Radiographics* **13**: 21-36.

Hartwig-Scherer S. and Martin R. D. (1992). Allometry and prediction in hominoids: A solution to the problem of intervening variables. *American Journal of Physical Anthropology* **88**: 37-57.

Harvey P. and Pagel M. (1991). *The Comparative Method in Evolutionary Biology.* Oxford: Oxford University Press.

Hata T., Makihara K., Aoki S., Hata K., and Kitao M. (1990). Magnetic resonance imaging of the fetus: initial experience. *Gynecological and Obstetrical Investigations* **29**: 255-258.

Heath M. E. (1984). The effects of rearing-temperature on body conformation and organ size in young pigs. *Comparative Biochemistry and Physiology* **77**: 63-72.

Heinon T., Dastidar P., Eskola H., Frey H., Ryymin P., Laasonen E. (1998). Applicability of semi-automated segmentation for volumetric analysis of brain lesions. *Journal of Medical Engineering and Technology* **22**: 173-178.

Hendrick R. E. and Osborn A. G. (1988). Introduction to MR imaging: Part II. Pulse sequences and image contrast. In (Stark D. D. and Bradley W. G., Eds) *Diagnostic categorical course in MR imaging*. Oak Brook: Radiological Society of North America.

Henkelman, R. M. and Bronskill, M. J. (1987). Artifacts in magnetic resonance imaging. *Reviews Magnetic Resonance in Medicine* **2**: 5-126.

Herring S. W. (1993). Epigenetic and functional influences on skull growth. In (Hanken J. and Hall B. K., Eds) *The skull: development*, pp 153-207. Chicago: Chicago University Press.

Hill R. E., Favor J., Hogan B. L. M., Tom C. C. T., Saunders G. F., Manson I. M., Posser J., Jordan T., Hastie N.D., and van Heynngen V. (1991). Mouse small eye results from mutations in paired-like homeobox-containing gene. *Nature* **354**: 522-525.

Hochstetter F. (1939). Über die Entwicklung und Differenzierung de Hüllen des Menschlichen Hehirns. *Morphologisches Jahrbuch* (Morphological year book) **83**: 359-494.

Hofman M. A. (1988). Allometric scaling in palaeontology: A critical review. *Human Evolution* **3**:177-188.

Hohl T. H. (1983). Masticatory muscle transposition in primates: effects on craniofacial growth. *Journal of Maxillo-Facial Surgery* **11**: 149-156.

Holloway R. L. (1988). "Robust" australopithecine brain endocasts: some preliminary observations. In (Grine F.E., Ed.) *Evolutionary History of the "Robust" Australopithecines,* pp. 97-106. New York: Aldine de Gruyter.

Holtzer H. (1964). Control of chondrogenesis in the embryo. *Biophysical Journal* **4**: 239-256.

Hoult D. I. and Richards R. E. (1976). The signal to noise ratio of the NMR experiment. *Journal of Magnetic Resonance* **24**: 71-85.

Houpt M. I. (1970). Growth of the craniofacial complex of the human fetus. *American Journal of Orthodontics* **58**: 373-383.

Hoyte D. A. (1971). Mechanisms of growth in the cranial vault and base. *Journal of Dental Research* **50**:1447-1461.

Hoyte D. A. (1975). A critical analysis of the growth in length of the cranial base. In (Bergsma D., Ed) *Morphogenesis and Malformations of the Face and Brain,* pp 255-282. **XI** (7).

Hoyte D. A. (1991). The cranial base in normal and abnormal growth. *Neurosurgery Clinics of North America* **2**: 515-537.

Hunt P., Gulisano M., Cook M., Sham M. H., Faiella A., Wilkinson D., Boncinelli E., and Krumlauf R. (1991). A distinct Hox code for the branchial region of the vertebrate head. *Nature* **353**: 861-864.

Huxley J. S. (1932). *Problems of Relative Growth.* London: Dial Press.

Huxley T. H. (1863). *Evidence as to man's place in nature*. London: Williams and Norgate.

Huxley T. H. (1867). On two widely contrasted forms of the human cranium. *Journal of Anatomy and Physiology* **1**: 60-77.

Inoue N. (1961). A study on the developmental changes of dentofacial complex during fetal period by means of roentgenographic cephalometrics. *Bulletin of Tokyo Medical and Dental University* **8**: 205-227.

Isobe, S., Hazlewood, C. F., Misra, L. K. and Klemm, W. R. (1994). Acute ethanol decreases NMR relaxation times of water hydrogen protons in fish brain. *Alcohol* **11**: 571-576.

Jack C. R. , Gehring D. G., Sharbrough F. W. (1988a). Temporal lobe volume measurement from MR images: accuracy and left-right asymmetry in normal persons. *Journal of Computer Assisted Tomography*. **12**: 21-29.

Jack C. R., Sharbrough F. W., Marsh W.R. (1988b). Use of MR imaging for quantitative evaluation of section for temporal lobe epilepsy. *Radiology*. **169**: 463-468.

Jack C. R., Twomey C. K., Zinsmeister A. R. (1989). Anterior temporal lobes and hippocampal formations: normative volumetric measurements from MR images in young adults. *Radiology* **172**: 549-554.

Jeffery N. and Spoor. F. (1999). Human fetal cranial base flexion and brain volumes: a high resolution Magnetic Resonance Imaging (hrMRI) study. *American Journal of Physical Anthropology* suppl. **27**: 161.

Jenkins G. B. (1921). Relative weight and volume of the component parts of the brain of the human embryo at different stages of development. *Contributions to Embryology* **29**: 41-60.

Johnson G. A., Benveniste H., Black R. D., Hedlund L. W., Maronpot R. R., Smith B. R. (1993). Histology by magnetic resonance microscopy. *Magnetic Resonance Quarterly* **9**: 1-30

Johnson K. E. (1988). *Human Developmental Anatomy.* New York: John Wiley & Sons.

Johnson, D. R. (1986). *The genetics of the Skeleton.* Oxford: Clarendon Press.

Johnston L. E. (1974). A cephalometric investigation of the sagittal growth of the second trimester fetal face. *Anatomical Record* **178**: 623-630.

Johnston L. E. (1976). The functional matrix hypothesis: reflections in a jaundiced eye. In (McNamara J.A., Ed) *Factors Affecting the Growth of the Midface,* pp 131-168. Ann Arbor: University of Michigan press.

Jones F. W. (1917). *Aboreal man.* Reprint 1964. New York: Hafner.

Joshi M., Cui J., Doolittle K., Joshi S., Van Essen D., Wang L., and Miller M. I. (1999). Brain segmentation and the generation of cortical surfaces. *Neuroimage* **9**: 461-467.

Julin P., Melin T., Andersen C., Isberg B., Svensson L., and Wahlund L. O. (1997). Reliability of interactive three-dimensional brain volumetry using MP-RAGE magnetic resonance imaging. *Psychiatry Research* **76**: 41-49.

Keith A. (1910). Description of a new craniometer and of certain age changes in the anthropoid skull. *Journal of Anatomy* **44**: 251-270.

Keith A. and Campion G. G. (1922). A contribution to the mechanism of growth of the human face. *International Journal of Orthodontics* **8**: 607-633.

Keith A. (1948). *Human Embryology and Morphology* (6th ed). London: William Clowes and Son.

Kennedy D. N. and Nelson A. C. (1987). Three-dimensional display from cross-sectional tomographic images: an application to magnetic resonance imaging. *IEEE Transactions in Medical Imaging* **1-6**: 134-140.

Kennedy D. N., Filipek P.A., and Caviness V. S. (1989). Anatomic segmentation and volumetric calculations in nuclear magnetic resonance imaging. *IEEE Transactions in Medical Imaging* **8**: 1-7.

Kessel M. and Gruss P. (1990). Murine developmental control genes. *Science* **249**: 374-379.

Kier E. L. (1976). Phylogenetic and ontogenetic changes of the brain relevant to the evolution of the skull. In (Bosma J. F., Ed) *Symposium on Development of the Basicranium*, pp 141-155. Bethesda: U.S. Government D. H. E. W. Publications No. (NIH) 76-989.

Kim S. G., Ugurbil K., and Stick P. L. (1994). Activation of a cerebellar output nucleus during cognitive processing. *Science* **265**: 949-951.

King M. C., and Wilson A. C. (1975). Evolution at two levels in humans and chimpanzees. *Science* **188**: 107-116.

Kingsbury B. K. (1924). The significance of the so-called law of cephalocaudal differential growth. *Anatomical Record* **27**: 305-321.

Kjaer I. (1990a).Ossification of the human fetal basicranium. *Journal of Craniofacial Genetics and Developmental Biology* **10**: 29-38.

Kjaer I. (1990b). Radiographic determination of prenatal basicranial ossification. *Journal of Craniofacial Genetics and Developmental Biology* **10**: 113-123.

Kjaer I. (1990c). Prenatal human cranial development evaluated on coronal plane radiographs. *Journal of Craniofacial Genetics and Developmental Biology* **10**: 339-351.

Kjaer I. and Fischer-Hansen B. (1995). The adenohypophysis and the cranial base in early human development. *Journal of Craniofacial Genetics and Developmental Biology* **15**: 157-161.

Kjaer I. (1998). Neuro-osteology. *Critical Reviews in Oral Biology and Medicine* **9**: 224-244.

Klintworth G. K. (1967). The ontogeny and growth of the human tentorium cerebelli. *Anatomical Record* **158**: 433-442.

Klintworth G. K. (1968). The comparative anatomy and phylogeny of the tentorium cerebelli. *Anatomical Record* **160**: 635-642.

Knowles C. C. (1963). The influence of cranial base structure on the orientation of the middle third of the face. *Dental Practice* **13**: 531-542.

Kodama G. (1973). Developmental studies on the squama occipitalis in the human skull: with special reference to the development of the os incae. *Hokkaido Journal of Medical Science* **48**: 351-363. (English Abstract of a Japanese article).

Kodama G. (1976a). Developmental studies on the presphenoid of the human sphenoid bone. In (Bosma J. F., Ed) *Symposium on Development of the Basicranium*, pp 141-155. Bethesda: U.S. Government D. H. E. W. Publications No. (NIH) 76-989.

Kodama G. (1976b). Developmental studies on the orbitosphenoid of the human sphenoid bone. In (Bosma J. F., Ed) *Symposium on Development of the Basicranium*, pp 166-176. Bethesda: U.S. Government D. H. E. W. Publications No. (NIH) 76-989.

Kodama G. (1976c). Developmental studies on the body of the human sphenoid bone. In (Bosma J. F., Ed) *Symposium on Development of the Basicranium*,

pp 156-165. Bethesda: U.S. Government D. H. E. W. Publications No. (NIH) 76-989.

Koop M., Rilling G., Herrmann A., and Kretschmann H. J. (1986). Volumetric development of the fetal telencephalon, cerebral cortex, diencephalon, and rhombencephalon including the cerebellum in man. *Bibliotheca Anatomica* **28**: 53-78.

Kretschmann H. J., Tafesse U., and Herrmann A. (1982). Different volume changes of cerebral cortex and white matter during histological preparation. *Microscopica Acta* **86**: 13-24.

Kurihara S., Enlow D. H., and Rangel R. D. (1980). Remodelling reversals in anterior parts of the human mandible and maxilla. *Angle Orthodontics* **50**: 98-100.

Kvinnsland S. (1967). A preliminary report on the angular changes of the cranial base in human foetuses. *Det Kgl. Norske Videnskabers selskaps forhandl* **40**: 55.

Kvinnsland S. (1971). The sagittal growth of the foetal cranial base. *Acta Odontologica Scandinavica* **29**: 699-715.

Laitman J. T. and Heimbuch R. C. (1982). The basicranium of Plio-Pleistocene hominids as an indicator of their upper respiratory systems. *American Journal of Physical Anthropology* **59**: 323-343.

Lang J. (1983). *Clinical anatomy of the head.* Berlin: Spinger-Verlag.

Larsell O. (1947). The development of the cerebellum in man in relation to its comparative anatomy. *Journal of Comparative Neurology* **87**: 85-129.

Larsell O. and Jansen J. (1972). *The comparative anatomy and histology of the cerebellum.* Minneapolis: Lund Press.

Larsen W. J. (1997). *Human Embryology* (2nd ed). New York: Churchill Livingstone.

Latham R. A. (1972). The sella point and postnatal growth of the human cranial base. *American Journal of Orthodontics*. **61**: 156-162.

Latham R. A. (1976). Malformations of the cranial base in human fetuses. In (Bosma J. F., Ed) *Symposium on Development of the Basicranium*, pp 203-221. Bethesda: U.S. Government D. H. E. W. Publications No. (NIH) 76-989.

Lauterbur P. C. (1973). Image formation by induced local interactions: examples employing nuclear magnetic resonance. *Nature* **242**: 190-191.

Lavelle C. (1987). An analysis of basicranial axis form. *Anatomischer Anzeiger* **164**: 169-180.

Lee H., Tarazi F. I., Chakos M., Wu H., Redmond M., Alvir J. M., Kinon B. J., Bilder R., Creese I., and Lieberman J. A. (1999). Effects of chronic treatment with typical and atypical antipyschotic drugs on rat striatum. *Life Sciences* **64**: 1595-1602.

Lee S., Kim Y., Jo Y, Seo J., and Chi J. E. (1996). Prenatal development of cranial base in normal Korean fetuses. *The Anatomical Record* **246**: 524-534.

Lemire R. J. (1986). *Embryology of the skull.* In (Cohen M. M., Ed) *Craniosynostosis: Diagnosis, evaluation and management.* New York: Raven Press.

Leutenegger W. (1987). Neonatal brain size and neurocranial dimensions in Pliocene hominids: implications for obstetrics. *Journal of Human Evolution* **16**: 291-296.

Levihn W. C. (1967). A cephalometric roentgenographic cross-sectional study of the craniofacial complex in fetuses from 12 weeks to birth. *American Journal of Orthodontics* **53**: 822-849.

Lewis R. (1990). *Practical Digital Image Processing.* London: Ellis Horwood.

Lieberman D. (1998). Sphenoid shortening and the evolution of modern human cranial shape. *Nature* **393**: 158-162.

Lieberman D. and McCarthy R. (1999). The ontogeny of cranial base angulation in humans and chimpanzees and its implications for reconstructing pharyngeal dimensions. *Journal of Human Evolution* **36**: 487-517.

Lieberman P., Laitman J. T., Reidenberg J. S., and Gannon P. J. (1992). The anatomy, physiology, acoustics and perception of speech: essential elements in the analysis of the evolution of human speech. *Journal of Human Evolution* **23**: 447-467.

Low A. (1991). *Introductory Computer Vision and Image Processing.* London: McGraw-Hill Book Company.

Luboga S. A. (1986). *Morphometric variation in the cranial base and facial skeleton of higher primates with special reference to modern humans.* PhD Thesis; Makerere University.

Lynch J. M., Wood C. G., and Luboga S. A. (1996). Geometric morphometrics in primatology: Craniofacial variation in *Homo sapiens* and *Pan troglodytes*. *Folia Primatologica* **67**: 15-39.

Mansfield P. and Pykett I. L. (1978). Biological and medical imaging by NMR. *Journal of Magnetic Resonance* **29**: 355-373.

Mansfield P., Maudsley A. A., and Baines T. (1976). Fast scan proton imaging by NMR. *Journal Physics and Scientific Instruments* **9**: 271-278.

Manson J. D. (1968). *A comparative study of the postnatal growth of the mandible.* London: Henry Kempton.

Marcus L. F., Corti M., Loy A., Naylor G. J. P., and Slice D. (eds). (1996). *Advances in Morphometrics.* New York: Plenum Press.

Marin-Padilla M. (1965). Study of the skull in human cranioschisis. *Acta Anatomica* **62**: 1-20.

Martin R. D. (1980). Adaption and body size in primates. *Zeitschrift fur Morphologie und Anthropologie* **71**: 115-124.

Matano S., and Hirasaki E. (1997). Volumetric comparisons in the cerebellar complex of anthropoids, with special reference to locomotor types. *American Journal of Physical Anthropology* **103**: 73-183.

McCarthy R. C. (submitted). Anthropoid cranial base architecture and scaling relationships. *Journal of Human Evolution.*

McCollum M. A. (1999). The robust Australopithecine face: A morphogenetic perspective. *Science* **248**: 301-305.

Meckel, J. F. (1811). Entwurf einer Darstellung der zwischen dem Embryozustande de höheren Tiere und dem permanenten der niederen stattfindenden Parallele. *Beträge zur vergleichenden Anatomie*, vol. **2** Leipzip: Reclam.

Melsen B. (1969). Time of closure of the cranial base in *Macaca rhesus* analyzed by the implant method. *Tandlaegebladet* **75**: 1320-1329.

Melsen B. (1971). The postnatal growth of the cranial base in *Macaca rhesus* analyzed by the implant method. *Tandlaegebladet* **75**: 1320-1329.

Mendel G. (1866). Versuche über Pflanzen-Hybriden. *Vehandlungen des naturforschenden Vereines, Abhandlungen, Brünn* **4**: 3-47.

Mestre J. C. (1959). A cephalometric appraisal of cranial and facial relationships at various stages of human fetal development. *American Journal of Orthodontics* **45**: 473.

Michejda M. (1971). Ontogenetic changes of the cranial base in *Macaca mulatta. Third International Conference on Primatology,* Zurich 1970; **1**: 215-225.

Michejda M. (1972). The role of the basicranial synchondroses in flexure processes and ontogenetic development of the skull base. *American Journal of Physical Anthropology* **37**: 143-150.

Michejda M. and Lamey D. (1971). Flexion and metric age changes of the cranial base in the *Macaca mulatta*: Infants and juveniles. *Folia Primatologica* **34**: 133-141.

Michiels J., Bosmans H., Pelgrims P., Vandermeulen D., Gybels J, Marchal G., Suetens P. (1994). On the problem of geometric distortion in magnetic resonance images for stereotactic neurosurgery. *Magnetic Resonance Imaging* **12**: 103-113.

Moloy H. S. (1942). Studies on head molding during labor. *American Journal of Obstetrics and Gynecology* **44**: 762-782.

Monteiro V. J. and Dias M. P. (1997). Morphogenic mechanisms in the development of ethmoidal sinuses. *Anatomical Record* **249**: 96-102.

Moore K. L. (1982). *The developing human.* Eastbourne: W. B. Saunders and Co.

Moore K. L and Persaud T. V. N. (1998). *The developing human.* London: W. B. Saunders and Co.

Moore R. N. (1978). A cephalometric and histologic study of the cranial base in foetal monkeys, *Macaca nemestrina. Archives of Oral Biology* **23**: 57-67.

Moore W. J. (1965). Masticatory function and skull growth. *Journal of Zoology* **146**: 123-131.

Moss M. L. (1958). The pathogenesis of artificial cranial deformation. *American Journal of Physical Anthropology* **16**: 269-286.

Moss M. L., Noback C. R., Robertson G. G. (1956). Growth of certain human fetal cranial bones. *American Journal of Anatomy* **98**: 191-204.

Moss M. L. and Young R. W. (1960). A functional approach to craniology. *American Journal of Physical Anthropology* **18**: 281-292.

Moss-Salentijn L. (1969). The capsular matrix. *American Journal of Orthodontics* **56**: 474-490.

Moyers R. E. and Bookstein F. L. (1979). The inappropriateness of conventional cephalometrics. *American Journal of Orthodontics* **75**: 599-617.

Müller F. and O'Rahilly R. (1980). The human chondrocranium at the end of the embryonic period, proper, with particular reference to the nervous system. *American Journal of Anatomy* **159**: 33-58.

Napier J. R. and Napier P. H. (1967). *A handbook of living primates*. London: Academic Press.

Nemzek W. R., Brodie H. A., Chong B. W., Babcook C. J., Hecht S.T., Salamat S., Ellis W. G., and Seibert J. A. (1996). Imaging findings of the developing temporal bone in fetal specimens. *American Journal of Neuroradiology* **17**: 1467-1477.

Nieuwenhuys R. and Bodenheimer T. S. (1966). The diencephalon of the primitive bony fish Polypterus in the light of the problem of homology. *Journal of Morphology* **188**: 415-450.

Noback C. R. (1944). The developmental anatomy of the human osseous skeleton during the embryonic, fetal and circumnatal periods. *Anatomical Record* **88**: 91-117.

Noback C. R. and Robertson G. (1951). Sequences of appearance of ossification centres in the human skeleton during the first five prenatal months. *American Journal of Anatomy* **89**:1-28.

Noback C. R. and Moss M. L. (1956). Differential growth of the human brain. *Journal of Comparative Neurology* **105**: 539-555.

Noden D. (1986). Origins and patterning of craniofacial mesenchymal tissues. *Journal of Craniofacial genetics and Developmental Biology* **2**:15-31.

Nur N. and Hasson O. (1984). Phenotypic plasticity and the handicap principle. *Journal of Theoretical Biology* **110**: 275-297.

O'Higgins P. and Dryden I. L. (1992). Studies of craniofacial development and evolution. *Perspectives in Human Biology* 2, *Archaeology in Oceania* **27**: 105-112.

O'Higgins P. and Jones N. (1998). Facial growth in *Cercocebus torquatus*: an application of three-dimensional geometric morphometric techniques to the study of morphological variation. *Journal of Anatomy* **193**: 251-272.

O'Rahilly R. (1963). The early embryology of the otic vesicle in staged human embryos. *Journal of Embryology and Experimental Morphology* **11**: 741-755.

O'Rahilly R. (1966). The early development of the eye in staged human embryos. *Contributions to Embryology* **38**: 5-42.

O'Rahilly R. and Gardner E. (1971). The timing and sequence of events in the development of the human nervous system during the embryonic period proper. *Zeitschrift fur Anatomie und EntwicklungsGeschichte* **134**: 1-12.

O'Rahilly R. (1975). The prenatal development of the human eye. *Experiments in Eye Research* **21**: 93-112.

O'Rahilly R., Müller F., Hutchins G. M., and Moore G. (1984). Computer ranking of the sequence of appearance of 100 features of the brain and related structures in staged human embryos during the first 5 weeks of development. *American Journal of Anatomy* **171**: 243-257.

O'Rahilly R. and Müller F. (1986). The meninges in human development. *Journal of Neuropathology and Experimental Neurology* **45**: 588-608.

O'Rahilly R. and Müller F. (1994). *The embryonic human brain.* New York: Wiley-Liss Inc.

Ortiz M. H. and Brodie A. G. (1949). On growth of the human head from birth to the third month of life. *Anatomical Record* **103**: 311-333.

Ostergaard M. (1997). Different approaches to synovial membrane volume determination by magnetic resonance imaging: manual versus automated segmentation. *British Journal of Rheumatology* **36**: 1166-1177.

Padgett D. H. (1957). The development of the cranial venous system in man, from the viewpoint of comparative anatomy. *Contributions to Embryology* **247**: 81-140.

Pagel M. D. and Harvey P. H. (1988). The taxon-level problem in the evolution of mammalian brain size: facts and artifacts. *American Nature* **132**: 344-359.

Pellerin C. (1983). *Le crane humain en orientation vestibulaire. Etude de neuf populations recentes.* Thèse Université René Descartes Paris V, Paris.

Powell M. C., Worthington B. S., Buckley J. M., and Symonds E. M. (1988). Magnetic resonance imaging (MRI) in obstetrics. II. Fetal anatomy. *British Journal of Obstetrics and Gynaecology* **95**: 38-46.

Pratt L. W. (1948). Experimental masseterectomy in the laboratory rat. *Journal of Mammology* **24**: 204-211.

Pratt W. K. (1978). *Digital Image Processing*. New York: John Wiley & Sons.

Prott F. J., Haverkamp U., Willich N., Resch A., Stöber U., and Pötter R. (1995). Comparison of imaging accuracy at different MRI units based on phantom measurements. *Radiotherapy and Oncology* **37**: 221-224.

Putz V. R. (1974). Schädelform und pyramiden. *Anatomischer Anzeiger* **135**: 252-266.

Rakic P. and Sidman R. L. (1970). Histogenesis of cortical layers in human cerebellum, particularly the lamina dissecans. *Journal of Comparative Neurology* **139**: 473-500.

Ravosa M. J. (1988). Browbridge development in Cercopithecidae: A test of two models. *American Journal of Physical Anthropology* **76**: 535-555.

Ravosa M .J. (1991). Interspecific perspective on mechanical and nonmechanical models of primate circumorbital morphology. *American Journal of Physical Anthropology* **86**: 369-396.

Rayner J. M. V. (1985). Linear relations in biomechanics: the statistics of scaling functions. *Journal of the Zoology* **206**: 415-439.

Reidel R. (1952). The relation of maxillary structures to the cranium in malocclusion and in normal occlusion. *Angle Orthodontics* **22**: 142-145.

Riesenfeld A. (1967). Biodynamics of head form and craniofacial relationships. *Homo* **18**: 233-251.

Rilling J. K. and Insel T .R. (1998). Evolution of the cerebellum in primates: Differences in relative volume among monkeys, apes and humans. *Brain, Behavior and Evolution* **6**: 623-641.

Rilling J.K. and Insel T.R. (1999) Evolution of the neocortical size and gyrification in hominids: evidence from comparative neuroanatomy. *American Journal of Physical Anthropology* suppl. **28**: 233.

Robert B., Sassoon D., Jacq B., Gerhring W., and Buckingham M. (1989). Hox-7: A mouse homeobox gene with a novel pattern of expression during embryogenesis. *EMBO Journal* **8**: 91-100.

Rönning O. and Kylämarkula K. (1982). Morphogenic potential of rat growth cartilages as isogeneic transplants in the interparietal suture area. *Archives of Oral Biology* **27**: 581-588.

Ross C. and Henneberg M. (1995). Basicranial flexion, relative brain size, and facial kyphosis in homo sapiens and some fossil hominids. *American Journal of Physical Anthropology* **98**: 575-593.

Ross C. F. and Ravosa M. J. (1993). Basicranial flexion, relative brain size and facial kyphosis in non-human primates. *American Journal of Physical Anthropology* **91**: 305-324.

Roth V. L. (1984). On homology. *Biological Journal of the Linnean Society of London* **22**: 13-29.

Ruiz i Altaba A. and Melton M. (1989). Involvement of the *Xenopus* homeobox gene Xhox 3 in pattern formation along the anterior-posterior axis. *Cell* **57**: 317-326.

Rusinek H., and Chandra R. (1993). Brain tissue volume measurements from magnetic resonance imaging. *Investigative Radiology* **28**: 890-895.

Sadler T. W. (1995). *Langman's Medical Embryology* (7th ed). London: Willaims and Wilkins.

Sarnat B. G. (1973). Craniofacial biology: animal surgical experimentation and clinical practice. *American Journal of Physical Anthropology* **38**: 315-323.

Sasaki H. and Kodama G. (1976). Developmental studies on the postsphenoid of the human sphenoid bone. In (Bosma J. F., Ed) *Symposium on Development of the Basicranium*, pp 177-190. Bethesda: U.S. Government D. H. E. W. Publications No. (NIH) 76-989.

Scammon R. E. and Calkins L. A. (1929). *The development and growth of the external dimensions of the human body in the fetal period.* Minneapolis: University of Minesota Press.

Schad L.R., Boesecke R., Schlegel W., Hartmann G. H., Sturm V., Strauss W. G., Lorenz W. J. (1987). Three dimensional image correlation of CT, MR, and PET studies in radiotherapy treatment planning of brain tumors. *Journal of Computer Assisted Tomography* **11**: 948-954.

Schultz A. H. (1940). The size of the orbit and eye in primates. *American Journal of Physical Anthropology* **26**: 389-408.

Schultz A. H. (1955). The position of the occipital condyles and of the face relative to the skull base in primates. *American Journal of Physical Anthropology* **13**: 97-120.

Scott J. H. (1953). The cartilage of the nasal septum. *British Dental Journal* **95**: 37-49.

Scott J. H. (1954). The growth of the human face. *Proceedings of the Royal Society of Medicine* **47**: 91-100.

Scott J. H. (1956). Growth at facial sutures. *American Journal of Orthodontics* **42**: 381.

Scott J. H. (1958). The cranial base. *American Journal of Physical Anthropology* **16**: 319-348.

Scott J. H. (1967). *Dento-facial development and growth.* Pergamon Press: Oxford.

Semendeferi K., Damasio H., Frank R., Hoesen G W. (1997). The evolution of the frontal lobes: a volumetric analysis based on three-dimensional reconstructions of magnetic resonance scans of human and ape brains. *Journal of Human Evolution* **32**: 375-388.

Shapiro R. and Robinson F. (1980). *The Embryogenesis of the Human Skull.* London: Harvard University Press.

Shizhe L., Gilmore J. A., Yang Q. X., Smith M. B. (1994). Three dimensional finite element calculations of magnetic susceptibility effects in high resolution anatomical models of human head. *In Proceedings of the Society of Magnetic Resonance* **2**: 831.

Sirianni J. E. (1985). Nonhuman primates as models for human craniofacial growth. In (Alan R., Ed) *Nonhuman primate models for human growth and development*, pp 95-124. New York: Liss Inc.

Sirianni J. E. and Newell-Morris L. (1980). Craniofacial growth of fetal *Macaca nemestrina*: A cephalometric roentgenographic study. *American Journal of Physical Anthropology* **53**: 407-421.

Sirianni J. E. and Swindler D. R. (1979). A review of postnatal craniofacial growth in old world monkeys and apes. *Yearbook of Physical Anthropology* **22**: 80-104.

Sirianni J. E. and Van Ness A. L. (1978). Postnatal growth of the cranial base in *Macaca nemestrina. American Journal of Physical Anthropology* **49**: 329-240.

Small C. S. and Peterson D. I. (1982). The reliability of dimensions of formalin-fixed brains. *Neurology* **32**: 413-415.

Smith B. R., Johnson G. A., Groman E. V., Linney E. (1994). Magnetic resonance microscopy of mouse embryos. *Proceedings of the National Academy of Sciences USA* **91**: 3530-3533.

Smith D. W. (1981). Mechanical forces and patterns of deformation. In (Connelly T. G., Ed) *Morphogenesis and Pattern Formation*, pp 215-223. New York: Raven Press.

Smith G. E. (1924). *The evolution of man.* London: Oxford University Press.

Smith R. J. (1980). Rethinking allometry. *Journal of Theoretical Biology* **88**: 97-111.

Snider R. S. and Stowell A. (1944). Receiving areas of the tactile, auditory and visual systems in the cerebellum. *Journal of Neurophysiology* **7**: 331-357.

Sokal R. R. and Rohlf F. J. (1995). *Biometry* (3rd ed). New York: W. H. Freeman and Co.

Solow B. (1966). The pattern of craniofacial associations. *Acta Odontologica Scandinavica* **46**: 75-83.

Sperber G. H. (1981). *Craniofacial embryology* (3rd ed). London: Wright-PSG.

Spoor F. (1997). Basicranial architecture and relative brain size of Sts 5. (*Australopithecus africanus*) and other Plio-Pleistocene hominids. *South African Journal of Science* **93**: 182-187.

Spoor F. and Zonneveld F. W. (1995). Morphometry of the primate bony labyrinth: a new method based on high-resolution computed tomography. *Journal of Anatomy* **186**: 271-286.

Spoor F. and Zonneveld F. W. (1998). Comparative review of the human bony labyrinth. *American Journal of Physical Anthropology* **27**: 211-251.

Spoor F., Jeffery N., and Zonneveld F. (In press). Imaging skeletal growth and evolution. In (O'Higgins P. and Cohen M., Eds) *Vertebrate ontogeny and phylogeny: Implications for the study of hominid skeletal evolution.* London: Academic Press.

Spoor F., O'Higgins P., Dean C., and Lieberman D. (1999). Anterior sphenoid in modern humans. *Nature* **397**: 572.

Srivastava H. C. (1992). Ossification of the membraneous portion of the squamous part of the occipital bone in man. *Journal of Anatomy* **180**: 219-224.

Steegman A. T. and Platner W. S. (1968). Experimental cold modification of craniofacial morphology. *American Journal of Physical Anthropology* **28**:17-30.

Stein J. F., Miall R. C., and Weir D. J. (1987). The role of the cerebellum in the visual guidance of movement. In (Glickstein M., Yeo C., and Stein J., Eds) *Cerebellum and neuronal plasticity.* pp212-230 New York: Plenum Press.

Stephan H., Frahm H., and Baron G. (1981). New and revised data on volumes of brain structures in Insectivores and Primates. *Folia primatologica* **35**: 1-29.

Strait D. S. (1999). The scaling of basicranial flexion and length. *Journal of Human Evolution* **37**:701-719.

Strait D. S. and Ross C. F. (1999). Kinematic data on primate head and neck posture: implications for the evolution of basicranial flexion, and an evaluation of registration planes used in paleoanthropology. *American Journal of Physical Anthropology* **108**: 205-222.

Streeter G. L. (1918). The developmental alterations in the vascular system of the brain of the human embryo. *Contributions to Embryology* **8**: 7-38.

Streeter G. L. (1920). Weight, sitting height, headsize, foot length, and menstrual age of the human embryo. *Contributions to Embryology* **55**: 143-159.

Sumanaweera T., Glover G., Song S., Adler J., Napel S. (1994). Quantifying MRI geometric distortion in tissue. *Magnetic Resonance in Medicine* **31**: 103-113.

Thach W. T. (1996). On the specific role of the cerebellum in motor learning and cognition: Clues from PET activation and lesion studies in man. *Behavioral and Brain Sciences* **19**: 411-431.

Thatcher R. W., Camacho M., Salazar A., Linden C., Biver C., and Clarke L. (1997). Quantitative MRI of the gray-white matter distribution in traumatic brain injury. *Journal of Neurotrauma* **14**: 1-14.

Thickman D. I., Kundel H. L., and Wolf G. (1983). Nuclear magnetic resonance characteristics of fresh and fixed tissue: the effect of elapsed time. *Radiology* **148**: 183-185.

Thomason J. J. and Russell A. P. (1986). Mechanical factors in the evolution of the mammalian secondary palate: A theoretical analysis. *Journal of Morphology* **189**: 199-213.

Thompson D. (1961). *On growth and form.* Cambridge: Cambridge University Press.

Thorogood P. (1987). Mechanisms of morphogenetic specification skull development. In (Wolff J.R., Sievers J., and Berry M., Eds) *Mesenchymal-Epithelial Interactions in Neural Development*, pp 141-152. Berlin: Spinger-Verlag.

Thorogood P. (1988). The developmental specification of the vertebrate skull. *Development* **103**: 141-153.

Tschermak, E. (1900). Über künstliche Kreuzung bei *Pisum sativum. Berichte der deutschen botanischen Gesellschaft* **18**.

Tucket F. and Morriss-Kay G. M. (1985). The ontogenesis of cranial neuromeres in the rat embryo. II. A transmission electron microscopy study. *Journal of Embryology and Experimental Morphology* **88**: 231-247.

Udupa J. K. (1982). Interactive segmentation and boundary surface formation for 3D digital images. *Computer Graphics and Image Processing* **18**: 213-235.

van den Eynde B., Kjaer I., Solow B., Graem N., Kjaer T. W. and Mathiesen M. (1992). Cranial base angulation and prognathism related to cranial and general skeletal maturation in human fetuses. *Journal of Craniofacial Genetics and Developmental Biology* **12**: 22-32.

Virapongse C., Shapiro R., Sarwar M., Bhimani S., and Crelin E. S. (1985). Computed tomography in the study of the development of the skull base:1. Normal development. *Journal of Computer Assisted Tomography* **9**: 85-94.

Virchow R. (1857). Untersuchungen über die Entwicklung des Schädelgrundes im gesunden und Frankhaften Zustande: Berlin.

von Bear K. E. (1828). Über Entwicklungsgeschichte der Tiere: Beobachtung und Reflexion. Königsberg: Borntraeger.

Vries H. (1900). Das Spaltungsgesetz der Bastarde. *Berichte der deutschen botanischen Gesellschaft* **18**.

Washburn S. L. (1947). The relation of the temporal muscle to the form of the skull. *Anatomical Record* **99**: 239-248.

Watt D. G. and Williams C. H. (1951). The effects of the physical consistency of food on the growth and development of the mandible and maxilla of the rat. *American Journal of Orthodontics* **37**: 895-928.

Weidenreich F. (1941). The brain and its role in the phylogenetic transformation of the human skull. *Transactions of the American Philosophical Society* **X, XI (V)**: 321-442.

Weinreb J.C., Lowe T., Cohen J.M., Kutler M. (1985). Human fetal anatomy: MR imaging. *Radiology* **157**: 715-720.

Westbrook C. and Kaut C. (1993). *MRI in practice*. Oxford: Blackwell Science.

Williams P. L., Bannister L. H., Berry M. M., Collins P., Dyson M., Dusseck J. E. and Ferguson M. W. J. (eds.). (1995). *Gray's Anatomy* (38th ed). Edinburgh: Churchill Livingstone.

Winter R. M. (1996). What's in a face. *Nature Genetics* **12**: 124-129.

Wragg L. E., Klein M., Steinworth G., and Warpeha R. (1970). Facial growth accommodating secondary palate closure in rat and man. *Archives of Oral Biology* **15**: 705-719.

Young R. W. (1959). The influence of cranial contents on postnatal growth of the skull in the rat. *American Journal of Anatomy* **105**: 383-415.

Zhu X. P., Checkley D. R., Hickey D.S., and Isherwood I. (1986). Accuracy of area measuremnts made from MR images compared with computed tomography. *Journal of Computer assisted Tomography* **10**: 96-102.

Zimmerman A. A., Armstrong E. L., and Scammon R. E. (1934). The change in position of the eyeballs during fetal life. *Anatomical Record* **59**: 109-134.

Zollikofer C. P. E, De Leon M. C. P., Martin R. D. (1998). Computer assisted paleoanthropology. *Evolutionary Anthropology* **6**: 41-54.

Zuckerman S. (1926). Growth changes in the skull of the baboon, *Papio porcarius*. *Proceedings of the Zoological Society of London* p.843.

Zuckerman S. (1955). Age changes in the basicranial axis of the human skull.

American Journal of Physical Anthropology **15**: 521.